University of Cambridge
Cambridge Institute for Medical Research

Dissertation

A MOLECULE-INHIBITOR OF THE INTEGRATED STRESS RESPONSE REGULATES ACTIVITY OF MAMMALIAN EUKARYOTIC TRANSLATION INITIATION FACTOR 2B

by Alisa Zyryanova

Darwin College

This dissertation is submitted for the degree of Doctor of Philosophy

July 2018

DISSERTATION: A MOLECULE-INHIBITOR OF THE INTEGRATED STRESS RESPONSE REGULATES ACTIVITY OF MAMMALIAN TRANSLATION INITIATION FACTOR 2B

BY ALISA ZYRYANOVA

The Integrated Stress Response (ISR) is a conserved eukaryotic translational and transcriptional program implicated in mammalian metabolism, memory and immunity. Although mainly considered to be a protective mechanism, prolonged and severe ISR can result in cell death. The ISR is activated by diverse stress pathways converged on phosphorylation of the alpha subunit of eukaryotic translation initiation factor 2 (eIF2) that inhibits the guanine nucleotide exchange activity of its partner eIF2B and attenuates overall rates of protein synthesis. Numerous mutations in eIF2B are linked to a fatal neurodegenerative disease of vanishing white matter. A new chemical inhibitor of the ISR (ISRIB), a bis-O-arylglycolamide, can reverse the attenuation of mRNA translation by phosphorylated eIF2 protecting mice from prion-induced neurodegeneration and traumatic brain injury.

The work presented in this dissertation describes identification of mammalian eIF2B as a cellular target of ISRIB by implementing biochemical, biophysical, structural and chemogenetic methods. The herein reported cryo-electron microscopy-based structure of eIF2B uncovers a novel allosteric site on the translation factor capturing the ISRIB-binding pocket at the interface between its β and δ regulatory subunits. The extensive CRISPR/ Cas9-based screen for ISRIB-resistant and analogue-sensitive phenotypes revealed residues on the eIF2B dimer interface important for ISRIB binding.

Based on the results reported in this dissertation along with the similar findings of others the potential molecular basis of ISRIB action, and its implication for the regulation of eIF2B's activity is broadly discussed. The identification of the ISRIB binding pocket away from the known interaction sites between eIF2B and eIF2 is also put into the context of a possible molecular mechanism of eIF2B's guanine exchange inhibition by phosphorylated eIF2.

The work described in this dissertation provides new insight into the translational regulation and points to the importance of fine-tuning the activity of translation factors by small chemical molecules.

Preface

Since I was young I was keen on sciences and languages, but I could have never imagined coming this far from my original birthplace at the geographical border between Europe and Asia in post-soviet Russia to pursue my scientific career. Doing a PhD at the University of Cambridge is a dream come true. And there are many people who helped me along my way and to whom I am extremely grateful.

I would like to say big thank you to my first host research institute, the Engelhardt Institute of Molecular Biology in Moscow, which gave me an opportunity to be immersed into the hidden and captivating world of science and scientists for the first time in my life. I am very grateful to my first research supervisor Tamara Mashkova, who was brave and enthusiastic to take me, an undergraduate student with an engineering background, on board of her lab. I would like to thank Nika Oparina, who actually responded to my self-advertisement on a job-seeking website stating “No experience. Big enthusiasm.” And I would like to thank the former head of our department, the late academician Lev Kisselev, who taught me to set goals and think about perspective.

Here in Cambridge, I was very lucky to get a position in the lab of Professor David Ron, who, being a brilliant mentor, taught me to think clearly and to be resilient. I will forever (as I can think) remember my days in his lab with lots of gratitude to him and to many of my colleagues with whom I shared laughs and tears. I am also thankful for all the networking opportunities my experience in Cambridge gave me, for all the collaborators, supporting staff, and all my new friends.

Coming back to my roots, I am of course very thankful to my family, who always supported my wish to pursue an academic career and did everything they could to make that happen. I am also very sorry that some of them are no longer around to celebrate this important step in my life. And I am very grateful to my partner Luca, who is always keen on listening to my eIF2B stories and whose support makes my days a lot brighter.

This dissertation is the result of my own work and includes nothing which is the outcome of work done in collaboration except as declared in the Preface and specified in the text and figure legends. It is not substantially the same as any that I have submitted, or, is being concurrently submitted for a degree or diploma or other qualification at the University of Cambridge or any other University or similar institution except as declared in the Preface and specified in the text. I further state that no substantial part of my dissertation has already been submitted, or, is being concurrently submitted for any such degree, diploma or other qualification at the University of Cambridge or any other University or similar institution except as declared in the Preface and specified in the text. It does not exceed the prescribed word limit for the relevant Degree Committee.

This dissertation is divided into four main Chapters: Introduction, Results, Discussion, and Materials and Methods, numbered 1-4 and split into corresponding sections. People who contributed to the design and/ or execution of any given experiment are acknowledged in the respective figure legends where indicated. Although a big consideration was taken and an honest attempt was made to cite the original works throughout, I do apologize for non-intentional omission of some authors from my Bibliography list.

Parts of the work documented in this dissertation were presented at various times between 2013-2017 at group lab meetings, internal institutional seminars and international conferences. Results in part are also featured in several publications: Sekine et al. 2015; Sekine et al. 2016; Zyryanova et al. 2017; Zyryanova et al. 2018.

I hope you will enjoy your reading.

Table of Contents

Summary

The Integrated Stress Response (ISR) is a conserved eukaryotic translational and transcriptional program implicated in mammalian metabolism, memory and immunity. Although mainly considered to be a protective mechanism, prolonged and severe ISR can result in cell death. The ISR is activated by diverse stress pathways converged on phosphorylation of the alpha subunit of eukaryotic translation initiation factor 2 (eIF2) that inhibits the guanine nucleotide exchange activity of its partner eIF2B and attenuates overall rates of protein synthesis. Numerous mutations in eIF2B are linked to a fatal neurodegenerative disease of vanishing white matter. A new chemical inhibitor of the ISR (ISRIB), a bis-O-arylglycolamide, can reverse the attenuation of mRNA translation by phosphorylated eIF2 protecting mice from prion-induced neurodegeneration and traumatic brain injury.

The work presented in this dissertation describes identification of mammalian eIF2B as a cellular target of ISRIB by implementing biochemical, biophysical, structural and chemogenetic methods. The herein reported cryo-electron microscopy-based structure of eIF2B uncovers a novel allosteric site on the translation factor capturing the ISRIB-binding pocket at the interface between its β and δ regulatory subunits. The extensive CRISPR/ Cas9-based screen for ISRIB-resistant and analogue-sensitive phenotypes revealed residues on the eIF2B dimer interface important for ISRIB binding.

Based on the results reported in this dissertation along with the similar findings of others the potential molecular basis of ISRIB action, and its implication for the regulation of eIF2B's activity is broadly discussed. The identification of the ISRIB binding pocket away from the known interaction sites between eIF2B and eIF2 is also put into the context of a possible molecular mechanism of eIF2B's guanine exchange inhibition by phosphorylated eIF2.

The work described in this dissertation provides new insight into the translational regulation and points to the importance of fine-tuning the activity of translation factors by small chemical molecules.

List of abbreviations

075B - ISRIB analogue, AAA1-075B

$075B^{SEN}$ - 075B sensitive cells

084 - ISRIB analogue, AAA1-084

084^{SEN} – 084 sensitive cells

ATF4 - Activating Transcription Factor 4

ATP – adenosine triphosphate

Cas9 – CRISPR associated protein 9

CBB – coomassie brilliant blue

CHOP - C/EBP-Homologous Protein

CRISPR - clustered regularly interspaced short palindromic repeats

CSC – catalytic sub-complex of eIF2B

CTD - C-terminal domain

eEF – eukaryotic elongation factor

eIF – eukaryotic translation initiation factor

eRF – eukaryotic release factor

ER – endoplasmic reticulum

FACS – fluorescence activated cell sorting

FAM – carboxyfluorescein

FP – fluorescence polarization

GCN2 - general control nonderepressible 2 kinase

gcn – general control nondepressible

gcd - general control depressible

GDF – GDI displacement factor (GDP-dissociation inhibitor displacement factor)

GDI – GDP-dissociation inhibitor

GDP - guanosine diphosphate

GEF – guanine exchange factor

GFP – green fluorescent protein

GSK - GlaxoSmithKline

GTP - guanosine triphosphate

HIS – histidinol

HRI - heme-regulated inhibitor kinase

IRES – internal ribosome entry site

ISR – integrated stress response

ISRIB – integrated stress response inhibitor

$ISRIB^{RES}$ – ISRIB resistant cells

$ISRIB^{SEN}$ – ISRIB sensitive cells

$Met\text{-}tRNA_i^{Met}$ – initiator methionyl tRNA

MS – mass spectrometry

NTD – N-terminal domain

PAM - protospacer adjacent motif

PERK - PKR-like endoplasmic reticulum kinase

PIC - pre-initiation complex

PKR - double-stranded RNA activatable kinase

PP1 – protein phosphatase 1

r.m.s.d. - root-mean-square deviation

PRMT5 - protein arginine N-methyltransferase 5

RSC – regulatory sub-complex of eIF2B

RT – room temperature

SEC – size exclusion chromatography

SEM – standard deviation of the mean

SD – standard deviation

SILAC - stable isotope labeling by amino acids in cell culture

TC – ternary complex

uORF – upstream open reading frame

UPR – unfolded protein response

VWM - leukoencephalopathy with vanishing white matter disease

WT - wildtype

ZBD – zinc binding domain

Chapter 1: Introduction

1.1 Overview of protein synthesis in eukaryotes

Across all the kingdoms of life, protein synthesis is indispensable in the pathway of gene expression and is a key component in its control. To produce a new protein a messenger RNA (mRNA), carrying information about a gene product transcribed from DNA, has to engage with many translational protein factors, ribosomes and transfer RNAs (tRNAs). This orchestrated process of mRNA translation is divided in four main stages: initiation, elongation, termination and recycling (Figure 1.1). Since the genetic code is universal, mRNA translation in eukaryotes shares many similarities with prokaryotes, varying in RNA modifications, utilized proteins and composition of ribosomes. In prokaryotes, however, mRNA translation is coupled with DNA transcription due to the absence of nucleus, whereas in eukaryotes mRNA translation is uncoupled from DNA transcription, occurring in the cytoplasm or on the endoplasmic reticulum (ER) membrane (reviewed in Hershey et al. 2012). And even though the elongation, termination and recycling phases in eukaryotes resemble those in bacteria, the translation initiation phase differs substantially between these two kingdoms of life, due to larger number and complexity of translational factors in the higher cellular forms of life (reviewed in Hershey et al. 2012; Dever et al. 2016).

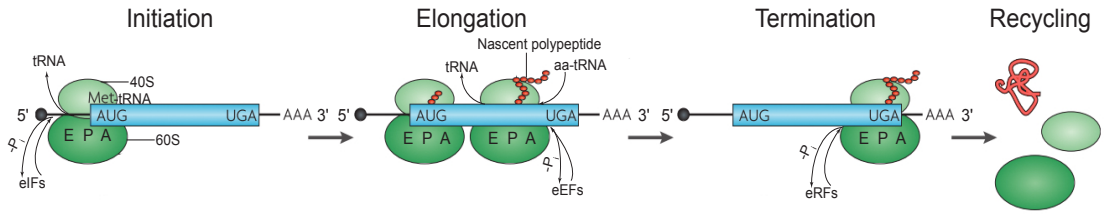

Figure 1.1: Overview of protein synthesis in eukaryotes.

Shown is a schema of the four stages of mRNA translation in eukaryotes: initiation, elongation, termination and recycling. The gene-coding region on mRNA is indicated in blue with marked start (AUG) and stop (UGA) codons. The ribosomal subunits (40S and 60S) are indicated in green, with marked acceptor (A), peptidyl (P) and exit (E) sites for channeling of charged aminoacylated/ deacylated tRNAs (aa-tRNAs/ tRNAs). The growing (or released) polypeptide chain is in red. Essential components of the translational machinery are indicated for each stage. Met – methionine; eIFs - eukaryotic translation initiation factors; eEFs - eukaryotic elongation factors; eRFs - eukaryotic release factors. Redrawn and modified from Scheper et al. 2007.

Translation initiation in eukaryotes requires association and dissociation of eukaryotic translation initiation factors (eIFs), selection of charged initiator aminoacyl-tRNA (aa-tRNA), search of the correct start site on mRNA and joining of ribosomal subunits (40S and 60S) (reviewed in Marintchev and Wagner 2004). The elongation phase is a series of steps where the actual polypeptide chain is being synthesized by the assembled 80S ribosome. It requires channeling of charged aa-tRNAs, facilitated by eukaryotic elongation factors (eEFs), between catalytic sites on the ribosome where they establish base-pairing between mRNA codons and their anticodons (acceptor (A) site), form peptide bonds with the peptide attached to a preceding tRNA (peptidyl (P) site) and clear the deacylated tRNA from the previous cycle (exit (E) site), while preserving the correct reading frame (reviewed in Marintchev and Wagner 2004). Finally, translation termination and recycling involves recognition of an in-frame stop codon on mRNA, release of a nascent polypeptide and dissociation of ribosomal complexes, facilitated by eukaryotic release factors (eRFs) (reviewed in Marintchev and Wagner 2004). All of the translation steps require ATP or GTP nucleotides to ensure high specificity of this sophisticated process (Hopfield 1974; Schimmel 1993).

Regulation of protein synthesis may occur at any step of the translational pathway. In eukaryotes, the translation initiation is thought to be the most complex and rate-limiting step of protein synthesis involving at least 11 eIFs, in contrast to just three IFs in bacteria, thus, being the most common target of the translational control machinery (reviewed in Hinnebusch and Lorsch 2012; Dever et al. 2016). Regulation of global protein synthesis is often based on activation/ inhibition of one or more components of the translational apparatus, while specific regulation may occur through trans-acting proteins or micro-RNAs (reviewed in Hershey et al. 2012).

1.1.1 Translation initiation and its regulation

The conventional initiation pathway in eukaryotic cells requires methionine-charged initiator tRNA (Met-$tRNA_i^{Met}$) together with the GTP-bound eIF2 to form a ternary complex (TC) that is recruited to the small 40S ribosomal subunit. Binding of the TC to the 40S is facilitated by eIF1, eIF1A, eIF5 and

eIF3, resulting in the formation of a 43 preinitiation complex (PIC), which is then able to bind mRNA. Mature mRNA usually contains 7-methylguanosine cap (m^7G) modification at its 5' end and polyadenylated (poly(A)) tail at its 3' end (reviewed in Dever et al. 2016). The 5'- m^7G mRNA is recognized by a group of cap-binding factors (eIF4B, eIF4H (in mammals), and eIF4F complex, comprising of eIF4G, eIF4E, and eIF4A factors), while the 3'-poly(A) mRNA tail interacts with poly(A)-binding protein (PABP) (Hinnebusch and Lorsch 2012; Llácer et al. 2015; Dever et al. 2016). The scaffolding protein eIF4G binds PABP assembling a circular messenger ribonucleoprotein (mRNP) and stimulating loading of 43S PIC onto mRNA forming the 48S PIC (Hinnebusch and Lorsch 2012; Llácer et al. 2015; Dever et al. 2016). The 43S PIC scans mRNA from its 5' end in search for an AUG codon to initiate protein synthesis. Recognition of an AUG codon triggers GTP hydrolysis on eIF2 and release of many eIFs, including GDP-bound eIF2. Large 60S ribosomal subunit joining is stimulated by another GTP-bound factor eIF5B, which gets hydrolyzed and released upon assembly of the 80S ribosomal complex marking the start of the next phase of translation, the elongation (Figure 1.1.1) (reviewed in Dever et al. 2016).

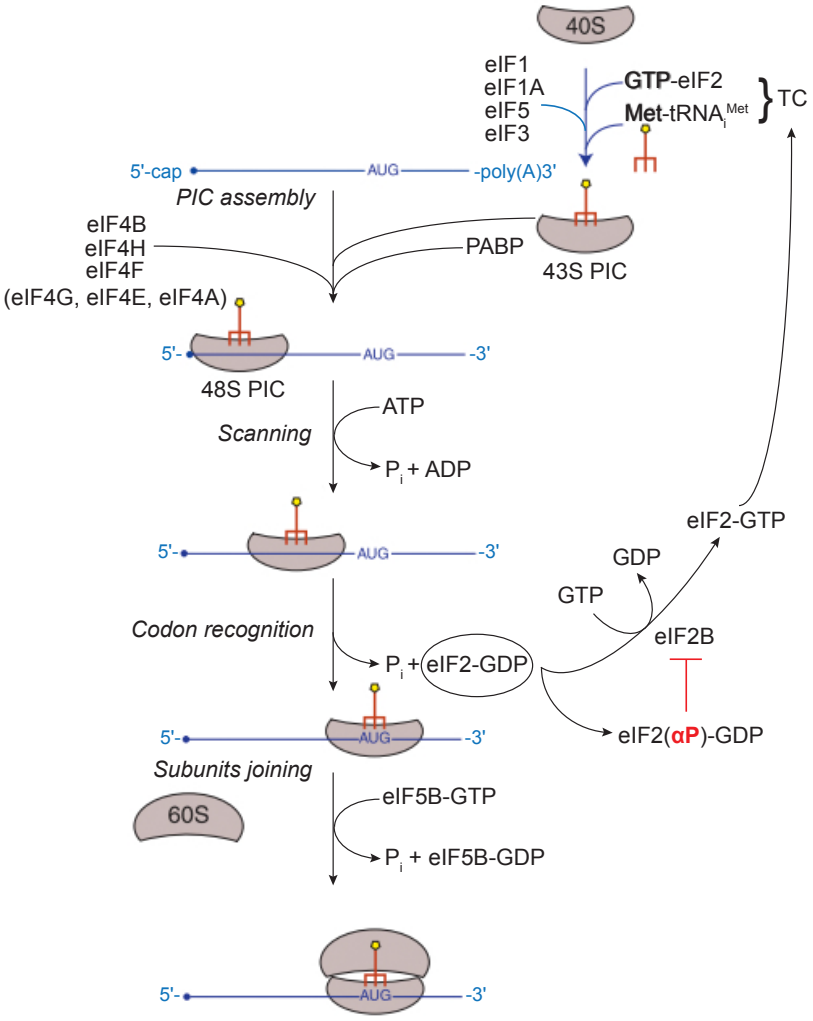

Figure 1.1.1: Conventional translation initiation in eukaryotes.

Shown is a simplified cartoon of cap-dependent translation initiation. Outlined are the steps of preinitiation complex (PIC) assembly, mRNA scanning, AUG codon recognition and 60S ribosomal subunit joining. The main participants of the translation initiation are indicated. The regeneration of eIF2-GDP with GTP, facilitated by eIF2B, after codon recognition is shown, as well as the inhibitory phosphorylation of eIF2α (in red). Mature mRNA is indicated in blue with 5'-m^{7}G-cap (circle) and 3'-poly(A) tail. 40S and 60S subunits are in grey. Met-tRNA$_i^{Met}$ is in red with yellow circle on top. Redrawn and modified from Hershey et al. 2012.

Reinitiation of translation requires recycling of eIF2 into a new TC (Figure 1.1.1). The eIF2-GDP dissociated from the PIC is unable to bind Met-tRNA$_i^{Met}$ and needs to acquire a fresh molecule of GTP in order to do so. Because of the large differences (up to 100 fold) in affinities between GDP and GTP towards eIF2 (Walton and Gill 1975), eIF2-GDP needs assistance in order to be recycled. eIF2B is a protein complex that serves as a guanine nucleotide exchange factor for eIF2 (eIF2 GEF), promoting GDP release and facilitating regeneration of eIF2 with GTP, subsequently initiating a new round of translation (Siekierka et al. 1982; Konieczny and Safer 1983). The activity of eIF2B is regulated by diverse mechanisms, and it can modulate overall rates of protein synthesis (reviewed in Proud 2005; Pavitt 2005). One of the best-studied mechanisms of regulation of eIF2B's activity is through phosphorylation of serine 51 (S51) of the α subunit of eIF2 (eIF2α) that converts eIF2-GDP from a substrate for eIF2B into a potent competitive inhibitor of eIF2B's GEF activity (Rowlands et al. 1988). Hence, the generally less abundant eIF2B becomes limiting, and the formation of productive interactions with eIF2 reduces considerably lowering down the levels of TC formation to the extend of global translation attenuation (Oldfield et al. 1994; Krishnamoorthy et al. 2001).

Inhibitory influence of eIF2α phosphorylation on TC formation is not the only regulatory event that can affect activity of eIFs and loading of 43 PIC onto mRNA. Phosphorylation is used quite often to regulate protein synthesis in cells (Hershey et al. 2012). And other mRNA-binding factors, like eIF4B and eIF4F, are reported to be a target of phosphorylation as well. Yet, unlike for eIF2, phosphorylation of these eIFs seems to cause or correlate with enhanced protein synthesis (reviewed in Merrick 1992). Another extensively studied regulatory event concerns formation of the eIF4F complex, focusing on the interactions between cap-binding eIF4E protein and scaffolding eIF4G protein. It was shown that members of a related protein family, eIF4E-binding proteins (4E-BPs), can compete with eIF4G for binding of eIF4E, thus inhibiting cap-dependent translation initiation. Additionally, phosphorylation of 4E-BPs was reported to weaken their interactions with eIF4E (Sonenberg and Hinnebusch 2009; Roux and Topisirovic 2012). Interestingly, the kinase

responsible for phosphorylation of 4E-BPs, mammalian target of rapamycin (mTOR) kinase, is also responsible for indirect phosphorylation of eIF4B and possibly eIF4G itself through the mTOR signaling pathway, potentially stimulating interaction of these eIFs with the PIC (Holz et al. 2005; Harris et al. 2006; Sonenberg and Hinnebusch 2009).

Other regulatory events occurring at the step of translation initiation are linked to changes in mRNA levels (regulated by micro-RNAs and trans-acting proteins), to the size of mRNA structural elements (like the size of 5' untranslated regions), to mRNA secondary structures, and to the unconventional ways (AUG-independent) of initiating protein synthesis (for e.g. through internal ribosome entry site – IRES) (reviewed in Hershey et al. 2012; Dever et al. 2016). I am, however, not going to further focus on that, and concentrate on details of one important translational control mechanism.

1.1.2 The integrated stress response

The aforementioned phosphorylation on S51 of eIF2α is probably one of the best-characterized mechanisms of translation initiation regulation in eukaryotes. In yeast, the only known protein kinase to phosphorylate eIF2α^{S51} is Gcn2p ("general amino acid control of gene expression non-depressing") that is activated by uncharged tRNAs during amino acid starvation (Dever et al. 1992). Gcn2p kinase was first characterized through its ability to stimulate translation of a transcriptional activator Gcn4p, which is a marker of the general amino acid control (GAAC) signaling pathway in yeast (Hinnebusch 1988; Wek 1989). This effect of enhanced translation upon activation of stress, during which translation of most mRNAs is attenuated, was shown to be associated with the presence of upstream open reading frames (uORFs) on a small subset of certain mRNAs, such as Gcn4p. Gcn4p has four short uORFs. During normal non-starvation conditions when the formation of TC is not limiting, the 40S ribosomal subunit can scan past first uORF, reinitiate at second uORFs but does not continue scanning further than that, thus not reaching the Gcn4p start codon. However, under stress conditions, when eIF2α is phosphorylated, eIF2(αP)-GDP cannot be efficiently regenerated and TC becomes limiting, then 40S ribosomal subunit keeps scanning mRNA past

the inhibitory downstream uORFs, three and four, stimulating Gcn4p translation (Hinnebusch 2011). It is known that Gcn4p promotes transcription of over 500 genes representing 12 different pathways, including amino acids, purines, and peroxisome biogenesis (reviewed in Hinnebusch and Natarajan 2002; Pavitt 2018).

The work on GAAC also contributed to identification of general control non-depressible (*gcn*) and general control depressible (*gcd*) genes. Mutation of *gcn* and *gcd* genes respectively gives rise to gcn$^-$ phenotype, resulting in insensitivity of translation to eIF2α phosphorylation, and to gcd$^-$ phenotype, causing constitutive suppression of protein synthesis even when eIF2α is not phosphorylated. Many *gcn* and *gcd* mutations were identified across genes encoding eIF2 and eIF2B protein subunits (Vazquez de Aldana et al. 1993; Vazquez de Aldana and Hinnebusch 1994; Pavitt et al. 1997; Pavitt et al. 1998; Krishnamoorthy et al. 2001; Dey et al. 2005; Dev et al. 2010). Such mutations, however, are not exclusively associated with just these two translation factors, and can affect formation of TC, PIC, and translation of uORFs containing mRNAs in other ways (Hinnebusch 2011).

In mammals, phosphorylation on S51 of eIF2α occurs in response to several distinct stress pathways mediated by four known kinases (Figure 1.1.2a). These kinases are: HRI ("hemin-regulated inhibitor") (Ranu and London 1976; Chen and London 1995; Lu et al. 2001); PKR ("protein kinase RNA-activated") (Levin and London 1978; Kaufman 1999); PERK ("PKR-like Endoplasmic Reticulum kinase") (Harding et al. 1999); and, a yeast ortholog, mammalian mGCN2 (Harding et al. 2000a). All these kinases share similarities in their activation mechanism, which requires dimerization and autophosphorylation of their C-terminal domains, while their N-terminal domains sense distinct changes in the cellular environment that trigger the response. HRI is mainly expressed in erythroid cells, red blood cell precursors, and is activated by heme deficiency, protecting cells from toxic globin aggregates (Han et al. 2001). It transitions between an inactive, heme-bound, dimeric form stabilized by disulfide bonds, and an active dimer stabilized by non-covalent interaction, promoting autohphosphorylation and kinase activity in the absence of heme

(Chefalo et al. 1998; Rafie-Kolpin et al. 2000). PKR is activated by binding of double-stranded RNAs to its N-terminal moiety and is important for limiting viral replication during infection. Its kinase activity is also dependent on dimerization and autophosphorylation of its C-terminal kinase domain (Kaufman 1999). PERK is an ER membrane resident that gets activated by the unfolded protein response (UPR). PERK is expressed in high levels in pancreas making these secretory cells particularly sensitive to changes in PERK's abundance (Harding et al. 2001). Its ER luminal domain is suggested to either bind ER chaperones that dissociate upon stress, or even bind misfolded proteins directly during stress, promoting dimerization and autophosphorylation of its cytosolic domain triggering its kinase activity (reviewed in Pakos-Zebrucka et al. 2016). GCN2 kinase possesses a domain homologous to histidyl-tRNA synthetase making it capable of binding to uncharged tRNAs that in its turn triggers its activity during amino acid starvation. It was also proposed that GCN2 is normally associated with ribosomes making it more efficient in sensing the deacylated tRNAs (Zhu and Wek 1998; Sattlegger and Hinnebusch 2000).

Similarly to yeast, phosphorylation of eIF2α in mammals promotes translation of mRNAs containing uORFs, such as transcriptional factor ATF4 (activating transcription factor 4) (Fawcett et al. 1999; Harding et al. 2000a; Vattem and Wek 2004; Zhou et al. 2008), despite inhibition of overall protein synthesis. Translational regulation of mammalian ATF4 is similar to that of Gcn4p in yeast, with the exception that ATF4 gene has fewer uORFs (two in mouse and three in human), and its last uORF overlaps the ATF4 coding sequence in an out-of-frame manner (reviewed in Pakos-Zebrucka et al. 2016). ATF4 controls the feedback loop of eIF2α phosphorylation helping to alleviate the stress by inducing expression of pro-apoptotic *CHOP/ GADD153* ("CCAAT/enhancer binding homologous protein"/ "growth arrest and DNA-damage inducible") and *ATF3* genes. This synergetic effect, in its turn, promotes expression of a regulatory subunit of eIF2α phosphatase encoded by *GADD34* (Novoa et al. 2001; Brush et al. 2003; Jiang et al. 2004). All the mentioned genes contain uORFs, and their translation relies on re-initiation mechanism, as described for yeast Gcn4p, or other Cap-independent

mechanisms, like IRES (reviewed in Pakos-Zebrucka et al. 2016). However, translation of some uORF-containing genes, like *CReP* that encodes a constitutively expressed eIF2α kinase, is independent of eIF2α phosphorylation (reviewed in Pavitt 2018). By analogy with GAAC in yeast, this stress adaptive mechanism of eIF2α phosphorylation that integrates several unrelated stress signals culminating in ATF4 translation, in mammals, was termed the integrated stress response (ISR) (Ron 2002; Harding et al. 2003).

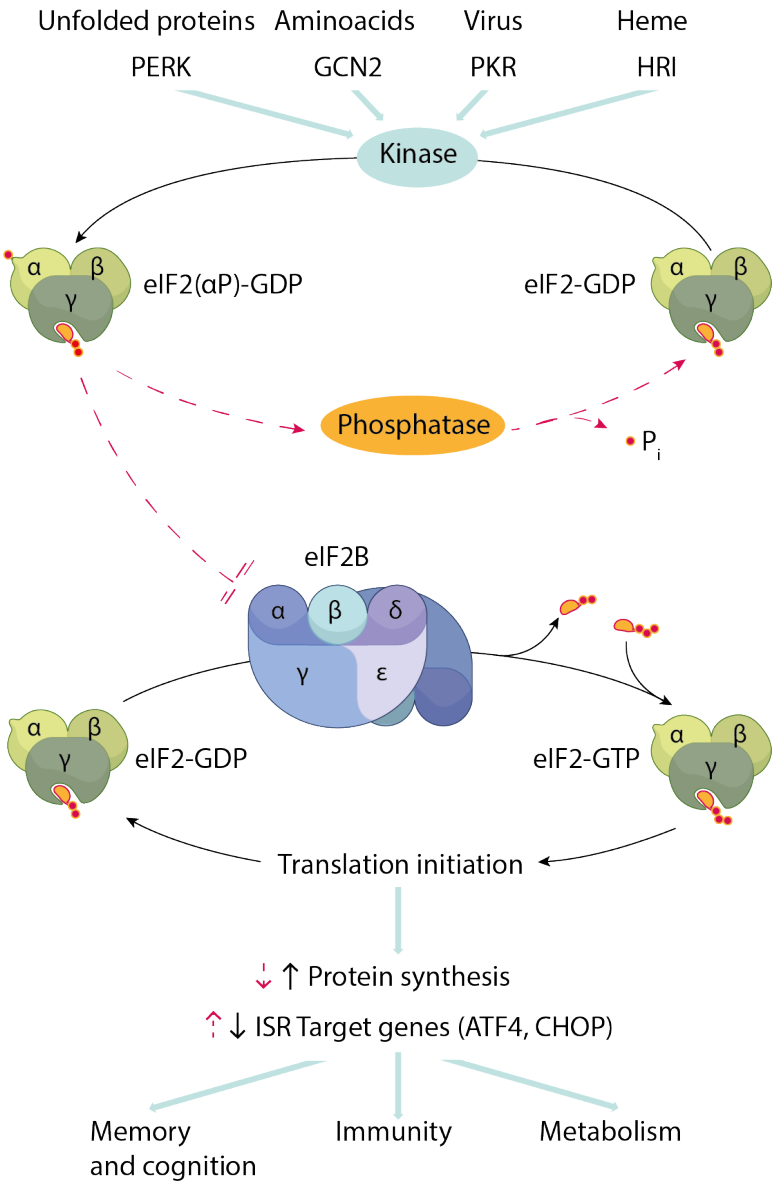

Figure 1.1.2a: eIF2 recycling and the integrated stress response (ISR).

Shown is a schematic representation of the ISR. Direction of processes under no stress conditions is indicated in black continuous lines, direction of processes under stress conditions is in red discontinuous lines. Heterotrimeric eIF2 complex is in green; heterodimeric eIF2B complex is in blue. Inorganic phosphate groups are in red, guanosine nucleoside is in orange. Drawn by A. Zyryanova, University of Cambridge.

The ISR was demonstrated to regulate important aspects of metabolism (Oyadomari et al. 2008), to play a role in memory formation (Costa-Mattioli et al. 2007), neurodegeneration (Ma et al. 2013), and, in general, to provide a protective role aimed at resolving stress and restoring homeostasis (Harding et al. 2000b; Harding et al. 2003; Chen 2007). The ISR, nonetheless, can play a dual role, and serves a pro-apoptotic function inducing cell death as well. The initial attenuation of mRNA translation is usually seen as a pro-survival measure meant to save energy (in case of HRI and GCN2 induction) and to restrict the load of proteins that are being produced (in case of PKR and PERK induction). Yet, the ISR induces pro-apoptotic genes, such as *CHOP*, that stimulate expression of *ERO1A* ("endoplasmic reticulum oxidoreductase 1 alpha"), which destabilizes oxidative homeostasis of the ER causing calcium release and leading to cellular death (Marciniak et al. 2004). The switch between these two roles (protective and pro-apoptotic) is not clearly defined. Therefore, when considering effect of the ISR on cellular fate one should probably take into account both the time it takes to be resolved and the extent to which it can be activated (Figure 1.1.2b) (Pakos-Zebrucka et al. 2016). Consequently, the beneficial effect of the ISR is most likely to vary between different cell types in contexts of either balancing the homeostasis or fighting the disease.

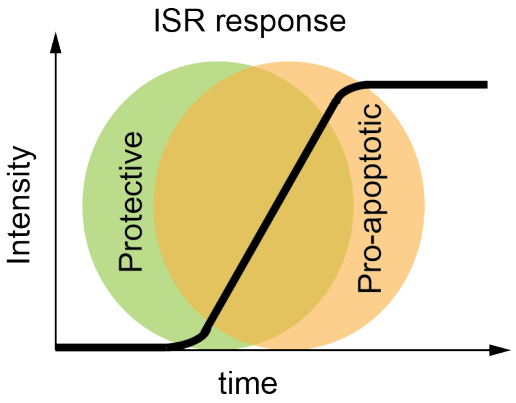

Figure 1.1.2b: Duality of the ISR.

Shown is a schematic intensity- and time-dependent activation of the ISR response. A dual effect of the ISR is indicated through overlapping protective (in green) and pro-apoptotic (in orange) outcomes that do not have a defined borderline.

1.2 Overview of eukaryotic initiation factors 2 and 2B (eIF2 and eIF2B)

1.2.1 eIF2

eIF2 is a member of a large family of G-proteins (GTPases) and its activity is regulated by the bound nucleotide stabilized by Mg^{2+} ions. GTP "activates" eIF2 (eIF2-GTP) so it is able to bind Met-$tRNA_i^{Met}$, forming a TC (GTP-eIF2*Met-$tRNA_i^{Met}$) and promoting PIC formation as the very first step of translation initiation (Figure 1.1.1). During the process of codon recognition, GTP hydrolysis stimulated by the GTPase activating protein (GAP) eIF5 "inactivates" eIF2 as it leaves PIC in a GDP-bound state (eIF2-GDP) (Mohammad-Qureshi et al. 2008; Dever et al. 2016). The activity of eIF2, therefore, should depend on the ratio between GDP and GTP, which in cells is about one to ten (Walton and Gill 1975). However, the affinity of eIF2 for GDP, in contrast to some translational GTPases (trGTPases), is about 100 fold higher than for GTP (Walton and Gill 1975; Dever et al. 2016; Maracci and Rodnina 2016). Spontaneous rates of nucleotide exchange on eIF2, therefore, are not sufficient to promote translation reinitiation in a timely manner posing a need for a GEF, eIF2B. eIF2 shares functional similarities with prokaryotic, EF-Tu, and eukaryotic, eEF1A, elongation factors, which also require GEFs, EF-Ts and eEF1B, respectively (Gromadski et al. 2002; Gromadski et al. 2007). Such GEF requirement might reflect the structural differences between the GTP- vs. GDP-bound states of the GTPases (Mohammad-Qureshi 2008; Maracci and Rodnina 2016).

eIF2 is a heterotrimeric protein complex consisting of α, β and γ subunits. Structural data on the full eIF2 complex is currently available for the yeast homologue bound to PIC (Llácer et al. 2015) and the archaeal homologue, aIF2, either free, bound to nucleotide, or engaged into TC (Yatime et al. 2007; Stolboushkina et al. 2008; Schmitt et al. 2012; Stolboushkina et al. 2013). The assembly of eIF2 complex reveals that α and β subunits bind γ but do not contact each other (Figure 1.2.1).

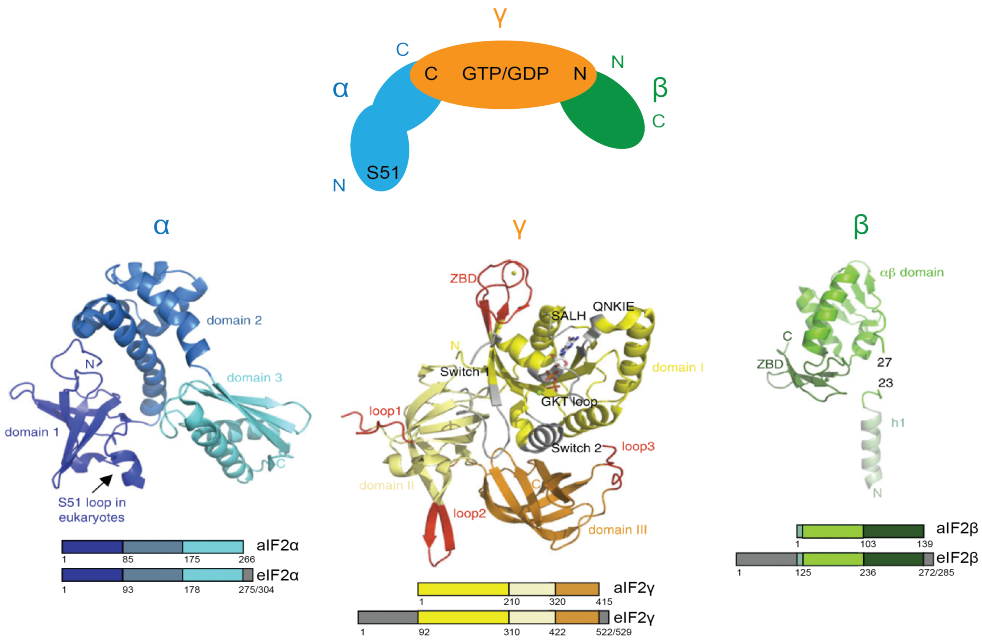

Figure 1.2.1: Structural organization of eIF2.

The α subunit: domain 1 in dark blue, domain 2 in marine, and domain 3 in cyan. The loop carrying S51 residue on eIF2α is indicated. The view is deduced from the structure of *Sulfolobus solfataricus* aIF2(αγ) (PDB: 2AHO). The γ subunit: domain 1 in yellow, domain 2 in pale yellow, and domain 3 in orange. GDP is shown as sticks, Mg^{2+} as a green sphere, and Zn^{2+} as a yellow sphere. Regions involved in the binding of the nucleotide are labeled and colored in grey. Regions characteristic of the initiation factor are labeled and colored in red. The view is deduced from the structure of *Pyrococcus abyssi* aIF2γ (PDB: 1KK3). The β subunit: helix 1 in pale green, domain 2 in green, and domain 3 in dark green. Zn^{2+} is shown as a green sphere. Residues 23–27 are not visible. The view is deduced from the structure of *Pyrococcus abyssi* aIF2(αβγ) (PDB: 2QMU). Below the cartoons are the schematic representations of e/ aIF2 subunits with numbering corresponding to *S. solfataricus* aIF2 and *S. cerevisiae* eIF2. Colors of the boxes are related to the colors of the structural domains. Domains specific of eukaryotic subunits are shown in grey. Shown above cartoons is a schema of mutual orientation of three subunits in eIF2 complex with marked N- and C-terminus. Structures and sequence schemas are redrawn from (Schmitt et al. 2010), eIF2 complex assembly schema is drawn by A. Zyryanova.

eIF2γ is a sequence and structural homologue of the prokaryotic, EF-Tu, and eukaryotic, eEF1A, elongation factors, and the selenocysteine-specific factor SelB (Gromadski et al. 2002; Roll-Mecak et al. 2004; Leibundgut et al. 2005; Gromadski et al. 2007). At the N-terminus, it possesses the flexible switch 1 and switch 2 regions, and nucleotide binding G-domain with a zinc-ribbon motif followed by two C-terminal β-barrel domains (Roll-Mecak et al. 2004). eIF2γ was reported to have an ability of binding Met-$tRNA_i^{Met}$ on its own although with a lower affinity than the full eIF2 heterotrimer (Nika et al. 2001; Roll-Mecak et al. 2004; Naveau et al. 2010).

eIF2β is attached to eIF2γ through its N-terminal helix, and its C-terminal zinc-binding domain (ZBD) is in close proximity of the GTP-binding pocket of eIF2γ (Sokabe et al. 2006; Stolboushkina et al. 2008; Llácer et al. 2015). eIF2β also possesses a helix-turn-helix (HTH) domain, through which it makes contacts with PIC and 40S ribosomal subunit (Llácer et al. 2015). eIF2β shares high sequence homology with the archaeal aIF2β, aside from its unique N-terminal portion bearing three lysine-rich K-boxes, which are absent from archaeal homologue (Schmitt et al. 2010; Dever et al. 2016). The K-boxes were shown to be important for cell viability as well as for binding eIF5 (the eIF2 GAP) and eIF2B (the eIF2 GEF) (Laurino et al. 1999; Asano et al. 1999; Das and Maitra 2000). This kingdom difference likely demonstrates the current notion that archaeal aIF2 neither has a GAP nor a GEF, even though some archaeal homologues of regulatory eIF2B subunits (aIF2B α, β and δ) are known (Schmitt et al. 2010; Gogoi and Kanaujia 2018). This concept is also consistent with some reports on eIF2β mutants suggesting that eIF2 possesses an intrinsic ability to hydrolyze GTP, and that eIF5 does not play a direct catalytic role in it (Dever 2002; Marintchev and Wagner 2004). The importance of eIF2β K-boxes for binding eIF5 and eIF2B were also reflected in the recently discovered function of eIF5 as the eIF2 guanine nucleotide displacement inhibitor (GDI), as well as in the novel function of eIF2B as the GDI dissociation factor (GDF) (Jennings and Pavitt 2010; Jennings et al. 2013; Jennings et al. 2016). Additionally, N-terminal parts of eIF5 and eIF1 were reported to share structural similarities with α/β domain and ZBD of eIF2β, which are conserved in aIF2β (Conte et al. 2006; Yatime et al. 2007).

Together with the reports of N-terminus of eIF5 binding the G-domain of eIF2γ (Alone and Dever 2006), these observations suggest the role of eIF2β, eIF5 and eIF1 in the GTP hydrolysis on eIF2 (Conte et al. 2006; Yatime et al. 2007).

eIF2α is structurally related to its archaeal homologue, aIF2α (Ito et al. 2004; Yatime et al. 2005). It consists of N-terminal (NTD) and C-terminal (CTD) domains, which are connected through a flexible linker. The eIF2α-CTD possesses an acidic C-terminal extension, which is not present in aIF2α-CTD (Schmitt et al. 2010). eIF2α-CTD is also structurally homologous to the CTD of the eukaryotic elongation factor eEF1Bα, which is a GEF for eEF1A. eEF1A, in its turn, is homologous to eIF2γ, altogether pointing to the role of eIF2α-CTD in mediating interactions between eIF2 α and γ subunits (Ito et al. 2004; Stolboushkina et al. 2008; Llácer et al. 2015). eIF2α-CTD was also shown to be important for eIF2α^{S51} phosphorylation-dependent binding to eIF2B (Krishnamoorthy et al. 2001). The eIF2α-NTD contains oligonucleotide/ oligosaccharide-binding (OB) fold formed of five β-strands, and α-helical subdomain (Nonato et al. 2002; Dhaliwal and Hoffman 2003). The OB fold contains S51, which resides within the phosphorylation loop (P-loop) and is phosphorylated in response to diverse stress signals (Dhaliwal and Hoffman 2003). Some evidence suggest that P-loop changes its conformation upon kinase binding, and that such flexibility is important for kinase selectivity since certain mutations identified in the P-loop can impair phosphorylation of S51 (Dey et al. 2011). Recent data also suggest the high flexibility of eIF2α-NTD and point to the importance of eIF2α NTD-CTD intersubunit interactions for regulation of the guanine nucleotide exchange (Bogorad et al. 2017).

1.2.2 eIF2B

eIF2B was originally discovered as a protein factor that reverses inhibition of protein synthesis stimulated by HRI kinase that phosphorylates eIF2α upon hemin depletion in rabbit reticulocytes without affecting phosphorylation state of eIF2α, therefore, named the anti-inhibitor or anti-HRI (Gross 1975; Gross 1976; Ralston et al. 1978; Amesz et al. 1979). eIF2B was also discovered independently as an eIF2 stimulating protein (ESP) that enhances formation

of the ternary complex between non-phosphorylated eIF2 and Met-tRNA$_i^{Met}$ (de Haro et al. 1978; de Haro and Ochoa 1979; Siekierka et al. 1981). Later on both anti-HRI and ESP were shown to be the same protein that possesses an ability to aid GDP release from eIF2, which is coupled to increase in TC formation, thus, named the eukaryotic recycling factor or eIF2B (Konieczny and Safer 1983; Matts et al. 1983; Panniers and Henshaw 1983; Siekierka et al. 1984; Salimans et al. 1984).

The first clean purifications of eIF2B from rabbit reticulocytes revealed that this translational factor is composed of five polypeptides, numbered from 1-5 or α-ε according to their increasing size, that in cells are usually found associated with the three subunits of eIF2 complex, α-γ, which could be dissociated by increasing salt concentration (Siekierka et al. 1982; Konieczny and Safer 1983; Panniers and Henshaw 1983; Matts et al. 1983; Salimans et al. 1984). Through yeast genetics it was shown that eIF2B α, β and δ subunits are required for regulation of the complex by eIF2(αP), therefore, labeled “regulatory subcomplex” (RSC) (Bushman et al. 1993; Vazquez de Aldana and Hinnebusch 1994; Yang and Hinnebusch 1996; Pavitt et al. 1997; Krishnamoorthy et al. 2001). eIF2B γ and ε subunits were demonstrated to be important for driving the catalysis of GDP/ GTP exchange on eIF2, thus, named “catalytic subcomplex” (CSC) (Bushman et al. 1993; Pavitt et al. 1998; Krishnamoorthy et al. 2001).

Since the discovery of eIF2B until recently it was considered a heteropentamer (Webb and Proud 1997). By integration of mass-spectrometry, chemical cross-linking, and biophysical experiments in one year several papers have provided strong evidence that eIF2B is a dimer of pentamers (Wortham et al. 2014; Bogorad et al. 2014; Gordiyenko et al. 2014). One argument that remained unresolved at the time was whether the decameric eIF2B complex is assembled through catalytic $(\gamma\varepsilon)_2$ (Gordiyenko et al. 2014) or regulatory $(\alpha\beta\delta)_2$ core (Wortham et al. 2014; Bogorad et al. 2014). The confusion was mainly caused by the existence of $(\gamma\varepsilon)_2$ tetramers amongst yeast but not mammalian eIF2B subcomplexes, which could be a true species-specific difference or mere misinterpretation of the mass

spectrometry data. In that argument, however, the dimerization model of the regulatory, $(\alpha\beta\delta)_2$, subcomplex was more in line with the information gained from crystal structures of archaeal homologue of eIF2B^{RSC}, *Pyrococcus horikoshii* aIF2Bα (PDB: 1VB5) (Kakuta et al. 2004), and human eIF2Bα subunit (PDB: 3ECS) (Hiyama et al. 2009) that were both suggesting dimerization of the monomeric regulatory subunits of eIF2B. This issue was finally resolved when a crystal structure of *Chaetomium thermophilum* eIF2B$(\beta\delta)_2$ tetramer (PDB: 5DBO) appeared in the literature (Kuhle et al. 2015), followed by a crystal structure of the full *Schizosaccharomyces pombe* eIF2B decameric complex (PDB: 5B04) (Kashiwagi et al. 2016), which confirmed the assembly of the hexameric eIF2B^{RSC} (eIF2B$\alpha_2(\beta\delta)_2$) at the core, and the heterodimeric eIF2B^{CSC} (eIF2B$(\gamma\varepsilon)$) at both of the exterior sides of the decamer (Figure 1.2.2).

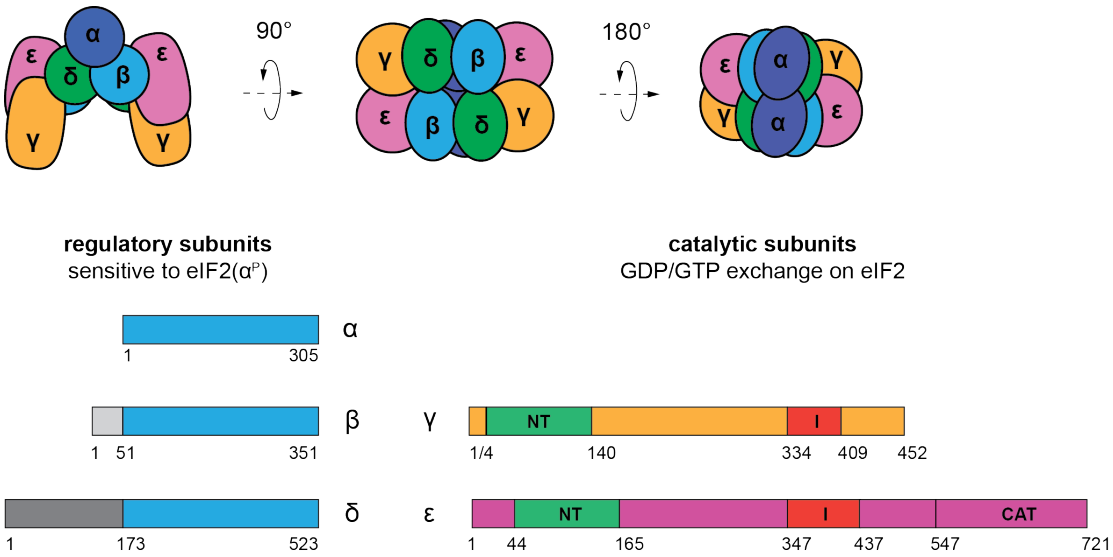

Figure 1.2.2 Structural organization of eIF2B.

Top: assembly of eIF2B complex in a dimer of pentamers with eIF2B$\alpha_2(\beta\delta)_2$ forming a regulatory subcomplex (RSC) at the core and eIF2B(γε) forming a catalytic subcomplexes (CSC) at the exteriors of the decamer. Bottom: homology between subunits of RSC and CSC. High sequence homology of RSC subunits is highlighted in blue and unique N-terminal regions in grey. Conserved nucleotidyl-transferase (NT) domains and isoleucine-rich patches (I-patch) on CSC subunits are marked in green and red, respectively. Approximate numbering is given for human eIF2B subunits. Drawing by A. Zyryanova, University of Cambridge.

Regulatory α, β, and δ subunits of eIF2B are close sequence homologues that differ in their unique N-terminal regions (Figure 1.2.2). Their structures are characterized by alpha helical and C-terminal Rossmann-fold-like domains (Paddon et al. 1989; Hiyama et al. 2009; Kuhle et al. 2015). The three regulatory subunits of the hexameric core of eIF2B (PDB: 5B04) are shaping a central cavity that is observed from the top of the subcomplex and was predicted to bind eIF2α (Kashiwagi et al. 2016). eIF2B^{RSC} is structurally closely related to the homohexameric *Thermococcus kodakarensis* ribose 1,5-bisphosphate isomerase (tkRBPI, PDB: 3VM6), suggesting its origin from sugar phosphate regulated enzymes (Nakamura et al. 2012; Kuhle et al. 2015). Another resemblance of eIF2B^{RSC} to a yeast methylthioribose-1-phosphate isomerase (Ypr118w, PDB: 1W2W), that shares the C-terminal sequence similarity with ribose-5-phosphate isomerase (RpiA) (Bumann et al. 2004), proposes that precursor of eIF2B might have served a dual function coupling methionine concentration in the cell with translation initiation (Anantharaman and Aravind 2006).

Catalytic γ and ε subunits are less well conserved and their ancestry is not well defined, although they share some common domains between each other (Figure 1.2.2) and with NDP-sugar pyrophosphorylases (Koonin 1995). Both catalytic subunits contain a nucleotidyl-transferase (NT) domain and an isoleucine-rich repeating motif region (I-patch) that forms a β-helical barrel. Both domains play an important role in the interaction between eIF2Bγ and ε subunits as well as the rest of the complex (Koonin 1995; Wang et al. 2012). The key motifs important for the nucleotide exchange activity, such as NF motif (Asparagine-Phenylalanine) and HEAT (Huntington, Elongation Factor 3, PR65/A, TOR) domain, are both found at the distal faces of eIF2Bε (Boesen et al. 2004; Wei et al. 2010; Kashiwagi et al. 2016). The HEAT domain at the C-terminal part of eIF2Bε contains multiple helices (Boesen et al. 2004; Wei et al. 2010) and is probably highly flexible, therefore, not resolved in the *S. pombe* eIF2B structure (PDB: 5B04) (Kashiwagi et al. 2016). Within the eIF2Bε's C-terminal region there are two AA-boxes, rich in aromatic and acidic residues, that are important for protein-protein

interactions, and multiple alanine substitutions in which result in disruption of eIF2Bε binding to eIF2β (Asano et al. 1999).

1.3 Function and regulation of eIF2B

1.3.1 Guanine nucleotide exchange activity

The main function of eIF2B determined to this date is to catalyze GDP/ GTP exchange on eIF2, analogous to prokaryotic EF-Tu/ EF-Ts system (Kaziro 1978; Hwang and Miller 1985). In yeast and mammalian cells, eIF2B catalysis leads to an increase in the amounts of eIF2-GTP binary complex, which promotes formation of GTP-eIF2*Met-tRNA$_i^{Met}$ ternary complex (TC) (Konieczny and Safer 1983). Like many other GEFs, eIF2B initiates the GDP release by conformational changes in the nucleotide binding pocket of eIF2 and destabilization of Mg^{2+} ion (Mohammad-Qureshi et al. 2008; Maracci and Rodnina 2016).

The typical eIF2B catalyzed reaction is represented in the following equation:

eIF2-GDP + GTP + eIF2B <-> eIF2-GTP + GDP + eIF2B,

in which eIF2 forms a transient complex with eIF2B resulting in the decrease of the affinity of eIF2 for GDP (Salimans et al. 1984). A relatively unstable eIF2-GTP complex, however, is considered to be a reaction intermediate, and a more stable TC is an actual product of eIF2B catalysis (Salimans et al. 1984; Gross et al. 1991). A typical eIF2B's GEF activity assay monitors exchange of radioactively or fluorescently labeled GDP for unlabeled GDP, since the rate of eIF2-GDP release from eIF2B is about an order of magnitude faster than the rate of eIF2-GTP release (Siekierka et al. 1982; Dholakia and Wahba 1989). Some works show that addition of the Met-tRNA$_i^{Met}$ to the reaction accelerates GDP release from eIF2 in the presence of unlabeled GTP but not GDP (Gross et al. 1991). Moreover, recent report suggests that yeast eIF2B binds both *apo*- and nucleotide-bound eIF2 (GDP or GTP) with similar affinities (Jennings et al. 2017), suggesting that directionality of the nucleotide exchange reaction catalyzed by eIF2B may indeed depend on the

presence of Met-$tRNA_i^{Met}$, as well as the guanine nucleotide displacement inhibitor (GDI), eIF5 (Jennings and Pavitt 2010; Jennings et al. 2013).

The mechanism by which guanine exchange is encouraged is not clearly defined, and there is couple of theories discussed in the literature for and against either substitutional or sequential mechanisms. The substitutional (Ping-Pong or double displacement) mechanism implies dissociation of GDP upon formation of eIF2B*eIF2 complex (Manchester 1997). It was suggested as possible mainly due to similarities between relationships of eukaryotic eIF2/ eIF2B and prokaryotic EF-Tu/ EF-Ts (Kaziro 1978; Rowlands et al. 1988). However, if the displacement of nucleotide from EF-Tu*GDP by EF-Ts has been shown (Miller and Weissbach 1970; Hwang and Miller 1985), the release of GDP from eIF2 upon eIF2B binding was not confirmed (Goss et al. 1984; Dholakia and Wahba 1989; Gross et al. 1991; Oldfield and Proud 1992).

The sequential (ternary complex) mechanism involves assembly of a ternary complex between eIF2B*eIF2 and GDP/ GTP through a quaternary eIF2B*eIF2-GDP/ GTP intermediate (Manchester 1997). In favor of this mechanism are the findings that eIF2B cannot displace GDP from eIF2 without presence of GTP (Goss et al. 1984; Dholakia and Wahba 1989; Gross et al. 1991; Oldfield and Proud 1992), that GTP but not GDP is required for dissociation of eIF2 from eIF2B (Goss et al. 1984), and that GTP binds eIF2B irrespective of eIF2 (Dholakia and Wahba 1989). To date there is no clear resolution on the question of the exact mechanism, by which the guanine exchange happens on eIF2. However, altogether these studies provide a great deal to understanding of the kinetics of guanine exchange reaction.

The main knowledge of the interactions between eIF2 and eIF2B subunits comes from yeast genetics (Pavitt 2005). The eIF2Bγ and ε subunits identified as constituents of a catalytic subcomplex make interactions with eIF2 and possess a guanine exchange activity (Pavitt et al. 1998). The supporting biochemical studies showed that eIF2Bε possesses catalytic activity on its own, which is much reduced (~10 fold) compared to a fully assembled complex (Fabian et al. 1997; Pavitt et al. 1998; Gomez and Pavitt 2000;

Williams et al. 2001). The eIF2Bγ alone does not possess guanine exchange activity, however, it stabilizes interactions between eIF2 and eIF2Bε (Pavitt et al. 1998; Gomez and Pavitt 2000). The minimal requirement for the GEF function, suggested by some reports, is a small 23 kDa fragment of eIF2Bε's C-terminal region (eIF2Bε^{cat}) containing about 200 amino acids. eIF2Bε^{cat} was shown to have similar activity as the full length protein, but it no longer could interact with the rest of the complex implying importance of eIF2Bε's N-terminus for stabilizing those interactions (Gomez and Pavitt 2000; Gomez et al. 2002). Other studies, however, could not provide reasonable evidence that eIF2Bε^{cat} is sufficient for full GEF activity advocating significance of N-terminal domain of eIF2Bε for nucleotide exchange (Asano et al. 1999; Anthony et al. 2000). C-terminal domain of eIF2Bε was also shown to be important for making contacts with eIF2β and eIF2γ, presumably stimulating binding of its catalytic region (Asano et al. 1999; Anthony et al. 2000; Mohammad-Qureshi et al. 2007). Three surface residues on eIF2Bε^{cat} (L568, E569, W699) were identified as critical for establishing interactions between eIF2β and eIF2γ, and for stimulating GEF activity *in vivo*. Single mutation of either E569 or W699 to alanine (E569A or W699A) cause a severe lethal phenotype in cells depleted of wt eIF2Bε, and E569A was also shown to be catalytically inactive *in vitro* (Boesen et al. 2004; Mohammad-Qureshi et al. 2007).

The yeast eIF2Bα subunit, encoded by *GCN3* gene, is the only non-essential gene amongst all the five subunits of eIF2B. The yeast eIF2Bα is also considered dispensable for eIF2B's GEF activity, but was demonstrated to play a critical role in sensing phosphorylation status of eIF2α (Hannig and Hinnebusch 1988; Dever et al. 1993; Bushman et al. 1993; Yang and Hinnebusch 1996). Research on mammalian eIF2B complex, however, suggested that GEF activity could only be observed when all five subunits of eIF2B are present. It was, therefore, proposed that the mammalian eIF2Bα plays an important role in guanine exchange catalysis and a possible reason for that is failure of eIF2B(βγδε) tetramer to establish contacts with eIF2 in mammalian cells (Craddock and Proud 1996). This potential species divergence is consistent with another piece of evidence suggesting that higher phosphorylation levels of eIF2 are required for inhibition of eIF2B's activity in

yeast (Dever et al. 1992). Such finding may be reflective of the differences in eIF2:eIF2B ratio between yeast and mammalian cells, where in the latter it may be higher. Or it could be indeed that yeast eIF2B(βγδε) tetramers are more potent than mammalian eIF2B(βγδε) tetramers. Moreover, the more potent yeast eIF2B(βγδε) tetramers may in fact be eIF2B$(\beta\gamma\delta\varepsilon)_2$ octamers that do not require bridging with eIF2Bα, and the existence of which was suggested by MS analysis of yeast eIF2B species (Gordiyenko et al. 2014).

1.3.2 Regulation of eIF2B by eIF2α phosphorylation

One of the strongest and shown to be physiologically most significant regulations of eIF2B's GEF activity is through phosphorylation of the α subunit of its substrate, eIF2, stimulated by diverse stressful events (Proud 2005; Sonenberg and Hinnebusch 2009; Dever et al. 2016). A suggested possible mechanism through which eIF2(αP) could inhibit its GEF is by sequestering eIF2B into an inactive complex. eIF2B is much less abundant (five-ten times less depending on the tissue) than eIF2 (Safer et al. 1982; Konieczny and Safer 1983; Oldfield et al. 1994), and phosphorylation affects about 25-30% of the total eIF2 (Safer and Jagus 1981; Leroux and London 1982). It is, therefore, feasible to assume that despite the major fraction of eIF2 remaining non-phosphorylated the formation of TC is stalled due to all active eIF2B engaging in non-productive interactions with eIF2(αP) (Leroux and London 1982; Konieczny and Safer 1983). Furthermore, some experiments showed that eIF2(αP) forms a more stable complex with eIF2B than non-phosphorylated eIF2 in the presence of nucleotides (Safer et al. 1982; Matts et al. 1983; Salimans et al. 1984). The mechanism by which eIF2(αP) sequesters eIF2B forming a non-productive complex, however, might not be due to simply tighter interactions between the two, as high enough levels of GTP (> 0.1 mM) may replace both eIF2B and GDP regardless of eIF2α phosphorylation status (Konieczny and Safer 1983; Goss et al. 1984). It was also shown by some that eIF2(αP) does not readily exchange eIF2 in a complex with eIF2B (Siekierka et al. 1984), and that eIF2(αP)*eIF2B complex itself dissociates quite rapidly (Rowlands et al. 1988). Under the light of all these studies, eIF2(αP) appears to be a competitive rather than an

irreversible inhibitor of eIF2B, that has an increased affinity (150-fold) and decreased Kd (10-fold) for eIF2B compared to eIF2 (Goss et al. 1984; Rowlands, Panniers et al. 1988; Price and Proud 1994). It then also follows that the higher the ratio between eIF2 and eIF2B the more sensitive the system to phosphorylation levels of eIF2α (Price and Proud 1994; Oldfield et al. 1994).

The critical eIF2α phosphorylation site is mapped on its N-terminal region, where serine 51 (S51) was determined to be a target for eIF2α kinases (Colthurst et al. 1987; Kaufman et al. 1989; Choi et al. 1992). It is also known that mutation of S51, as well as S48, on eIF2α to alanine can reduce inhibition of eIF2B's GEF activity upon induction of eIF2α kinases (Kaufman et al. 1989; Choi et al. 1992; Murtha-Riel et al. 1993; Ramaiah et al. 1994). The proposed mechanism suggests that phosphorylation of S51 directly impairs eIF2B's activity, while S48 residue is important for maintaining interactions between phosphorylated eIF2(αP) and eIF2B (Ramaiah et al. 1994; Sudhakar et al. 1999). Mutation of S51 to aspartic acid (S51D) mimics phosphorylation modification and promotes formation of higher affinity complex between eIF2(α^{S51D}) and eIF2B resulting in reduced translation (Kaufman et al. 1989; Sudhakar et al. 2000). Reciprocal mutation of S48 (S48D), however, does not result in altered phosphorylation pattern of eIF2 nor does it affect protein synthesis (Kaufman et al. 1989). Altogether these findings suggest that S48 residue does not contribute to eIF2α phosphorylation-dependent inhibition of eIF2B's GEF activity directly, but may rather contribute to its inhibition in an indirect way.

The eIF2B subunits that participate in sensing the phosphorylation state of eIF2α were mainly identified through yeast genetics (Pavitt 2005). Multiple gcn^- mutations identified on the eIF2Bα, β and δ subunits are able to reduce sensitivity of eIF2B towards eIF2(αP) (Vazquez de Aldana and Hinnebusch 1994; Pavitt et al. 1997; Pavitt et al. 1998; Krishnamoorthy et al. 2001; Dev et al. 2010). When mapped onto the structure, these mutations localize either on the solvent exposed area or at the interface between the subunits of $eIF2B^{RSC}$. This arrangement is probably indicative of the role of these

residues in lowering the affinity of eIF2(αP) towards eIF2B or stabilizing eIF2B in some other way favorable for catalysis (Bogorad et al. 2014; Kashiwagi et al. 2016). In contrast, the gcd$^-$ mutations identified on the same subunits that evoke constant inhibition of eIF2B activity localize more on the buried surfaces. The position of the inhibitory gcd$^-$ mutations is more likely to be in agreement with either lowered GEF activity of eIF2B or altered integrity of the eIF2B complex, rather than with changes in the affinity of eIF2B towards eIF2/ eIF2(αP) (Dev et al. 2010; Bogorad et al. 2014). The importance of eIF2Bα, β and δ subunits for sensing eIF2(αP) is substantiated by over-expression experiments revealing formation of eIF2B^{RSC} that does not possess guanine exchange activity, but is able to rescue cells from the inhibitory effect of eIF2(αP), which is sequestered by eIF2B^{RSC} into a higher affinity complex (Yang and Hinnebusch 1996; Pavitt et al. 1998).

The topic of regulation of eIF2B's GEF activity by eIF2(αP) is one of the most discussed in eIF2B field. The molecular basis of such regulation remains yet to be determined. Some hypothesis suggests the engagement of the eIF2α at a cavity formed by the convergence of the α, β and δ regulatory subunits of the eIF2B decamer. This cavity is distant from the catalytic (γε) subcomplex of eIF2B that engage the nucleotide binding γ subunit of eIF2. Engagement of eIF2αP into the eIF2B^{RSC} cavity might propagate some allosteric changes reaching eIF2B^{CSC} and making productive interactions between non-phosphorylated eIF2 and eIF2B less favourable (Bogorad et al. 2014; Kuhle et al. 2015; Kashiwagi et al. 2016; Kashiwagi et al. 2017; Bogorad et al. 2017).

eIF2B is a dimer possessing two regulatory and two catalytic sites. The current literature does not provide clear evidence on whether eIF2B is able to engage one or two molecules of eIF2/ eIF2(αP) at the same time. Without a full structural data on the complexes forming between eIF2B and eIF2/ eIF2(αP) this question and many others will possibly remain unanswered.

1.3.3 Other regulators of eIF2B

The GEF activity of eIF2B may be subject to regulation not only by phosphorylated eIF2α, but also by allosteric effectors and other covalent

modifications (Price and Proud 1994) reflecting its lineage from metabolic-regulated enzymes (Koonin 1995; Kuhle et al. 2015).

The ε subunit of eIF2B, for example, has multiple phosphorylation sites that are targeted by various kinases altering eIF2B's GEF activity independent of eIF2α phosphorylation. Phosphorylation of eIF2Bε by casein kinases I and II (CK I and CK II) results in increased amount of GTP bound to eIF2B, and in enhancement of its GEF activity (Dholakia and Wahba 1988; Oldfield and Proud 1992; Aroor et al. 1994; Singh et al. 1994; Singh et al. 1996). Glycogen synthase kinase-3β (GSK-3β) is also able to phosphorylate eIF2Bε inhibiting its activity, while insulin inactivates GSK-3β and stimulates eIF2B's GEF activity (Welsh and Proud 1992; Welsh and Proud 1993; Welsh et al. 1998; Wang et al. 2001; Pap and Cooper 2002). Two isoforms of dual-specificity tyrosine phosphorylated and regulated kinase (DYRK2 and DYRK1A) phosphorylate S539 on eIF2Bε permitting phosphorylation of its S535 by GSK-3β (Woods et al. 2001; Wang et al. 2001). The former event is also connected to the control of programmed cell death where inactivation of GSK-3β prevents apoptosis (Pap and Cooper 2002). Another eIF2Bε phosphorylation site on S525 was even shown to directly influence sensitivity of human eIF2B to amino acids availability regardless of eIF2α phosphorylation (Wang and Proud 2008). All these studies indicate the existence of a regulatory phosphorylation site on eIF2Bε, which lies N-terminally from the known C-terminal catalytic domain and possibly is important for establishing contacts with eIF2.

eIF2B's GEF activity can also be stimulated by sugar phosphates (Gross et al. 1988) and by polyamines, like spermine and spermidine (Gross and Rubino 1989; Oldfield and Proud 1992). In contrast, heparin (Singh et al. 1995), NAD^+, $NADP^+$ and ATP (Dholakia et al. 1986; Dholakia and Wahba 1988; Kimball and Jefferson 1995) can inhibit eIF2B's GEF activity, where spermidine and NADPH can reverse this inhibitory effect. Yeast eIF2B and its γ subunit is a subject of regulation by fusel alcohols, such as butanol, a by-product of yeast fermentation process, that inhibit eIF2B's GEF activity (Ashe et al. 2001).

Considering size and complexity of eIF2B complex, and its pivotal role in regulation of global protein synthesis in cells, it is not unreasonable to hypothesize that some of the aforementioned regulatory mechanisms might be more relevant to certain cell types or in yet undiscovered circumstances. Identification of the novel pathways regulating eIF2B's GEF activity independent of the well known ISR and GAAC, thus, should be of a big interest.

1.3.4 eIF2B related diseases

Multiple missense mutations found across all five subunits of eIF2B were linked to an inherited tissue-specific human brain disease called leukoencephalopathy with vanishing white matter (VWM), or childhood ataxia with central nervous system hypomyelination (CACH) (Leegwater et al. 2001; Van Der Knaap et al. 2002). There are a few inherited genetic diseases associated with translational pathway. VWM disease, however, is the only one linked to mutations in a single translation initiator factor, probably due to many of such genes being essential, and severe mutants being not viable (Scheper et al. 2007).

The VMW disease is recessive mainly affecting glial cells, astrocytes and oligodendrocytes, with a typical onset in late infancy or early childhood and fatal outcome (Leegwater et al. 2001; Pavitt 2005; Dietrich et al. 2005), and a few cases reported in adults (Labauge et al. 2009; Matsukawa et al. 2011). The onset usually correlates with a head trauma or viral infection indicating lowered tolerance to stress of mutated tissues and enfeebled recovery capacity.

Majority of mutation associated with VWM are found on *EIF2B5* gene encoding a catalytic eIF2Bε subunit. The least number of VWM mutations are within *EIF2B1* gene encoding a regulatory eIF2Bα subunit that in yeast was shown to be non-essential and dispensable for eIF2B's GEF activity (Pronk et al. 2006; Pavitt and Proud 2009), but in mammals is important for stimulating GEF activity and dimerization of eIF2B pentamer (Craddock and Proud 1996; Wortham et al. 2014). The VWM mutations were shown to affect eIF2B in

different ways, for example, by reducing formation of the full complex or by disrupting connections with eIF2 (Richardson et al. 2004; Li et al. 2004; Fogli et al. 2004; Pavitt 2005). Many of the VMW mutations that are responsible for the loss of the complex integrity go in hand with the decrease in GEF activity (20-70% compared to control) (Richardson et al. 2004; Fogli et al. 2004; Schiffmann and Elroy-Stein 2006). The loss of the complex integrity and the reduction in GEF activity, however, is not necessarily a characteristic of a mutated eIF2B. Some reports suggest that certain VMW mutations inflict rise in GEF activity proposing loss of an alternative eIF2B function (Liu et al. 2011; Wortham and Proud 2015).

Cells bearing VMW mutations exhibit increased ISR and UPR signaling upon activation of stress judging by the heightened phosphorylation levels of eIF2α, and by the increased translation of ATF4 and expression of pro-apoptotic *CHOP* gene (Li et al. 2004; Kantor et al. 2005; van der Voorn et al. 2005; Scheper et al. 2006; Schiffmann and Elroy-Stein 2006; Sekine et al. 2016). Despite that certain mutations cause lowered eIF2B's GEF activity, it does not correlate with measurable effects on global protein synthesis rate, nor does it affect cell survival under normal circumstances (Kantor et al. 2005; Van Kollenburg et al. 2006). However, the first mouse model of CACH, bearing a mild VWM mutation on eIF2Bε subunit (*EIF2B5R*^{136H} in human or *Eif2b5*^{R132H} in mouse) and associated with just 20% reduction in GEF activity of mutated eIF2B, revealed delays in development of brain white matter, as well as abnormally high levels of myelin protein and increased abundance of oligodendrocytes and astrocytes (Geva et al. 2010). Another two CACH mouse models with severe mutations in eIF2Bε, *Eif2b5*^{R191H}, and eIF2Bδ subunit, *Eif2b4*^{R484W} (corresponding to *EIF2B5*^{R195H} and *EIF2B4*^{R483W} in human, respectively), also showed abnormalities in development of oligodendrocytes and astrocytes suggesting the potential therapeutic target (Dooves et al. 2016). In the light of these facts, the sensitivity of glia to stress in VMW could be explained by the importance of the ER homeostasis in oligodendrocytes producing large amounts of myelin, and by the general sensitivity of astrocytes to apoptosis (Scheper et al. 2007).

Since major bulk of studies on VWM mutations come from yeast or mammalian epithelial cells demonstrating their diverse effect on eIF2B's GEF activity, more studies need to be conducted in specialized tissue types to confirm validity of those findings. Further assessment of animal CACH models revealing genomic and proteomic profiles of the affected tissues together with system biology approaches can facilitate understanding of the disease pathology and designing of appropriate screening techniques and treatments for real-life patients (Marom et al. 2011; Gat-Viks et al. 2015).

1.4 ISR modulators

Phosphorylation of eIF2α and the ISR have important homeostatic functions. Impairment of the ISR is linked to a number of human pathologies, including inflammation, diabetes, neurodegeneration, and cancer. Whilst in some circumstances the ISR provides protective function increasing cellular fitness, in others, a benefit arises from attenuation in the ISR signalling (Ye et al. 2010; Chen et al. 2011; Pakos-Zebrucka et al. 2016). The ongoing search for modulators of the ISR that can shift the balance in either way is, thus, of great interest.

The enhanced ISR was shown to be beneficial in diseases associated with protein misfolding, like amyotrophic lateral sclerosis, where reduction of GADD34*PP1 (protein phosphatase 1) activity, the ISR-induced eIF2α phosphatase complex, helped to delay the disease onset and prolonged survival of model animals (Wang et al. 2014). Over more than a decade efforts of many people were concentrated on search for a specific and selective inhibitors of eIF2α phosphatase. Amongst the discovered drugs are Salubrinal, Guanabenz, and Sephin 1 that were all shown to target the regulatory GADD34 subunit of the eIF2α phosphatase complex (Boyce et al. 2005; Tsaytler et al. 2011; Das et al. 2015). Moreover, Sephin 1 was even shown to supress the development of neurodegenerative protein-misfolding diseases in mice (Das et al. 2015). However, the exact molecular mechanisms of these known "phosphatase inhibitors" were recently

questioned, suggesting that they might activate an alternative pathway (Crespillo-Casado et al. 2017, Crespillo-Casado et al. 2018).

On the other side, a substantial body of research centred on the repression of the ISR is focused on searching for compounds that inhibit eIF2α kinases (Pakos-Zebrucka et al. 2016). The findings in this field include discovery of GSK compounds, selective and potent inhibitors of the PERK kinase (IC_{50} 0.4 nM), that can suppress tumor growth in vivo (Axten et al. 2012; Axten et al. 2013) and can even contribute to neuroprotection in mice models of prion disease (Moreno et al. 2013). Activity of GSK compounds, however, was also shown to interfere with normal insulin production in vitro (Harding et al. 2012), and was linked to weight loss and hyperglycemia in mice (Moreno et al. 2013), altogether suggesting serious potential side effects resulting in pancreatic insufficiency. Such effects of GSK compounds are not surprising since PERK is an ubiquitously expressed kinase, and $PERK^{-/-}$ knockout mice experience rapid and progressive decline in endocrine and exocrine pancreatic function leading to development of diabetes (Harding et al. 2001).

The toxicity caused by complete repression of the ISR with GSK once again point at the importance of tissue-specific regulation of the ISR. This notion implies a need for a different approach in a search for “fine-tuners” of the ISR focusing on its down-stream effectors instead of targeting upstream eIF2α kinases. Pursuit of such compounds resulted in the discovery of a novel ISR inhibitor, ISRIB (Sidrauski et al. 2013).

ISRIB is a partial and reversible inhibitor of the ISR. Its effect is observed despite persistent elevated levels of eIF2α phosphorylation indicating that ISRIB’s site of action lies downstream of the stress-induced kinases phosphorylating eIF2α (Sidrauski et al. 2013). ISRIB has proven efficacious in certain mouse models of neurodegeneration (Halliday et al. 2015) and traumatic brain injury (Chou et al. 2017), in normal rats as a memory-enhancing drug (Sidrauski et al. 2013), and even in pancreatic ductal adenocarcinoma improving its chemosensitivity to gemcitabine (Palam et al. 2015). Moreover, the reported therapeutic effects of ISRIB showed no

adverse effects on pancreatic function. All these findings, unsurprisingly, led to an increased interest in ISRIB's mechanism of action, especially since its target was proposed to be the ever more captivating eIF2B.

1.5 Goal of the study and experimental approach

During the course of my PhD project I applied biochemical, biophysical, structural and chemogenetic methods to identify the target of ISRIB and to provide insight into ISRIB's mode of action. I also attempted to shed light onto regulation of eIF2B's GEF activity and its importance for the ISR. The original work described in this Thesis follows the steps that I undertook in collaboration with my co-workers in pursuit of the main goal of the project.

The important techniques used for this study include, but are not limited to:

1) Flow cytometry and fluorescence activated cell sorting (FACS) – a laser-based biophysical method that allows counting, sorting and collection of cells, for example, based on the level of the activated fluorescent cell reporter that they bear;
2) Cryo-electron microscopy (cryo-EM) and single particle analysis (SPA) – a technique for structural analysis of biological macro-molecules that combines electron microscopy conducted under cryogenic conditions, with the help of which the information about a specimen frozen in time and space is gathered through analysis of micrographs containing 2D views of the biological material; and a computational method that processes the cryo-EM micrographs identifying individual 2D-representation of the studied biological material, and performing a 3D reconstruction of a full-size molecule;
3) CRISPR/ Cas9 (Clustered Regularly Interspaced Short Palindromic Repeats/ CRISPR associated protein 9) – a genomic DNA modification technique that is used to alter the genome of mammalian cells.

Chapter 2: Results

2.1 Identification of a molecular target of the integrated stress response inhibitor (ISRIB)

2.1.1 ISRIB and its active analogues inhibit the ISR in mammalian cells

The original method used to identify the first ISRIB compound (Sidrauski et al. 2013) suggested that ISRIB action could be tracked by its effects on the activity of a stably-integrated ISR-responsive reporter genes in live mammalian cells. We utilized a similar system that relied on the activation of a *CHOP* gene under endogenous promoter fused to GFP protein in hamster CHO-C30 cells (Novoa et al. 2001) to monitor ISRIB activity. Treatment of these cells with L-histidinol (HIS), a precursor of L-histidine, that inhibits binding of L-histidine to histidyl-tRNA synthetase, leading to increase in the amount of uncharged histidyl-tRNAs and consequent activation of GCN2 kinase that phosphorylates α subunit of eIF2. eIF2(αP) inhibits the eIF2B's GEF activity, initiating the ISR and culminating in *CHOP::GFP* activation, which is detected by flow cytometry method (Figure 2.1.1a – "WT cells").

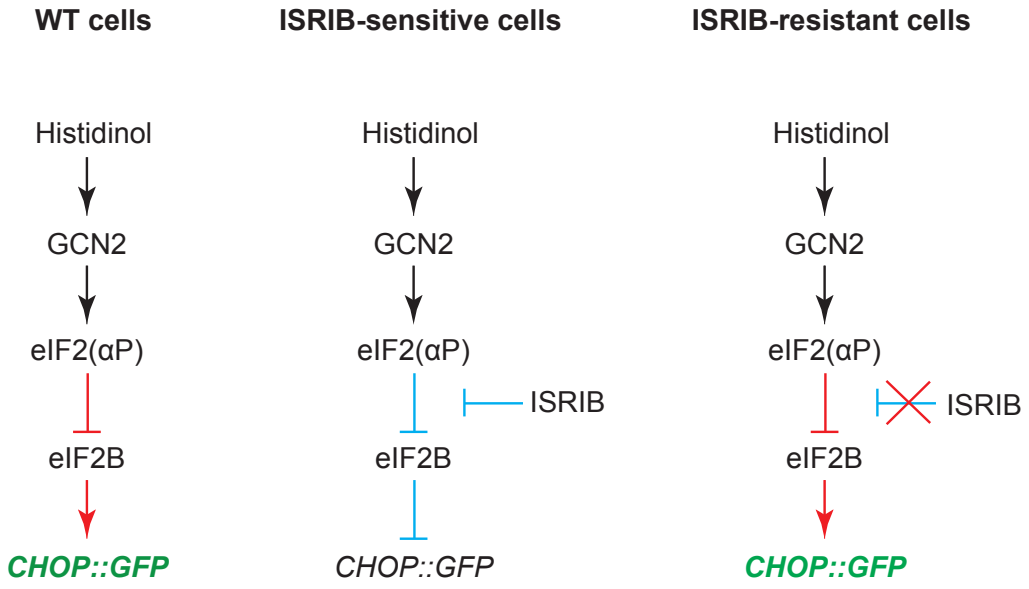

Figure 2.1.1a: Tracking the ISR activation in fluorescent reporter cell-lines.

Shown is a schema of the ISR activation by histidinol (HIS) in CHO-C30 cells bearing *CHOP::GFP* reporter. Note the effect downstream of phosphorylated eIF2α in three different cases: 1) in wild-type, parental, cells treated with HIS *CHOP::GFP* is activated (green highlight); 2) in ISRIB-sensitive cells treated with HIS and ISRIB *CHOP::GFP* is inhibited; 3) in ISRIB-resistant cells treated with HIS and ISRIB *CHOP::GFP* is activated (green highlight). Figure was draw by A. Zyryanova, University of Cambridge.

In ISRIB-sensitive ($ISRIB^{SEN}$) HIS-stressed cells, the presence of ISRIB attenuated the response of the *CHOP::GFP* reporter (Figure 2.1.1a, and figure 2.1.1b left panel - note divergence of continuous red, HIS^+, and discontinuous green, HIS^+ISRIB^+, traces). We used HIS instead of other common drugs utilized for activation of the ISR (like thapsigargin and tunicamycin), because the complete attenuation of CHOP::GFP signal by ISRIB was only observed in HIS-treated CHO-C30 cells. In thapsigargin- or tunicamycin-treated cells, CHOP::GFP signal was only partially reversed by ISRIB (Sekine et al. 2015). This possibly indicates that HIS triggers the ISR-specific branch of eIF2α phosphorylation pathway (GCN2), and that it does not stimulate other stress response pathways, like unfolded protein response (UPR) that activates PERK.

Screening of CHO-C30 cells for chemically induced somatic mutations that reversed ISRIB's effect on ISR led to the discovery of the ISRIB-resistant ($ISRIB^{RES}$) clones (Sekine et al. 2015), in which *CHOP::GFP* reporter remained active under HIS treatment despite ISRIB's presence (Figure 2.1.1a, and figure 2.1.1b right panel – note convergence of continuous red, HIS^+, and discontinuous green, HIS^+ISRIB^+, traces). Identified amino acid substitutions in $ISRIB^{RES}$ cells all clustered at the unique N-terminal portion of eIF2Bδ (Figure 2.1.1c) (Sekine et al. 2015). Targeted CRISPR/ Cas9 mutagenesis of that region on eIF2Bδ in parental cells confirmed the finding, and led us to suggest that a cellular target of ISRIB is eIF2B.

At the time, the reported crystal structure of *C. thermophilum* $eIF2B(\beta\delta)_2$ tetramer (Kuhle et al. 2015) suggested that together with $eIF2B\alpha_2$ (Hiyama et al. 2009) it forms a regulatory subcomplex ($eIF2B^{RSC}$) shaping the core of the eIF2B decamer. ISRIB-resistant mutations identified on eIF2Bδ in our screen (Figure 2.1.1c), and plotted on the model of $eIF2B\alpha_2(\beta\delta)_2$ hexamer revealed their clustering at the dimeric $(\beta\delta)_2$ interface next to the core cavity that spatially seemed to allow accommodation of a symmetrical *trans*-ISRIB molecule (Figure 2.1.1d, e).

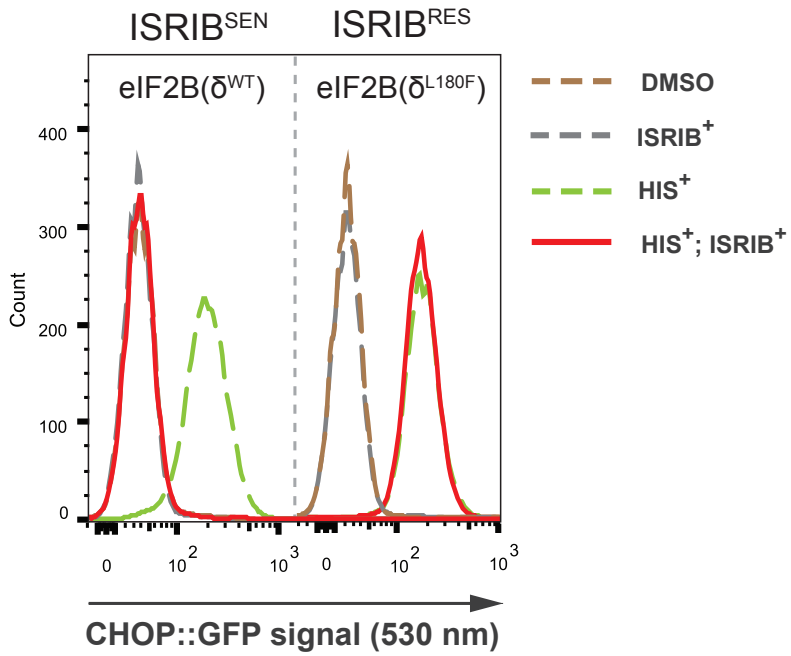

Figure 2.1.1b: ISR activation in ISRIB-sensitive and ISRIB-resistant cell lines.

Shown are histograms of *CHOP::GFP* activity in ISRIB-sensitive (ISRIB^{SEN}, δ^{wt}, clone S7) and ISRIB-resistant (ISRIB^{RES}, δ^{L180F}, clone S9) (Sekine et al. 2015) CHO-C30 cells revealed by flow cytometry. Each pool was treated for 20 hours as indicated with histidinol (HIS, 0.5 mM), ISRIB (200 nM) or both. Note the difference between wildtype and δ^{L180F} in their ability to inhibit the ISR-activated CHOP::GFP signal when treated with ISRIB (compare continuous red trace, His^{+}ISRIB^{+}, on the left and right panels). Clone S7 was used for CRISPR/ Cas9 mutagenesis (Section 2.3) and in fluorescence polarization experiments (Section 2.1.7). Clone S9 was used in fluorescence polarization experiments (Section 2.1.7). Shown is a representative experiment repeated more than three times. Cell culturing, treatments and flow cytometry done by A. Zyryanova, University of Cambridge.

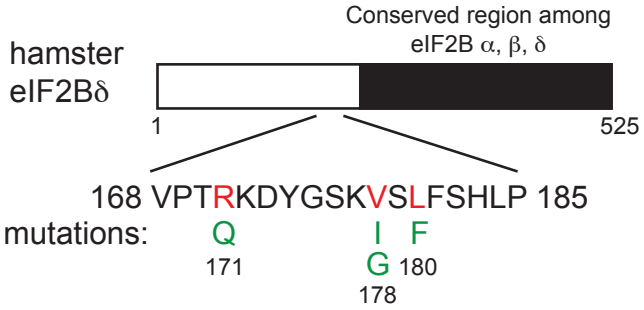

Figure 2.1.1c: ISRIB-resistant mutations.

Shown is a schema of the hamster eIF2B δ subunit with the indicated positions of the mutations associated with the ISRIB^{RES} phenotype. Note that mutations are clustered at the unique N-terminal region of eIF2Bδ not conserved in the other regulatory subunits (α, β) of eIF2B (Sekine et al. 2015). Figure was drawn by Y. Sekine, University of Cambridge.

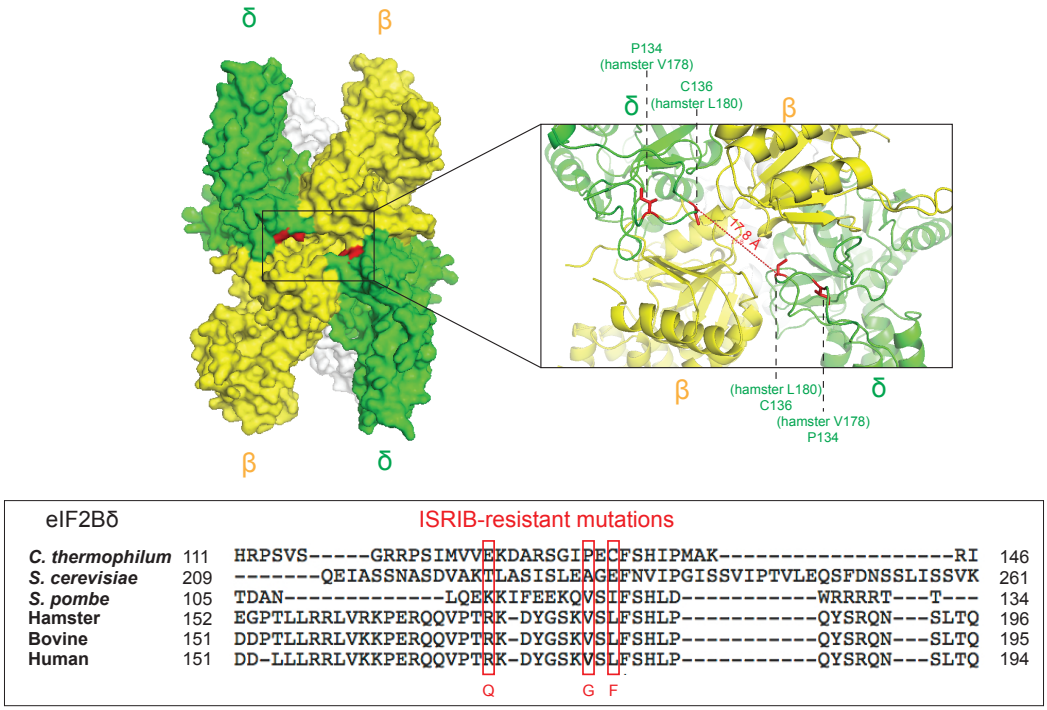

Figure 2.1.1d: Dimer interface of the regulatory eIF2B subcomplex.

Top: surface representation of a model of regulatory eIF2Bα$_2$(βδ)$_2$ hexameric subcomplex (eIF2B^{RSC}) from crystal structures of *Chaetomium thermophilum* (βδ)$_2$ tetramer (PDB: 5DBO) and human α$_2$ dimer (PDB: 3ECS), where α is in light grey, β in yellow, and δ in green. Marked on the surface in red are two ISRIB^{RES} mutations (δV178 and δL180 - in hamster; P134 and C136 – in *C. thermophilum*) identified on the δ subunit of hamster eIF2B (in green) revealing their position at the core of the eIF2B^{RSC} between the symmetrical (βδ)$_2$ dimer interface. Note the distance between the symmetrical residues (17.8 Å), which is roughly corresponding to the size of a symmetrical *trans*-ISRIB molecule (23 Å). Bottom: eIF2Bδ protein sequences alignment between lower and higher eukaryotes with highlighted ISRIB-resistant mutations identified in hamster (δR171Q, δV178G, δL180F). Note the conservation of the highlighted residues between mammalian species but not yeast species. Structure was modified using PyMOL (by Schrödinger) to highlight the ISRIB resistant residues and calculate the distance, done by A. Zyryanova. Alignment was done using UniProt website by A. Zyryanova, University of Cambridge.

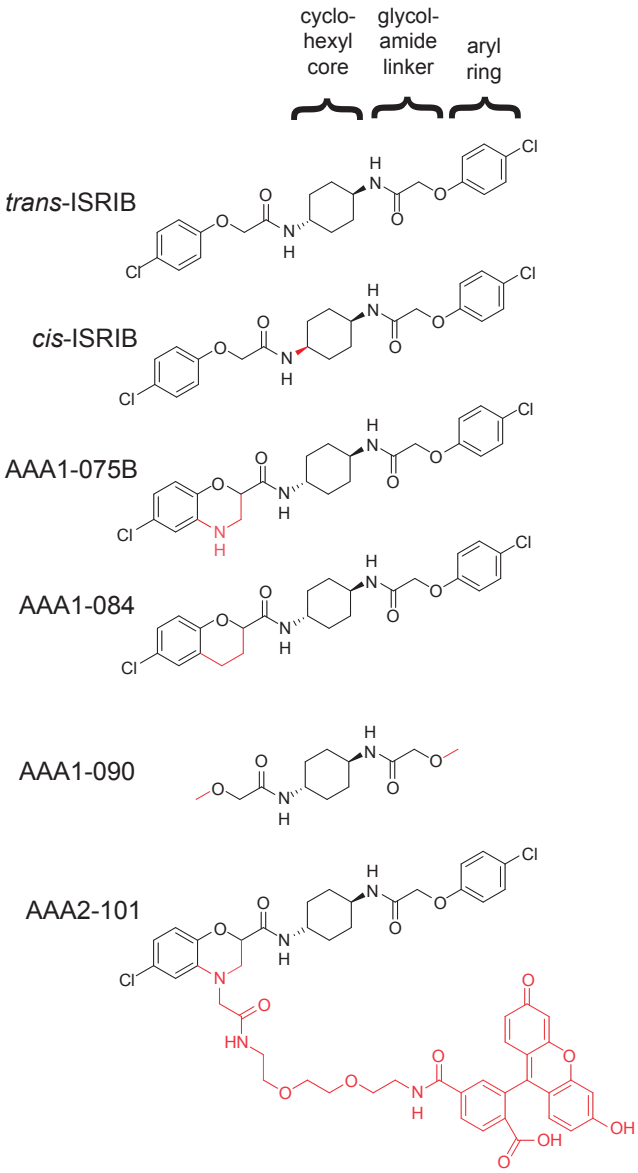

Figure 2.1.1e: ISRIB compounds.

Shown are structures of ISRIB and ISRIB analogues used in this study. Active analogues: *trans*-ISRIB, *cis*-ISRIB, AAA1-075B, and AAA1-084 (used in ISRIB cellular activity experiments and FACSorting analysis in Section 2.1.1 and section 2.3.2); inactive analogue: AAA1-090 (used in ISRIB cellular activity experiments in Section 2.1.1); fluorescein-labeled analogue: AAA2-101 (used in fluorescence polarization experiments to measure direct binding to eIF2B in Section 2.1.7 and Section 2.3.3). Compounds design and synthesis was executed by A. A. Alard, C. Fromont and P. M. Fischer, University of Nottingham.

ISRIB is a potent molecule with an IC_{50} reported to be around 5 nM in cells (Sidrauski et al. 2013). Despite its potential in treating brain-associated illnesses (Halliday et al. 2015; Chou et al. 2017), its solubility limit of only 5 mM in 100% DMSO raised concerns of whether it could be safely and easily delivered to human brain cells. Attempts to search for a better soluble and a more potent compound resulted in better understanding of structure-activity relationships of ISRIB analogues (Hearn et al. 2016). In collaboration with Peter Fischer's group from the University of Nottingham, we too were successful in learning that major modifications of the central *trans*-cyclohexyl group and the glycolamide linkages are poorly tolerated, while changes to the terminal aryl groups in some cases maintained or even enhanced activity (Figure 2.1.1e partial results are shown; note the structural divergence of analogues from the original *trans*-ISRIB molecule highlighted in red). In this manuscript, I present two active (AAA1-075B and AAA1-084) and one inactive (AAA1-090) ISRIB analogues, activities of which were evaluated by the ISR inhibition assay (Figure 2.1.1a). Using this assay, CHOP::GFP signal was measured across the various concentrations of ISRIB and its analogues to estimate their EC_{50} (Figure 2.1.1f). Tethering of the glycolamide C^{α} of one of the cyclohexyl substituents to the neighboring phenyl in the form of a chromane group (AAA1-084, Figure 2.1.1e) retained activity, and the new AAA1-084 compound was only 8.5-fold less active than *trans*-ISRIB in cells (Figure 2.1.1f). Replacement of the chromane with the dihydro-benzoxazine system afforded a compound AAA1-075B (Figure 2.1.1e) only 3-fold less active than *trans*-ISRIB in cells (Figure 2.1.1f). The aniline function in AAA1-075B compound was then used to elaborate the first fluorescently labeled ISRIB analogue, which contains a flexible linker terminating in a 6-carboxyfluorescein moiety (AAA2-101, Figure 2.1.1e). This labeled ISRIB analogue was later used in fluorescence polarization experiments to study direct binding of ISRIB to purified eIF2B (Section 2.1.7 and Section 2.3.3).

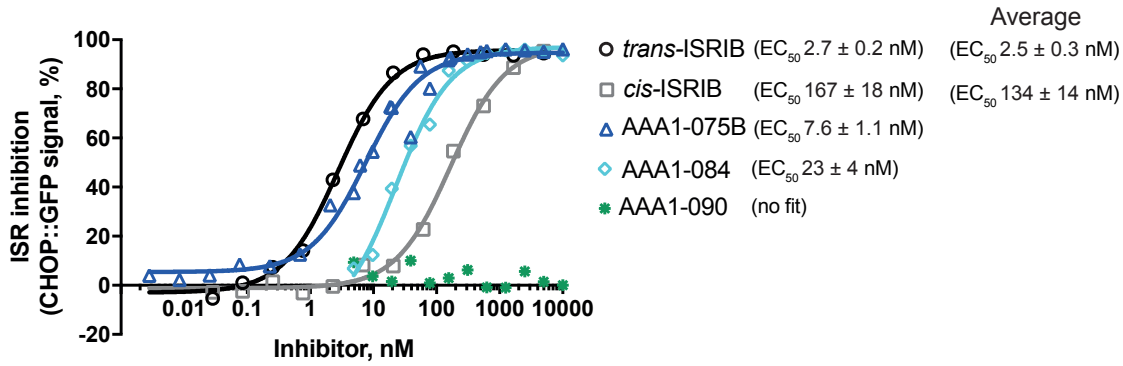

Figure 2.1.1f: The ISR inhibition assay.

Shown is a plot of inhibition of the ISR-activated CHOP::GFP signal induced upon treatment of CHO-C30 cells with 0.5 mM HIS in the presence of escalating concentrations of either ISRIB or its analogues. Displayed is a representative of two independent experiments conducted for *trans* and *cis*-ISRIB, and of single experiment conducted for analogues. Indicated are EC_{50} ± SD for the experiment and mean EC_{50} ± SD for n=2, where applicable. Concentration of ISR inhibitor is represented on a $\log_{10}$ scale. Curves fitting, EC_{50}, and SD was generated using agonist vs. response function on GraphPad Prism. *Trans* and *cis*-ISRIB were tested by A. Crespillo-Casado, University of Cambridge. Compounds AAA1-075B, AAA1-084, and AAA1-090 were tested by A. Zyryanova, University of Cambridge.

2.1.2 Effect of ISRIB on eIF2/ eIF2(αP) association with eIF2B in mammalian cells

One of the hypothesis suggests that the ISR halts protein synthesis by a mechanism of sequestration of the active eIF2B into inactive complex with eIF2(αP) (Leroux and London 1982; Konieczny and Safer 1983). Since the evidence says that ISRIB reverses this impediment to protein synthesis without altering phosphorylation levels of eIF2α (Sidrauski et al. 2013), we aimed to test whether ISRIB could have an effect on the formation of the catalytic and regulatory interactions between eIF2B and eIF2/ eIF2(αP) in live cells.

To conduct such experiments, we used CHO cells bearing constitutively expressed cytosolic version of the eIF2α PERK kinase (Fv2E-PERK) that has its luminal and transmembrane domains substituted for a ligand-activatable Fv2E moiety. Addition of the AP20187 drug promotes dimerization of the cytosolic Fv2E-PERK stimulating recombinant PERK's kinase activity and phosphorylation of eIF2α independently of the ISR pathway (Lu et al. 2004). On top of that, we introduced a constitutively expressed recombinant C-terminally 3xFlag-tagged wild-type human eIF2α. We hoped recombinant eIF2α would associate with endogenous hamster eIF2 β and γ subunits, forming eIF2 heterotrimer that could interact with endogenous hamster eIF2B complex. We could regulate the association of eIF2B with eIF2 during purification procedure by increasing salt concentration promoting eIF2B complex dissociation and yielding a fairly pure eIF2 complex (Figure 2.1.2a compare left and right gels). Analytical centrifugation revealed that a mixture of proteins purified under low salt conditions (Figure 2.1.2a right panel) consisted of free recombinant 3xFlag-tagged human eIF2α, hamster eIF2(hu_α-3xFLAG) heterotrimer, and hamster eIF2B*eIF2(hu_α-3xFLAG) complexes (Figure 2.1.2b, left and right panels), which validated our system to be suitable for studying interactions between eIF2 and eIF2B.

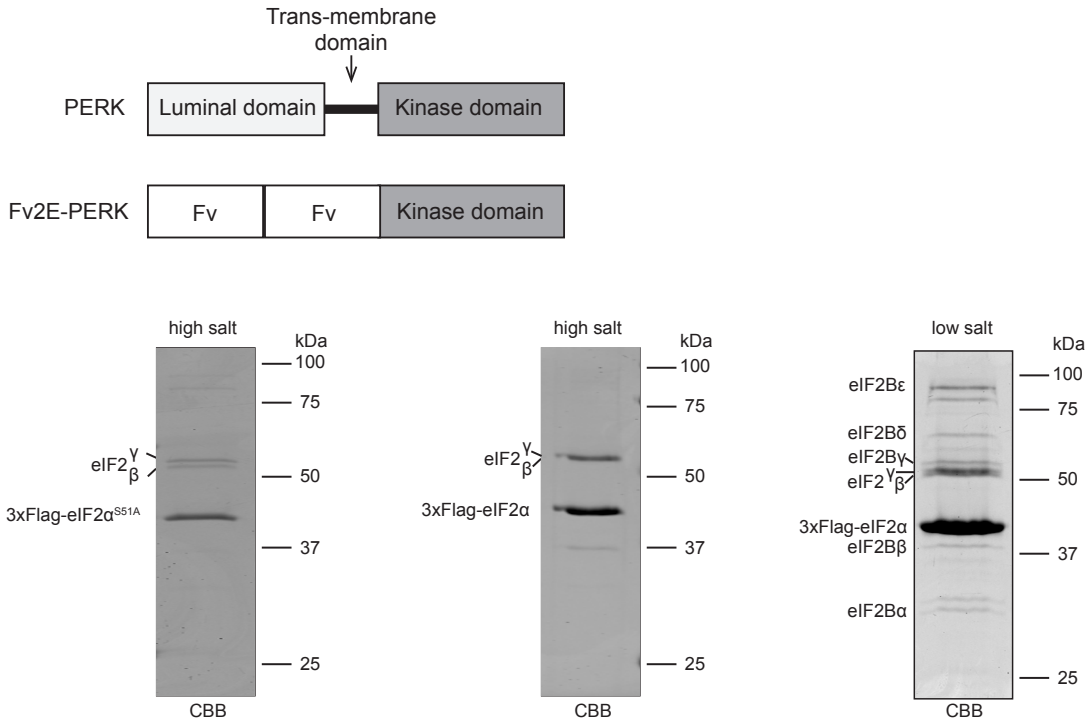

Figure 2.1.2a: Purification of hamster eIF2 and eIF2B complexes.

Coomassie-stained SDS-PAGE gel of purified eIF2/ eIF2(α^{S51A}) (left and central) in high salt (450 mM), or eIF2 purified in complex with eIF2B (right) in low salt (100 mM) from CHO cell lines bearing constitutively expressed recombinant human 3xFlag-tagged eIF2α^{WT}/ eIF2(α^{S51A}) (3xFlag-hu_eIF2$\alpha^{WT/S51A}$) and ligand-activatable cytosolic Fv2E-PERK. Complexes were purified by pulling on the 3xFlag-tagged human eIF2α under conditions promoting phosphorylation of eIF2α by Fv2E-PERK dimerizing upon AP20187 treatment (100 nM) or under conditions of not stimulated phosphorylation. 3xFlag-hu_eIF2$\alpha^{WT/\ S51A}$ along with endogenous hamster eIF2β and γ subunits was believed to assemble into the hamster eIF2(3xFlag-hu_$\alpha^{WT/\ S51A}$) complex. Purified eIF2 heterotrimer was used in experiments studying association of eIF2/ eIF2(αP) with eIF2B (Section 2.1.2), and as a GDP-loaded substrate for measuring GEF activity of eIF2B (Section 2.1.3). Top cartoon is showing recombinant Fv2E-PERK protein in comparison to endogenous PERK with indicated domains. Generation of cartoons, cell lines and purification of complexes was done by A. Zyryanova, University of Cambridge.

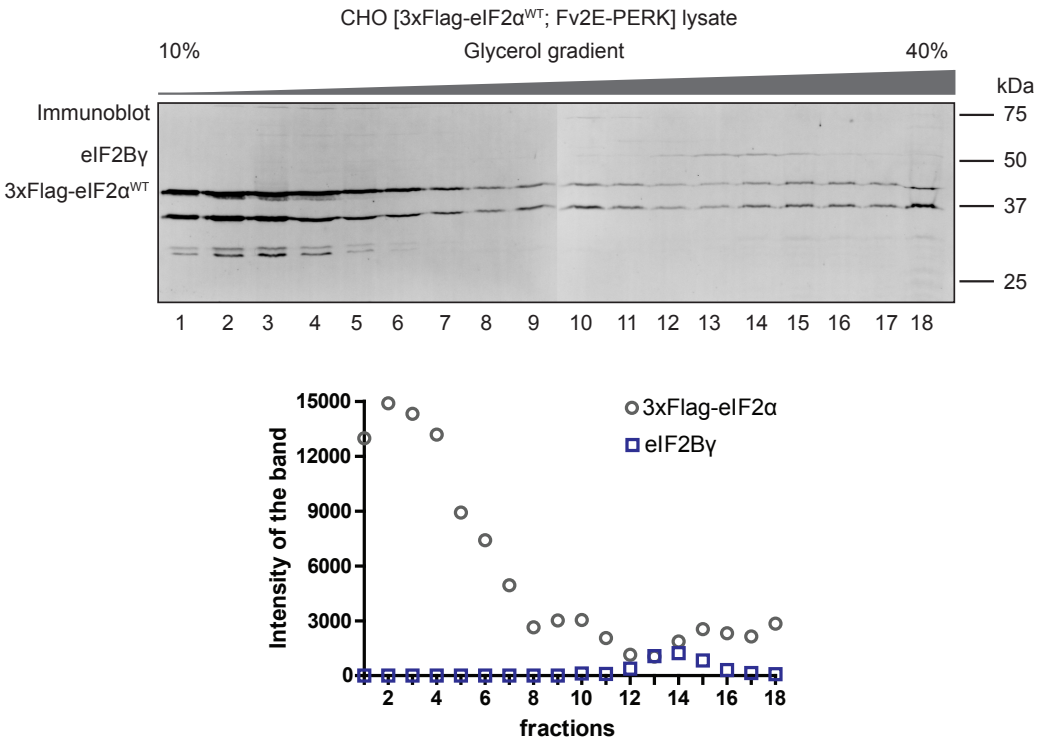

Figure 2.1.2b: Association of eIF2 and eIF2B.

Top: immunoblot of 3xFlag-hu_eIF2α^{WT} (39.6 kDa) and hamster eIF2Bγ (50.5 kDa) detected with anti-FLAG M2 and anti-eIF2Bγ antibodies, respectively, in CHO [Fv2E-PERK; 3xFlag-hu_eIF2α^{WT}] cell lysates resolved on a 10-40% glycerol density gradient. Bottom: quantification of the immunoblot bands (top) tracking mobility of free human 3xFlag-hu_eIF2α^{WT} (fractions 2 and 3), hamster eIF2(3xFlag-hu_α^{WT}) complex (assuming association of recombinant human 3xFlag-tagged eIF2α^{WT} with endogenous hamster eIF2β and γ subunits, fractions 9 and 10), and of the high molecular weight complex between hamster eIF2(3xFlag-hu_α^{WT}) and eIF2B (assuming that eIF2Bγ signal is indicating presence of the full endogenous hamster eIF2B complex, fractions 13-15). The experiment was performed under conditions promoting phosphorylation of eIF2α by Fv2E-PERK upon AP20187 treatment (100 nM), repeated three times. Quantification was done using ImageJ1 software (Wayne Rasband, NIH USA). Culture maintenance, treatments, analytical centrifugation, and analysis performed by A. Zyryanova, University of Cambridge.

We then intended to find out whether we could monitor phosphorylation-dependent increase in association of eIF2B with eIF2(αP), since some reports suggest that phosphorylation promotes formation of high affinity regulatory, eIF2B*eIF2(αP), complex (Safer et al. 1982; Matts et al. 1983; Salimans et al. 1984; Sudhakar et al. 2000). By immunoblotting anti-FLAG M2 affinity pull downs of 3xFlag-eIF2α/ 3xFlag-eIF2αP under low salt conditions with anti-FLAG and anti-eIF2Bγ antibodies, we could detect eIF2/ eIF2(αP) and eIF2B complexes, respectively. Under non-phosphorylating conditions the two complexes were believed to predominantly form productive catalytic, eIF2B*eIF2, interactions (Figure 2.1.2c lane 1). Addition of AP20187 compound increased phosphorylation of eIF2α by 5 fold (Figure 2.1.2c lanes 1&2), which we thought would promote formation of higher affinity regulatory, eIF2B*eIF2(αP), complex. The association of eIF2B with eIF2(αP), however, was enhanced just ever so slightly (Figure 2.1.2c lanes 1&2). Moreover, that modest increase in eIF2B signal associated with eIF2(αP) could not be consistently reproduced suggesting that either all the available eIF2B was already associated with eIF2 prior induced phosphorylation, or our eIF2(αP) did not promote formation of a more stable complex with eIF2B.

Nonetheless, we then tried to challenge interactions between lightly phosphorylated or highly phosphorylated eIF2 and eIF2B with ISRIB (Figure 2.1.2c lane 3&4). ISRIB could stimulate association of eIF2B with eIF2 under conditions in which eIF2α phosphorylation was not induced (Figure 2.1.2c lane 1&3). The association of eIF2B with eIF2(αP), however, did not seem to be altered by ISRIB (Figure 2.1.2c lane 2&4). Withal, the effect of ISRIB on catalytic interactions between eIF2B and eIF2 was also hardly reproduced, and led us to believe that ISRIB does not measurably weaken nor strengthens interactions between eIF2B and eIF2/ eIF2(αP). Though, we admit that our system may have its flaws, and may not be optimal for capturing differences in such a dynamic system. Besides, it does not allow us to unambiguously monitor formation of catalytic and regulatory interactions between eIF2B and eIF2/ eIF2(αP), since in our system they are mixed together.

In an attempt to uncouple catalytic, eIF2B*eIF2, from regulatory, eIF2B*eIF2(αP), complexes, we created a similar cell line that has an original phosphorylatable serine 51 (S51) on recombinant 3xFlag-tagged human eIF2α substituted with non-phosphorylatable alanine (S51A). We reasoned that the mutant form of eIF2α^{S51A} would allow us to focus exclusively on catalytic interactions between eIF2B and eIF2. The association of eIF2B with eIF2(hu_α^{S51A}-3xFLAG) was lower compared to the association of eIF2B with eIF2(hu_α^{WT}-3xFLAG) (Figure 2.1.1c lanes 1&5) suggesting that we were able to capture the catalytic interactions between eIF2B and eIF2 without mixed in regulatory interactions. Moreover, induction of eIF2α phosphorylation stripped off eIF2B from eIF2(hu_α^{S51A}-3xFLAG) proposing that eIF2B was sequestered by higher affinity interactions with endogenous hamster eIF2(αP) (Figure 2.1.1c lanes 5&6). Compellingly, addition of ISRIB was enough to rescue association of eIF2B with eIF2(hu_α^{S51A}-3xFLAG) to its original level, but did not encourage any further association (Figure 2.1.1c compare lanes 7&8 to lane 5). Since the effect observed with eIF2α^{S51A} mutant was reproducible, we were encouraged to conclude that in the presence of ISRIB more eIF2B becomes available for catalytic interactions with eIF2.

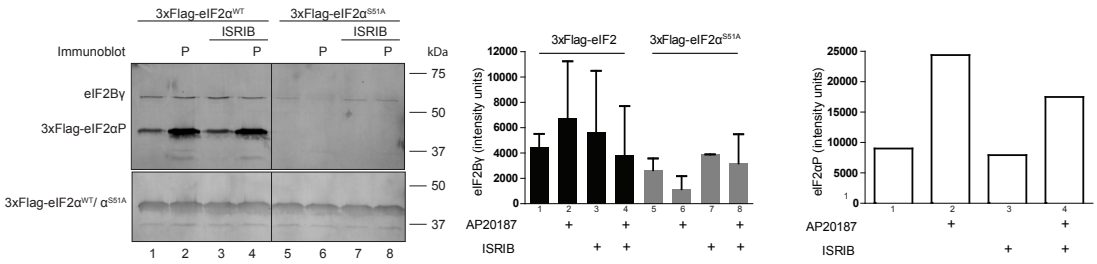

Figure 2.1.2c: Effect of ISRIB on association between eIF2B and eIF2/ eIF2(αP).

Immunoblot of 3xFlag-hu_eIF2α and eIF2Bγ purified from CHO [Fv2E-PERK; 3xFlag-hu_eIF2α^{WT}] cells (lanes 1-4) or CHO [Fv2E-PERK; 3xFlag-hu_eIF2α^{S51A}] (lanes 5-8) using anti-FLAG M2 affinity resin, and detected with anti-phospho-eIF2α, anti-FLAG M2, and anti-eIF2Bγ antibodies. Where indicated the samples were treated with AP20187 (P, 100 nM), ISRIB (100 nM) or both. Lanes 1-4: addition of AP20187 to cells bearing eIF2α^{WT} triggered a 5-fold increase in eIF2αP signal, and a modest increase in association of eIF2Bγ with eIF2αP (lanes 1&2). ISRIB treatment did not influence phosphorylation-dependent association of eIF2Bγ with eIF2αP (lanes 2&4), and increased association of eIF2Bγ with eIF2α under no phosphorylation conditions (lanes 1&3). Both findings were not highly reproducible. Lanes 5-8: association of eIF2Bγ with non-phosphorylatable S51A mutant of eIF2α was less strong than with eIF2α^{WT} (lanes 1&5), possibly indicating formation of a transient catalytic eIF2*eIF2B complex. Addition of AP20187 to cells with eIF2α^{S51A} triggered disappearance of eIF2Bγ signal (lanes 5&6), potentially reflecting sequestration of eIF2B by endogenous phosphorylated hamster eIF2(αP) complex. ISRIB was able to rescue catalytic eIF2*eIF2B complex (lanes 6&8). Bar graphs show quantification of bands corresponding to eIF2Bγ signal (mean ± SD, n=4 from four independent blots, note high variability for eIF2α^{WT} in lanes 1-4), and eIF2αP signal (this blot only), both normalized to the total 3xFlag-eIF2α. Quantification was done using ImageJ1 software (Wayne Rasband, NIH USA). Executed by A. Zyryanova, University of Cambridge.

In order to reveal the regulatory interactions between eIF2B and eIF2(αP), we needed to decrease the amount of catalytic interactions between eIF2B and eIF2 in our pull downs. Some reports suggest that addition of GTP promotes dissociation of eIF2B from eIF2 by shifting the equilibrium towards formation of TC (Matts et al. 1983; Salimans et al. 1984). We, therefore, decided to use GTP in an attempt to wash off catalytic interactions, and focus on regulatory interactions between eIF2B and eIF2(αP). Testing different nucleotides against the system with human eIF2α^{S51A} mutant showed that both GDP and GTP, but not ATP, nucleotides promote dissociation of eIF2B from eIF2(hu_α^{S51A}-3xFLAG) complex, potentially indicating that catalytic interactions are being stripped off (Figure 2.1.2d lanes 5-8). Consequently, we utilized GTP wash in the system with human eIF2α^{WT}, and observed decrease in the amount of eIF2B associated with eIF2(hu_α^{WT}-3xFLAG) under no promoted phosphorylation conditions (Figure 2.1.2d, lanes 1&3). The amount of eIF2B associated with eIF2(hu_α^{WT}-3xFLAG), nonetheless, did not seem to change under conditions of promoted phosphorylation with or without GTP wash (Figure 2.1.2d lanes 2&4). Both findings suggested that by using GTP wash we potentially could focus more on regulatory interactions between eIF2B and eIF2(αP).

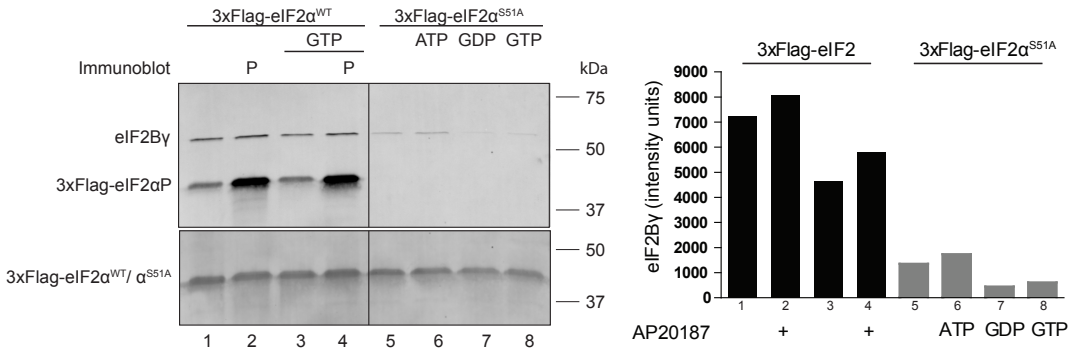

Figure 2.1.2d: Capturing regulatory interactions between eIF2B and eIF2(αP).

Immunoblot of 3xFlag-hu_eIF2α and eIF2Bγ purified from CHO [Fv2E-PERK; 3xFlag-hu_eIF2α^{WT}] cells (lanes 1-4) or CHO [Fv2E-PERK; 3xFlag-hu_eIF2α^{S51A}] (lanes 5-8) using anti-FLAG M2 affinity resin, and detected with anti-phospho-eIF2α, anti-FLAG M2, and anti-eIF2Bγ antibodies. Where indicated the samples were treated with AP20187 (P, 100 nM), nucleotide (1 mM) or both. Lanes 5-8: addition of GTP/ GDP but not ATP to cell lysates bearing eIF2α^{S51A} triggered disappearance of eIF2Bγ signal indicating dissociation of catalytic eIF2*eIF2B complex. Lanes 1-4: addition of GTP to cell lysates bearing eIF2α^{WT} potentially decreased amount of catalytic interactions between eIF2 and eIF2B exposing regulatory interactions between eIF2(αP) and eIF2B, where slight increase in association of eIF2Bγ signal with eIF2αP was observed (lanes 3&4). Bar graph shows quantification of bands corresponding to eIF2Bγ signal (this blot only, note decrease of signal in lanes 3&4 vs. 1&2, and 7&8 vs. 5&6) normalized to the total 3xFlag-eIF2α. Quantification was done using ImageJ1 software (Wayne Rasband, NIH USA). Experiments were repeated twice. Executed by A. Zyryanova, University of Cambridge.

We tried to use GTP in order to unravel the effect of ISRIB on regulatory interactions (Figure 2.1.2e). In contrast to the previous similar experiment without GTP (Figure 2.1.2c lanes 1-4), we could now observe a conspicuous phosphorylation dependent increase in association of eIF2B with eIF2(αP) (Figure 2.1.2e lanes 1&2). Moreover, we observed the rise in the amount of eIF2B associated with eIF2 under conditions in which eIF2α phosphorylation was not induced, and no change in association of eIF2B with eIF2(αP) under conditions promoting phosphorylation (Figure 2.1.2e, lanes 1&3 and 2&4) consistently with the previously noted effect (Figure 2.1.2c, lanes 1&3 and 2&4). Those findings led us to propose that whatever ISRIB compound might be doing it is unlikely facilitating dissociation of eIF2B from eIF2(αP). If anything, in the presence of ISRIB, eIF2B might adopt an allosterically more favorable conformation facilitating catalysis despite persistent high levels of phosphorylated eIF2α, or maybe more active eIF2B could be drawn from some other source in the cell.

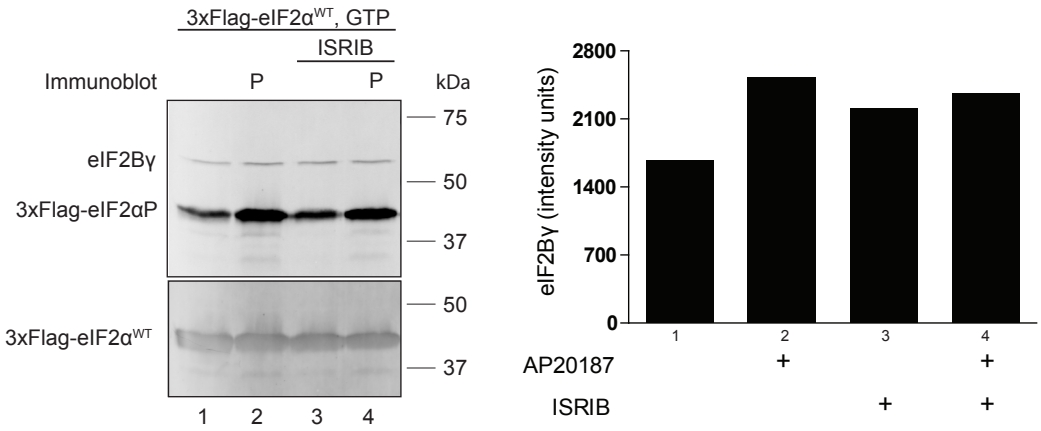

Figure 2.1.2e: Effect of ISRIB on regulatory interactions between eIF2B and eIF2(αP).

Immunoblot of 3xFlag-hu_eIF2α^{WT} and eIF2Bγ purified from CHO [Fv2E-PERK; 3xFlag-hu_eIF2α^{WT}] using anti-FLAG M2 affinity resin in the presence of GTP (1 mM), and detected with anti-phospho-eIF2α, anti-FLAG M2, and anti-eIF2Bγ antibodies. Where indicated samples were treated with AP20187 (P, 100 nM), ISRIB (100 nM) or both. As in (Figure 2.1.2d lanes 3&4), presence of GTP potentially reduced amount of catalytic, eIF2*eIF2B, interactions exposing regulatory association of eIF2(αP) with eIF2B (lanes 1&2). Addition of ISRIB did not decrease association of eIF2Bγ with eIF2αP under high phosphorylation conditions (lanes 2&4), but increased association of eIF2Bγ with eIF2α under no phosphorylation conditions (lanes 1&3). Experiments were repeated twice. Bar graph shows quantification of bands corresponding to eIF2Bγ signal (this blot only, note increase of signal in lane 3 vs. 1) normalized to the total 3xFlag-eIF2α. Quantification was done using ImageJ1 software (Wayne Rasband, NIH USA). Executed by A. Zyryanova, University of Cambridge.

2.1.3 ISRIB's effect on the GEF activity of eIF2B

To address a question of whether eIF2B is a primary target for ISRIB, and whether the compound has an effect on eIF2B's GEF activity, we required a purified active mammalian eIF2B decamer to conduct the experiments. We chose to focus on the mammalian complex since there is evidence that ISRIB does not have an effect on intact yeast cells or purified yeast eIF2B complex (data not shown). As a source of eIF2B substrate we decided to use nucleotide loaded hamster eIF2(hu_α-3xFLAG), eIF2(hu_αP-3xFLAG) or eIF2(hu_α^{S51A}-3xFLAG) complex purified from CHO cells as described in Section 2.1.2.

At the time of our experimental design, there was no available bacterial over-expression system for purification of high amounts of full-length mammalian eIF2B complex. Moreover, some of our own experience (data not shown) along with reports of others (Bogorad et al. 2014) suggested that over-expression of some subunits of eIF2B, and the assembly of the full eIF2B complex under non-stoichiometric conditions, could be challenging. Purification of eIF2B from liver tissues or rabbit reticulocytes is long and tedious, and requires multiple dialysis and chromatography steps (Salimans et al. 1984; Kimball et al. 1987). We, therefore, designed a system to purify an endogenous human eIF2B complex by introducing a 3xFlag-tag at the N-terminus of eIF2Bβ, encoded by *EIF2B2* gene, utilizing CRISPR/Cas9 and homologous DNA repair template (more details in Section 4.2.2). Introduction of 3xFlag into the endogenous eIF2B subunit proved to be not detrimental for the gene expression, and allowed us to purify fully assembled stoichiometric human eIF2B decamer using a single step of affinity purification (Figure 2.1.3a left panel). The further cleanup using size-exclusion chromatography confirmed homogeneity of the purified endogenous eIF2B eluting as a single peak at the size of a decamer (530 kDa) (Figure 2.1.3a middle & right panels). Following similar logic, we later designed purification systems for endogenous hamster eIF2B, which was 3xFlag-tagged at its γ subunit by targeting *Eif2b3* locus (more details in Section 4.2.3). In the context of hamster 3xFlag-tagged eIF2B, ISRIB^{RES} mutant (δ^{L180F}) (Section 2.3.3, Figure 2.1.3b) and VWM

mutant (δ^{A392D}) were created (Figure 2.1.3b). The discussion of the behavior of the hamster eIF2B during SEC will follow.

To confirm that the purified human eIF2B is an active guanine exchange factor, and to learn whether ISRIB has an effect on eIF2B's GEF activity, we tested the complex in a nucleotide exchange assay. We designed a nucleotide exchange assay by combining features of a well-established [^{3}H]GDP-release assay (Kimball et al. 1989) with a modern fluorescence intensity-based assay for nucleotide binding to other G-proteins (Sajid et al. 2011; Shang et al. 2012). A commercially available fluorescent compound, Bodipy-FL conjugated GDP ([b]GDP), is quenched by photo-induced electron transfer from proximal guanosine bases when it is free in solution (*The Molecular Probes Handbook. a Quide to Fluorescent Probes and Labeling Technologies* 2010). Loading of [b]GDP onto eIF2 leads to increase in probe's fluorescence due to dequenching of the fluorophore by burial of the base in the protein's hydrophobic pocket (McEwen et al. 2001). The release of the bound [b]GDP nucleotide from the non-phosphorylated eIF2 or phosphorylated eIF2(αP) substrates promoted by purified human eIF2B in the excess of unlabeled GDP could be monitored continuously by the decline of the fluorescence signal as quenching by the base was re-established (Figure 2.1.3c). The rate of [b]GDP release from phosphorylated eIF2 declined by approximately 35% compared to non-phosphorylated substrate (Figure 2.1.3d) consistent with the inhibitory effect of eIF2(αP) on eIF2B GEF activity (Kimball et al. 1998). Addition of ISRIB increased the rate of [b]GDP release from both non-phosphorylated and phosphorylated eIF2 substrates by around 22% and 20%, respectively, suggesting the direct effect of ISRIB on promoting GEF activity of eIF2B towards eIF2 and eIF2(αP) (Figure 2.1.3d).

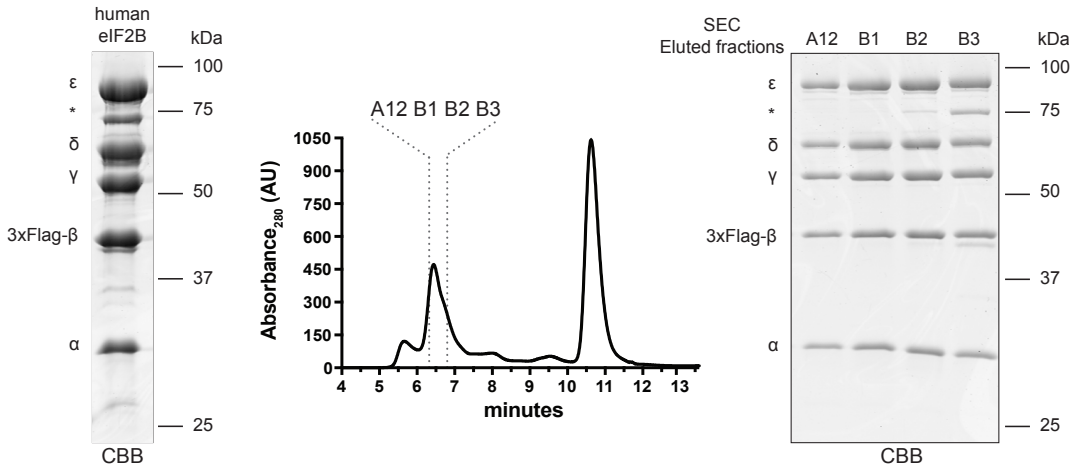

Figure 2.1.3a: Purification of endogenous human eIF2B.

Coomassie-stained SDS-PAGE gel of the endogenous human eIF2B purified from HeLa cells bearing 3xFlag-tag at the N-terminus of eIF2B gel of the endogenous human eIF2B purified from HeLa cells bearing 3xFlag-*EIF2B2*) using anti-FLAG M2 affinity resin, and resolved by size exclusion chromatography (SEC) on a SEC-3 300 Å chromatography column (middle) with the indicated fractions analyzed on a Coomassie-stained SDS-PAGE gel (right) (*PRMT5 – a contaminant). The human eIF2B eluted from the affinity resin with 3xFlag peptide without further SEC run (left) was used in GEF activity assays (Section 2.1.3) and in fluorescence polarization experiments measuring direct binding of ISRIB to eIF2B (Section 2.1.7). The SEC eluted fractions (right) were used for structural analysis (Section 2.2). Human eIF2B was purified using the described system multiple times. Generation of cell lines and eIF2B purifications were executed by A. Zyryanova, University of Cambridge.

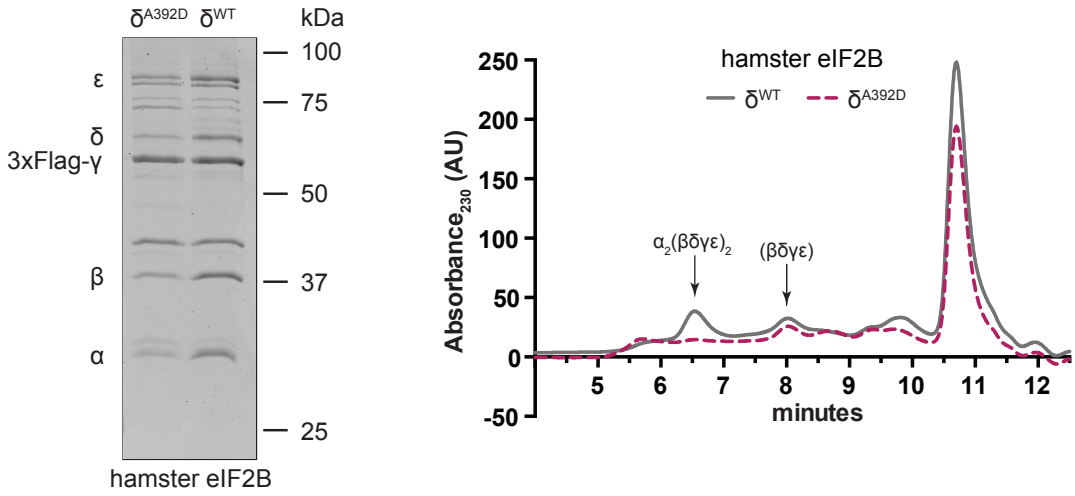

Figure 2.1.3b: Purification of endogenous hamster eIF2B.

Left: Coomassie-stained SDS-PAGE gel of the endogenous hamster eIF2B(δ^{WT}) and eIF2B(δ^{A392D}) bearing 3xFlag-tag at the C-terminus of eIF2Bγ (introduced by CRISPR/ Cas9 and homologous recombination into the *Eif2b3* locus), purified using anti-FLAG M2 resin, and loaded in equimolar concentrations. Note the substoichiometric ratio of eIF2B subunits (the eIF2Bα in particular) of the mutant compared to wildtype complex. Right: chromatograms of the purified endogenous hamster eIF2B(δ^{WT}) and eIF2B(δ^{A392D}) protein complexes (as on the left) resolved by size exclusion chromatography on a SEC-3 300 Å chromatography column. Note the two main species running at the sizes of a full hamster eIF2B decamer (490 kDa) and a partial hamster eIF2B(βγδε) tetramer (220 kDa), which are both present in the eluted wildtype complex (grey continuous trace) but not in eIF2B(δ^{A392D}) (red discontinuous trace) that runs only at the size of a tetramer. CHO [3xFlag-eIF2Bγ, δ^{WT}] was also used in complex stability experiments (Section 2.1.5), purified hamster eIF2B was used in fluorescence polarization experiments (Section 2.3.2). Cell lines were designed and created by Y. Sekine, purifications were done by A. Zyryanova, University of Cambridge. SEC analysis was performed by A. Zyryanova, University of Cambridge.

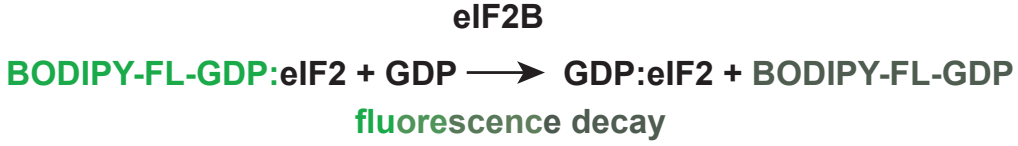

Figure 2.1.3c: GDP-release assay.

Shown is a schema of a fluorescence-based GDP-release assay monitoring fluorescence decay of Bodipy-FL-GDP in the presence of eIF2B and access of unlabeled GDP, as it is being released from eIF2 substrate. Figure drawn by A. Zyryanova, University of Cambridge.

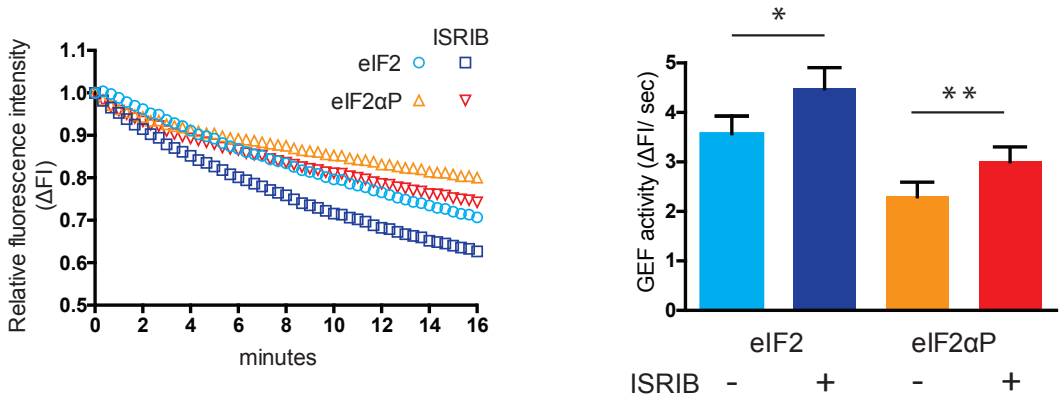

Figure 2.1.3d: GDP-release assay with purified GEF eIF2B.

Left: GEF activity of the human eIF2B (1.5 nM) observed as time-dependent decrease of relative fluorescence intensity of Bodipy-FL-GDP (ΔFI) loaded onto weakly (blue circles and dark blue squares) or heavily phosphorylated eIF2 (orange triangles and red upside down triangles) (100 nM), and incubated with unlabeled GDP (1.5 mM) in the presence or absence of ISRIB (200 nM). ΔFI was calculated as a ratio between the starting FI signal at time "0" (FI_0) and the subsequently measured FI points at time "n" (FI_n): $\Delta FI = FI_0 / FI_n$. Shown is a representative experiment repeated more than three times. Right: GEF activity reflected in the initial velocities (ΔFI/ sec) of Bodipy-FL-GDP release reactions (as on the left). Note accelerated GEF activity of weakly phosphorylated vs. heavily phosphorylated eIF2 substrates (compare blue to orange in both panels), as well as stimulation of GEF activity upon addition of ISRIB for either of substrates (compare blue to dark blue and orange to red in both panels). Mean ± SEM (n=8). *P=0.012, **P =0.0054 (Student's t test). Executed by A. Zyryanova, University of Cambridge.

To exclude the potential contamination of eIF2 substrate with its phosphorylated form, and to rule out the assumption that ISRIB-mediated acceleration of GEF activity is selective for eIF2(αP), we decided to use purified non-phosphorylatable eIF2(α^{S51A}) as a non-phosphorylated eIF2 substrate (described in Section 2.1.2). To save the purified eIF2B for other experiments, and to compare eIF2B's GEF activity in the context of various mutations, we switched to using mammalian cell lysates as a source of GEF (Kimball et al. 1989). In concordance with the experiments using purified eIF2B (Figure 2.1.3d), we observed decrease in GEF activity of wildtype cell lysate towards phosphorylated eIF2(αP) compared to eIF2(α^{S51A}), and increase in GEF activity of cell lysate promoted by ISRIB towards both substrates (Figure 2.1.3e, wt lysate). These findings altogether demonstrated that ISRIB can exert its effect on GEF activity of eIF2B in the absence of any phosphorylated eIF2. When comparing activity of the wildtype cell lysate to the ISRIB^{RES} cell lysate bearing eIF2Bδ^{L180F} mutation, we saw no effect of ISRIB on the GEF activity of the latter consistently with our working hypothesis that eIF2B is a target of ISRIB (Figure 2.1.3e). Even though we cannot estimate precisely the amount of eIF2B present in cell lysates used in our assays, our rough estimation suggests that concentration of eIF2B in cell lysates is comparable to the concentration of purified human eIF2B. Hence, it is interesting to note that the GEF activity of cell lysates observed by us, on average, is enhanced by ISRIB by more than 30-40% compared to around 20% when using purified eIF2B (Figure 2.1.3d, e). This observation made us wonder if there is some cellular component essential for ISRIB's activity that is missing from the assay with purified eIF2B.

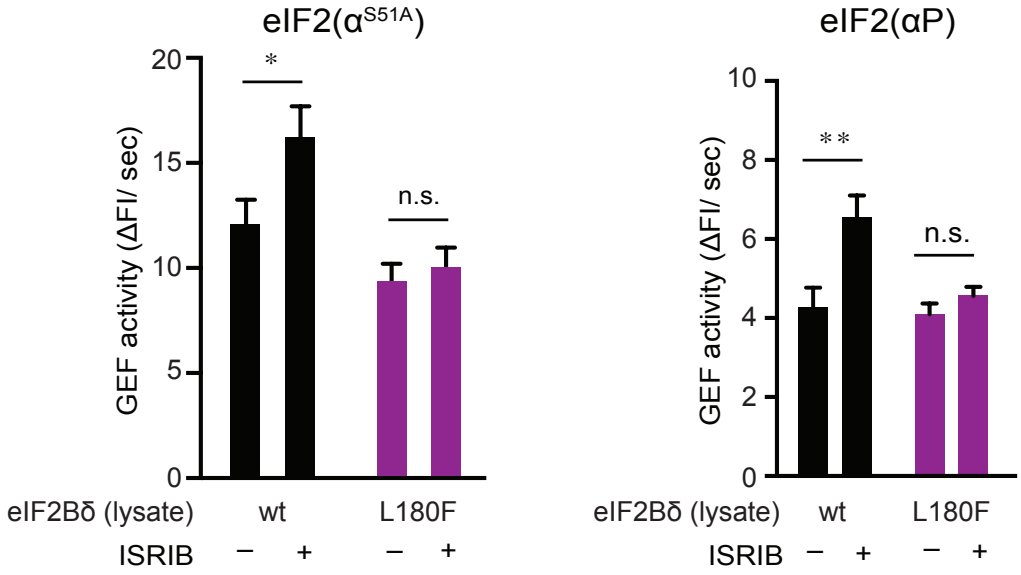

Figure 2.1.3e: GDP-release assay with cell lysate as a source of GEF.

GEF activity of CHO cell lysates (wt or eIF2Bδ^{L180F} ISRIB^{RES} mutant) reflected in the initial velocities (ΔFI/ sec) of Bodipy-FL-GDP release reactions (as in Figure 2.1.3d) towards non-phosphorylatable eIF2(α^{S51A}) (left) or phosphorylated eIF2(αP) (right) substrates in the presence or absence of ISRIB. Note the decreased GEF activity of wildtype and δL180F lysates towards eIF2(αP) compared to eIF2(α^{S51A}) substrate, and increased GEF activity in the presence of ISRIB towards both substrates when using wildtype lysate but not δL180F lysate. Note decreased GEF activity of δL180F lysate towards eIF2(α^{S51A}) compared to wildtype lysate. Shown are mean ± SEM (n = 7 for eIF2(α^{S51A}) substrate, n=5 for eIF2(αP) substrate), *P<0.01, **P<0.05, n.s. - not significant (Student's t test). Executed by Y. Sekine, University of Cambridge.

2.1.4 Searching for a "missing" component that promotes eIF2B's GEF activity in the presence of ISRIB in cells

To address the question of whether ISRIB's accelerating effect on eIF2B's GEF activity in cell lysates is due to enhanced stimulated association of some other proteins with eIF2B, for instance, translational factors, like eIF2, or due to reduced association of usual eIF2B's interactors, we designed the following experiment. We decided to use a quantitative technique of stable isotope labeling by amino acids in cell culture (SILAC) coupled with mass spectrometry (MS) analysis to detect eIF2B's associates. SILAC allowed us to label proteins in live HeLa cells bearing 3xFlag-eIF2Bβ, with light or heavy isotopes of carbon and nitrogen (^{12}C/ ^{13}C and ^{14}N/ ^{15}N) by feeding cells with medium containing respective isotopic versions of arginine and lysine. Using anti-FLAG M2 resin we could pull on the 3xFlag-tag of eIF2Bβ, and quantify by MS peptides associated with the tagged protein under various conditions, for example, treated or untreated with ISRIB.

First, we wanted to check the specificity of our designed method by comparing the amount of specific and non-specific eIF2B associates that could be detected (Figure 2.1.4a). We prepared parental untagged HeLa cells cultured in media containing light isotopic version of Arg and Lys ($HeLa^{PL}$), and tagged HeLa cells bearing 3xFlag-tagged eIF2Bβ (described in Section 2.1.3) cultured in media containing heavy isotopic mixture of Arg and Lys ($HeLa^{\beta H}$). After adapting and expanding both cultures, we lysed the cells, combined lysates from $HeLa^{PL}$ and $HeLa^{\beta H}$ in equal amounts, and performed affinity pull down by dragging on the 3xFlag-tag of eIF2Bβ bait. The pull down was then eluted from the beads with 3xFlag peptide and sent for MS analysis. Since the proteins in the two cell cultures, $HeLa^{PL}$ and $HeLa^{\beta H}$, were labeled by either "L" or "H" amino acids, we could quantify the corresponding peptides by MS analysis tracking their origin. The data was then plotted as a logarithmic ratio of (H/L) peptides against the intensity of the signal (Figure 2.1.4a). The intensity of the peptide count indicated the level of association of the corresponding protein with the 3xFlag-tagged eIF2Bβ bait. The log(H/L) ratio of a given peptide, therefore, revealed whether the corresponding protein

comes from the HeLa^{PL} (log(H/L)<0) or HeLa$^{\beta H}$ (log(H/L)>0) culture, demonstrating specificity of the pull down (Figure 2.1.4a).

We expected to see all the proteins strongly interacting with 3xFlag-eIF2Bβ to accumulate on the right side of the graph (log(H/L)>0) since these associates should come primarily from the tagged HeLa$^{\beta H}$ culture. As predicted, we detected peptides corresponding to all the eIF2B subunits on the right side of the graph (Figure 2.1.4b), including an eIF2Bδ isoform that was previously shown to make eIF2B complex insensitive to eIF2α phosphorylation (Martin et al. 2010). This observation was indicative of the stable interaction between eIF2B subunits, although a slight shift to the left and lessened intensity signal of peptides corresponding to eIF2Bα subunit and eIF2Bδ isoform were observed. These findings suggested weaker association of eIF2Bα and eIF2Bδ isoform with the rest of the eIF2B complex (Figure 2.1.4b) consistently with observations of others (Craddock and Proud 1996; Martin et al. 2010).

We anticipated that all the peptides accumulated on the left side of the graph (log(H/L)<0) should correspond to non-specific associates of 3xFlag-eIF2Bβ or of the anti-FLAG M2 affinity resin, since they predominantly come from untagged HeLa^{PL} culture (Figure 2.1.4b). Not many peptides of high intensity were found on the left side of the graph, which demonstrated specificity of our pull down.

The main bulk of peptides identified in this experiment fell on the center of the plot (log(H/L)~0) suggesting that their signal is equally contributed by the proteins coming from both untagged HeLa^{PL} and tagged HeLa$^{\beta H}$ cultures (Figure 2.1.4b). Amongst many of such peptides are the ones corresponding to translation initiation factors, including eIF2, the most well-known eIF2B associate (Figure 2.1.4b). This result is probably indicative of the transient nature of these associations with the bait, and not of the lack of assay's specificity. Even though these transient associates were derived from both untagged and tagged cells, they probably had time to adopt some equilibrium between each other and between the 3xFlag-tagged eIF2Bβ bait during affinity pull down procedure.

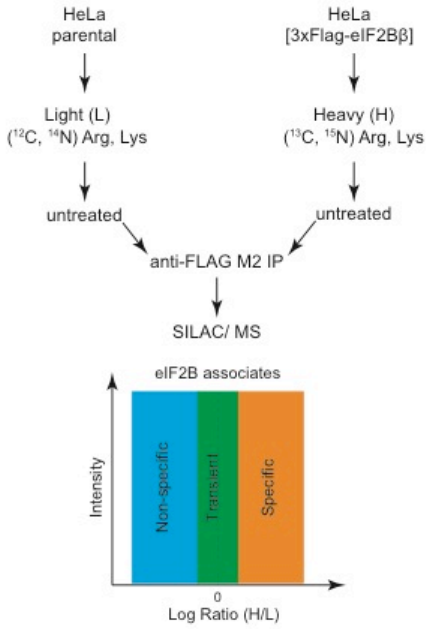

Figure 2.1.4a: SILAC/ MS experiment I.

Shown is a schema of a SILAC/ MS experiment. HeLa parental cells, and tagged HeLa cells bearing 3xFlag-eIF2Bβ were adapted to media containing either light (L) isotopic contents or heavy (H) isotopic contents of arginine and lysine, respectively. Equal amounts of untreated cell lysates from “H” and “L” cultures were mixed together, 3xFlag-tagged eIF2B was purified using anti-FLAG M2 affinity resin under low salt conditions (150 mM), and eluted from the resin using 3xFlag peptide (as in Section 2.1.3). The eluted sample containing a mixture of “H”- and “L”-labeled proteins was analyzed by MS, and the peptides containing “H” and “L”-labeled peptides were counted. The log ratio of (H/L) peptides was calculated, and the results were plotted revealing species purified alongside tagged eIF2B. Comparison between parental and tagged cell lines reveals the specificity of the pull-down, since all the associates making specific interactions with eIF2B should fall to the right on log(H/L)>0, and all the non-specific associates should fall to the left on log(H/L)<1. Everything on the line (log(H/L)=0) can be considered as potentially specific but transient interactors that are in equilibrium within “H” and “L” lysates, and eIF2B. Drawn by A. Zyryanova, University of Cambridge.

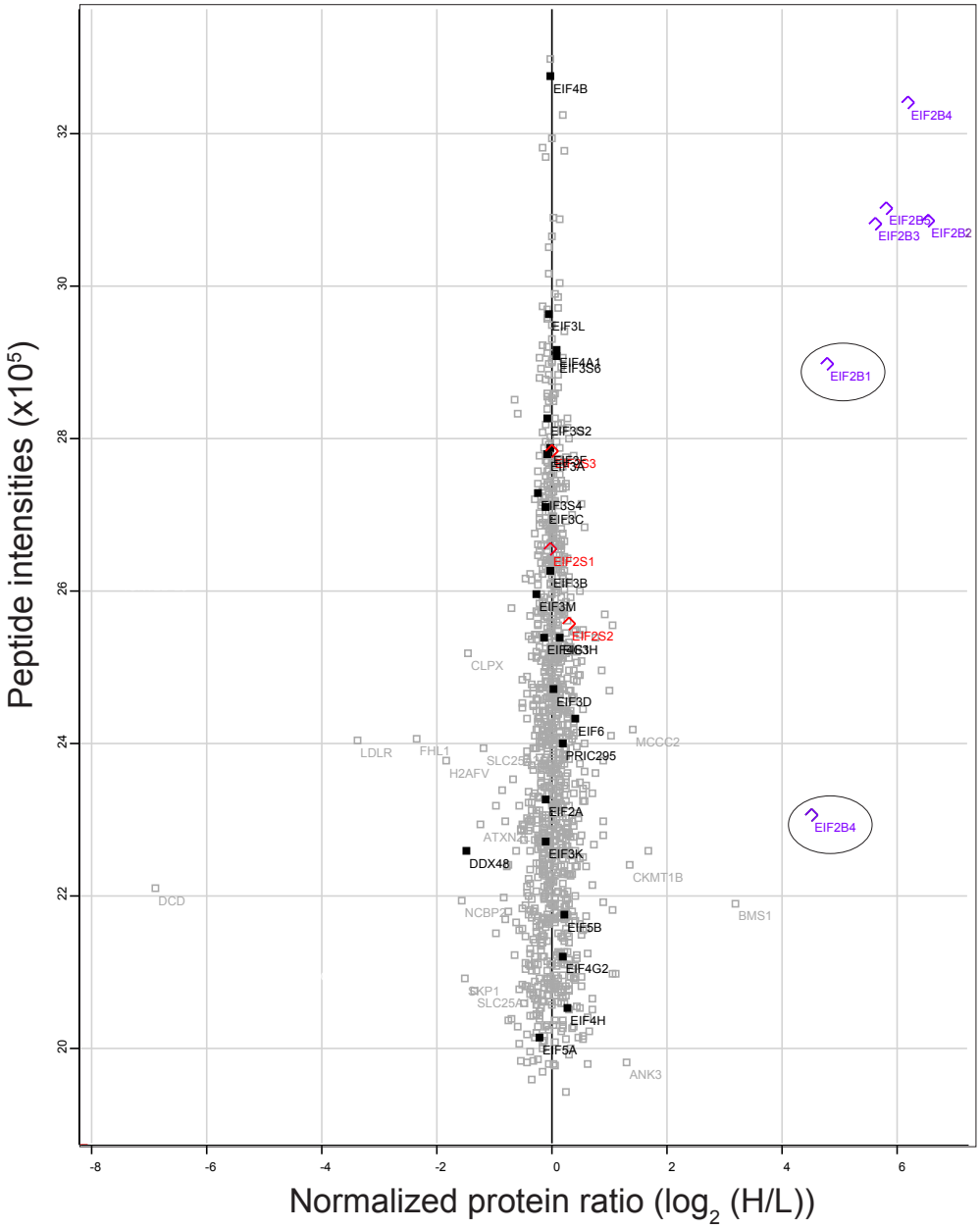

Figure 2.1.4b: Results of SILAC/ MS experiment I.

Plotted are protein ratios of “heavy” (H) to “light” (L) labeled peptides (on a logarithmic scale) against summed peptides intensities derived from SILAC/ MS experiment (as described in Figure 2.1.4a). The intensity reflects abundance of the peptides and the accuracy of quantification. $Log_2(H/L)>0$ showed all eIF2B subunits, including an isoform of eIF2Bδ, amongst primary associates of 3xFlag-eIF2Bβ. $Log_2(H/L)<0$ showed the associates non-specifically co-purifying with the anti-FLAG M2 resin. (continued on the next page)

Log_2(H/L)~0 showed transient associates of eIF2B. The signal for transient associates is contributed by peptides from both pools (“H”- and “L”-labeled) that presumably reached equilibrium with eIF2B when they were mixed together in equal amounts. Amongst the transient associates are many translational factors, including eIF2. eIF2B subunits are labeled in lilac by their gene name (*EIF2B1*, *EIF2B2*, *EIF2B3*, *EIF2B4*, *EIF2B5*), eIF2 subunits in red (*EIF2S1*, *EIF2S2*, *EIF2S3*), other translation initiation factors in black. Marked in black circles are eIF2Bα (*EIF2B1*) and eIF2B isoform (*EIF2B4*). Data analysis and plotting was performed using MaxQuant Perseus software (version 1.5.2.6, Computational Systems Biochemistry). Adaptation of cells to SILAC medium, treatments, pull downs, and figure preparation were performed by A. Zyryanova. MS and data analysis was done by R. Antrobus, University of Cambridge.

We then set up a different SILAC/ MS experiment in which we only used the tagged HeLa cells adapted to either “L” (HeLa$^{\beta L}$) or “H” (HeLa$^{\beta H}$) amino acids (Figure 2.1.4c). Prior to combining lysates from “L” and “H” cultures and performing the pull down, we treated the “H”-labeled culture with ISRIB (ISRIB-HeLa$^{\beta H}$) and left the “L”-labeled culture untreated (UT-HeLa$^{\beta L}$). After performing pull-down and MS analysis, we obtained a data set of peptides counts revealing 3xFlag-eIF2Bβ associates under two different conditions (Figure 2.1.4c).

This time we saw the peptide corresponding to the 3xFlag-eIF2Bβ bait aligned in the center of the plot (log(H/L)~0) indicating the equally mixed UT-HeLa$^{\beta L}$ and ISRIB-HeLa$^{\beta H}$ cell lysates (Figure 2.1.4d). The regular and transient eIF2Bβ’s associates were also expected to be found in the center of the plot (log(H/L)~0), where we observed very strong peptide signals corresponding to all the eIF2B subunits, and other peptide signals matching the many translation initiation factors, eIF2 inclusive (Figure 2.1.4d). In the previous experiment the peptide signal corresponding to eIF2Bα subunit was exhibiting weakened association with the bait containing eIF2Bβ subunit (Figure 2.1.4b). In the new experiment, however, the eIF2Bα shifted to the right from the rest of eIF2B subunits (log(H/L)>0) (Figure 2.1.4d) suggesting that ISRIB-treatment enhanced the recovery of eIF2Bα in complex with the eIF2Bβ bait. This observation is also in line with the assumption that ISRIB stabilizes eIF2B complex (Sidrauski et al. 2015). Nothing in particular drew our attention amongst the peptide to the left of the plot (log(H/L)<0) proposing that ISRIB did not promote dissociation of any proteins from eIF2B that normally would strongly interact with it (Figure 2.1.4d).

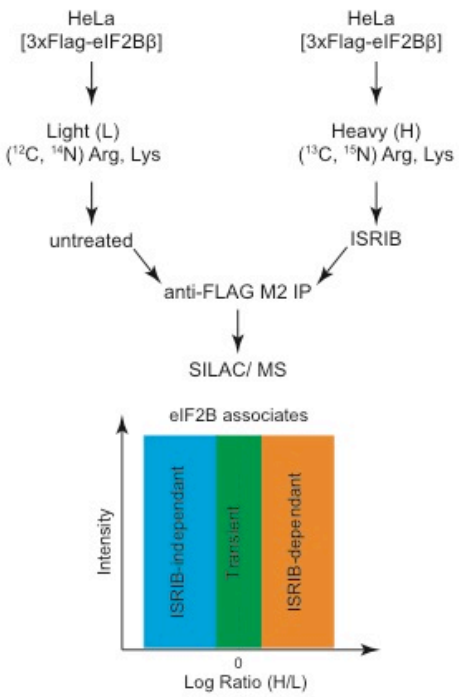

Figure 2.1.4c: SILAC/ MS experiment II.

Shown is a schema of SILAC/ MS experiment similar to the one in Figure 2.1.4a with an exception of using untreated tagged HeLa cells and ISRIB-treated (200 nM) tagged HeLa cells both bearing 3xFlag-eIF2Bβ. Cell cultures were “L”- or “H”-labeled, respectively. Log(H/L)~0 reveals all the transient eIF2B’s associates, strength of interaction with which doesn’t change upon ISRIB treatment. Log(H/L)>0 should indicate all the eIF2B’s associates, interaction with which is enhanced upon ISRIB treatment. Log(H/L)<0 should indicate all the eIF2B’s associates, interaction with which is decreased upon ISRIB treatment. Drawn by A. Zyryanova, University of Cambridge.

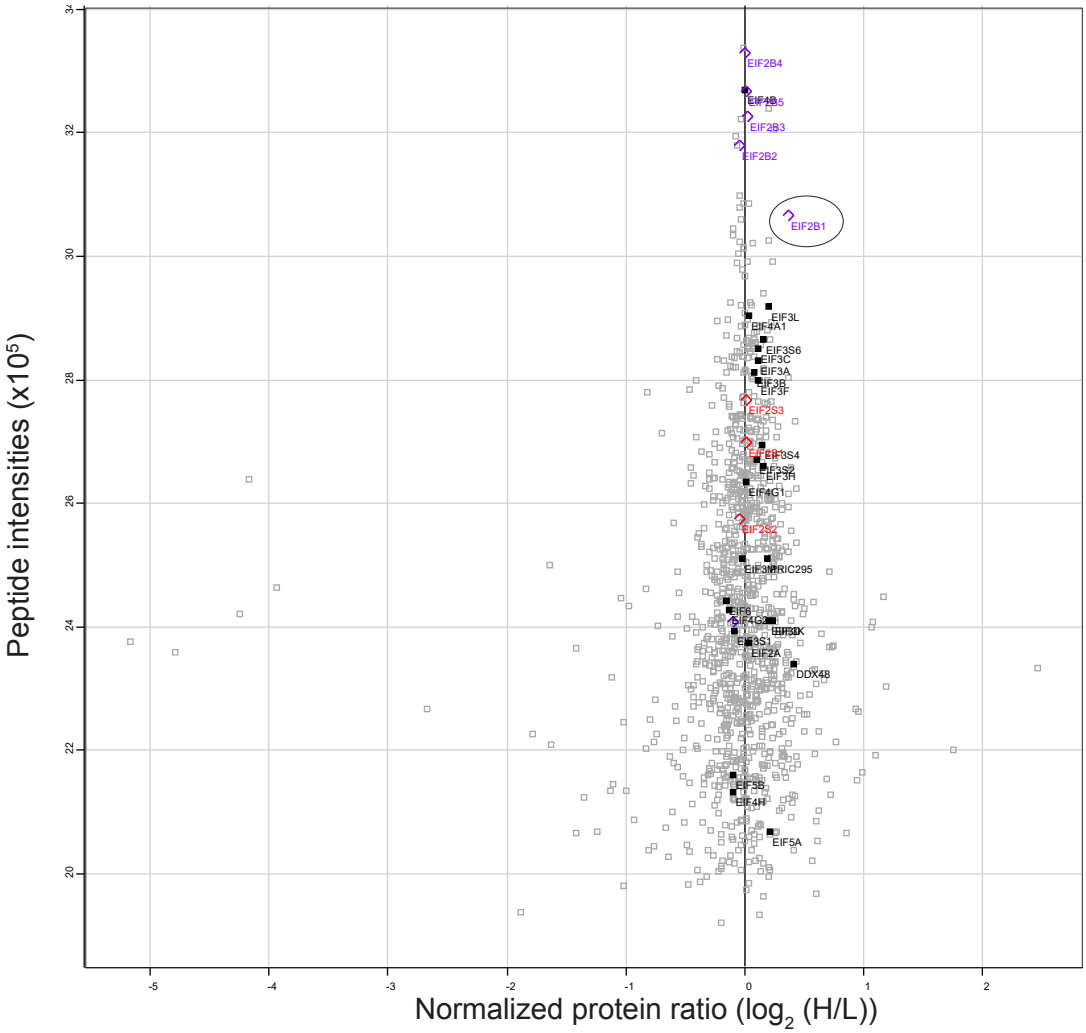

Figure 2.1.4d: Results of SILAC/ MS experiment II.

Plotted are protein ratios of “heavy” (H) to “light” (L) labeled peptides (on a logarithmic scale) against summed peptides intensities derived from SILAC/ MS experiment (as described in Figure 2.1.4c). The intensity reflects abundance of the peptides and the accuracy of quantification. $Log_2(H/L)\sim0$ showed all the eIF2B subunit (and eIF2Bδ isoform) and many translational factors, including eIF2, amongst the primary associates of 3xFlag-eIF2Bβ, also indicating equal mixing of “H”- and “L”-labeled samples. $Log_2(H/L)>0$ showed that association of eIF2Bα with the rest of the complex could potentially be enhanced upon ISRIB treatment. $Log_2(H/L)<0$ showed the associates specific to untreated conditions. (continued on the next page)

eIF2B subunits are labeled in lilac by their gene name (*EIF2B1*, *EIF2B2*, *EIF2B3*, *EIF2B4*, *EIF2B5*), eIF2 subunits in red (*EIF2S1*, *EIF2S2*, *EIF2S3*), other translation initiation factors in black. Marked in black circle is eIF2Bα (*EIF2B1*). Data analysis and plotting was performed using MaxQuant Perseus software (version 1.5.2.6, Computational Systems Biochemistry). Adaptation of cells to SILAC medium, treatments, pull downs, and figure preparation were performed by A. Zyryanova. MS and data analysis was done by R. Antrobus, University of Cambridge.

Even though the results of both SILAC/ MS experiments suggested that nothing interacts with eIF2B as strong as its own subunits, one associate could be worth mentioning since the intensity of its peptide signal stood out above the others in both SILAC/ MS experiments (log(H/L)~0) (Figure 2.1.4b, d) suggesting the potentially strong interaction of the corresponding protein with eIF2B. This protein is a translation initiation factor eIF4B that stimulates the ATP-dependent RNA helicase activity of eIF4A and interacts with eIF3 (Hinnebusch 2006). There is no mention of interactions between eIF2B and eIF4B in the current literature, and, therefore, it could be potentially interesting to look at more carefully.

2.1.5 ISRIB stabilizes eIF2B

Encouraged by the idea of ISRIB's stabilizing effect on eIF2B complex observed by (Sidrauski et al. 2015) and ourselves (Figure 2.1.4d), we set out to explore this idea further and conducted more in vitro experiments.

To observe changes in migration of the full endogenous eIF2B complex untreated or treated with ISRIB, we performed analytical centrifugation experiments similarly to the ones described previously (Sidrauski et al. 2015). We tracked migration of 3xFlag-tagged human eIF2Bβ from HeLa cell lysates and 3xFlag-tagged hamster eIF2Bγ subunit from CHO cell lysates (described in Section 2.1.3) through a density gradient under low and high (facilitating dissociation of eIF2 complex) salt conditions, untreated or treated with ISRIB. Addition of ISRIB under low salt condition did not affect migration of the main eIF2B peak fraction in neither of cell lines (Figure 2.1.5a left panels, fraction 11), but the peak itself got sharpened, and signal from LMW species became more faint (Figure 2.1.5a left panels). When we increased salt concentration we saw a conspicuous shift of eIF2B treated with ISRIB towards HMW species in both cell lines (Figure 2.1.5a right panels) in concordance with the published results (Sidrauski et al. 2015). Both of these observations (under low and high salt conditions) could be either reflective of native cell conditions, or of the potentially destabilizing nature of the analytical procedure itself. The noted stabilizing effect of ISRIB on eIF2B complex could, thus, be due to a change in subunits composition of eIF2B, or conformational change that

eIF2B might undergo upon treatment with ISRIB making it less flexible, i.e. more stable.

In an attempt to confirm the observed stabilizing effect of ISRIB on eIF2B, we decided to implement a different analytical method. We applied CHO cell lysates bearing endogenous 3xFlag-tagged eIF2Bγ on a native PAGE gel, and immunoblotted it with anti-FLAG M2 antibodies (Figure 2.1.5b left panel). We observed a specific signal arising from anti-FLAG M2 antibodies, as judged by the absence of such when immunoblotting non-tagged parental CHO cell lysates (Figure 2.1.5b left panel, compare lanes 1-3 to 4-6). We then repeated the experiment comparing untreated and ISRIB-treated tagged CHO cells (Figure 2.1.5b right panel). We hoped to improve the resolution of the signal by using various detergents. However, none of the conditions tested were of benefit, and it was hard to judge whether we see any difference between migration of untreated and ISRIB-treated species (Figure 2.1.5b, right panel). To learn if ISRIB could evoke any change in the migration of the purified eIF2B complex, we applied purified human eIF2B protein (described in Section 2.1.3) untreated or ISRIB-treated on a native PAGE gel, and stained it with Coomassie. Even though we could track quite clearly migration of the purified eIF2B complex, possibly its decameric form (as judged by its SEC profile in Figure 2.1.3a), no change to eIF2B's migration pattern was observed when treated with ISRIB (Figure 2.1.5c). We, therefore, concluded that the method of native PAGE might not be very suitable for observing effect of ISRIB on native eIF2B in cell lysates, and maybe not sensitive enough to resolve different conformations of purified eIF2B if such exist.

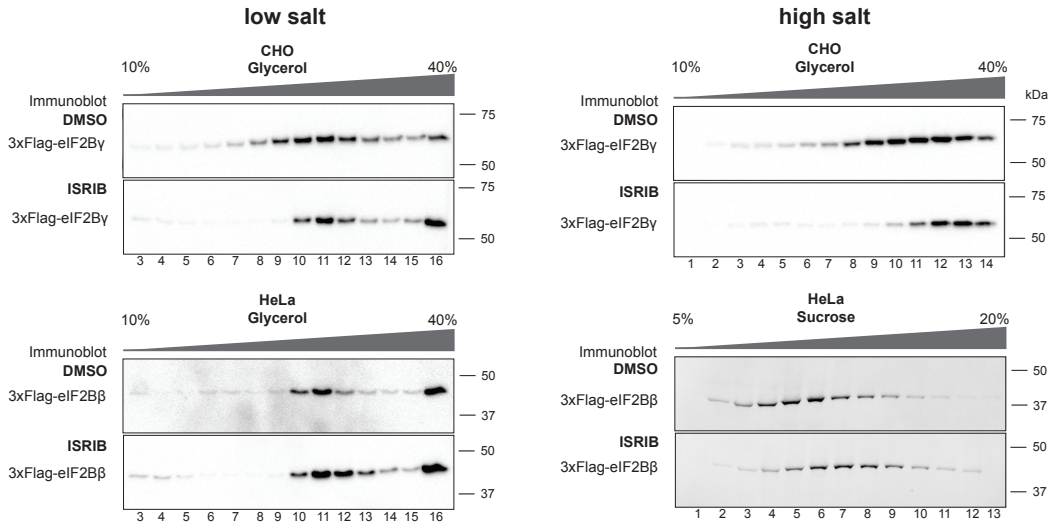

Figure 2.1.5a: Stabilization of endogenous eIF2B across analytical gradient.

Immunoblots of 3xFlag-tagged eIF2Bγ and eIF2Bβ detected with anti-FLAG M2 antibodies in CHO and HeLa cell lysates (described in Section 2.1.3), respectively, treated with DMSO (top panels) or ISRIB (200 nM) (bottom panels), and resolved on a 10-40% glycerol gradient or on a 5-20% sucrose density gradient, as indicated. Left: comparison of migration of hamster and human eIF2B under low (150 mM) salt conditions. Note that upon ISRIB treatment the peak fraction (fraction 11) does not shift position, however, the peak itself becomes sharper. Right: comparing CHO and HeLa lysates under high (500 mM) salt conditions. Note that upon ISRIB treatment the main peak fractions shift towards the HMW species. Experiments performed once. Executed by H. P. Harding and A. Zyryanova, University of Cambridge.

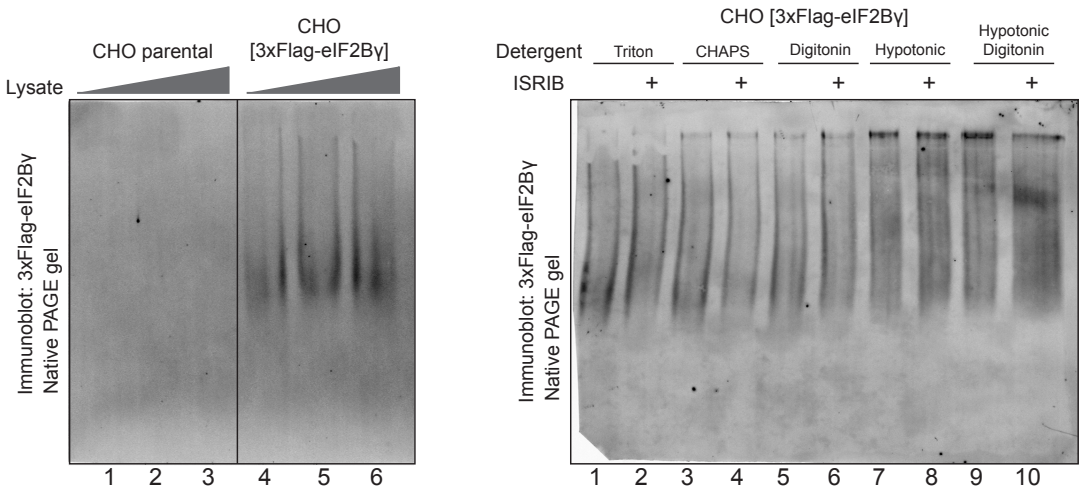

Figure 2.1.5b: Effect of ISRIB on a native endogenous eIF2B in cells.

Left: immunoblot of native 3xFlag-tagged eIF2Bγ detected with anti-FLAG M2 antibodies in increasing concentrations of parental (lanes 1-3) or tagged CHO cell lysates (lanes 4-6) (described in Section 2.1.3) resolved on a native PAGE gel, and showing the specificity of the signal. Right: the same but only for one concentration of tagged CHO cell lysate tested across various detergents, and treated with DMSO or ISRIB (2 μM), as indicated. No obvious effect of ISRIB on the migration of native 3xFlag-eIF2Bγ species in cell lysates was observed. Executed by A. Zyryanova, University of Cambridge.

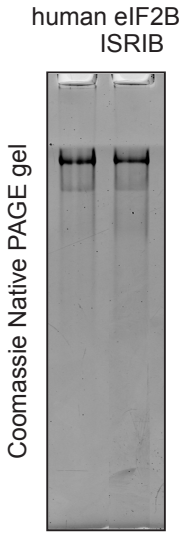

Figure 2.1.5c: Effect of ISRIB on a purified native endogenous eIF2B.

Coomassie-stained native PAGE gel of a purified human eIF2B protein (described in Section 2.1.3) treated with DMSO or ISRIB (10 μM). No obvious effect of ISRIB on migration of native purified eIF2B was observed. Executed by A. Zyryanova, University of Cambridge.

2.1.6 ISRIB binds directly to purified mammalian eIF2B

To observe ISRIB's interaction with eIF2B directly, we [1] designed a fluorescently labeled derivative (AAA2-101, Section 2.1.1) based on the known structure–activity relationships of ISRIB analogues reported by (Hearn et al. 2016), and also established by ours and Peter Fischer's groups (University of Nottingham) (partial data presented in Section 2.1.1).

Using this compound, we measured the effect of added purified eIF2B on the fluorescence polarization (FP) signal. FP increased with increasing concentrations of eIF2B (Figure 2.1.6a). At the concentrations of eIF2B available for testing, the FP signal was not saturated, thus, we were unable to extract a reliable dissociation constant from this assay. Unlabeled ISRIB, however, effectively competed for eIF2B in the FP assay with an EC_{50} in the nanomolar range, as observed for ISRIB action in cells (Figure 2.1.6b and figure 2.1.1f), whilst less active congeners competed less successfully (Figure 2.1.6c and figure 2.1.1f). The FP assay, thus, likely reported on engagement of the FAM-labeled ISRIB derivative at a site(s) on eIF2B that is relevant to ISRIB action.

[1] Design and synthesis by A. A. Alard, C. Fromont and P. Fischer, University of Nottingham

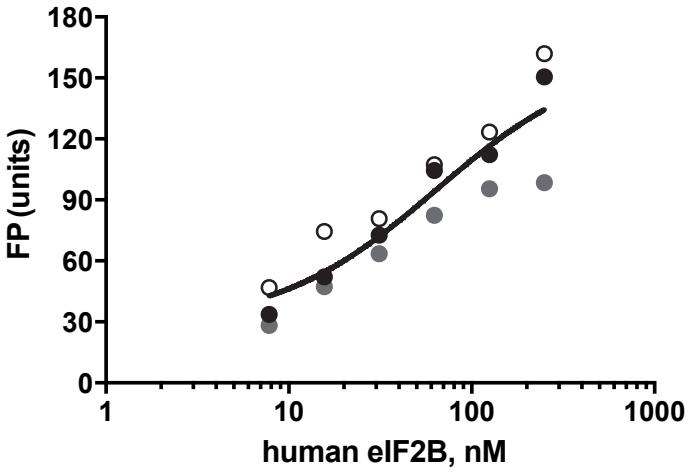

Figure 2.1.6a: Binding of ISRIB to human eIF2B.

Fluorescence polarization (FP) assays showing binding of ISRIB to human eIF2B. A plot of the FP signal arising from fluorescein-labeled ISRIB analogue (2.5 nM AAA2-101, Figure 2.1.1e,) as a function of the concentration of eIF2B in the sample. Concentrations of eIF2B are represented on a $\log_{10}$ scale. Curve fitting and EC_{50} was generated using agonist vs. response function on GraphPad Prism. Shown are values of three independently acquired measurements. Executed by A. Zyryanova, University of Cambridge.

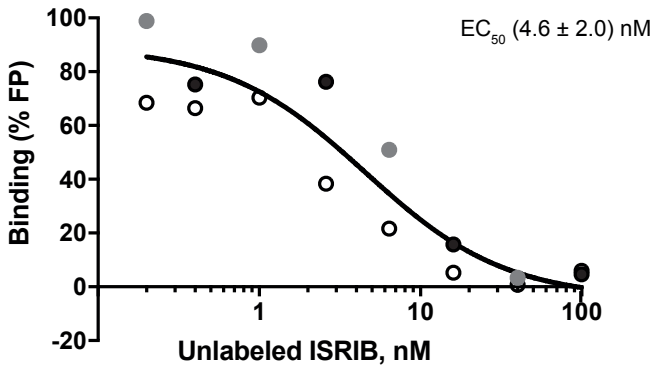

Figure 2.1.6b: Competition between labeled and unlabeled ISRIB for binding human eIF2B.

Plot of the relative FP signal arising from samples with fluorescein-labeled AAA2-101 (2.5 nM, Figure 2.1.1e) bound to purified human eIF2B (30 nM) in the presence of the indicated concentration of unlabeled *trans*-ISRIB introduced as a competitor. Concentrations of ISRIB on respective plots are represented on a $\log_{10}$ scale. Shown is a mean EC_{50} ± SD for three independently acquired measurements. Curve fitting, EC_{50}, and SD were generated using agonist vs. response function on GraphPad Prism. Executed by A. Zyryanova, University of Cambridge.

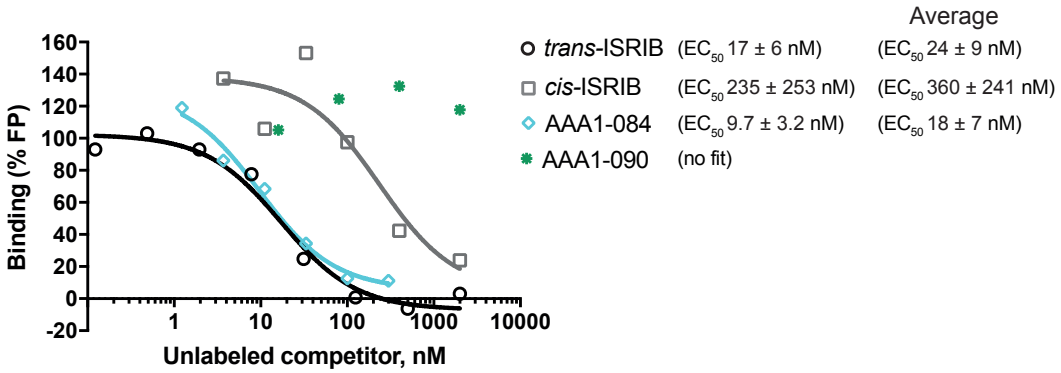

Figure 2.1.6c: Competition of labeled ISRIB with ISRIB analogues for binding human eIF2B.

Plot of the relative FP signal arising from samples with fluorescein-labeled AAA2-101 (100 nM, Figure 2.1.1e) bound to purified human eIF2B (250 nM) in the presence of the indicated concentration of unlabeled ISRIB analogues (Figure 2.1.1e) introduced as competitors. Shown is a representative from three independent experiments. Indicated are EC_{50} ± SD for the experiment and mean EC_{50} ± SD for n=3. Concentration of inhibitor is represented on a $\log_{10}$ scale. Curve fitting, EC_{50}, and SD were generated using agonist vs. response function on GraphPad Prism. Executed by A. Zyryanova, University of Cambridge.

2.1.7 Summary of Section 2.1

1) ISRIB and its derivatives can inhibit the ISR in live cells (Figures 2.1.1a, f); 2) ISRIB directly binds eIF2B (Figures 2.1.6a, b and c) and affects its GEF activity in vitro (Figures 2.1.3d, e); 3) ISRIB does not disrupt regulatory interactions between eIF2B and eIF2(αP), however, it may promote catalytic contacts between eIF2B and eIF2 (Figures 2.1.2c, e); 4) ISRIB does not promote association of eIF2B with other translational factors (Figures 2.1.4d); 5) ISRIB may have a stabilizing effect on eIF2B's subunits composition (Figures 2.1.4d and figure 2.1.5a).

2.2 Cryo-EM reveals an ISRIB binding pocket in eIF2B

2.2.1 Overall human eIF2B structure and resolution

After gathering evidence that ISRIB might directly bind to eIF2B and affect eIF2B's GEF activity, we decided to learn the molecular basis of ISRIB's mechanism. Since at the time the only available eIF2B-related complexes solved by X-ray crystallography were the human α_2 dimer (Hiyama et al. 2009) and the *C. thermophilum* $(\beta\delta)_2$ regulatory subcomplexes (Kuhle et al. 2015), we set out to obtain a structure of full human eIF2B complex bound to ISRIB by methods of cryo-electron microscopy (cryo-EM) and single particle analysis (SPA) (the complete *S. pombe* eIF2B decamer structure (Kashiwagi et al. 2016) appeared in the literature after we obtained our first density maps).

We purified endogenous human eIF2B from HeLa cell lysates (described in Section 2.1.3) in the presence of ISRIB (Figure 2.2.1a) and determined the structure of the ISRIB-eIF2B complex at an overall resolution of 4.1-Å (Figure 2.2.1b) (for details of data collection and processing refer to Section 4.12 and table 4.12.3b). We[2] also measured ISRIB contents in the final sample applied onto grids to assess the occupancy of the eIF2B complex with ISRIB (data not shown). It is interesting to note that only 20% of eIF2B was occupied by ISRIB which correlates with the fraction of the particles used for the 3D model building of the complex (Figure 4.12.2c). The fact that ISRIB-bound eIF2B was the only class that was representative enough to build a 3D density map is consistent with the idea of ISRIB stabilizing eIF2B.

[2] Liquid chromatography-tandem mass spectrometry performed by Dr. Catharine Ortori and Prof. David Barrett from the University of Nottingham

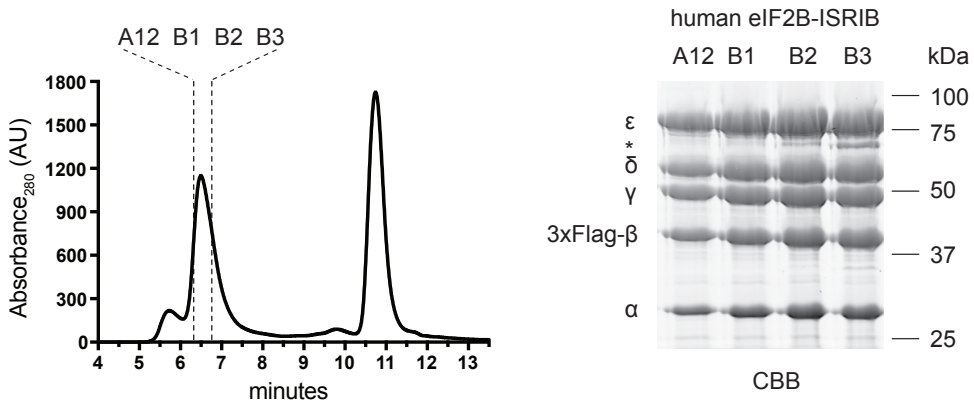

Figure 2.2.1a: Purification of human eIF2B with ISRIB.

Left: chromatogram of the endogenous human eIF2B bearing 3xFlag-tag at the N-terminus of eIF2Bβ subunit (described in Section 2.1.3 and section 4.8.2), purified from HeLa cells in the presence of ISRIB (200 nM) using anti-FLAG M2 affinity resin, and resolved by size exclusion chromatography on a SEC-3 300 Å chromatography column. Right: the indicated fractions from SEC run (left) analyzed on a Coomassie-stained SDS-PAGE gel (*PRMT5 – a contaminant) and used for structural analysis. Generation of cell line and purification of the protein was executed by A. Zyryanova, University of Cambridge.

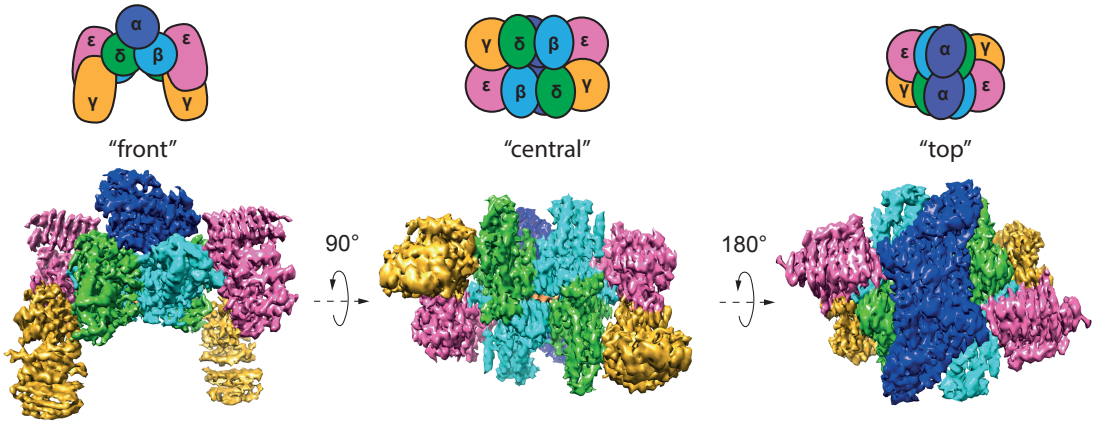

Figure 2.2.1b: cryo-EM map of ISRIB-bound human eIF2B.

Shown are representative views of the cryo-EM map of the ISRIB-bound decameric human eIF2B complex (EMDB: EMD-4162). Density is colored according to the subunits architecture indicated in the cartoons on the top: α – blue, β – cyan, δ – green, γ – gold, ε – pink, ISRIB - orange. The experimental density was generated by F. Weis using RELION software (MRC LMB), Laboratory of Molecular Biology. The structural model was assembled by A. Faille using Coot software, and the figure was made by A. Zyryanova using Chimera software (UCSF), University of Cambridge.

The local resolution of the map varies from 3.7 Å in the core to >6 Å at the periphery (Figure 2.2.1c). In particular, the resolution of the γ and ε human catalytic subcomplex was lower compared to the regulatory core, consistent with flexibility of this region in both human and yeast eIF2B structures (Kashiwagi et al. 2016). Similar to the *S. pombe* eIF2B crystal structure, we were unable to resolve the catalytically important C-terminal HEAT domain of the ε subunit in our cryo-EM map. Within the β and δ regulatory core, in the most central part of the map, protein side chains are clearly resolved, resulting in a near complete atomic model (Figure 2.2.1d).

Due to lack of sufficient high-quality cryo-EM images of an apo-eIF2B complex, we were unable to calculate a difference map of eIF2B with and without ISRIB. However, a nearly continuous density with a shape and size of a single ISRIB molecule was conspicuously present at the interface of the β and δ regulatory subunits. The quality of the map in this position provided sufficient detail to confidently model the ISRIB molecule (Figure 2.2.1e).

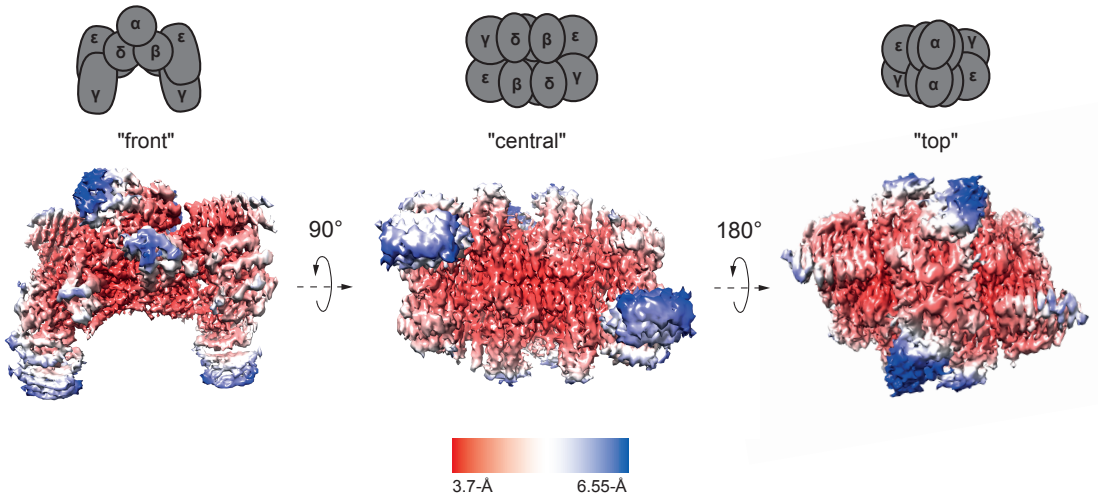

Figure 2.2.1c: Resolution of cryo-EM map of ISRIB-bound eIF2B.

Shown is a cryo-EM density map colored according to local resolution for the ISRIB-bound eIF2B complex. The highest resolution is at the core of the $(\beta\delta)_2$ dimer interface where the putative density of ISRIB was detected. The red-blue palette covers resolution range from 3.70 Å to > 6.55 Å. The local resolution map was generated by A. Faille using RELION software (MRC LMB), and the figure was assembled by A. Zyryanova using Chimera software (UCSF), University of Cambridge.

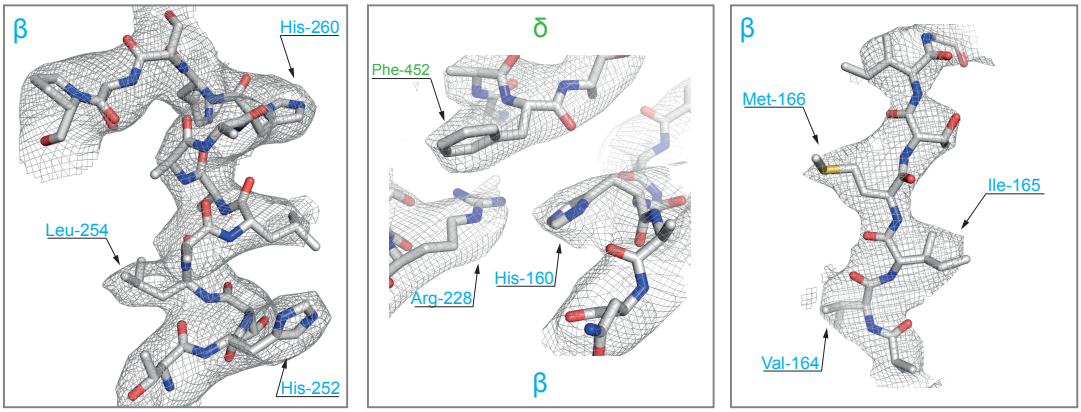

Figure 2.2.1d: High-resolution of eIF2B's side-chains.

Shown is representative density depicted as a mesh around the eIF2B atomic model including well-resolved side chains from the core of $(\beta\delta)_2$ dimer interface. Individual residues of β (blue) and δ (green) subunits are labeled for reference. Generated by A. Faille using Chimera software (UCSF), University of Cambridge.

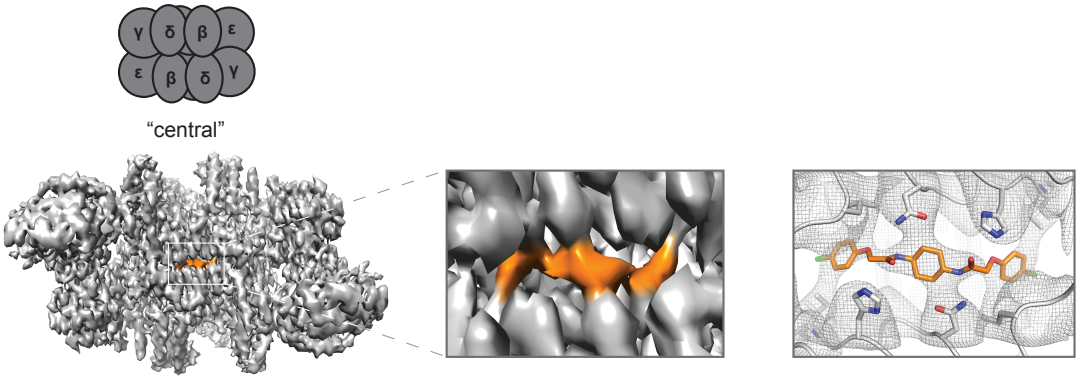

Figure 2.2.1e: ISRIB density identified on cryo-EM map.

Shown is a cryo-EM map of human eIF2B (in grey) bound to ISRIB (in orange) (“central” view as in Figure 2.2.1a). Two close-ups: density corresponding to ISRIB (orange) at the $(\beta\delta)_2$ dimer interface, and atomic model of $(\beta\delta)_2$ dimer interface with ISRIB (orange sticks) superimposed onto density in mesh. Generated by A. Faille using Chimera software (UCSF), University of Cambridge.

2.2.2 ISRIB-binding pocket

The ISRIB binding pocket is located at the plane of symmetry between the β and δ subunits (Figure 2.2.2a). In the central part of the pocket, residue H188 of the β subunit is notable, as its side chain is positioned in the vicinity of the essential carbonyl moiety of ISRIB (Hearn et al. 2016). Residue N162 of the β subunit also stabilizes the diaminecyclohexane moiety of ISRIB, possibly through hydrogen bonding interactions. More distally in the pocket, various residue side chains – namely δL179 (the human counterpart of ISRIB sensitive hamster δL180), δF452, δL485, δL487, βV164, βI190, βT215, and βM217 – form the hydrophobic end of the symmetrical pocket that accommodates the aryl groups of ISRIB (Figure 2.2.2b). The observation that a hamster *Eif2b4*^{L180F} mutation (δL179 in the human) disrupts ISRIB action in cells (Sekine et al. 2015) is consistent with a clash between the bulkier side chain of phenylalanine and the bound ISRIB molecule (Figure 2.2.2b). The ISRIB binding site identified in the map is also consistent with the lack of a corresponding density in the *S. pombe* apo-eIF2B map (PBD: 5B04) (Kashiwagi et al. 2016).

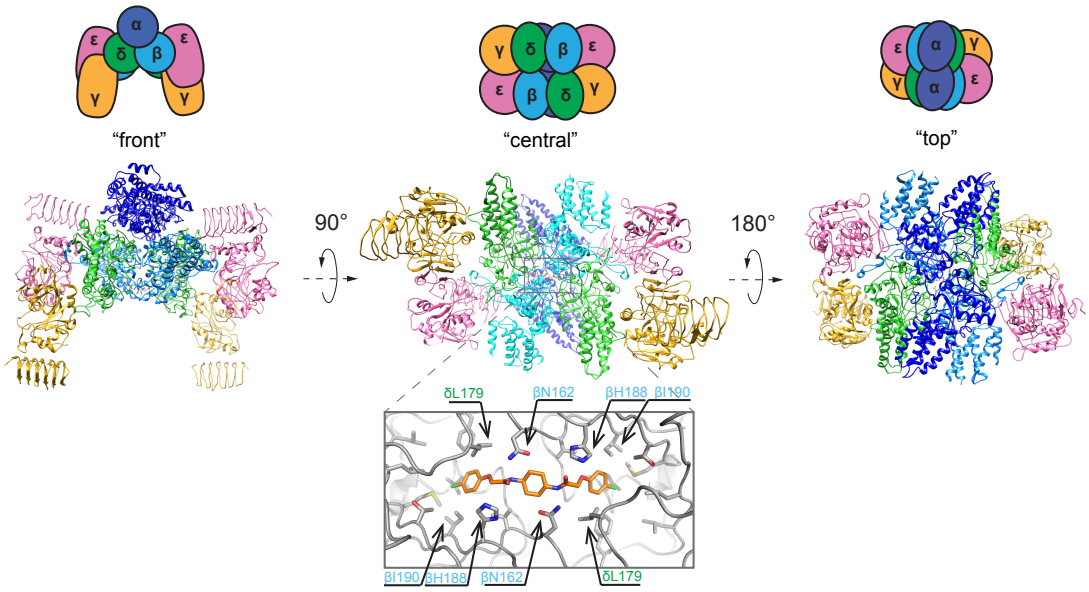

Figure 2.2.2a: Structural model of ISRIB-bound human eIF2B.

Ribbon representation of the ISRIB-bound decameric human eIF2B complex (PDB: 6EZO) colored according to the subunit architecture indicated in the cartoons: α – blue, β – cyan, δ – green, γ – gold, ε – pink, ISRIB - orange. Close-up of the "central" view is showing the ISRIB binding site. A single ISRIB molecule (orange sticks) is docked into the cavity at the $(\beta\delta)_2$ dimer interface. Residues βN162, βH188, βI190 and δL179 contacting ISRIB in the central part of the pocket from the β (blue) and δ (green) subunits are indicated. Structural model was generated by A. Faille using Coot software, and figure was assembled by A. Zyryanova using Chimera software, University of Cambridge.

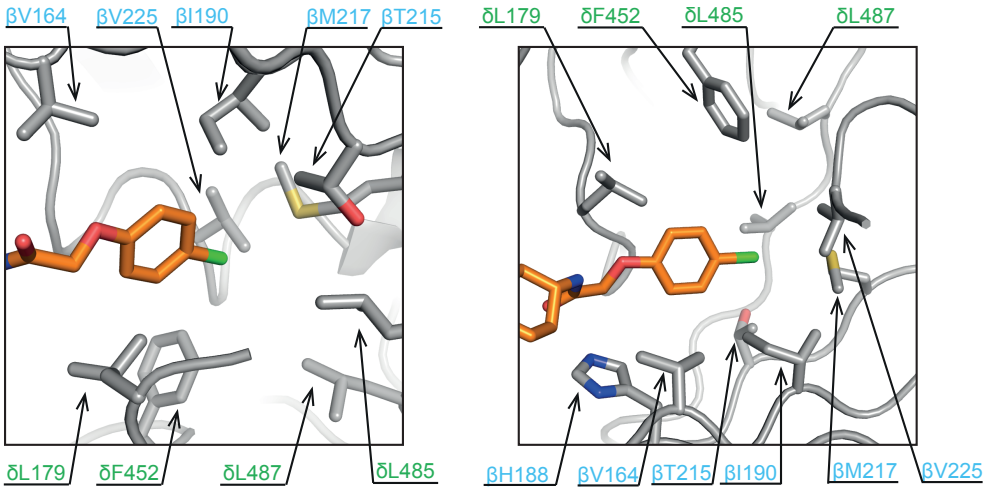

Figure 2.2.2b: Close-up of the hydrophobic end of the ISRIB-pocket.

Two views of the eIF2B complex core are presented, showing the symmetrically opposite sides of the pocket. The left panel view is from the solvent area looking at the core of the protein. The right panel is from the core looking at the solvent area. Residues making the hydrophobic end of the ISRIB pocket from the β (blue) and δ (green) subunits are indicated. Structural modeling was performed by A. Faille using Coot software, and figure was assembled by A. Zyryanova using Chimera software, University of Cambridge.

Overall the human and yeast structures are highly similar (r.m.s.d of 2.57 Å over 3049 alpha carbons) with no evidence of major domain movements that might be attributed to ISRIB binding in the human complex (Figure 2.2.2c). The region corresponding to the N-terminal ~166 residues of the human δ subunit remains unresolved (in both yeast and human structures) (Figure 2.2.2d). However, residues 167-204 of the human protein, which can be reliably placed in the density, assumed a very different conformation from the corresponding segment of the yeast δ subunit (Figure 2.2.2d). It is unclear if this difference reflects species-divergence in the structure of eIF2B, a crystallization-induced difference or is a consequence of ISRIB binding. It is noteworthy that this divergent region emerges from the putative ISRIB density at the $(\beta\delta)_2$ interface and that it contains two residues, human eIF2B δ R170 and V177, whose mutation interferes with ISRIB action in hamster cells, δ R171 and V178 (Figure 2.1.1c) (Sekine et al. 2015).

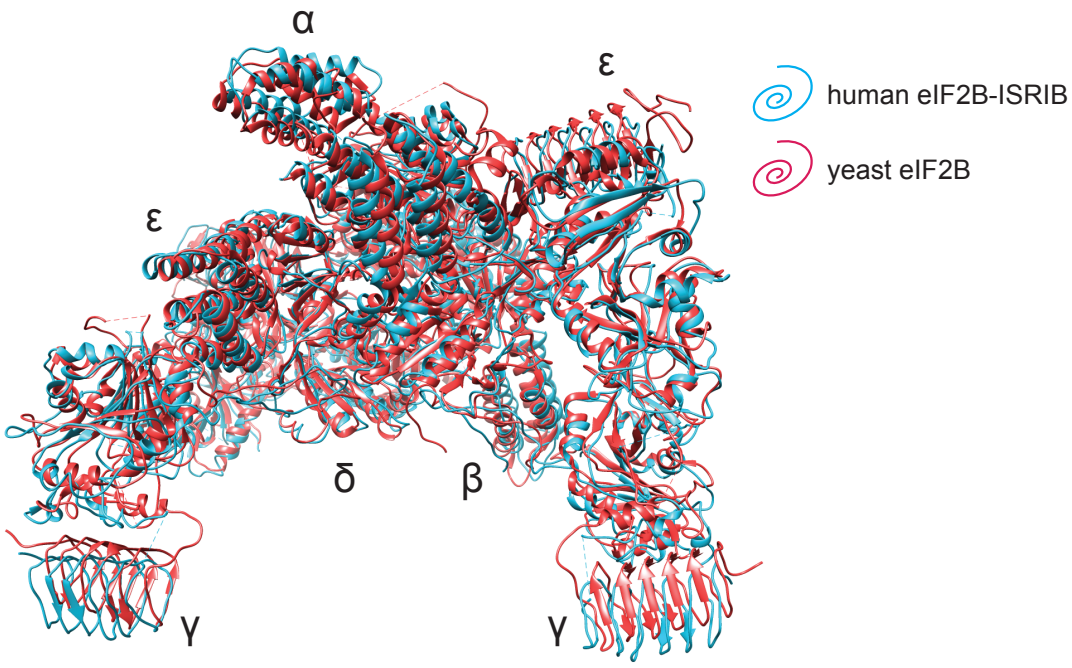

Figure 2.2.2c: Overall structural homology of human and yeast eIF2B.

Superimposition of ISRIB-bound human (cyan) (PDB: 6EZO) and yeast eIF2B (red) (PDB: 5B04) lacking bound ISRIB from the “front view” (as in Figure 2.2.2a), showing high convergence of the two species. Alignment was performed by A. Faille using Chimera software (UCSF), and figure was assembled by A. Zyryanova, University of Cambridge.

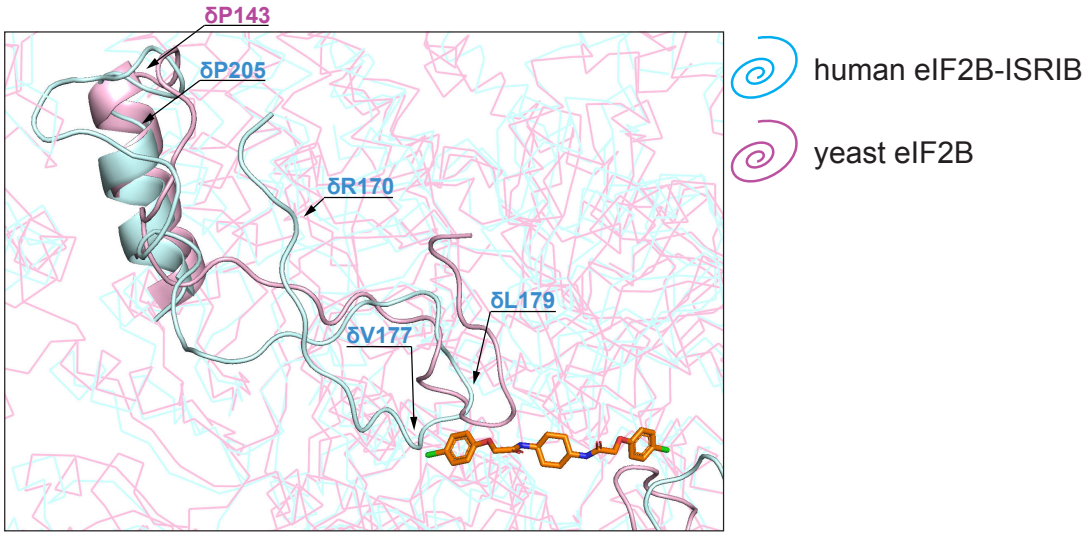

Figure 2.2.2d: Structural divergence of human and yeast eIF2B.

Cartoon showing the divergence in orientation of the N-terminal portion of the ISRIB-bound human δ subunit (residues 167-204, PDB: 6EZO, in cyan) and yeast δ subunit (residues 114-142, PDB: 5B04, in light magenta). Three residues (human δ R170, V177, L179 in cyan) important for ISRIB activity in cells (Sekine et al. 2015) and ISRIB (orange sticks) are indicated. Note the convergence of the structure at δ Proline 205 (human, in cyan)/ δ Proline 143 (yeast, in light magenta), which cap the closely-aligned helix I of the human and yeast eIF2Bδ. Alignment was performed by A. Faille using Chimera (UCSF), and figure was assembled by D. Ron using Chimera (UCSF), University of Cambridge.

2.2.3 Summary of Section 2.2

1) Human eIF2B is a dimer of pentamers where two catalytic (γε) dimers are flanking the regulatory, $\alpha_2(\beta\delta)_2$, hexameric core of the complex (Figure 2.2.1b and figure 2.2.2a); 2) ISRIB binds human eIF2B at the symmetrical $(\beta\delta)_2$ interface where four residues (βN162, βH188, βI190 and δ179) are potentially making critical contacts with the compound (Figure 2.2.2a); 3) No major conformational shifts were identified between ISRIB-bound human eIF2B and *apo*-yeast structures, except for a slightly different disposition of the eIF2Bδ N-terminus (Figure 2.2.2d).

2.3 Chemogenetic analysis of the putative ISRIB-binding pocket

2.3.1 Randomized CRISPR/Cas9 mutagenesis reveals ISRIB resistant mutants of the eIF2B β subunit

To validate the mode of ISRIB binding revealed by the structural data (Figure 2.2.2a), we decided to mutagenize the residues predicted by the model to line the ISRIB-binding pocket in hope of eliciting a correlation between amino acid substitutions and ISRIB's activity in such mutagenized cells.

To achieve this, we used CRISPR/ Cas9 to target the aforementioned *Eif2b2* locus of CHO-K1 cells, encoding β subunit of eIF2B, and provided a repair template randomized at *Eif2b2*^{N162}, *Eif2b2*^{H188} or *Eif2b2*^{I190} codons (Figure 2.3.1a). After mutagenesis, for each given codon (*Eif2b2*^{N162}, *Eif2b2*^{H188} or *Eif2b2*^{I190}), we obtained a pool of mutagenized cells represented by a mixture of clones bearing various codon substitutions, including a substitution to an original amino acid. We then performed a phenotypical screen and sorting of these mutagenized pools of cells exposed to an ISR inducer, histidinol (HIS), based on the activity of the CHOP::GFP reporter (described in Section 2.1.1).

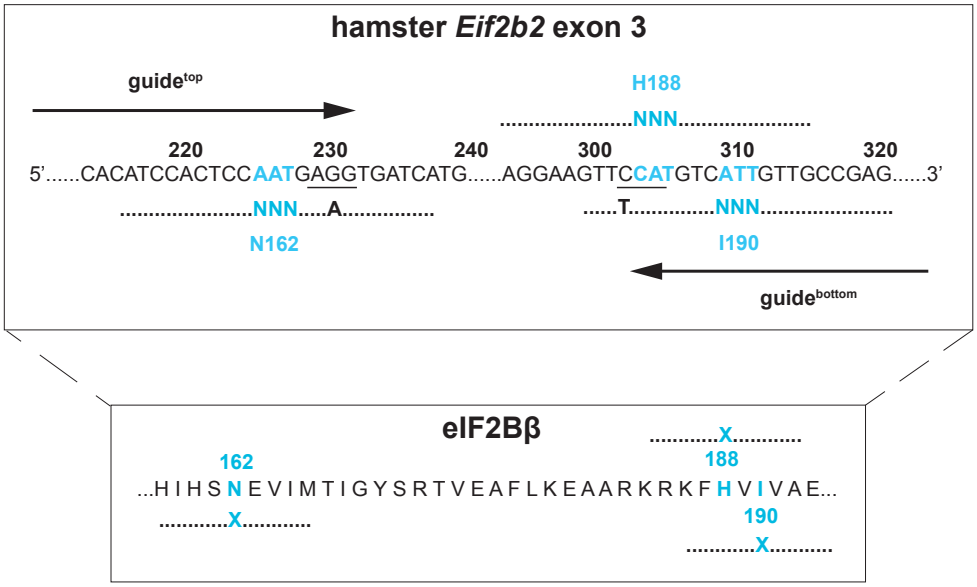

Figure 2.3.1a: Strategy for mutagenizing the ISRIB-binding pocket.

CRISPR/Cas9 directed mutagenesis of the hamster *Eif2b2* gene at the locus encoding ISRIB contact sites on the eIF2B β subunit revealed by the structure: N162, H188 or I190 (marked in cyan). Hamster *Eif2b2* exon 3 with the two RNA guides (top - for mutagenesis of N162, bottom - for H188 or I190) directing Cas9 to mediate double strand break, and the aligned single-strand repair templates are indicated. The randomized substitution of the original codon is marked (NNN, in blue), as are the silent mutations disrupting PAM sequence (underlined). Nucleotide numbering corresponds to GeneBank accession NW_003613913.1. Guides and templates were co-designed by D. Ron and A. Zyryanova. Cloning, cell cultures and mutagenesis was performed by A. Zyryanova, University of Cambridge.

In the first round of sorting (Figure 2.3.1b), HIS-treated, mutagenized pools of cells were segregated by phenotypic selection into ISRIB sensitive (ISRIB^{SEN}, CHOP::GFP inhibited, i.e. “GFP-dull”], and ISRIB resistant (ISRIB^{RES}, CHOP::GFP activated, i.e. “GFP-bright”) classes. In the second round of sorting (Figure 2.3.1b), untreated populations from the ISRIB^{SEN} and ISRIB^{RES} pools were purged of cells that had acquired a constitutively active ISR phenotype and, therefore, remained “GFP-bright” even under no HIS treatment. Thus, using fluorescence activated cell sorting (FACS), we successfully isolated ISRIB^{SEN} cells, in which ISR induction by HIS was readily counteracted by ISRIB, and ISRIB^{RES} cells, in which ISR induction was maintained upon ISRIB treatment (Figure 2.3.1c, note red traces). To determine which mutations were enriched in these phenotypically-distinguished pools, we subjected genomic DNA derived from each population to next generation sequencing (NGS) analysis (Figure 2.3.1d).

Mutagenesis of *Eif2b2*^{N162} (N162X) did not generate a pool of strongly ISRIB-resistant cells (Figure 2.3.1c, panels 1&2). This probably does not reflect the failure of the homologous recombination strategy since the incorporation of a silent PAM disrupting mutation (Figure 2.3.1a) enabled us to restrict the sequencing analysis to alleles that had successfully undergone homologous recombination. The high frequency with which the parental asparagine had been retained in both ISRIB^{SEN} and ISRIB^{RES} pools (82% and 44%, respectively) suggests that replacement of this residue is selected against (*Eif2b2* is an essential gene) (Figure 2.3.1d top panel and table). The only other residue, except the parental Asn, that was greatly enriched (26%) in the ISRIB^{RES} pool was threonine (Figure 2.3.1d top panel and table).

Targeting of *Eif2b2*^{H188} (H188X) was more successful, as ISRIB^{RES} pool of cells (Figure 2.3.1c panels 3&4) diverged dramatically from the parental sequence (Figure 2.3.1d middle panel and table). Of a total of 250,617 reads, collected for ISRIB^{RES} population, histidine was present in only 6,443 (2.6%), with arginine, glycine, leucine, lysine and glutamine dominating (24%, 21%, 18%, 8.2% and 6.2%, respectively) (Figure 2.3.1d middle panel and table). The design of the H188X repair template did not allow us to select for non-

targeted alleles in ISRIB^{SEN} cells, because PAM sequence was partially encoded by the repair codon itself (Figure 2.3.1a). Hence, histidine was largely preserved in the ISRIB^{SEN} pool (269,253 of 328,113 reads, 82%), which was constituted mainly of parental alleles that probably escaped targeting altogether and targeted alleles that had acquired a synonymous mutation (Figure 2.3.1d, middle panel and table). These observations point to the importance of histidine at position 188 of the β subunit in mediating ISRIB sensitivity. The bias in a favor of certain substitutions in the ISRIB^{RES} pool likely arises by their ability to preserve eIF2B function whilst eliminating responsiveness to ISRIB.

The ISRIB^{RES} pool of cells targeted at *Eif2b2*^{I190} (I190X) was also successful (Figure 2.3.1c panels 5&6) and dominated by tryptophan, methionine and tyrosine (28%, 24% and 15%, respectively) (Figure 2.3.1d bottom panel and table). This finding is consistent with a role for these bulky side chains in occluding the ISRIB binding pocket, in addition to the previously reported ISRIB^{RES} mutation (Sekine et al. 2015) (δL180F in hamster, δL179 in human) (Figures 2.2.2a, b). The relative enrichment of the parental isoleucine (14%) in ISRIB^{RES} pool probably indicates its not entirely pure phenotype (Figure 2.3.1c, panels 5&6). The ISRIB^{SEN} pool constituted largely of the original isoleucine (90%) (Figure 2.3.1d bottom panel and table). However, a slight enrichment of ISRIB^{SEN} pool in small residues, like valine (4.3%) and leucine (2.3%) (Figure 2.3.1d, bottom panel and table), could be of interest, since it may further support the link between ISRIB resistance and acquisition of bulky side chains in this locus.

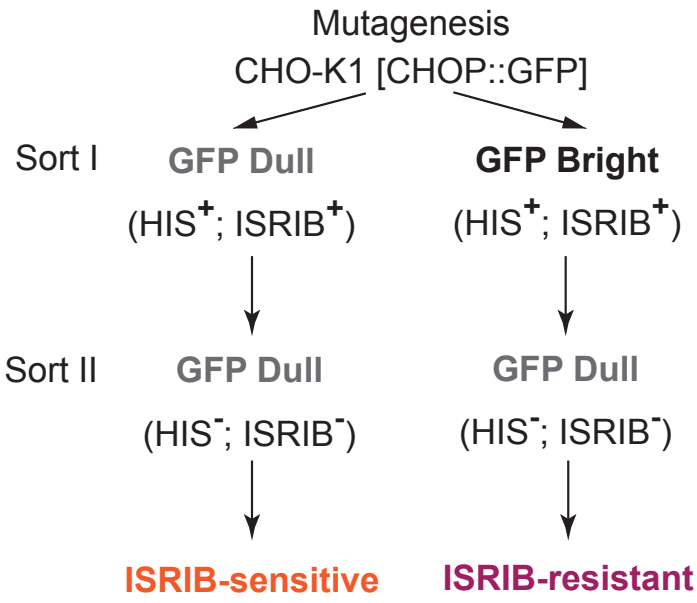

Figure 2.3.1b: Sorting strategy for ISRIB-sensitive and ISRIB-resistant clones.

Shown is a schema of selection for ISRIB-sensitive ($ISRIB^{SEN}$) and ISRIB-resistant ($ISRIB^{RES}$) cells (Sort I), and elimination of cells with constitutive ISR (Sort II) following CRISPR/Cas9 mutagenesis, based on the ISR-activated CHOP::GFP fluorescent reporter upon histidinol (HIS) treatment of CHO-K1 cells. Sorting strategy was co-designed by H. P. Harding and A. Zyryanova, cultures and treatments prepared by A. Zyryanova, operation of the FACSorter and collection of cells was executed by G. Grondys-Kotarba, C. Cossetti, R. Schulte, University of Cambridge.

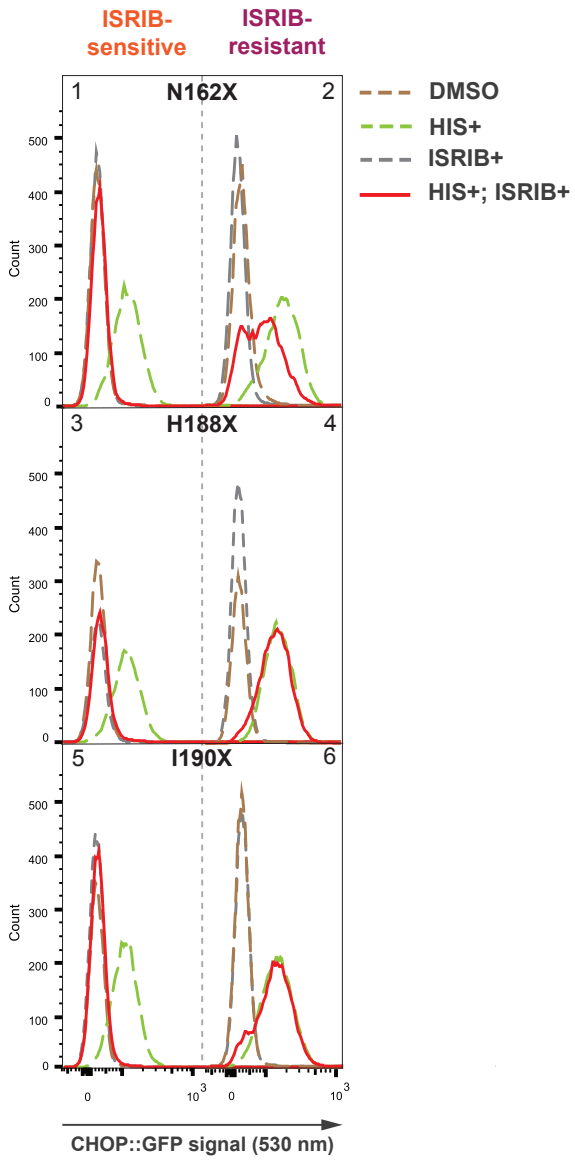

Figure 2.3.1c: Phenotypes of ISRIB-sensitive and ISRIB-resistant clones.

Histograms of the ISR-responsive CHOP::GFP fluorescent reporter activity induced by histidinol (HIS^+, 0.5 mM) in ISRIB-sensitive ($ISRIB^{SEN}$) (left panels) and ISRIB-resistant ($ISRIB^{RES}$) (right panels) pools of CHO-K1 cells selected for their responsiveness to ISRIB (200 nM) following CRISPR/Cas9-induced random mutagenesis of the indicated codon of *Eif2b2*. Cultures, treatments and phenotypical flow cytometry screens were performed by A. Zyryanova, University of Cambridge. Data analysis was done using FlowJo (LLC) software.

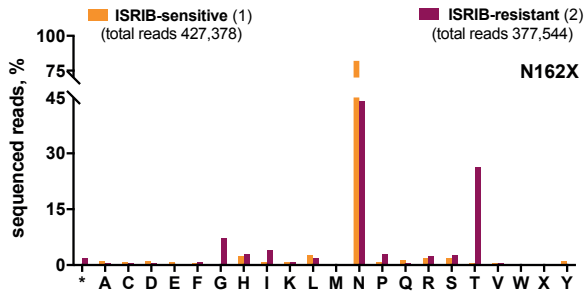

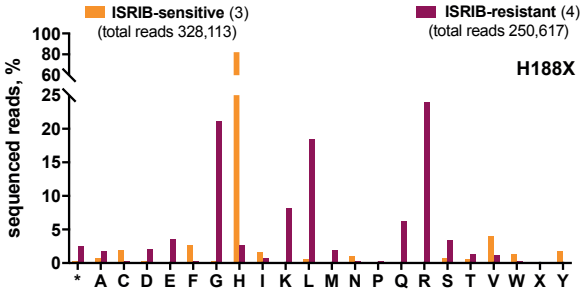

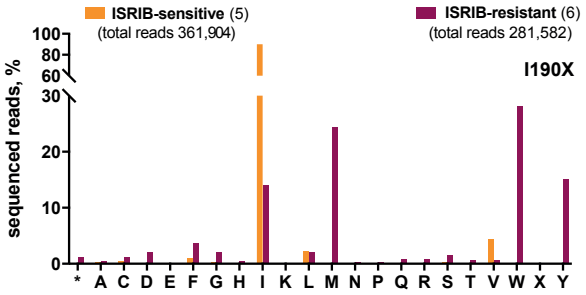

Amino Acid	N162X				H188X				I190X			
	ISRIB-SEN		ISRIB-RES		ISRIB-SEN		ISRIB-RES		ISRIB-SEN		ISRIB-RES	
	Reads	% Reads	Reads	% Reads	Reads	% Reads	Reads	% Reads	Reads	% Reads	Reads	% Reads
*	855	**0.20**	6575	**1.74**	1025	**0.31**	6215	**2.48**	340	**0.09**	3467	**1.23**
A	3953	**0.92**	1768	**0.47**	2248	**0.69**	4305	**1.72**	1106	**0.31**	1213	**0.43**
C	2429	**0.57**	1654	**0.44**	5992	**1.83**	716	**0.29**	1416	**0.39**	3145	**1.12**
D	3953	**0.92**	1436	**0.38**	662	**0.20**	5075	**2.03**	419	**0.12**	5912	**2.10**
E	2655	**0.62**	867	**0.23**	227	**0.07**	8902	**3.55**	426	**0.12**	574	**0.20**
F	2064	**0.48**	2798	**0.74**	8730	**2.66**	682	**0.27**	3363	**0.93**	10199	**3.62**
G	419	**0.10**	26632	**7.05**	965	**0.29**	52762	**21.05**	949	**0.26**	5716	**2.03**
H	9410	**2.20**	10487	**2.78**	269253	**82.06**	6443	**2.57**	208	**0.06**	1315	**0.47**
I	2804	**0.66**	14912	**3.95**	4980	**1.52**	1749	**0.70**	326077	**90.10**	39307	**13.96**
K	3520	**0.82**	2809	**0.74**	499	**0.15**	20494	**8.18**	139	**0.04**	359	**0.13**
L	10772	**2.52**	7055	**1.87**	1794	**0.55**	46099	**18.39**	8405	**2.32**	5827	**2.07**
M	1211	**0.28**	724	**0.19**	350	**0.11**	4795	**1.91**	192	**0.05**	68523	**24.34**
N	350813	**82.08**	165829	**43.92**	3058	**0.93**	668	**0.27**	398	**0.11**	770	**0.27**
P	2485	**0.58**	11242	**2.98**	425	**0.13**	648	**0.26**	331	**0.09**	947	**0.34**
Q	5727	**1.34**	1589	**0.42**	443	**0.14**	15550	**6.21**	207	**0.06**	2403	**0.85**
R	7597	**1.78**	8707	**2.31**	411	**0.13**	59827	**23.87**	548	**0.15**	2188	**0.78**
S	8007	**1.87**	9712	**2.57**	2208	**0.67**	8331	**3.32**	829	**0.23**	4443	**1.58**
T	2143	**0.50**	99150	**26.26**	1737	**0.53**	3153	**1.26**	452	**0.12**	1932	**0.69**
V	1721	**0.40**	2101	**0.56**	13035	**3.97**	2950	**1.18**	15627	**4.32**	1749	**0.62**
W	428	**0.10**	142	**0.04**	4038	**1.23**	618	**0.25**	147	**0.04**	79154	**28.11**
X	253	**0.06**	209	**0.06**	329	**0.10**	256	**0.10**	63	**0.02**	48	**0.02**
Y	4159	**0.97**	1146	**0.30**	5704	**1.74**	379	**0.15**	262	**0.07**	42391	**15.05**
Total Reads	**427378**		**377544**		**328113**		**250617**		**361904**		**281582**	

(continued on the next page)

Figure 2.3.1d: Distribution of residues in the mutagenized β subunit of eIF2B in ISRIB-sensitive and ISRIB-resistant cells.

Shown are bar graphs of the distribution of residues identified at the indicated positions of mutagenized *Eif2b2*, analyzed by the next generation sequencing (NGS). Shown is the number of sequenced reads in ISRIB^{SEN} pools (orange bars) or ISRIB^{RES} pools (plum bars) encoding each amino acid (* - stop codon, X – ambiguous sequence). NGS strategy was co-designed, co-executed, and data co-analyzed by H. P. Harding and A. Zyryanova, University of Cambridge. Extraction of sequenced data was done by F. Allen, Wellcome Sanger Institute.

I should also note that drawing a link between the selected residues and the acquired phenotypes cannot be as straightforward. The nature of the conducted NGS analysis does not allow us to pair up the alleles, hence, we cannot make any statements as to which are the dominant mutations, unless we clone out the pools or reproduce each individual mutation separately. Another consideration should be taken with regards to the results of the screen since we are working with live cells. This kind of mutagenesis may put selective pressure on cells permitting only those substitutions that are best tolerated by the cell, thus, negatively selecting for some residues that could potentially evoke ISRIB^{RES} or ISRIB^{SEN} phenotypes, and making those residues under-represented in our screen.

2.3.2 ISRIB analogues alter sensitivity of ISRIB resistant mutants targeted at *Eif2b*^{H188}

The finding of ISRIB^{RES} mutations suggests that they may exert their effect by altering the character of an ISRIB-binding pocket. Therefore, it may be possible to adapt ISRIB molecule to the new mutated environment of the ISRIB-pocket. To examine this idea, we tested pools of ISRIB^{RES} cells for their responsiveness to ISRIB analogues, using the CHOP::GFP inhibition assay (described in Section 2.1.1).

Compounds AAA1-075B (075B) and AAA1-084 (084) (Figure 2.1.1e) are 3- to 11-fold less potent than ISRIB in inhibiting the ISR of wildtype and ISRIB^{SEN} H188X pool (targeted at *Eif2b2*^{H188}) (Figure 2.1.1f and figure 2.3.2a, left panel). However, both compounds were relatively more potent than ISRIB in reversing the ISR of the ISRIB^{RES} pool of H188X cells (targeted at *Eif2b2*^{H188}), attainting nearly complete inhibition (60-70%) when applied at micromolar concentration (Figure 2.3.2a, right panel). The faint biphasic response of the mutant ISRIB^{RES} H188X pool to ISRIB is reproducible but currently lacking an explanation.

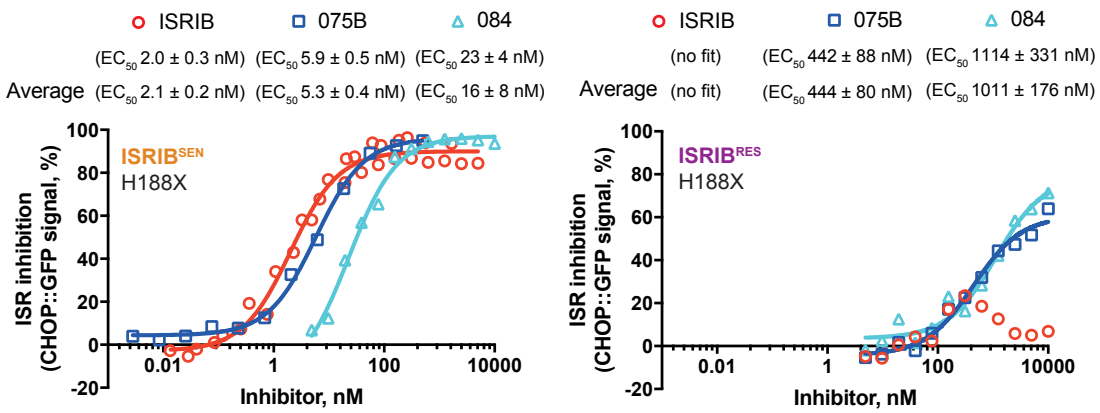

Figure 2.3.2a: ISRIB-resistant cells respond to ISRIB analogues.

Graphs showing inhibition of the ISR-activated CHOP::GFP reporter by ISRIB or two related analogues, compound AAA1-075B (075B) and compound AAA1-084 (084), in ISRIB^{SEN} (left) and ISRIB^{RES} (right) mutant pools of *Eif2b2*^{H188X} (as in Figure 2.3.1c panels 3&4). Shown is a representative from three independent experiments for each of the compounds. Indicated are EC_{50} ± SD for the experiment and mean EC_{50} ± SD for n=3. Concentration of inhibitor is represented on a log_{10} scale. Curve fitting, EC_{50}, and SD were generated using agonist vs. response function on GraphPad Prism. Cultures were co-maintained, treatments were co-administered and flow cytometry was co-performed by A. Crespillo-Casado and A. Zyryanova, University of Cambridge. Analysis of phenotypical data and figures assembly was done by A. Zyryanova using FlowJo (LLC) software.

To consolidate the aforementioned findings, we set out to perform a new round of FACSorting on ISRIB^{RES} H188X pool to select for sub-pools that retained their sensitivity to ISRIB (ISRIB^{SEN}, CHOP::GFP inhibited, “GFP dull”) or acquired sensitivity to ISRIB analogues 075B or 084 (075B^{SEN} or 084^{SEN}, CHOP::GFP inhibited, “GFP dull”) (Figure 2.3.2b). We also selected for another ISRIB^{RES} sub-pool without activating the CHOP::GFP channel, to serve as a control population of the original ISRIB^{RES} H188X pool (Figure 2.3.2b). As before, we then assessed the phenotypes of the collected sub-pools and sequenced their *Eif2b2* alleles using NGS analysis (Figure 2.3.2c, d).

As expected, sorting for ISRIB sensitivity enriched by over 20-fold for those rare wildtype H188 alleles that persisted the pool of ISRIB^{RES} H188X cells (Figure 2.3.2d, compare plum to orange bars). H188 was also somewhat enriched (about 5-fold) in the pools sorted for their sensitivity to compounds 075B (075B^{SEN}) or 084 (084^{SEN}) (Figure 2.3.2d, compare blue and cyan bars to plum bars). However, unlike the ISRIB^{SEN} pool, 075B^{SEN} and 084^{SEN} pools were also enriched for residues other than histidine (Figure 2.3.2d, compare blue and cyan bars). Importantly, selecting for sensitivity to these ISRIB analogues enriched for different residues than those found in the original ISRIB^{RES} pool, for e.g. arginine, glycine and leucine were depleted and replaced by lysine, serine, alanine and threonine (Figure 2.3.2d, compare blue and cyan bars to plum bars).

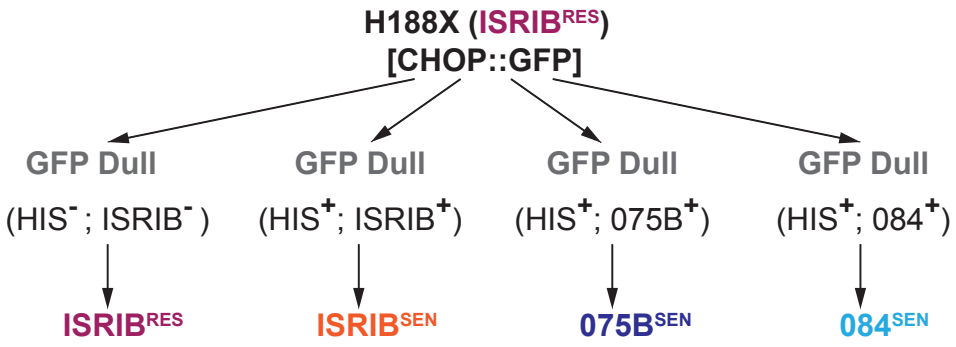

Figure 2.3.2b: Strategy for sorting ISRIB-resistant mutants sensitive to ISRIB analogues.

Shown is a schema of selection for ISRIB^{RES}, ISRIB^{SEN}, AAA1-075B sensitive (075B^{SEN}) and AAA1-084 sensitive (084^{SEN}) cells, based on the ISR-activated CHOP::GFP fluorescent reporter upon histidinol (HIS) treatment in *Eif2b2*^{H188X} mutant population. Sorting strategy was co-designed by H. P. Harding and A. Zyryanova, cultures and treatments prepared by A. Zyryanova, operation of the FACSorter and collection of cells was executed by G. Grondys-Kotarba, C. Cossetti, R. Schulte, University of Cambridge.

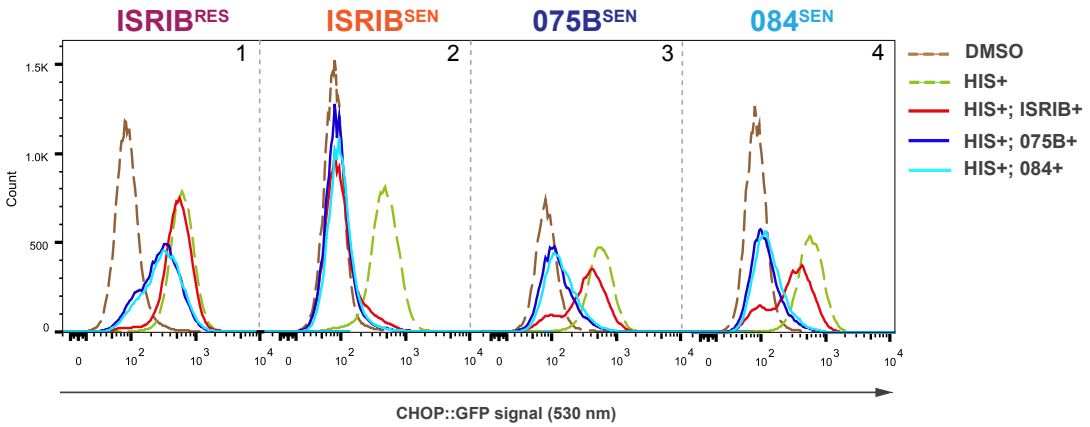

Figure 2.3.2c: Phenotypes of ISRIB-analogue sensitive cells.

Histograms of the activity of the ISR-responsive CHOP::GFP fluorescent reporter induced by histidinol (HIS^+, 0.5 mM) in $ISRIB^{RES}$, $ISRIB^{SEN}$, compound $075B^{SEN}$ and compound 084^{SEN} sub-pools selected for their responsiveness to ISRIB or respective analogues (2.5 μM) from a population of originally $ISRIB^{RES}$ *Eif2b2*^{H188X} mutant cells. Cultures, treatments and phenotypical flow cytometry screens were performed by A. Zyryanova, University of Cambridge. Data analysis was done using FlowJo (LLC) software.

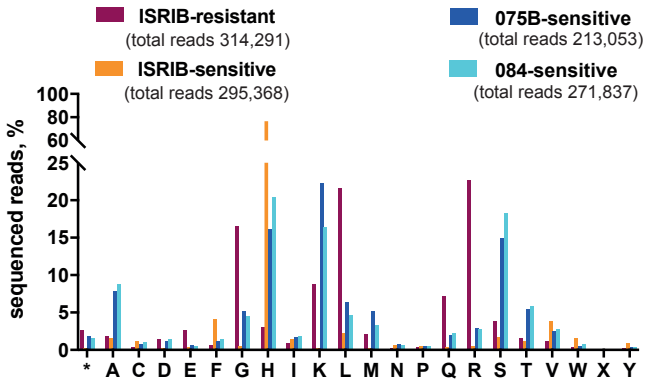

Amino Acid	H188X ISRIB-RES							
	ISRIB-RES		ISRIB-SEN		075B-SEN		084-SEN	
	Reads	% Reads	Reads	% Reads	Reads	% Reads	Reads	% Reads
*	8309	**2.64**	648	**0.22**	4001	**1.88**	4428	**1.63**
A	5809	**1.85**	4595	**1.56**	16814	**7.89**	23876	**8.78**
C	1346	**0.43**	3465	**1.17**	1687	**0.79**	2635	**0.97**
D	4608	**1.47**	797	**0.27**	2338	**1.10**	3892	**1.43**
E	8292	**2.64**	920	**0.31**	1228	**0.58**	1311	**0.48**
F	1776	**0.57**	12004	**4.06**	2450	**1.15**	3853	**1.42**
G	52131	**16.59**	1558	**0.53**	10887	**5.11**	12264	**4.51**
H	9311	**2.96**	226030	**76.53**	34473	**16.18**	55443	**20.40**
I	2684	**0.85**	4081	**1.38**	3612	**1.70**	4906	**1.81**
K	27535	**8.76**	803	**0.27**	47373	**22.24**	44470	**16.36**
L	67765	**21.56**	6498	**2.20**	13552	**6.36**	12728	**4.68**
M	6690	**2.13**	666	**0.23**	11051	**5.19**	8943	**3.29**
N	772	**0.25**	1915	**0.65**	1587	**0.75**	1816	**0.67**
P	1193	**0.38**	1520	**0.52**	1038	**0.49**	1298	**0.48**
Q	22530	**7.17**	1111	**0.38**	4152	**1.95**	6029	**2.22**
R	71454	**22.74**	1397	**0.47**	6097	**2.86**	7651	**2.82**
S	11841	**3.77**	4824	**1.63**	31921	**14.98**	49558	**18.23**
T	4857	**1.55**	3513	**1.19**	11650	**5.47**	15931	**5.86**
V	3537	**1.13**	11438	**3.87**	5317	**2.50**	7625	**2.81**
W	1177	**0.37**	4767	**1.61**	1123	**0.53**	2019	**0.74**
X	61	**0.02**	61	**0.02**	48	**0.02**	56	**0.02**
Y	613	**0.20**	2757	**0.93**	654	**0.31**	1105	**0.41**
Total Reads	**314291**		**295368**		**213053**		**271837**	

Figure 2.3.2d: Distribution of residues in the mutagenized β subunit of eIF2B in analogue-sensitive cells.

Bar graph of the distribution of residues identified at *Eif2b2* codon 188 in phenotypically divergent pools of CHO-K1 cells. The number of sequenced reads in ISRIB^{RES} (plum), ISRIB^{SEN} (orange), compound 075B^{SEN} (blue) and compound 084^{SEN} (cyan) pools encoding each amino acid (* - stop codon, X – ambiguous) is plotted. NGS strategy was co-designed, co-executed, and data co-analyzed by H. P. Harding and A. Zyryanova, University of Cambridge. Extraction of sequenced data was done by F. Allen, Wellcome Sanger Institute.

To examine more carefully the sensitivity of certain substitutions at position 188 of β subunit to ISRIB analogues, we decided to clone out one of the ISRIB^{RES} H188X sub-pools sensitive to either of ISRIB analogues from the latest experiment. We selected four clones from 084^{SEN} sub-pool with unambiguous genotypes (Figure 2.3.2e), and tested their sensitivity to ISRIB and compound 084 (Figure 2.3.2f). Clone A1 bearing parental wildtype *Eif2b2*^{H188} allele retained its responsiveness to both ISRIB and 084, as expected. However, responsiveness of the mutant clones (B3, A5 and A3) to ISRIB was greatly enfeebled, which can be noted in the shift to the right in the concentration-response curves and in the magnitude of inhibition observed at the highest concentration of compound (Figure 2.3.2f, red traces). Once again the biphasic response to ISRIB observed in the pools of mutagenized cells (Figure 2.3.2a) was also evident in the clonal populations (Figure 2.3.2f). A similar shift to the right was noted in the response of the mutant clones to compound 084, nonetheless, the ISR inhibitory effect observed at the higher concentration was reaching almost 90%, comparable to the wildtype clone (Figure 2.3.2f, blue traces). It should be noted that the selected clones bearing substitutions to lysine (clone B3), methionine (clone A5) and serine/ threonine (clone A3) were found amongst the most populated in the 084^{SEN} sub-pool, and also most divergent from the original ISRIB^{RES} H188X pool (Figure 2.3.2d, compare cyan to plum bars).

The observation of altered hierarchy of the potency of ISRIB analogs indicates that ISRIB^{RES} mutations, at position 188 of the β subunit, alter the binding properties of the ISRIB pocket. That notion argues against an allosteric effect of ISRIB binding elsewhere, and against of ISRIB^{RES} mutations disrupting communication between such ISRIB binding site and the relevant catalytic activity of eIF2B. Altogether these findings, however, support the validity of ISRIB binding at the $(\beta\delta)_2$ interface of eIF2B.

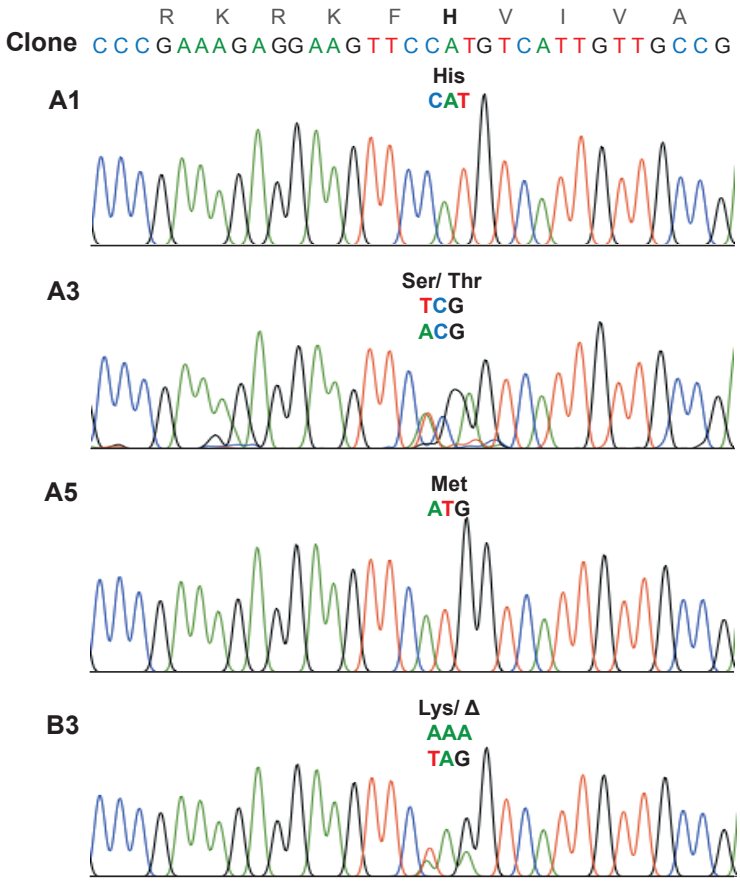

Figure 2.3.2e: ISRIB analogue-sensitive clones.

Traces of dye-termination sequencing reactions of PCR amplified *Eif2b2* exon 3 from indicated cell clones: A1 (parental, wt), A3 (H188S/ T), A5 (H188M), B3 (H188K/ Δ). H188 is highlighted. Cloning, screening, and data analysis was executed by A. Zyryanova using MacVector (Inc), University of Cambridge.

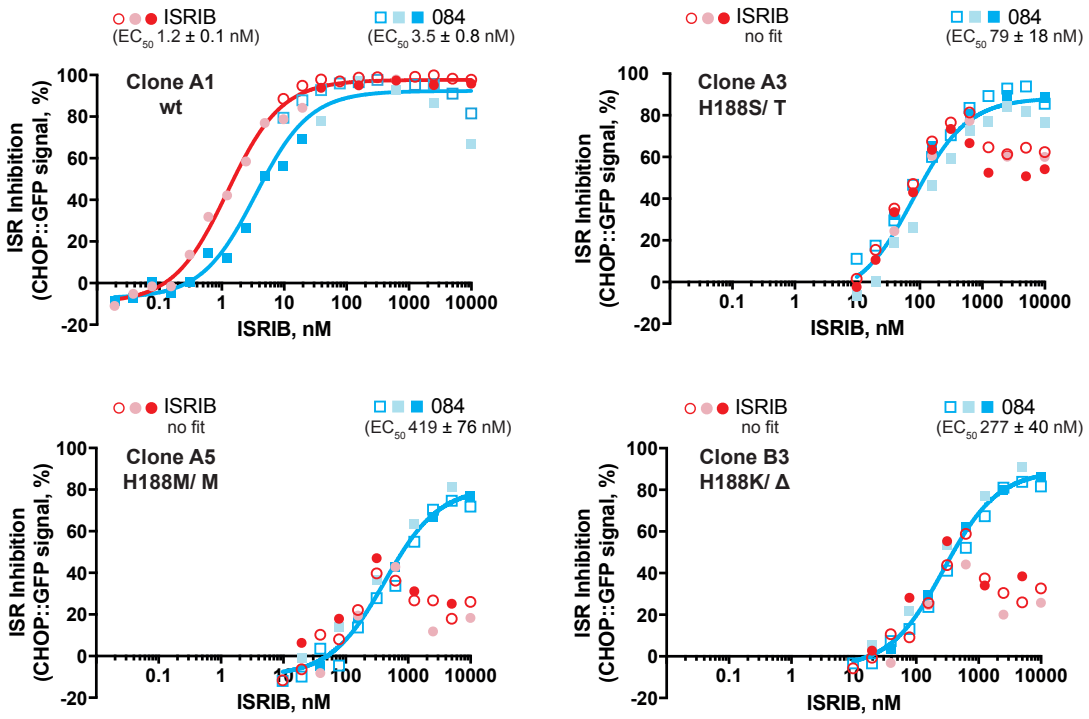

Figure 2.3.2f: The ISR-inhibition in analogue-sensitive clones.

Graphs showing inhibition of the ISR-activated CHOP::GFP signal induced upon treatment with HIS (0.5 mM), by ISRIB and AAA1-084 (084) in individual clones from 084^{SEN} pool (as in Figure 2.3.2c, d). Shown is data from three independent experiments for each of the compounds. Indicated are mean EC_{50} ± SD for n=3. Concentration of ISRIB is represented on a $\log_{10}$ scale. Curve fitting, EC_{50}, and SD were generated using agonist vs. response function on GraphPad Prism. Cultures were co-maintained, treatments were co-administered and flow cytometry was co-performed by A. Crespillo-Casado and A. Zyryanova, University of Cambridge. Analysis of phenotypical data and figures assembly was done by A. Zyryanova using FlowJo (LLC) software.

2.3.3 ISRIB insensitivity links to loss of ISRIB binding

ISRIB resistant mutations could alter the ISRIB-binding pocket in at least two different ways. If a sole ISRIB function is to stabilize eIF2B active decameric form than ISRIB resistant mutations may prevent binding of ISRIB to the relevant site. However, if ISRIB resistant mutations could still allow binding of ISRIB without propagating its effect on eIF2B's GEF activity than it should reflect an allosteric nature of ISRIB function that might alter the regulatory or catalytic interactions between eIF2B and its substrate eIF2/ eIF2(αP).

To address the effect of ISRIB-resistant mutations in eIF2B on binding of ISRIB we used the fluorescence polarization (FP) assay (described in Section 2.1.6). We purified eIF2B from wildtype, *Eif2b4*^{L180F} and *Eif2b2*^{H188K} CHO cells by exploiting a 3xFlag-tag knocked into the endogenous eIF2Bγ subunit (Figure 2.3.3a, described in Section 2.1.3) and tested their ability to bind FAM-labeled ISRIB (AAA2-101, figure 2.1.1e). The wildtype hamster eIF2B gave rise to a conspicuous concentration-dependent FP signal in the presence of a FAM-labeled AAA2-101 (Figure 2.3.3b right panel, circular pictograms). Validity of this FP signal was confirmed by competition with unlabeled ISRIB (Figure 2.3.3b, right panel). However, hamster eIF2B purified from the mutant cells failed to give rise to an FP signal (Figure 2.3.3b, right panel, square and triangle pictograms). This observation suggested that ISRIB resistance in those mutant cells might be due to the defective ISRIB binding, therefore, supporting the notion that ISRIB exerts its effect on eIF2B's GEF activity possibly through stabilizing the active eIF2B decamer. However, the fact that we did not identify the ISRIB^{RES} mutations that do not disrupt ISRIB binding to the pocket does not exclude the existence of such and the potential validity of an allosteric idea of ISRIB mechanism of action.

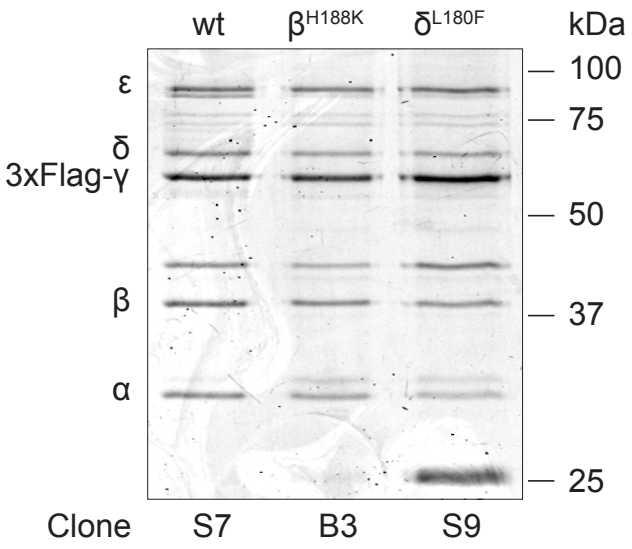

Figure 2.3.3a: Purification of hamster eIF2B from ISRIB-resistant clones.

Coomassie-stained SDS-PAGE gel of endogenous hamster eIF2B purified from wildtype (wt, clone A1), *Eif2b2*^{H188K} (clone B3) and *Eif2b4*^{L180F} (clone S9, generated by Y. Sekine) CHO cells via a 3xFlag-tag knocked into *Eif2b3* locus (encoding the γ subunit, described in Section 2.1.3). Cultures were maintained and purifications were done by A. Zyryanova, University of Cambridge.

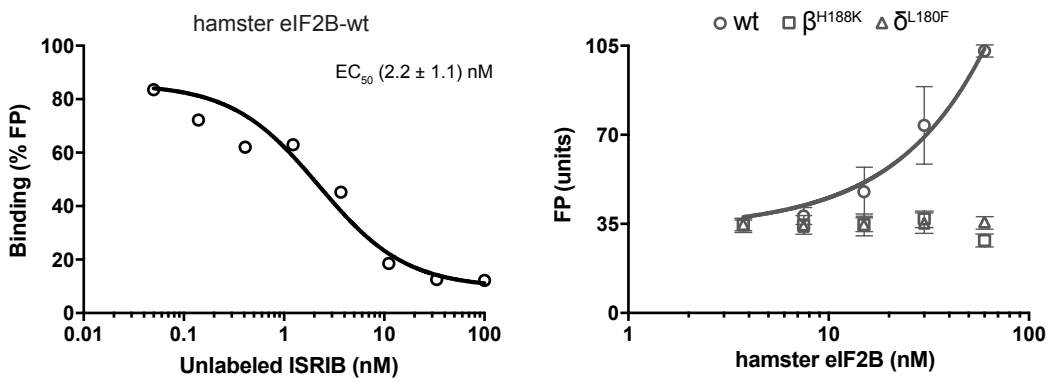

Figure 2.3.3b: ISRIB-resistant clones do not bind ISRIB.

Left: plot of the relative FP signal arising from samples with fluorescein-labeled AAA2-101 (2.5 nM) bound to purified hamster eIF2B (30 nM) in the presence of the indicated concentration of unlabeled ISRIB introduced as a competitor (represented on a $\log_{10}$ scale, done once). Indicated is EC_{50} ± SD. Curve fitting, EC_{50}, and SD were generated using "agonist vs. response" function on GraphPad Prism. Right: plot of the FP signal arising from fluorescein-labeled AAA2-101 (2.5 nM) as a function of the concentration of wildtype (wt) or mutant eIF2B (δ^{L180F} or β^{H188K}) in the sample. Shown are mean ± SD (n=3). Concentrations of eIF2B are represented on a $\log_{10}$ scale. Proteins were purified and FP experiment was executed by A. Zyryanova, University of Cambridge.

2.3.4 Summary of Section 2.3

1) Mutagenesis of the residues at positions 162, 188 or 190 of the eIF2Bβ subunit, lining the putative ISRIB-binding pocket, evokes ISRIB resistant phenotype in live mammalian cells (Figure 2.3.1c); 2) the ISRIB resistant phenotype of the cells mutated at position 188 of the eIF2Bβ subunit could be rescued by ISRIB analogs (Figure 2.3.2a); 3) ISRIB analogs select for analog-sensitive mutations at position 188 of the eIF2Bβ subunit (Figure 2.3.2f), that lost their ability to bind ISRIB (Figure 2.3.3b).

Chapter 3: Discussion

The past few years were really exciting for all the people working on understanding of structure and regulation of the surprising and elusive eIF2B complex. Starting from the first claims of five subunit eIF2B complex to adopt a stoichiometry of a decamer in 2014 (Wortham et al. 2014; Bogorad et al. 2014; Gordiyenko et al. 2014) to a very recent progress made on structural architecture and assembly of a full eIF2B decamer (Kuhle et al. 2015; Kashiwagi et al. 2016; Zyryanova et al. 2018; Tsai et al. 2018), this knowledge revealed new insight and opened up opportunities to explore in more detail the function and regulation of eIF2B, and implication of changes in its GEF activity to the protein synthesis in eukaryotes and to development of human neurological diseases.

In the course of my PhD project I in collaboration with my co-workers determined the cryo-EM structure of the full human eIF2B complex together with its regulatory synthetic compound ISRIB. Our structure is the first full human eIF2B structure revealing eIF2B's assembly through the regulatory $\alpha_2(\beta\delta)_2$ core flanked on either sides by opposing catalytic ($\gamma\varepsilon$) subcomplexes, in concordance with the previously obtained biochemical, biophysical and structural data (Wortham et al. 2014; Bogorad et al. 2014; Kuhle, Eulig et al. 2015; Kashiwagi et al. 2016).

Accompanying our structural work (Zyryanova et al. 2018) another cryo-EM structure of the full human eIF2B in complex with ISRIB appeared in the literature (Tsai et al. 2018). Both structural studies independently provided complementary evaluation of each others highly similar findings and unequivocally contributed to the fast-developing cryo-EM field that focuses more and more on high resolution (< 2 Å) structures of "small" (< 500 kDa) proteins and dynamic assemblies, uncovering a high potential of this technique for drug discovery (Merk et al. 2016; Dubochet et al. 2018).

3.1 Structure of eIF2B and ISRIB binding pocket

The human eIF2B-ISRIB structure obtained by (Tsai et al. 2018) is of higher resolution (PDB: 6CAJ, overall 2.8Å) than ours (PDB: 6EZO, overall 4.1Å). Nonetheless, the two human eIF2B structures (PDB: 6CAJ and 6EZO) are highly similar to each other and to the *S. pombe* eIF2B decamer (PDB: 5B04, overall 2.99Å) (Kashiwagi et al. 2016), and all of them lacking the catalytic HEAT domain of the ε subunit, once again suggesting its highly flexible nature. Additionally, both human structures (PDB: 6CAJ and 6EZO) share one key finding that reveals a novel regulatory site on eIF2B at the core of its regulatory $\alpha_2(\beta\delta)_2$ subcomplex, between the symmetrical interface of $(\beta\delta)_2$ subunits - the ISRIB-binding pocket. This discovery was based on the experimentally-derived unambiguous cryo-EM density identified in the aforementioned cavity, that was not assigned to any of the surrounding protein residues (Figure 2.2.1e).

The residues contacting ISRIB were identified and characterized in an extensive CRISPR/Cas9-based random mutagenesis phenotypical screen (Section 2.3). We were able to determine that substitution of residues at position 162, 188 or 190 of the eIF2B β subunit led to the loss of sensitivity to ISRIB in cultured cells, and to the loss of ISRIB binding *in vitro* (Figures 2.3.1c, d and figure 2.3.3b). Additionally, we identified that the same substitutions are instead more sensitive to certain ISRIB analogues in live cells (Figures 2.3.2c, d, f).

Tsai et al. also performed *in vitro* biochemical analysis of the residues lining the ISRIB-binding pocket. Having the flexibility of working in a recombinant over-expression system, Tsai et al. generated several mutant eIF2B complexes with substitutions at the position 160 and 188 on its β subunit, and at the position 179 on its δ subunit, and characterized them separately. Interestingly, the βH188A identified by Tsai et al. was resistant to stabilization by ISRIB across the density gradient, which in some way is consistent with our results from phenotypical screen where the same mutation (βH188A) appeared with higher frequency in ISRIB-resistant and 075B/ 084-sensitive

cells (Figures 2.3.1d and figure 2.3.2d). On a contrary, the βH188Y and βH188F mutants in hands of Tsai et al. were stabilized by ISRIB on a density gradient even to a greater extend than the wildtype. In our phenotypical screen, both βH188Y and βH188F substitutions appeared with higher frequency in ISRIB-sensitive population as well (Figures 2.3.1d and figure 2.3.2d). These alleles, however, were still much less represented than the wildtype, a finding that could reflect a potential cost of such substitutions to cell viability or proliferation that would not be picked-up in *in vitro* experiments conducted by Tsai et al.

Our previous findings also showed that L180F substitution on the hamster eIF2B δ subunit (δL179 in human) evokes strong ISRIB-resistant phenotype in live cells (Sekine et al. 2015), and exhibits loss of ISRIB binding *in vitro* (Figures 2.1.1b and 2.3.3b). Tsai et al. discovered two new substitutions at the same position on the human eIF2Bδ. The δL179A, which is selective for one of the ISRIB analogues, and the δL179V, which is insensitive to ISRIB but has wildtype levels of GEF activity when assembled along three other eIF2B subunits (β, γ and ε) omitting the α, reflecting stabilization effect of δL179V mutation on eIF2B$(\beta\gamma\delta^{L179V}\varepsilon)_2$ octamer. Withal, both works, ours and Tsai's, present structural, biochemical and chemogenetic results that altogether point to an important role for ligand engagement at the aforementioned pocket in ISRIB action.

3.2 Molecular mechanism of ISRIB action

Though we can now be more certain of ISRIB's engagement in the core cavity of eIF2B dimer interface, clarity has to be provided on how does ISRIB exert its effect on eIF2B's GEF activity and regulate translation initiation. By understanding the mode of ISRIB action, we could get further insight into eIF2B's relationship with its substrate eIF2.

Two models of ISRIB action come to mind: "direct" and "allosteric". The "direct" model argues in favor of ISRIB's engagement with the pocket that leads to direct effect on GEF activity through stabilizing eIF2B in its most active form of a decamer. The "allosteric" model suggests the possibility of

ISRIB binding in a way that propagates conformational changes to the relevant regulatory or catalytic domains of eIF2B leading to the change in GEF activity or in its sensitivity to inhibition by eIF2(αP). We shall now discuss the validity of both hypotheses.

3.2.1 "Allosteric" model

The regulatory subcomplex of eIF2B (eIF2B^{RSC}) is formed of α, β and δ subunits, which share sequence and structural homology, comprising mainly of an N-terminal helix bundles and a C-terminal Rossmann-like folds (Figure 2.2.2a). This hexameric, $\alpha_2(\beta\delta)_2$, eIF2B^{RSC} is assembled in a way that subunits' CTDs form the core of the subcomplex, and their NTDs form two cavities (Figure 2.2.2a, "central" view) (Kuhle et al. 2015; Kashiwagi et al. 2016; Tsai et al. 2018). eIF2B^{RSC} is believed to have evolved from a family of metabolic enzymes, like ribose-1,5-bisphosphate isomerases (RBPIs) and methylthioribose-1-phosphate isomerases (MTNAs), that share a high structural similarity with eIF2B^{RSC} (Bogorad et al. 2014; Kuhle et al. 2015). One of such enzymes, *Thermococcus kodakarensis* R15Pi, forms a homohexamer that can transition from "closed" (substrate-bound) to "open" (product-bound) state accompanied by multiple interactions between its N- and C-terminal domains (Nakamura et al. 2012). Hence, it is very plausible to suggest that just like its ancestors an early-emerged eIF2B^{RSC} could undergo ligand-induced allosteric changes that might have been repurposed later on to respond directly to changes in phosphorylation state of eIF2α making eIF2B^{RSC} a translational regulator (Figure 3.2.1a) (Kuhle et al. 2015).

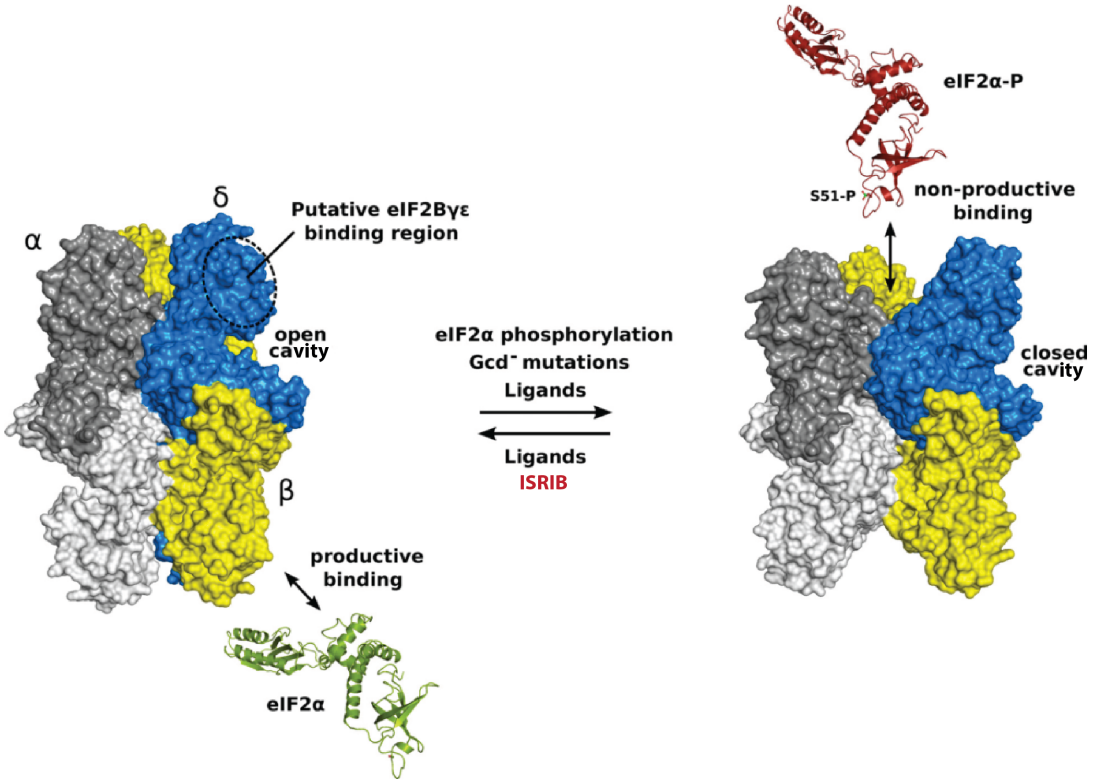

Figure 3.2.1a: Model of interaction between the eIF2B regulatory subcomplex ($eIF2B^{RSC}$) and eIF2α.

Shown is a hexameric, $\alpha_2(\beta\delta)_2$, $eIF2B^{RSC}$ that might transition between two conformational states. Left: an "open" state with the NTDs of the two heterotrimers close together providing surface for the productive binding of non-phosphorylated eIF2 (green cartoon). Right: "closed" state with the NTDs far apart from each other disrupting productive binding site, and allowing non-productive binding of eIF2(αP) (red cartoon). A possible transition between two conformational states might be influenced by allosteric ligands (e.g. AMP, GMP, ATP, GTP, NADP+ and even ISRIB) that could stabilize either the "open" or "closed" state. A possible binding site for the catalytic eIF2B(γε) complex is indicated. The two structural models are based on the crystal structures of *apo* and R15BP-bound tkRBPI (PDB: 3A11 and 3VM6). Redrawn and modified from Kuhle et al. 2015.

The potential of eIF2B to transition from “active” (allowing catalytic interactions with eIF2) to “inactive” (sequestered by unproductive interactions with eIF2(αP)) state is also based on the assumptions that phosphorylated eIF2α makes contacts primarily with the cavity of $eIF2B^{RSC}$ (Kashiwagi et al. 2016; Kashiwagi et al. 2017) formed by all three regulatory subunits (α, β and δ), while non-phosphorylated eIF2 mainly interacts with the eIF2B β subunit (Dev et al. 2010). In addition, existence of active-inactive conformation of $eIF2B^{RSC}$ is consistent with some gcn^- and gcd^- mutations identified in yeast that are mapped onto the surface exposed (αβδ) cavity, and respectively promote productive and non-productive eIF2α interactions (Vazquez de Aldana and Hinnebusch 1994; Pavitt et al. 1997; Dev et al. 2010; Kashiwagi et al. 2016).

Considering the hypothesis mentioned above one could speculate that the effect of ISRIB molecule could be in shifting the eIF2B complex into a more productive state favoring guanine-exchange and disfavoring the inhibitory eIF2(αP) interactions (Figure 3.2.1b).

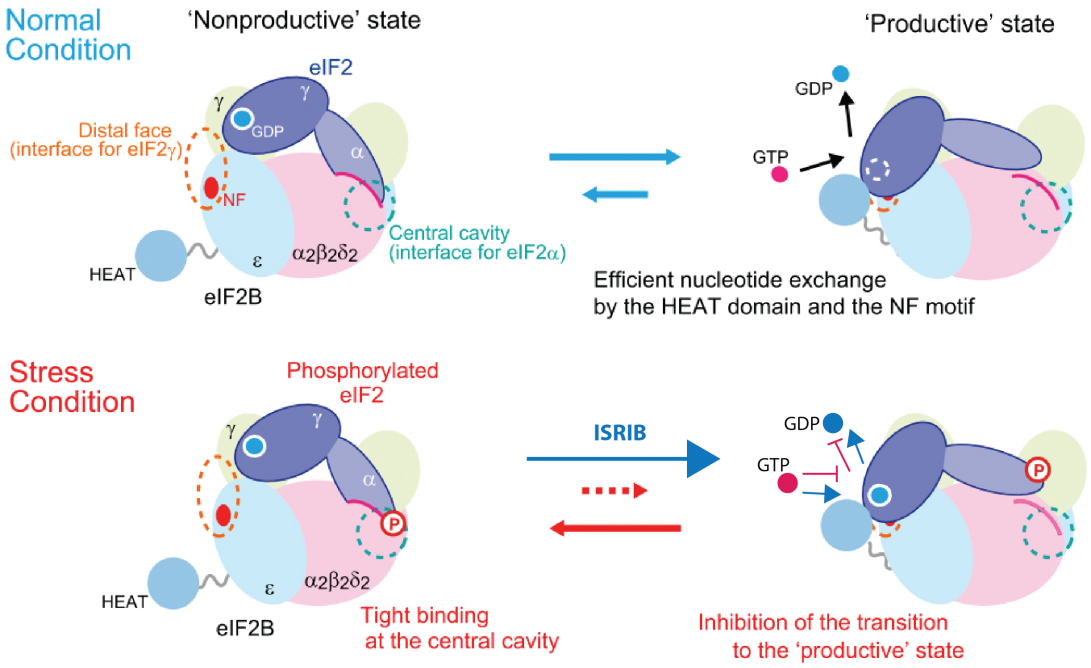

Figure 3.2.1b: Model mechanism of the stress-induced inhibition of the eIF2B's nucleotide exchange activity by phosphorylated eIF2.

Top: the "productive", nucleotide exchange state is favored under normal conditions when eIF2α is not phosphorylated and eIF2B catalytic HEAT domain can facilitate exchange of GDP for GTP. Bottom: under stress conditions, phosphorylated eIF2α inhibits catalytic activity of eIF2B disfavoring nucleotide exchange. ISRIB potentially shifts the "unproductive" state to "productive" despite phosphorylation of eIF2α. Redrawn and modified from Kashiwagi et al. 2017).

3.2.11 Conformational shift

The best way to observe ISRIB-induced conformational shift in eIF2B complex is by comparison of two structures of eIF2B, with and without ISRIB. Unfortunately, we could not obtain a cryo-EM structure of the human eIF2B without ISRIB compound (the structure of an “apo” complex was also absent from Tsai et al.). But we could compare the ISRIB-ligated human eIF2B (PDB: 6EZO) to *S. pombe* eIF2B (PDB: 5B04) crystallized in the absence of ISRIB. Both human (PDB: 6EZO) and yeast (PDB: 5B04) structures share a great deal of similarity (r.m.s.d. of 2.57 Å over 3049 alpha carbons, Figure 2.2.2c), which argues against large domain movements as the basis of ISRIB action. Certain elements of both regulatory and catalytic subcomplexes remain unresolved in the structure. It is, therefore, possible to propose that ISRIB stabilized an active conformation of the human eIF2B (PDB: 6EZO) entailing changes in the disposition of the unobserved C-terminal HEAT repeats of the catalytic ε subunit, and that the same conformation was assumed by the yeast eIF2B in the crystal (PDB: 5B04). Nonetheless, without an *apo*- eIF2B structure we cannot make any confident statements on the effect of ISRIB on eIF2B conformation.

When comparing our human eIF2B-ISRIB structure (PDB: 6EZO) to *S. pombe* *apo*-eIF2B (PDB: 5B04), however, one divergence was noted that suggested a difference in the disposition of the not fully resolved N-terminal extension of their δ subunits (Figure 2.2.2d). The divergent region of the human δ subunit contains two residues (R170 and V177) that are distant from the ISRIB binding pocket (Figure 2.2.2d), yet important for ISRIB action, as mutations, R171Q and V178G, found in the δ subunit of hamster eIF2B (R170 and V177 in human) evoke ISRIB resistant phenotype (Sekine et al. 2015). Such potentially ISRIB-induced change in the disposition of this segment of the δ subunit could contribute to the increase in eIF2B’s GEF activity. Even though this observation could not be considered only in favor of “allosteric” mode of ISRIB action, we could speculate that ISRIB-induced conformational change might propagate all the way through the regulatory core of eIF2B to the top cavity of the complex assembled by regulatory α, β and δ subunits. In its turn,

such ISRIB effect might enfeeble binding of the phosphorylated eIF2α implicated in formation of high affinity unproductive interactions with eIF2B (Vazquez de Aldana and Hinnebusch 1994; Pavitt et al. 1997; Kashiwagi et al. 2016; Kashiwagi et al. 2017; Bogorad et al. 2017), perhaps, favoring more productive catalytic interactions (Figure 3.2.1b). The flexibility of that top cavity region (Figure 2.2.1c) might have masked the important allosteric changes.

3.2.12 Catalytic and regulatory interactions between eIF2B and eIF2/ eIF2(αP)

The potential conformational transition of eIF2B between "active" and "inactive" states might favor either productive (catalytic) or non-productive (regulatory) interactions with eIF2/ eIF2(αP). ISRIB, thus, can increase Kd of eIF2(αP) promoting its dissociation from eIF2B, and making eIF2B available for catalytic interactions. However, our pull-down experiments, through which we could monitor association of eIF2/ eIF2(αP) with eIF2B, showed no evidence for such dissociation effect induced by ISRIB (Figure 2.1.2c, e). On the contrary, the experiments with non-phosphorylatable eIF2α^{S51A} mutant indicated that more eIF2B becomes available for productive catalytic interactions with eIF2 in the presence of ISRIB (Figure 2.1.2c). Both of these results are not disfavoring the possibility of an allosteric regulation of eIF2B's GEF activity by ISRIB, suggesting it might work similarly to gcn$^-$ mutations by converting eIF2(αP) into eIF2B's substrate instead of its competitive inhibitor. An alternative possibility of drawing more active eIF2B from a different source stimulated by ISRIB could not be excluded either.

3.2.2 "Direct" model

It is known that the α subunit of yeast eIF2B encoded by a non-essential *GCN3* gene (Hannig and Hinnebusch 1988) is dispensable for yeast eIF2B's GEF activity (Bushman et al. 1993). However, mammalian eIF2Bα, although still being the most readily dissociating subunit (Craddock and Proud 1996; Liu et al. 2011; Wortham et al. 2014), serves an important function in stimulating mammalian eIF2B's GEF activity since α-depleted eIF2B(βγδε)

complex promotes GDP-release from its substrate only partially (Liu et al. 2011) or abolishes it almost entirely (Craddock and Proud 1996; Tsai et al. 2018). Hence, the idea of ISRIB stabilizing the active mammalian eIF2B decamer is very compelling (Sidrauski et al. 2015; Tsai et al. 2018).

This potential function of ISRIB fits nicely with the fact that it is a symmetrical molecule straddling the two-fold axis of symmetry at the core of the regulatory eIF2B subcomplex, and engaging the same residues from opposing protomers of the $(\beta\delta)_2$ dimer of dimers (Figure 2.2.2a) (Tsai et al. 2018). The potential increase in abundance of active eIF2B decamer driven by ISRIB may then explain the ability of this compound to inhibit the ISR and to restore protein synthesis in cells despite the persistent phosphorylation of eIF2α leading to sequestration of all the generally available active eIF2B decamer into a non-productive complex with eIF2(αP) (Safer et al. 1982; Konieczny and Safer 1983; Oldfield et al. 1994). This hypothesis, however, is based on some concepts that have not been tested so far. For example, the notion that cells possess a considerable pool of eIF2B(βγδε) tetramers readily available for the assembly of eIF2B decamer. And the notion that assembly of eIF2B decamer from two eIF2B(βγδε) tetramers and eIF2B$(\alpha)_2$ dimer is a rate-limiting step. There are a few findings in the literature that could argue in favor of this hypothesis.

3.2.21 eIF2B subcomplexes and assembly

Previously, analysis of purified mammalian eIF2B subcomplexes by MS and affinity pull-downs already hinted at the existence of eIF2B(βγδε) heterotetramers and eIF2B$(\alpha)_2$ homodimers, proposing the way for a full eIF2B decamer assembly through stabilization of the two parts of the former by one part of the latter (Figure 3.2.21) (Wortham et al. 2014; Wortham et al. 2016). Though being important findings, these studies were conducted in overexpression system ideally requiring confirmative experiments on endogenous species found in cells.

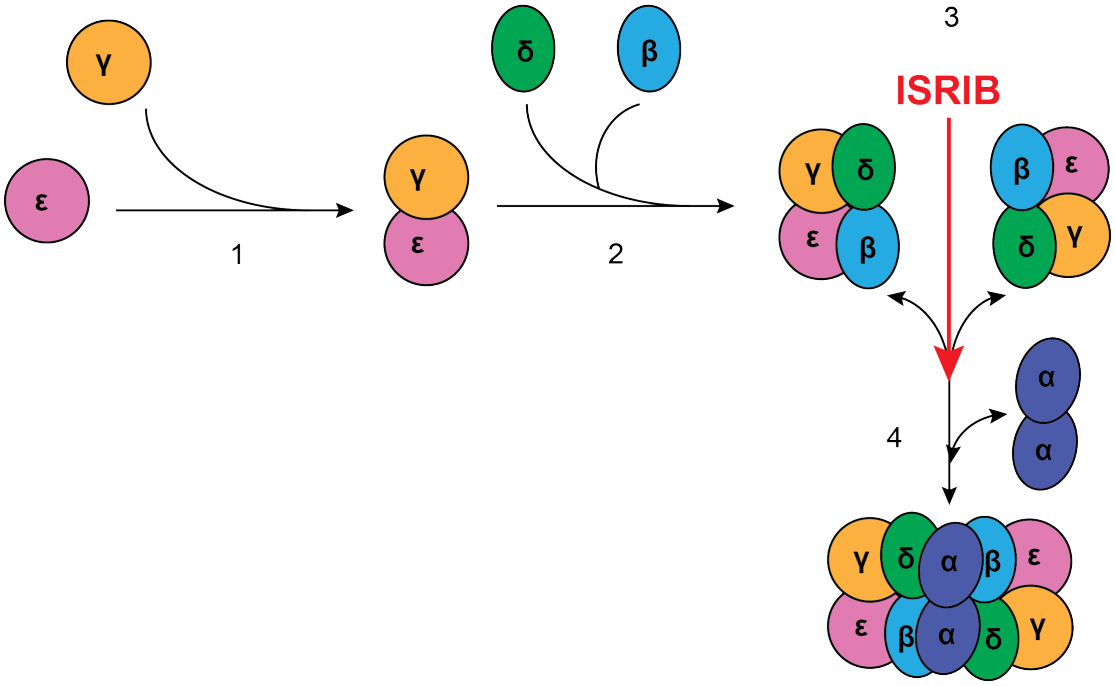

Figure 3.2.21: Model of stoichiometric assembly of eIF2B complex.

1) eIF2Bε subunit binds to eIF2Bγ to form eIF2B(γε) heterodimer. 2) The eIF2B(γε) heterodimer then binds to eIF2Bβ and δ to form eIF2B(βγδε) tetramers. 3) Two eIF2B(βγδε) tetramers are associating together with the help of eIF2B$(\alpha)_2$ homodimer. 4) Formation of an eIF2B$\alpha_2(\beta\gamma\delta\varepsilon)_2$ decamer. The unstable association between $(\alpha)_2$ dimer and (βγδε) tetramers (steps 3&4) is indicated by reverse arrows. The potential $(\beta\gamma\delta\varepsilon)_2$ octomer-stabilization (step 3) effect of ISRIB is highlighted in red. Drawn by A. Zyryanova, University of Cambridge.

Some of the observations from our own experiments indicated existence of eIF2B(βγδε) tetramers in cells. As noted from the chromatography profile of the purified endogenous hamster eIF2B complex, it eluted in two main peaks corresponding to the sizes of decameric and tetrameric forms of eIF2B (Figure 2.1.3b). Even the endogenous human eIF2B, although predominantly eluted as a decamer, might have some hints of the presence of tetrameric species (Figure 2.1.3a), which disappeared in the presence of ISRIB (Figure 2.2.1a). Though the observations from chromatography profiles of eIF2B complexes might indicate the presence of a pool of tetrameric eIF2B species in cells, they still argue against the idea of a fast dissociation rate of $(\alpha)_2$ dimer from the rest of the complex. In the light of the new knowledge, even the SILAC experiment potentially indicated that the eIF2Bα subunit loosely associated with the rest of the complex got stabilized by ISRIB (Figure 2.1.4d).

On the note of existence of eIF2B subcomplexes in cells, we should also consider a few findings obtained through the studies of VWM mutations found on eIF2B. Several experiments done on purified VWM mutants of human eIF2B complexes from overexpressed systems suggest the impairment in the full eIF2B complex assembly (Li et al. 2004; Liu et al. 2011; Wortham et al. 2014; Wortham and Proud 2015; Wong et al. 2018). It was recently observed that a few of those VWM mutant complexes seem by large to adopt a form of eIF2B(βγδε) tetramer (Wong et al. 2018). We too observed such destabilizing effect of one VWM mutation, δA391D (δA392D in hamster), on the endogenous hamster eIF2B complex assembly (Sekine et al. 2016). The chromatography profile of this VWM δA392D mutant also revealed that it eluted mainly as tetrameric species (Figure 2.1.3b). Additionally, the recombinant VWM mutants studied by Wong et al. were able to transition from tetrameric to decameric species upon addition of ISRIB. These observations are also consistent with the reports of stabilizing effect of ISRIB on wildtype mammalian eIF2B complex, which shifted towards HMW species across the density gradient in response to ISRIB in both endogenous (Figure 2.1.5a) (Sidrauski et al. 2015) and over-expression set-ups (Tsai et al. 2018).

3.2.22 eIF2B's GEF activity

The new findings by Tsai et al. further substantiate the aforementioned model of eIF2B decamer assembly highlighting the importance of formation of eIF2B(βδγε)$_2$ octamer, which serves as a platform for eIF2B(α)$_2$ dimer joining (Figure 3.2.21). Tsai et al. propose that ISRIB "staples" eIF2B(βδγε) tetramers, shifting the equilibrium of eIF2B subcomplexes towards eIF2B(βγδε)$_2$ octamer formation, thereby, stimulating the eIF2B's GEF activity. They further suggest that GEF activity of the fully assembled human eIF2B measured *in vitro* is not affected by ISRIB as much as the activity of eIF2B(βδγε) tetramers, which is credited to the assembly of an eIF2B(βδγε)$_2$ octamer (Tsai et al. 2018). This very compelling idea, however, requires more thorough assessment of the rates of eIF2B complex assembly from eIF2B(βδγε) tetramers and eIF2B(α)$_2$ dimers. Knowing the association/ dissociation constants for eIF2B(α)$_2$ dimer would be necessary in order to confirm the relevance of the aforementioned *in vitro* findings to processes happening in live cells.

The absence of ISRIB effect on the GEF activity of the fully assembled human eIF2B complex revealed by Tsai et al. is also not in line with some other results suggesting that ISRIB does increase the GEF activity of the purified full mammalian eIF2B complex towards non-phosphorylated eIF2 (Sekine et al. 2015; Sidrauski et al. 2015; Wong et al. 2018) and phosphorylated eIF2(αP) (Sekine et al. 2015) substrates (Figure 2.1.3d). In our experience, however, the observed effect of ISRIB on purified eIF2B was weaker than the effect observed when using mammalian cell lysates as a source of GEF (the amounts of eIF2B in each case were comparable) (Figures 2.1.3d, e) (Sekine et al. 2015). This observed ISRIB effect on lysates could be explained by the presence of eIF2B(βγδε) tetramers in cells, which were promoted to eIF2B(βγδε)$_2$ octamers upon addition of ISRIB, thereby, exhibiting higher GEF activity than the purified decameric eIF2B. The smaller delta of ISRIB's effect on purified eIF2B compared to lysates (Figures 2.1.3d, e), and the absence of ISRIB effect on the full eIF2B's GEF (Tsai et al. 2018) is then consistent with the "direct" model of ISRIB action. And the "residual" GEF acceleration effect

of ISRIB observed on the purified eIF2B in our hands could be indicative of an existing fast equilibrium between eIF2B(βδγε) tetramers and $(\alpha)_2$ dimers in the reaction mixture. The apparent stability of the human eIF2B decamer (Figure 2.1.3a), however, argues against a fast exchange between the eIF2B subcomplexes and in favor of the "allosteric" model of ISRIB action.

The finding of an octamer-stabilizing mutation, δL179V, on human eIF2B that is not further influenced by ISRIB (Tsai et al. 2018) is also a valuable clue to understanding the complex assembly and regulation, especially in comparison to the yeast eIF2B. The aforementioned observations that yeast eIF2Bα is dispensable for eIF2B's GEF activity (Bushman et al. 1993), that residues in yeast eIF2Bδ species equivalent to human L179 are not conserved as in mammals (Figure 2.1.1d), and that ISRIB does not influence eIF2B's GEF activity in yeast (data not shown) - all point, firstly, to the importance of mammalian eIF2Bα in bridging two eIF2B(βδγε) tetramers (Wortham et al. 2014; Tsai et al. 2018) and, secondly, to the effect of ISRIB on stabilizing mammalian eIF2B$(\beta\delta\gamma\varepsilon)_2$ octamers providing a platform for eIF2B$(\alpha)_2$ joining (Tsai et al. 2018). This idea also supports the previous studies on yeast eIF2B's activity and assembly (Dever et al. 1992; Gordiyenko et al. 2014), suggesting that yeast might possess a pool of active eIF2B$(\beta\gamma\delta\varepsilon)_2$ octamers that are more stable than mammalian octamers, thus, making the yeast eIF2B capable of retaining its full GEF activity even in the absence of eIF2Bα.

3.3 Commentary and future experimental approach

Taking into consideration all the arguments for and against of "direct" or "allosteric" models of molecular mechanism of ISRIB action, we cannot decisively come to a single conclusion maybe because this two hypothesis are mutually non-exclusive.

The presented "direct" model, based on the structural specifics of the discovered ISRIB-binding pocket, and the stabilization effect ISRIB has on the recombinant eIF2B(βδγε) tetramers and VWM mutants, seems to be very logical and appealingly straightforward. However, the many uncertainties around the molecular mechanism of eIF2B's GEF activity and the modes of

interaction between eIF2B and eIF2/ eIF2(αP), as well as the remoteness of ISRIB-binding pocket from the main sites of eIF2B's regulatory and catalytic activity, still leave room for the proposed allosteric shifts in eIF2B that stabilization of its decameric form can evoke.

Understanding the function of ISRIB molecule provided not only insight into its own molecular mode of action, but also shed light onto the potential mechanism governing assembly and regulation of eIF2B in cells, and opened up new exciting questions. Further elucidation of the ways by which eIF2B communicates with eIF2/ eIF2(αP) is the key to understanding the fundamental principals governing regulation of protein synthesis in cells and cellular fitness in general.

3.3.1 Searching for eIF2B subcomplexes in mammalian cell

In recent years, various lines of evidence coming from the analysis of overexpressed recombinant mammalian eIF2B complexes, and from the examination of endogenous eIF2B subunits expression levels, suggested a model for eIF2B assembly in cells (Wortham et al. 2014; Wortham et al. 2016; Tsai et al. 2018). According to that model assembly of a full mammalian eIF2B decamer requires its subunits to sequentially come together in the following manner: (γ+ε) and (β+δ) to form (βδ+γε) heterotetramers, which in their turn are dimerized, and stabilized by (α+α) homodimer generating $(\alpha)_2$+$(\beta\delta\gamma\varepsilon)_2$ decamer (Figure 3.2.21). Revealing the existence of the endogenous eIF2B subcomplexes in cells, and assessing their mutual association rates would be of great interest, in general, and for affirmation of the mechanism of ISRIB action, in particular.

In order to examine distribution of eIF2B subunits and subcomplexes (and the effect of ISRIB on them) in mammalian cells, one could apply mammalian cell lysates on a SEC column since utilizing density gradient and Native PAGE seems to produce not highly definitive results (Figures 2.1.5a, b). This may work particularly well in the context of VWM mutants that exhibit high tetramer contents in the overexpression system (Wong et al. 2018).

Chasing the eIF2B subcomplexes in cells could be challenging if the exchange rates of $(\alpha)_2$ dimer and $(\beta\delta\gamma\varepsilon)$ tetramers in the $(\alpha)_2(\beta\delta\gamma\varepsilon)_2$ decamer are too fast. Therefore, assessing the association/ dissociation rates between subcomplexes in the eIF2B decamer would be of interest as well. In a proposed experiment one could measure, for instance, the exchange rate of a tagged/ labeled (α_2) dimer for an untagged $(\alpha)_2$ species in the assembled $(\alpha)_2(\beta\delta\gamma\varepsilon)_2$ decamer.

3.3.2 Allostery vs. stabilization

The existence of the ISRIB-resistant mutants that lost their ability to bind ISRIB (Figure 2.3.3b) does not discriminate between a "direct" or "allosteric" model of ISRIB's action. However, finding ISRIB-resistant mutants that are capable of binding the molecule would be supportive of "allosteric" model. For example, testing of ISRIB-resistant mutants with substitutions in eIF2B subunits that are not interfering with the eIF2B decamer formation and are retaining their ability to bind ISRIB could provide an answer to that. One such human eIF2B mutant, βH188A, seems to be a good candidate since it has a stoichiometry of a wildtype complex that is not altered by ISRIB on a density gradient (Tsai et al. 2018). Two other ISRIB-resistant mutants identified in a previously published mutagenesis screen in hamster eIF2B, δR171Q and δV178G (δR170 and δV177 in human), could also be readily tested for their stoichiometry and ISRIB-binding capacity (Sekine et al. 2015).

Since one of the hypothesis of the mechanism of eIF2B's GEF activity suggests that eIF2B might undergo some allosteric changes when interacting with the eIF2 substrate or the eIF2(αP) competitive inhibitor (Kuhle et al. 2015), it may be that the conformational shift evoked by ISRIB in eIF2B could only be illuminated when the GEF is interacting with eIF2/ eIF2(αP). Therefore, an experiment alternative to an ambiguous GEF activity assay could be performed, in which binding ability of eIF2(αP) to eIF2B decamer could be tested in the presence of ISRIB. Similarly to the fluorescence polarization assay done by Bogorad et al. showing increase in the affinity of phosphomimetic $eIF2\alpha^{S51D}$-NTD towards $eIF2B^{RSC}$ compared to wildtype eIF2α-NTD (Bogorad et al. 2017), we could additionally try titrating ISRIB in. If

ISRIB could trigger dissociation of eIF2(αP) from eIF2B it will be indicative of allosteric changes happening in eIF2B arguing against of the idea that ISRIB merely shifts the balance between eIF2B(βδγε) tetramers and eIF2B$(βδγε)_2$ octamers in cells. Incidentally, use of the full-length eIF2/ eIF2(αP) should be considered when performing this kind of binding assay since some evidence suggest that eIF2α-CTD is important for phosphorylation dependent binding of eIF2α to eIF2B^{RSC} (Krishnamoorthy et al. 2001).

If only the "direct" model is correct than not only it argues against of "allosteric" mode of ISRIB action, but also discourages existence of any allostery associated with eIF2B's GEF activity (Kuhle et al. 2015). Instead, the "direct" model favors the concept of sole subunits stoichiometry governing eIF2B's catalytic activity (Wortham et al. 2016). The fact that different cell types have varying levels of eIF2B (Wortham et al. 2014), and have varied sensitivity to ISR explained by differences in the ratio between eIF2 and eIF2B (Price and Proud 1994; Oldfield et al. 1994) is also in line with the "direct" model. It is, thus, legitimate to speculate that effects of stress and its resolution might affect the eIF2B decamer assembly.

3.3.3 Re-thinking eIF2B's GEF activity assay

Previously, some discrepancies were outlined between stimulatory effect of purified eIF2B and cell lysates on GDP-release from eIF2/ eIF2(αP) in the presence of ISRIB (Figure 2.1.3d, e). Such inconsistencies in measuring the rate of GDP-release are not only observed when comparing purified eIF2B to the cell lysates, but also between similar measurements done with purified eIF2B. For example, Tsai et al. could not observe stimulation of GDP-release by ISRIB on purified eIF2B decamer in contrast to several other reports (Sekine et al. 2015; Sidrauski et al. 2015; Wong et al. 2018). Another example of such variations in measuring purified eIF2B's GEF activity could be drawn from VWM mutants, that, in some cases, despite affecting eIF2B complex integrity were reported not to influence eIF2B's GEF activity or even enhance it (Liu et al. 2011; Wortham and Proud 2015).

One explanation to those differences could be attributed to some cellular factor missing from purified eIF2B. As we already hypothesized, according to the findings by Tsai et al. this missing component could be the eIF2B(βδγε) tetramer, dimerization of which is a potentially rate-limiting step in the assembly of an active eIF2B decamer. On the other hand, this could be a different cellular factor, like Met-tRNA$_i^{Met}$, that participates in the formation of a TC together with GTP-bound eIF2, and is actually considered the product of eIF2B catalysis, while the eIF2-GTP is being only an intermediate (Salimans et al. 1984; Gross et al. 1991; Bogorad et al. 2018).

The current measurement of eIF2B's GEF activity relies on measurement of the release of the bound labeled GDP nucleotide from eIF2 substrate, so that eIF2 could acquire a fresh molecule of GDP and then be released from eIF2B. Such measurement of GEF activity couples changes in eIF2B's potency to the changes in its affinity towards eIF2 substrate, which in some cases may obscure the real rate of GDP release (Bogorad et al. 2018). Perhaps, the better way of revealing a wider amplitude of eIF2B stimulation is by introducing a charged Met-tRNA$_i^{Met}$ into the assay to promote TC formation that was shown to boost nucleotide release from eIF2 (Gross et al. 1991).

Still, even that might not be enough to provide a GEF assay that captures all the functions of eIF2B. Recent evidence suggested that eIF2B could compete with Met-tRNA$_i^{Met}$ for binding of eIF2-GTP, thus, showing that TC complex is not really stable and is not the end product of eIF2B catalysis (Jennings et al. 2017). Instead, it is proposed that eIF5 possessing dual function of GAP and GDI (Jennings and Pavitt 2010) is stabilizing the TC by decreasing the affinity of eIF2B for eIF2-GTP, and by forming a more stable quaternary complex eIF5*eIF2-GTP*Met-tRNA$_i^{Met}$ (Jennings et al. 2017). Therefore, more accurate measurement of eIF2B's GEF activity probably requires reconstitution of the full eIF2 recycling system, including eIF2-GDP, GTP, eIF2B, Met-tRNA$_i^{Met}$ and eIF5.

3.3.4 An alternative model for regulation of eIF2B by eIF2(αP)

Considering some evidence disfavoring allosteric changes that eIF2B might undergo upon interaction with eIF2/ eIF2(αP), the regulation of eIF2B's GEF activity needs a different explanation. A recent study suggests that, instead of or additionally to eIF2B, the big conformational change is imposed on the α subunit of eIF2 since its N-terminal (eIF2α-NTD) and C-terminal domains (eIF2α-CTD) able to form inter-subunit interactions (Bogorad et al. 2017). This conformational change allows eIF2 to exist in two forms: "extended" (bound to GDP) and "closed" (*apo*, nucleotide free) (Figure 3.3.4a). In line with the cross-linking data (Kashiwagi et al. 2016), the nucleotide-bound "extended" conformation promotes interactions of the extended eIF2α-NTD with $eIF2B^{RSC}$. The "closed" *apo* form promotes catalytic interactions between eIF2γ and $eIF2B^{CSC}$ followed by GTP binding, and eIF2-GTP release stimulated by formation of TC with $Met\text{-}tRNA_i^{Met}$. The proposed driving force of guanine exchange catalysis in this model is the shift of equilibrium between eIF2-GDP and *apo*-eIF2 towards the latter (Bogorad et al. 2017) since eIF2B has higher affinity for *apo*-eIF2 than for eIF2-GDP (Goss et al. 1984; Panniers et al. 1988).

Interestingly, the same study shows that phosphorylated eIF2α exists in an "extended" conformation, as does eIF2-GDP, since the phosphorylation modification destabilizes NTD-CTD eIF2α inter-subunit interactions (Bogorad et al. 2017). Moreover, it is proposed that the inhibition of eIF2B's GEF activity by eIF2(αP) might be contributed not only by the sequestration of eIF2B in an unproductive complex, due to tighter interactions of eIF2αP-NTD with $eIF2B^{RSC}$ compared to non-phosphorylated eIF2α-NTD (Kashiwagi et al. 2016; Bogorad et al. 2017). The inhibition of eIF2B's GEF activity by eIF2(αP) could also be explained by a "thermodynamical" effect where nucleotide exchange of eIF2(αP)-GDP for eIF2(αP)-GTP is disfavored due to similar affinities of eIF2(αP)-GDP and *apo*-eIF2(αP) intermediate for eIF2B (Bogorad et al.2017; Bogorad et al. 2018), which are lower than the affinity of *apo*-eIF2 for eIF2B (Goss et al. 1984). This hypothesis is also consistent with reports

suggesting that eIF2(αP) dissociates from eIF2B as fast as non-phosphorylated eIF2 (Rowlands et al. 1988).

According to the aforementioned view, we could speculate that ISRIB might be pushing the equilibrium between “extended” eIF2-GDP and “closed” *apo*-eIF2 conformations even more towards the latter. ISRIB could do so by enfeebling interactions between eIF2α/ eIF2αP and $eIF2B^{RSC}$, or by enhancing interactions between eIF2γ and $eIF2B^{CSC}$, thus, stimulating the guanine exchange catalysis regardless of eIF2α phosphorylation (Figure 3.3.4b). Accordingly, this hypothesis does not exclude the possibility of allosteric changes that eIF2B might undergo upon ligand binding in order to push this equilibrium.

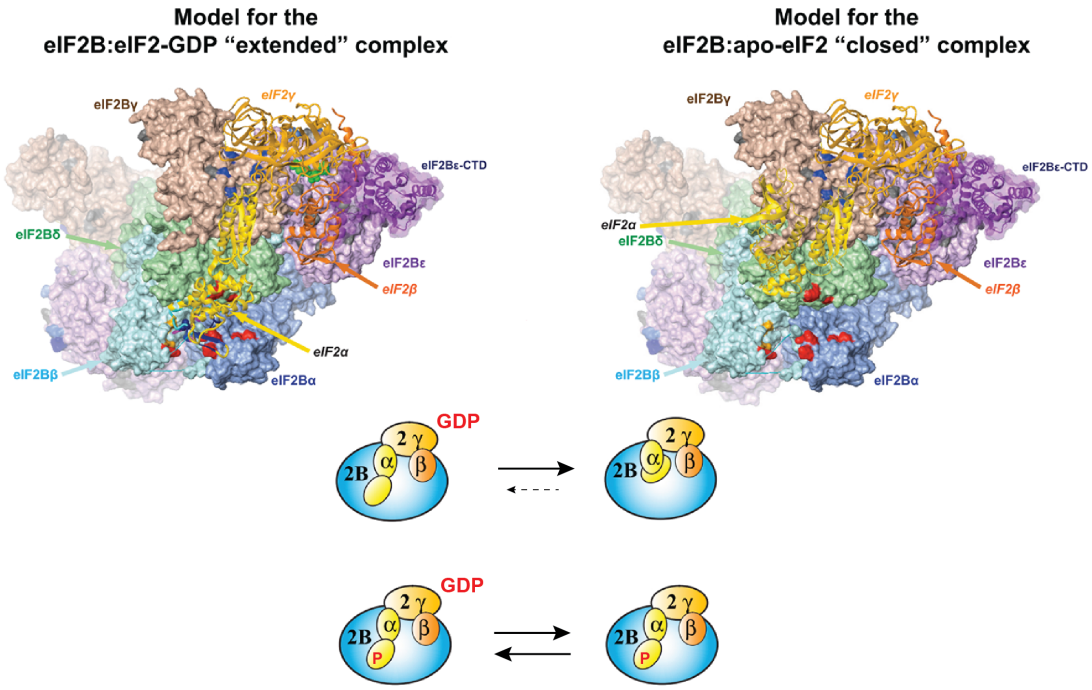

Figure 3.3.4a: Model of eIF2B interaction with eIF2.

Top: shown are two structural model of eIF2B/ eIF2 interactions: eIF2B complex with nucleotide-bound eIF2 in "extended" conformation (left), eIF2B*(*apo*-) eIF2 complex in "closed" conformation. eIF2B subunits (PDB: 5B04) are shown in surface representation; eIF2α (PDB: 1Q8K), eIF2β (PDB: 3V11) and eIF2γ (PDB: 3V11) are shown as ribbons. Crosslinking data for eIF2B^{RSC} ($\alpha_2(\beta\gamma)_2$) residues to both phosphorylated and non-phosphorylated eIF2α is indicated in red; crosslinking data for eIF2B^{RSC} residues only to non-phosphorylated eIF2α is indicated in orange (Kashiwagi et al. 2016). Crosslinking data for eIF2B(γε) residues to eIF2γ are navy, except the two residues with lower efficiency of crosslinking, which are light blue (Kashiwagi et al. 2016). The sites of VWM mutations are gray. Cartoon representation of the respective complexes is shown on the bottom of each panel, including a cartoon of phosphorylated eIF2 interacting with eIF2B. According to the model the nucleotide exchange is favored by higher affinity of "closed" conformation of *apo*-eIF2 for eIF2B. When eIF2α is phosphorylated the "closed" conformation is disrupted and the affinities of the nucleotide bound and *apo*-eIF2 states for eIF2B become similar, therefore, providing no driving force. Redrawn and modified from Bogorad et al. 2017.

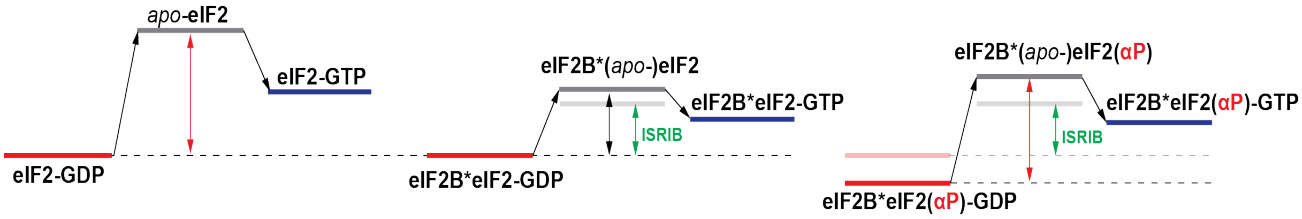

Figure 3.3.4b: Thermodynamic description of the eIF2B catalytic cycle.

Shown are activation energies (indicated in black) for spontaneous nucleotide exchange on eIF2 (left), in the presence of eIF2B (central), and when phosphorylated in the presence of eIF2B (right). The potential ISRIB's effect in lowering the activation energies of nucleotide release on both phosphorylated and non-phoshorylated eIF2 in the presence of eIF2B is highlighted in green. Red bars mark starting energy level of GDP-bound eIF2, grey bars – *apo*-eIF2, blue bars – GTP-bound eIF2, either phosphorylated or not and with or without eIF2B. Faint red and faint grey bars indicate potential shift in energy levels of GDP-bound and *apo*-eIF2 with eIF2B in the presence of ISRIB. Redrawn and modified from Bogorad et al. 2018.

3.3.5 Why is eIF2B so big?

eIF2B complex shares functional similarities with other translational GEFs, like bacterial EF-Ts (EF-1B) and eukaryotic (eEF-1B) elongation factors (Janssen and Moller 1988; Gromadski et al. 2002; Maracci and Rodnina 2016). Unlike many other GEFs, which are monomeric, eIF2B is surprisingly more complex being a dimer of pentamers. This suggests its pivotal role in regulating the global cellular fitness by being a target of diverse effectors not limited to only phosphorylated eIF2(αP).

3.3.51 Novel functions of eIF2B

The so far described consequences of ISRIB binding to eIF2B only reflected the possibility of influencing eIF2B's GEF activity through altering its relationship with eIF2/ eIF2(αP). The new independent function of eIF2B, as a GDP-dissociation inhibitor displacement factor (GDI displacement factor or GDF) (Jennings et al. 2013; Jennings and Pavitt 2014), opens up room for an alternative proposal. As was shown in yeast, the eIF2B's GDF activity promotes dissociation of eIF2-GDP from eIF5, a multifunctional eIF2 GAP and GDI, that reduces the chance of spontaneous nucleotide release from eIF2-GDP by antagonizing eIF2B's GEF activity and restricting eIF2 recycling to TC (Singh et al. 2006; Jennings and Pavitt 2010; Jennings et al. 2013). It was also indicated that γ and ε subunits of $eIF2B^{CSC}$ are important for the GDF activity of eIF2B, and that this GDF activity is not dependent on phosphorylation status of eIF2 (Jennings et al. 2013). In the light of these findings, we could speculate that, instead of acting solely on eIF2B's GEF activity, ISRIB could also accelerate the GDF activity of eIF2B contributing to ISR resistance. This concept, however, will require uncovering the role of mammalian eIF5 in its relationship with mammalian eIF2 and eIF2B complexes (Sokabe et al. 2012).

3.3.52 Other regulators of eIF2B

The regulatory and catalytic subunits of eIF2B evolved from ligand-regulated protein ancestors and possess nucleotide binding sites (Gordiyenko et al.

2014; Kuhle et al. 2015). The catalytic (γ and ε) subunits share similarities with nucleotide-binding ADP-glucose pyrophosphorylase (AGP) (Koonin 1995; Jin et al. 2005; Reid et al. 2012), However, the structure of eIF2B (PDB: 5B04) revealed that the proposed GTP-binding site identified on eIF2Bγ does not correspond to the nucleotide-binding site of AGP (PDB: 1YP4), and its importance for eIF2B's GEF activity still remains elusive (Nika et al. 2000; Gordiyenko et al. 2014; Kashiwagi et al. 2017). The regulatory (α, β and δ) subunits share similarity with ribose-1,5- bisphosphate isomerase (*tk*RBPi) and possess the same highly-conserved phospho-sugar binding pocket (Kuhle et al. 2015). Although by now eIF2B most likely lost its isomerase activity and became the main target of ISR, it retained its ability to bind some sugar-phosphate ligands proposing existence of an alternative to eIF2α phosphorylation regulation by low energy metabolites (Kuhle et al. 2015). Moreover, the potential ligand-binding sites of eIF2B mapped onto its structure overlap the putative eIF2 binding sites suggesting the likelihood of the aforementioned effectors to influence the relationship between these two translational factors (Bogorad et al. 2017). The role of other known allosteric effectors of eIF2B's GEF activity, like ATP, NADPH and polyamines (Gross and Rubino 1989; Oldfield and Proud 1992; Kimball and Jefferson 1995) remains to be uncovered.

The discovery of the ISRIB-binding pocket led us to speculate whether it is a conserved feature of eIF2B, and whether there are other endogenous or exogenous ligands that could engage into the identified cavity, evoking the ISR resistance. One of the four ISR-triggering pathways involves activation of PKR kinase by double-stranded viral RNAs (dsRNAs). Since it is important for the viral replication machinery to avoid the protein arrest caused by eIF2α phosphorylation, many viruses evolved mechanisms targeting PKR-eIF2α pathway (Walsh et al. 2013). Interestingly enough, some viruses acquired an ability to avoid translational arrest independent of eIF2α phosphorylation (Qin et al. 2011; Khaperskyy et al. 2014; Sharon and Frenkel 2017). It is, thus, not unreasonable to hypothesize that some of those viral gene-products could target anything downstream of eIF2(αP), like eIF2B itself.

3.4 Concluding remarks

The importance of the integrated stress response (ISR) and regulation of protein synthesis governing cellular homeostasis cannot be appreciated enough. Although the balancing between maintaining cellular fitness and inducing cell death seems to be quite robust under “normal” circumstances in healthy cells, under stress in dysregulated environment this balance may become fragile leading to irreversible sequence of events with a fatal outcome. An animal organism consists of a number of cell types sharing the same genetic material but providing various needs depending on their localization and function. Therefore, it is of vital importance to consider those tissue-specificities when trying to combat a given disease.

The diseases caused by or linked to the mutations targeting any part of the cellular homeostasis apparatus are plentiful. The outcome of the mutations in translational machinery, in particular, is probably the most elusive. The ubiquitous translational factors cannot be simply considered as “house-keepers” since deeper understanding of their functions beyond the conventionally assumed reveals their versatile roles. When attempting to “fix” such mutations, a consideration should be taken not to turn to the extreme measures of complete activation or inhibition.

The need for fine-tuning the ISR becomes apparent since the complete inhibitors of the ISR, like GSK, turn out to be toxic for pancreatic secretory cell types with high load of protein production. The discovery of a partial reversible inhibitor of the ISR (ISRIB) is a first example of a small molecule that is able to “gently” shift the balance of translation attenuation, potentially, helping dysregulated brain cells to recover from stress without causing protein-toxicity. The apparent benefit of a temporary switch off the energy-saving mode of the cell caused by phosphorylation of eIF2α is evident even in non-diseased circumstances.

Excitingly, eIF2B, one of the largest translational factors lying at the heart of the ISR, mutations in which are linked to the development of a neurodegenerative vanishing white matter disease (VWM), was identified as a

target of the ISRIB compound. The link between ISRIB and eIF2B uncovers a new frontier in searching for treatments for brain-associated illnesses, and provides a new tool that can help to elucidate many of the unanswered questions regarding the maintenance of the cellular fitness.

Chapter 4: Materials and Methods

4.1 Cell culturing and reagents

4.1.1 HeLa-derived cell lines

HeLa-derived adherent cell lines were maintained in DMEM (D6546, Sigma Aldrich) supplemented with 2 mM L-glutamine (G7513, Sigma Aldrich), 1x Penicillin/ Streptomycin (P0781, Sigma), 1x non-essential amino acids solution (M7145, Sigma), and 55 µM β-mercaptoethanol at 37°C with 5% CO_2. HeLa-derived suspension cell lines were maintained in DMEM Joklik's modification (M0518, Sigma) supplemented with 0.2% $NaHCO_3$ (S8761, Sigma), Newborn Calf serum (N4637, Sigma), 1x Penicillin/ Streptomycin, 1x non-essential amino acids solution, and 55 µM β-mercaptoethanol. Suspension cultures were grown in either Erlenmeyer flasks in a Minitron shaker (Infors HT) at a shaking speed 70 rpm, 37°C, and 8% CO_2, or in a Cellbag (BC10, GE Healthcare) using a WAVE Bioreactor 20/50 EHT system (GE Healthcare) at 37°C, 8% CO_2, air flow 0.3 sp, angle 5°-7.5°, and rotation speed 15-18.5 rpm.

4.1.2 CHO-derived cell lines

CHO-K1-derived adherent cell lines were maintained in Nutrient Mixture F12 (N4888, Sigma), 10% Fetal Calf serum (FetalClone II, Thermo), 2 mM L-glutamine (G7513, Sigma Aldrich), and 1x Penicillin/Streptomycin (P0781, Sigma) at 37°C with 5% CO_2 for. CHO-K1-derived suspension cell lines were maintained in MEM Alpha (M8042, Sigma) with 10% Fetal Calf serum, 2 mM L-glutamine, 1x Penicillin/ Streptomycin, 1x non-essential amino acids solution (M7145, Sigma), and 55 µM β-mercaptoethanol in Erlenmeyer flasks in Minitron shaker (Infors HT) at a shaking speed 70 rpm, 37°C, and 8% CO_2.

4.2 Generation of cell lines

Gene	Exon	Cells	Clone name	Description	Mutagenized region (number shows amino acid position at which mutagenesis occurred)	Results Section	Methods Section
constitutive	NA	CHO-K1	**C4**	compound activatable Fv2E-PERK cells with integrated 3xFlag-tagged eIF2αWT	314_**ERPLERADYKDHDGDYKDHDIDYKDDDDK***	**2.1.2 2.1.3**	**4.2.1**
constitutive	NA	CHO-K1	**C12**	compound activatable Fv2E-PERK cells with integrated non-phosphorylatable 3xFlag-tagged eIF2αS51A mutant	314_**ERPLERADYKDHDGDYKDHDIDYKDDDDK***	**2.1.2 2.1.3**	**4.2.1**
Eif2b2	1	HeLa	**2C2**	eIF2Bβ-3xFlag-tagged cells	2_**PGSDYKDHDGDYKDHDIDYKDDDDK**	**2.1.3-6 2.2**	**4.2.2**
Eif2b3	11	CHO-C30	**S7**	eIF2Bγ-3xFlag-tagged cells	451_**EFCRYPAQWRPLERADYKDHDGDYKDHDIDYKDDDDK***	**2.1.1 2.1.3 2.1.5 2.3.1 2.3.3**	**4.2.3**
Eif2b3	6	CHO-C30	**S9**	eIF2Bγ-3xFlag-tagged ISRIB-resistant (δL180F) cells	180_**F**FSHLPQYSRQNSLTQYMS	**2.1.1 2.1.3 2.3.3**	**4.2.4**
Eif2b3	10	CHO-C30	**C3-2**	eIF2Bγ-3xFlag-tagged VWM mutant (δA392D) cells	392_**D**SYVLPE	**2.1.3**	**4.2.5**
Eif2b2	3	CHO-K1	**N162X**	mixed population of ISRIB-resistant cells	162_**X**EVIMTIGYSRTVEAFLKEAARKRKFHVIV	**2.3.1**	**4.2.6 4.3**
Eif2b2	3	CHO-K1	**H188X**	mixed population of ISRIB-resistant cells	188_**X**VIVAECAPFCQVRG	**2.3.1 2.3.2**	**4.2.6 4.3**
Eif2b2	3	CHO-K1	**I190X**	mixed population of ISRIB-resistant cells	190_**X**VAECAPFCQVRG	**2.3.1**	**4.2.6 4.3**
Eif2b2	3	CHO-K1	**H188X-075B**	mixed population of 075B-sensitive cells	188_**X**VIVAECAPFCQVRG	**2.3.2**	**4.2.6 4.3**
Eif2b2	3	CHO-K1	**H188X-084**	mixed population of 084-sensitive cells	188_**X**VIVAECAPFCQVRG	**2.3.2**	**4.2.6 4.3**
Eif2b2	3	CHO-K1	**A3**	H188S/T, heterozygous, 084-sensitive, mildly ISRIB-resistant	188_**S**VIVAECAPFCQVRG; 188_**T**VIVAECAPFCQVRG	**2.3.2**	**4.2.6 4.3**
Eif2b2	3	CHO-K1	**A5**	H188M, homozygous, 084-sensitive, strongly ISRIB-resistant	188_**M**VIVAECAPFCQVRG	**2.3.2**	**4.2.6 4.3**
Eif2b2	3	CHO-K1	**B3**	H188K/Δ, heterozygous, 084-sensitive, strongly ISRIB-resistant	188_**K**VIVAECAPFCQVRG	**2.3.2 2.3.3**	**4.2.6 4.3**

Table 4.2a: The genotypes and descriptions of the cell lines.

ID	Plasmid name	Description	Methods Section
UK1223	heIF2a_WT_3XFLAG_pCEFL_neo MP1	mammalian expression C-terminal 3xFlag-tagged human eIF2αWT	**4.2.1**
UK1224	heIF2a_S51A_3XFLAG_pCEFL_neo MP5	mammalian expression C-terminal 3xFlag-tagged non-phosphorylatable human eIF2αS51A mutant	**4.2.1**
UK1406	EIF2B2_CRSPR1_pSpCas9(BB)-2A-GFP	GFP-tagged CRISPR/Cas9 plasmid with guide RNA for targeting N-terminus of human *EIF2B2* gene exon 1	**4.2.2**
UK1467	hEIF2B2_CRISPR1-G_pSpCas9(BB)-2A-GFP	GFP-tagged CRISPR/Cas9 plasmid with guide RNA for targeting N-terminus of human *EIF2B2* gene exon 1	**4.2.2**
UK1469	hEIF2B2_HDR_3XFLAG_N_pBS	homologous DNA repair template for N-terminal 3xFlag-tagged human *EIF2B2*	**4.2.2**
UK1491	haEIF2B3_g299541_pSpCas9_GFP	GFP-tagged CRISPR/Cas9 plasmid with guide RNA for targeting C-terminus of hamster *Eif2b3* exon 11	**4.2.3**
UK1500	haEIF2B3_3XFLAG_C_tgt1_pBS	homologous DNA repair template for C-terminal 3xFlag-tagged hamster *Eif2b3*	**4.2.3**
UK1376	haEIF2B4_g216083_pSpCas9Puro	Puro-labeled CRISPR/Cas9 plasmid with guide RNA for targeting hamster *Eif2b4* exon 6	**4.2.4**
UK1377	haEIF2B4_g212220_pSpCas9Puro	Puro-labeled CRISPR/Cas9 plasmid with guide RNA for targeting hamster *Eif2b4* exon 6	**4.2.4**
UK1385	haEIF2B4_L180F_Tgt1_mCherry	homologous DNA repair template for ISRIB-resistant L180F mutant in hamster *Eif2b3*	**4.2.4**
UK1596	haEIF2B4_g257788_pSpCas9_GFP	GFP-tagged CRISPR/Cas9 plasmid with guide RNA for targeting hamster *Eif2b3* exon 10	**4.2.5**
UK2105	EIF2B2_CRISPR7_pSpCas9(BB)-2A-mCherry	mCherry-tagged CRISPR/Cas9 plasmid with guide RNA for targeting hamster *Eif2b2* exon 3 bottom strand	**4.2.6**
UK2106	EIF2B2_CRISPR8_pSpCas9(BB)-2A-mCherry	mCherry-tagged CRISPR/Cas9 plasmid with guide RNA for targeting hamster *Eif2b2* exon 3 top strand	**4.2.6**

Table 4.2b: Plasmids list.

ID	Primer name	Sequence	Description	Methods Section
Oligo852	hEIF2B2_5HA_2S	CCTCATCTCTAATTTCGCCGTCTTCTGTTAGACGTG	screen for 3xFlag insertion at N-terminus of human *EIF2B2*, sense primer	**4.2.2**
Oligo896	hEIF2B2_3HA_3AS	GTCTGTTCCACTCCACAGATCTGTAGTCTATC	screen for 3xFlag insertion at N-terminus of human *EIF2B2,* anti-sense primer	**4.2.2**
Oligo992	haEIF2B3_OUT_AS	CAGCCCTTTAATTCTTGATCCTCCT	screen for 3xFlag insertion at C-terminus of hamster *Eif2b3,* anti-sense primer	**4.2.3**
Oligo1029	haEIF2B3_5OUT_S	TGCATGCATGTGGTATACGTACGTG	screen for 3xFlag insertion at C-terminus of hamster *Eif2b3,* sense primer	**4.2.3**
Oligo837	haEIF2B4_EX5_IN1F	GTCGAAGGGCCCACACTTCTGAGGAGGCTTGTTAGA	screen for L180F mutation in hamster *Eif2b4,* sense primer	**4.2.4**
Oligo840	haEIF2B4_EX7_IN1R	GGAGCCACTGATGAGGCCCTGGGAGTAC	screen for L180F mutation in hamster *Eif2b4,* anti-sense primer	**4.2.4**
Oligo1161	haEIF2B4_EX10 _1F	CTTAGAGAAGCCATTGATCGG	PCR DNA repair template for hamster *Eif2b4* VWM A392D mutation, sense primer	**4.2.5**
Oligo1162	haEIF2B4_A392D_1R	AGCACATAGGAATCGGCGGGAATCAGCAGGTAGGAGGTGG	PCR DNA repair template for hamster *Eif2b4* VWM A392D mutation, anti-sense primer	**4.2.6**
Oligo1163	haEIF2B4_A392D_1F	CCCGCCGATTCCTATGTGCTCCCAGAGGTGA	PCR DNA repair template for hamster *Eif2b4* VWM A392D mutation, sense primer	**4.2.7**
Oligo1164	haEIF2B4_INT11_1R	TAAGGGCCAGTGAGGTGGCTCAAT	PCR DNA repair template for hamster *Eif2b4* VWM A392D mutation, anti-sense primer	**4.2.8**
Oligo1159	haEIF2B4_INT9_OUT1F	CTCAACATTTAGGCAAAGTCAG	screen for A392D mutation in hamster *Eif2b4,* sense primer	**4.2.9**
Oligo1160	haEIF2B4_INT11_OUT1R	TATAGGCTACACAGAGAAACCC	screen for A392D mutation in hamster *Eif2b4,* anti-sense primer	**4.2.10**
Oligo1922	EIF2B2_H188X_ssODN_S	CTCTGGAGCACATCCACTCCAATGAGGTGATCATGACCATTG GCTATTCTAGAACAGTAGAAGCCTTCCTTAAAGAGGCAGCC CGAAAGAGGAAGTTCNNNGTCATTGTTGCCGAGTGTGCTCC TTTCTGCCAGGTAAGAGGGGCTGCTAAGAGTTGCTAAGAAA AGGTGAAGAGGGAATAAATAAAGGAGGAATGGAG	sense single strand ODN repair template for *Eif2b* H188X clone	**4.2.6**
Oligo1923	EIF2B2_I190X_ssODN_S	CTGGAGCACATCCACTCCAATGAGGTGATCATGACCATTGG CTATTCTAGAACAGTAGAAGCCTTCCTTAAAGAGGCAGCCC GAAAGAGGAAGTTTCATGTCNNNGTTGCCGAGTGTGCTCCT TTCTGCCAGGTAAGAGGGGCTGCTAAGAGTTGCTAAGAAAA GGTGAAGAGGGAATAAATAAAGGAGGAATGGAGTGA	sense single strand ODN repair template for *Eif2b* I190X clone	**4.2.6**
Oligo1924	EIF2B2_N162X_ssODN_A S	GAGCACACTCGGCAACAATGACATGGAACTTCCTCTTTCGG GCTGCCTCTTTAAGGAAGGCTTCTACTGTTCTAGAATAGCCA ATGGTCATGATCACTTCNNNGGAGTGGATGTGCTCCAGAGC TTGGGCTGCAATGTTCTCCGTTGTGCCTTCTGCAAGAACAGT TTTGCAAGGGAATGTGAAACGGCCATGCTTCATC	anti-sense single strand ODN repair template for *Eif2b* N162X clone	**4.2.6**
Oligo1975	P1_pKLV-EIF2B2_1975	TGAGGCCACTTGTGTAGCGCCAAGTGCAGAAGGCACAACG GAGAAC	1st round PCR, NGS sequencing of mutations in hamster *Eif2b2* exon 3, adaptor sense primer	**4.3**
Oligo1976	P2_EIF2B2_NGS_1976	ACACTCTTTCCCTACACGACGCTCTTCCGATCTCTTAGCAGCC CCTCTTACCTGGC	1st round PCR, NGS sequencing of mutations in hamster *Eif2b2* exon 3, adaptor anti-sense primer	**4.3**
Oligo1977	P5_Truseq Universal_1977	AATGATACGGCGACCACCGAGATCTACACTCTTTCCCTACAC GACGCTCTTCCGATCT	2d round PCR, NGS sequencing of mutations in hamster *Eif2b2* exon 3, adaptor anti-sense primer	**4.3**
Oligo1759	pKLV_NEBNXT01_1759	CAAGCAGAAGACGGCATACGAGATCGTGATGTGACTGGAG TTCAGACGTGTGCTCTTCCGATCTGAGGCCACTTGTGTAGCG CCAAG	2d round PCR, NGS sequencing of mutations in hamster *Eif2b2* exon 3, barcoded sense primer	**4.3**
Oligo1760	pKLV_NEBNXT02_1760	CAAGCAGAAGACGGCATACGAGATACATCGGTGACTGGAG TTCAGACGTGTGCTCTTCCGATCTGAGGCCACTTGTGTAGCG CCAAG	2d round PCR, NGS sequencing of mutations in hamster *Eif2b2* exon 3, barcoded sense primer	**4.3**
Oligo1761	pKLV_NEBNXT04_1762	CAAGCAGAAGACGGCATACGAGATTGGTCAGTGACTGGAG TTCAGACGTGTGCTCTTCCGATCTGAGGCCACTTGTGTAGCG CCAAG	2d round PCR, NGS sequencing of mutations in hamster *Eif2b2* exon 3, barcoded sense primer	**4.3**
Oligo1762	pKLV_NEBNXT05_1763	CAAGCAGAAGACGGCATACGAGATCACTGTGTGACTGGAGT TCAGACGTGTGCTCTTCCGATCTGAGGCCACTTGTGTAGCGC CAAG	2d round PCR, NGS sequencing of mutations in hamster *Eif2b2* exon 3, barcoded sense primer	**4.3**
Oligo1763	pKLV_NEBNXT06_1764	CAAGCAGAAGACGGCATACGAGATTATTGGCGTGACTGGA GTTCAGACGTGTGCTCTTCCGATCTGAGGCCACTTGTGTAGC GCCAAG	2d round PCR, NGS sequencing of mutations in hamster *Eif2b2* exon 3, barcoded sense primer	**4.3**
Oligo1764	pKLV_NEBNXT07_1765	CAAGCAGAAGACGGCATACGAGATTGATCTGGTGACTGGA GTTCAGACGTGTGCTCTTCCGATCTGAGGCCACTTGTGTAGC GCCAAG	2d round PCR, NGS sequencing of mutations in hamster *Eif2b2* exon 3, barcoded sense primer	**4.3**
Oligo1765	pKLV_NEBNXT08_1766	CAAGCAGAAGACGGCATACGAGATTTCAAGTGTGACTGGA GTTCAGACGTGTGCTCTTCCGATCTGAGGCCACTTGTGTAGC GCCAAG	2d round PCR, NGS sequencing of mutations in hamster *Eif2b2* exon 3, barcoded sense primer	**4.3**
Oligo1766	pKLV_NEBNXT09_1767	CAAGCAGAAGACGGCATACGAGATTCTGATCGTGACTGGAG TTCAGACGTGTGCTCTTCCGATCTGAGGCCACTTGTGTAGCG CCAAG	2d round PCR, NGS sequencing of mutations in hamster *Eif2b2* exon 3, barcoded sense primer	**4.3**
Oligo1767	pKLV_NEBNXT10_1768	CAAGCAGAAGACGGCATACGAGATAAGCTAGTGACTGGAG TTCAGACGTGTGCTCTTCCGATCTGAGGCCACTTGTGTAGCG CCAAG	2d round PCR, NGS sequencing of mutations in hamster *Eif2b2* exon 3, barcoded sense primer	**4.3**

Table 4.2c: Primers list.

4.2.1 CHO-K1 [Fv2E-PERK; 3xFlag-eIF2α^{WT}/ 3xFlag-eIF2α^{S51A}]

CHO-K1 [Fv2E-PERK] cell line bearing a cytosolic version of the ER kinase, PERK, was previously described (Lu et al. 2004). The cytosolic PERK has its luminal domain substituted for cytosolic Fv2E moiety able to dimerize upon addition of AP20187 compound, thereby, activating kinase activity towards eIF2α without induction of stress response. Derivative Fv2E-PERK expressing CHO-K1 cell lines that coexpress C-terminally 3xFlag-tagged full length human eIF2α^{WT} or non-phosphorylatable mutant eIF2α^{S51A} were, respectively, generated by stable transduction of plasmids UK1223 and UK1224 possessing a neomycin resistance gene for clone selectivity and an EF1 promoter to drive expression of the recombinant eIF2α subunit in mammalian cells (Sekine et al. 2015).

For transfection, 15 µg of plasmid UK1223 or UK1224 were linearized using AatII (FD0994, Thermo Fischer) using a standard procedure, the linearized DNA was phenol-chloroform extracted according to a standard method, and resuspended in 50 µL of sterile H_2O. On a day of transfection, CHO-K1 [Fv2E-PERK] cells on 100 mm dishes (2 x 10^5 cells/ mL) were transfected with 50 µL of linearized DNA using polyethylenimine (PEI) according to a standard protocol. 48 hours after transfection, cells were treated with 500 µg/ mL of neomycin G418 (G0175, Melford) to select for successfully transduced clones. Cultures were maintained under selective conditions, and clones were picked 14 days later. The selected clones were expanded and analyzed by a standard western blot procedure using mouse monoclonal anti-FLAG M2 antibodies (F1804, Sigma Aldrich) according to the manufacturer's protocol. Clones with the expression levels of tagged human eIF2α closest to the expression levels of the endogenous hamster eIF2α were carried over for experiments (human eIF2α^{WT} – Clone 4, human eIF2α^{S51A} – clone 12). The ability of Fv2E-PERK to phosphorylate the coexpressed 3xFlag-tagged full length human eIF2α^{WT} was tested by treatment of cells with 100 nM AP20187, followed by a standard western blot procedure using polyclonal rabbit anti-phospho-eIF2α antibodies (1090-1, Epitomics) according to the manufacturer's protocol.

4.2.2 HeLa [3xFlag-*EIF2B2* in/in]

HeLa [3xFlag-*EIF2B2* in/in] cell line was created using CRISPR/ Cas9 directed mutagenesis and homologous DNA repair template to N-terminally tag an endogenous human eIF2B β subunit with 3xFlag tag (Sekine et al. 2015) following published procedure (Ran et al. 2013).

HeLa cells in 6-well plates (1.3 x 10^5 cells/ mL) were transfected with 1.5 µg of homologous DNA repair plasmid (UK1469) alongside the two guide RNA plasmids (1 µg each, UK1406 and UK1467). The DNA repair plasmid contained an in-frame 3xFlag tag at codon 4 of *EIF2B2* gene, and 5' and 3' homology arms with respective sizes of 606 and 859 base pairs. The guide RNA plasmids carried Cas9 nuclease targeting the first exon of the *EIF2B2* gene, and a GFP marker for selection of successfully transfected cells. Transfection was done using Lipofectamine LTX (15338500, Invitrogen) according to the manufacturer's protocol. 24 hours post-transfection, GFP-positive cells were FACSorted, collected into 96-well plates, and expanded as single clones. The insertion of 3xFlag was analyzed by sequencing the PCR-amplified (Oligos852 and 896) targeted locus of the genomic DNA extracted from the clones. Successful clones were analyzed by a standard western blot procedure using mouse monoclonal anti-FLAG M2 antibodies (F1804, Sigma Aldrich) according to the manufacturer's protocol. Finally, the clone 2C2 expressing highest amount of 3xFlag-eIF2Bβ with both alleles bearing insertion was used for further experimentation.

4.2.3 CHO-C30 [3xFlag-*Eif2b3* in/+]

CHO-30 cells, derivatives of CHO-K1 cells, bearing *CHOP::GFP* reporter for tracking the ISR in live cells were described before (Novoa et al. 2001). CHO-C30 [3xFlag-*Eif2b3* in/+] cell line was created using CRISPR/ Cas9 directed mutagenesis and homologous DNA repair template to C-terminally tag an endogenous hamster eIF2B γ subunit with 3xFlag tag (Sekine et al. 2016) following published procedure (Ran et al. 2013).

CHO-C30 cells in 6-well plates (1.3 x 10^5 cells/ mL) were transfected with 1 µg of homologous DNA repair plasmid (UK1500) alongside a 1 µg guide RNA plasmid (UK1491). The DNA repair plasmid contained an in-frame 3xFlag tag at C-terminus of *Eif2b3* gene with 5' and 3' homology arms of respective sizes of 497 and 465 base pairs. The guide RNA plasmid carried Cas9 nuclease targeting the exon 11 of the *Eif2b3* gene, and a GFP marker for selection of successfully transfected cells. Transfection was done using Lipofectamine LTX (15338500, Invitrogen) according to the manufacturer's protocol. 24 hours post-transfection, GFP-positive cells were FACSorted, collected into 96-well plates, and expanded as single clones. Genomic DNA isolated from the clones was screened by PCR (Oligo992 and 1029) and EcoRI (FD0274, Thermo Fischer) digestion. Cells that acquired 3xFlag should have also received an exogenous EcoRI site at the C-terminus of *Eif2b3* gene derived from the repair template. The insertion of 3xFlag was confirmed by sequencing. Successful clones were analyzed by a standard western blot procedure using mouse monoclonal anti-FLAG M2 antibodies (F1804, Sigma Aldrich) according to the manufacturer's protocol. Finally, the clone S7 expressing the highest amount of 3xFlag-eIF2Bγ with one allele bearing insertion and another allele intact was used for further experimentation.

4.2.4 CHO-C30 [3xFlag-*Eif2b3* in/in; *Eif2b4_L180F in/ Δ*]

To generate CHO-C30 [3xFlag-*Eif2b3* in/+; *Eif2b4*_L180F in/Δ] cell line a 3xFlag tag was incorporated into the *Eif2b3* gene of CHO-C30 [*Eif2b4*_L180F in/Δ] cells at the C-terminus of eIF2Bγ subunit by a CRISPR/ Cas9 mediated homology-directed repair as described in Section 4.2.3. The clone S9 expressing highest amount of 3xFlag-eIF2Bγ with both alleles bearing insertion was used for further experimentation.

The CHO-C30 [*Eif2b4*_L180F in/Δ] cells, in their turn, were generated using CRISPR/ Cas9 directed mutagenesis and homologous DNA repair template to target an endogenous hamster eIF2B δ subunit (Sekine et al. 2015) following published procedure (Ran et al. 2013).

CHO-C30 cells in 6-well plates at (1.3 x 10^5 cells/ mL) were transfected with 1 µg of homologous DNA repair plasmid (UK1385) alongside two guide RNA plasmids (1 µg each, UK1376 & UK1377). The DNA repair plasmid contained L180F mutation in *Eif2b4* gene, and 5' and 3' homology arms with respective sizes of 212 and 329 base pairs. The guide RNA plasmids carried Cas9 nuclease targeting the exon 6 of the *Eif2b4* gene, and mCherry marker for selection of successfully transfected cells. Transfection was done using Lipofectamine LTX (15338500, Invitrogen) according to the manufacturer's protocol. 24 hours post-transfection, mCherry-positive cells were FACSorted, collected, and expanded as a pool. After 13 days of recovery, the cells were treated with 0.5 mM histidinol and 100 nM ISRIB for 24 hours, and FACSorted for GFP-bright populations (top 1-2%). Collected pool of cells was expanded, its genomic DNA was isolated and screened by PCR (Oligo837and 840) and BamHI (FD0054, Thermo Fischer) digestion. The mutagenized DNA should have lost the BamHI restriction site. Finally, the insertion of mutation was confirmed by sequencing.

4.2.5 CHO-C30 [3xFlag-*Eif2b3* in/in; *Eif2b4_A392D in/ Δ*]

The CHO-C30 [3xFlag-*Eif2b3* in/+, *Eif2b4*_A392D in/in] cells were generated using CRISPR/ Cas9 directed mutagenesis and homologous DNA repair template to target an endogenous hamster eIF2B δ subunit (Sekine et al. 2016) following published procedure (Ran et al. 2013).

CHO-S7 [3xFlag-*Eif2b3* in/+] cells in 6-well plates (1.3 x 10^5 cells/ mL) were transfected with 1 µg of homologous DNA repair PCR product (Oligo1161 & 1162 and Oligo1163 & 1164, knitted by Oligo1161 and 1164) alongside a 1 µg guide RNA plasmid (UK1596). The DNA repair PCR product contained A392D mutation in *Eif2b4* gene, and 5' and 3' homology arms with respective sizes of 406 and 322 base pairs. The guide RNA carried Cas9 nuclease targeting the exon 10 of the *Eif2b4* gene, and a GFP marker for selection of successfully transfected cells. Transfection was done using Lipofectamine LTX (15338500, Invitrogen) according to the manufacturer's protocol. 24 hours post-transfection, GFP-positive cells were FACSorted, collected in 96-well plates, and expanded as single clones. Cell clones were expanded, their genomic

DNA isolated and screened by PCR (Oligo1159 & 1160) and PstI (FD0614, Thermo Fischer) digestion. The mutagenized DNA should have lost the PstI restriction site. Finally, the insertion of mutation was confirmed by sequencing. Clone 3-2 was used for further experimentation.

4.2.6 CHO-C30 genome edited cells with altered ISRIB responsiveness

Site-directed random mutagenesis of hamster *Eif2b2* was carried out using CRISPR/ Cas9-directed homologous repair using an equimolar mixture of single-stranded oligo deoxynucleotides (ssODN) as repair templates containing combination of all possible codons (n=64) for each targeted site providing the diversity of substitutions (Figure 2.3.1a). Each set of ssODNs was transfected alongside guide RNA plasmids (UK2105, UK2106) inserted into a vector containing mCherry-marked Cas9 nuclease as follows: UK2105 with ssODN-1922 or ssODN-1923, UK2106 with ssODN-1924. See Tables 4.2b, c for further description of repair templates and guide vectors.

For transfection, 20 x 10^3 CHO-S7 cells (described in Section 4.2.3) (Sekine et al. 2016) were plated on 6-well plates 36 hours prior being transfected with equal amounts of 1 µg guide and 1 µg ssODN using standard Lipofectamine protocol. Transfected cells were sorted 48 hours later (Figure 2.3.1b). Before sorting for ISRIB resistance or sensitivity, a technical “mCherry-positive” sort for successfully transfected cells was done, and 240K, 360K and 330K cells were collected for respective N162X, H188X and I190X templates. Cells were plated and expanded in 100 mm dishes. Five days later, the recovered cell pools were treated with 0.5 mM histidinol (228830010, Acros Organics) and 200 nM ISRIB. 20 hours later, pools were sorted for “GFP-bright” (ISRIB-resistant) and “GFP-dull” (ISRIB-sensitive) phenotypes (Sort I, Figure 2.3.1b). 37K, 126K and 240K cells for each of the respective ISRIB-resistant pools (N162X, H188X and I190X), and 500K cells for each of the ISRIB-sensitive pools were collected. Cells were plated and expanded in 100 mm dishes. 10 days later, “GFP-dull” sort of untreated pools was carried out (Sort II, Figure 2.3.1b) to eliminate clones with a constitutively active ISR. 1 x 10^6 cells were collected for each of ISRIB-resistant and ISRIB-sensitive pools. Cells were plated and expanded in 100 mm dishes.

For a new round of sorting to reselect analogue-sensitive pools from ISRIB-resistant *Eif2b*^{H188X} pool (Figure 2.3.2a), 1 x 10^6 cells were plated on 100mm dishes. 36 hours later, cells were treated with 0.5 mM histidinol, and 2.5 µM of ISRIB or ISRIB analogue (AAA1-075B or AAA1-084). 20 hours later, cells were sorted for "GFP-dull" (analogue-sensitive) phenotype, and 1 x 10^6 cells were collected for each respective pool (ISRIB-sensitive, 075B-sensitive and 084-sensitive) (Figure 2.3.2c). Note that a newly selected ISRIB-resistant pool did not undergo any treatments prior being sorted, serving as a control population (Figure 2.3.2b). Cells were plated and expanded in 100 mm dishes.

Cell pools were phenotypically characterized, and their genomic DNA obtained for subsequent next-generation sequencing (NGS) analysis. Individual clones were genotyped following Sanger sequencing of PCR products amplified from genomic DNA.

For FACSorting procedure, all cells were washed with PBS once, collected in PBS containing 4 mM EDTA and 0.5% BSA, and sorted on INFLUX cell sorter.

4.3 NGS sequencing of *Eif2b2* containing targeted mutations

Genomic DNA was prepared from 1 x 10^7 cells using Blood and Cell culture Midi Kit (13343, Qiagen). Two rounds of PCR were performed to isolate amplicons for NGS sequencing. The first round of 18 cycles with primers 1975 and 1976 to amplify a 244 bp region of *Eif2b2* from 31 µg of DNA (corresponding to genomic DNA from 19,300 cells) divided into five 50 µL PCR reactions using Q5 polymerase (M0493, NEB) according to the manufacturer's protocol. The PCR products were pooled together and combined with 250 µL of solubilisation buffer from Gene-Jet gel purification kit (K0691, Thermo Fisher). Thereafter, mixes were purified following the standard Gene-Jet gel purification protocol (without adding the isopropanol recommended for smaller products). The second round of PCR used 11-15 cycles with a universal Illumina P5 primer (1977) and individually barcoded P7 primers for each sample (1762-1768). The resulting products were purified as

above, and quantified using Agilent DNA chip 1000 and qPCR with Illumina P5 and P7 primers. The NGS sequencing was performed using Illumina SE150bp (Figure 2.3.1d) or SE50bp kits (Figure 2.3.2d). Primers details are provided in Table 4.2c.

The sequencing reads were converted to BAM files aligned to the hamster *Eif2b2* locus. The corresponding SAM files were aligned to 31 bp templates surrounding each mutation: N162 (NNNGAXGTGATCATGACCATTGGCTATTCT), H188 (CGAAAGAGGAAGTTCNNNGTCATTGTTGCC) and I190 (CGAAAGAGGAXGTTXCATGTCNNNGTTGCCS). Reads that differed by less than three residues outside the degenerate sequence were counted for codons and amino acids at each position using Python scripts.

4.4 Measuring ISRIB action in cultured cells

ISRIB action was tracked by its effects on the activity of a stably-integrated ISR-responsive *CHOP::GFP* reporter gene in CHO-K1 cells (CHO-C30) as described in (Novoa et al. 2001). Inhibition of histidyl-tRNA synthetase by histidinol activates the eIF2α kinase GCN2 that phosphorylates eIF2. eIF2(αP) inhibits its GEF eIF2B, initiating the ISR, and culminating in *CHOP::GFP* activation, which is detected by FACS. In wild-type, ISRIB-sensitive, cells the presence of ISRIB attenuates the response of the *CHOP::GFP* reporter, whereas, in ISRIB-resistant, mutant cells, the *CHOP::GFP* reporter remains active despite ISRIB's presence.

40 x 10^3 CHO-C30 were plated in 6-well plates. Two days later, the culture medium was replaced with 2 mL of fresh medium, and compounds were added. Immediately before analysis, cells were washed with PBS, and collected in PBS containing 4 mM EDTA. Fluorescent signal from single cells (10,000/ sample) was measured by FACS Calibur (Beckton Dickinson). FlowJo software was used to analyze the data.

4.5 eIF2/ eIF2B pull-down assays

1-3 x 10^7 CHO-K1 [Fv2E-PERK; 3xFlag-eIF2α^{WT}] or CHO-K1 [Fv2E-PERK; 3xFlag-eIF2α^{S51A}] cells were used for one pull-down per sample. Cells were treated with 100 nM AP20187 (in EtOH) to promote phosphorylation of wild-type eIF2α, or 100 nM ISRIB (in DMSO), or both, or treated with respective amounts of EtOH or DMSO (not more than 1% of the growth media) as an "untreated" control for 0.5-1 hour at 37℃. For simultaneous treatment, ISRIB was added couple of minutes before AP20187 to allow ISRIB to bind its target before phosphorylating eIF2α. After the treatments, cells were washed twice with ice-cold PBS, harvested in PBS with 4 mM EDTA, pelleted at 367 x g for 5 min at 4℃, and lysed for 10 min on ice in 200 µL of harvest buffer [10 mM HEPES pH 7.9, 100 mM NaCl, 0.5% Triton, 0.5 M Sucrose, 0.1 mM EDTA, 1 mM DTT, 2 mM PMSF, 8 µg/ ml aprotinin, 4 µg/ mL pepstatin, 17.5 mM β-glycerophosphate, 10 mM tetrasodium pyrophosphate, 100 mM NaF]. Supernatants were cleared at 21,130 x g for 15 min at 4℃, and their concentration was measured using Bradford assay reagent (5000006, Bio-Rad) according to the manufacturer's protocol. 30 µL of anti-FLAG M2 affinity resin (A2220, Sigma Aldrich) resuspended 1:1 in harvest buffer was added to the equalized amounts of samples supernatants, and rotated for 1-2 hours at 4℃. After the incubation, resin was washed quickly three times with 500 µL of harvest buffer containing 100 mM NaCl to preserve eIF2*eIF2B interactions. Then, all the liquid was discarded and 30 µL of loading Laemmli buffer [100 mM Tris pH 6.8, 20% glycerol, 4% SDS, 0.2% bromophenol blue, 200 mM DTT] was added to the resin with bound material. Afterwards, samples were denatured at 70℃ for 10 min, loaded onto 12.5 % SDS-PAGE gel, and run for 1 hour at constant voltage (180 V) using a Mini-PROTEAN vertical electrophoresis system (Bio-Rad). Samples were then transferred from the gel onto PVDF membrane at constant voltage (110 V) for 70 min using transfer buffer [190 mM glycine, 25 mM Tris-base] with 20% MetOH. Membrane was then briefly washed with transfer buffer without MetOH, and blocked with 5% BSA (BP1600-100, Fischer Scientific) for 30 min at room temperature (RT) prior to incubation for 2 hours at RT with primary polyclonal rabbit anti-eIF2Bγ

antibody (H-300, Santa Cruz Biotech) to assess the amount of eIF2B bound to eIF2, and with primary polyclonal rabbit anti-phospho-eIF2α to assess the amount of phosphorylated eIF2α followed by incubation with secondary goat anti-rabbit-IR800 for 1 hour at RT according to the manufacturer's procedure. The same membrane was then incubated for 2 hours at RT with primary monoclonal mouse anti-FLAG M2 antibodies (F1804, Sigma) to assess the equal amounts of loading followed by incubation with secondary goat anti-mouse-IR680 for 1 hour at RT according to the manufacturer's procedure. Membranes were scanned on Odyssey imager (LI-COR Biosciences) and image analysis was done using ImageJ software (NIH, SciJava).

4.6 Analytical Gradient Centrifugation

4.6.1 Sucrose Gradient

HeLa-2C2 (3xFlag-*EIF2B2* in/in) cells suspension (7.5 x 10^7 cells in 75 mL) was treated for 20 minutes with either 150 µL DMSO or 200 nM ISRIB prior to harvesting and lysing in 3 x cell pellet volume of the lysis buffer [50 mM Tris pH 7.4, 400 mM KCl, 4 mM $Mg(OAc)_2$, 0.5% Triton, 5% Sucrose, 1 mM DTT, 2 mM PMSF, 8 µg/ ml aprotinin, 4 µg/ mL pepstatin, 4 µM leupeptin]. Lysates were cleared at 21,130 x g in a chilled centrifuge. 0.5 mL of the supernatant was applied on 5 mL of 5-20% sucrose gradient prepared in the cell lysis buffer with respective amounts of sucrose using SG15 Hoefer Gradient Maker, and equilibrated for 24 hours on ice. Velocity gradient centrifugation was performed on a SW50.1 rotor at 40,000 rpm for 14 hours and 20 minutes, after which the gradient was manually divided into 13 fractions of 420 µL. Each fraction was diluted two-fold with lysis buffer without sucrose, and incubated with 20% TCA for 16 hours at 4 ℃ to precipitate proteins. Proteins were then pelleted at 21,130 x g for 20 minutes in a chilled centrifuge, pellets were washed twice with ice-cold acetone, air-dried, resuspended in 60 µL of alkaline SDS loading buffer, and 5 µL of protein resuspension was resolved on a 12.5% SDS-PAGE gel. Protein gel was then transferred onto PVDF membrane (as described in Section 4.5), and incubated with primary monoclonal mouse anti-FLAG M2 antibody (F1804, Sigma) followed by

incubation with secondary polyclonal goat anti-mouse-IR800. Membranes probed with antibodies were scanned on Odyssey imager (LI-COR Biosciences) and image analysis was done using ImageJ software.

4.6.2 Glycerol Gradient

CHO [Fv2E-PERK; 3xFlag-eIF2α^{WT}] adherent cells (1 x 10^7 cells) were harvested, lysed in 500 µL of lysis buffer [10 mM HEPES pH7.9, 50 mM NaCl, 0.1 mM EDTA, 0.5% Triton, 8% Glycerol, 1mM DTT, 2 mM PMSF, 8 µg/ ml aprotinin, 4 µg/ mL pepstatin], and lysate was cleared as described in Section 4.5. 270 µL (2.3 mg) of cleared supernatant was applied on chilled equilibrated 4 mL of 10-40% glycerol gradient prepared in lysis buffer with respective amounts of glycerol using SG15 Hoefer Gradient Maker, and centrifugation was done using SW60 (Beckman Coulter) rotor at 27,500 rpm for 21 hours at 4℃. After the centrifugation, the gradient was manually fractionated into 18 fractions of 235 µL, and 23 µL of each fraction was taken for western blot analysis. Fractions were run on 12.5% SDS-PAGE gel, transferred onto PVDF membrane, incubated with primary monoclonal mouse anti-eIF2α (ascites) antibody to track migration of free 3xFlag-tagged eIF2α, and eIF2 complex, and with primary polyclonal rabbit anti-eIF2Bγ antibody (H-300, Santa Cruz Biotech) to track migration of eIF2B complex for 2 hours at RT, sequentially, followed by incubation with secondary goat anti-mouse-IR800 and with secondary goat anti-rabbit-IR800 according to the manufacturer's protocol. Probed membranes were scanned on Odyssey imager (LI-COR Biosciences), and image analysis was done using ImageJ software.

CHO-S7 [*Eif2b3*-3xFlag in/in; *Eif2b4*^{wt}] and HeLa [*EIF2B2*-3xFlag] cells (9 x 10^7 cells/ sample) were harvested, lysed in 250-500 µL of lysis buffer [50 mM HEPES pH7.5, 150 mM NaCl, 1% Triton, 5% Glycerol, 1mM DTT, 2 mM PMSF, 8 µg/ml aprotinin, 4 µg/mL pepstatin] either with 250 nM ISRIB (in 100% DMSO) or equivalent amount of DMSO, and lysates were cleared as described in Section 4.5. 250 µL of cleared supernatant was applied on 5 mL of 10-40% glycerol gradient prepared in lysis buffer (without triton) with

respective amounts of glycerol using SG15 Hoefer Gradient Maker, and centrifuged using SW50 (Beckman Coulter) rotor at 45,000 rpm for 13 hours or 14 hours 48 min at 4°C. After the centrifugation gradients were manually fractionated into 16 fractions of 325 µL, and 30 µL of each fraction was taken for western blot analysis. Fractions were run on 10% SDS-PAGE gel, transferred onto PVDF membrane, incubated for 2 hours at RT with primary monoclonal mouse anti-FLAG M2 antibody (F1804, Sigma Aldrich) to track migration of 3xFlag-tagged eIF2B complex, followed by incubation for 45 min at RT with secondary goat anti-mouse-IR800 and with secondary goat anti-mouse-HRP antibodies according to the manufacturer's protocol. Membranes were developed with enhanced chemiluminescence kit following the manufacturer's procedure, scanned on CheminDoc (Bio-Rad) and image analysis was done using ImageJ software.

4.7 Stable isotope labeling with amino acids in cell culture (SILAC)

HeLa parental or HeLa [*EIF2B2*-3xFlag] cell lines were adapted to SILAC DMEM medium (89985, Thermo Scientific) supplemented with 10% dialysed serum (26400-044, Life-Technologies), 2 mM L-glutamine (G7513, Sigma Aldrich), 1x Penicillin/ Streptomycin (P0781, Sigma), 55 µM β-mercaptoethanol, and freshly added 50 mg/ L L-arginine (A6969, Sigma Aldrich), 50 mg/L L-lysine (L8662, Sigma Aldrich), and 280 mg/L L-proline (P5607, Sigma Aldrich) according to ATCC animal cell culture guide (*ATCC® Cell Culture Media* 2012) at 37°C with 5% CO_2. Once the cells were adapted to SILAC medium, they were split, and one part of them started receiving SILAC medium supplemented with heavy-labeled 50 mg/L L-arginine ($^{13}C_6$/ $^{15}N_4$, CNLM-539, CK Gas Products) and 50 mg/L L-lysine ($^{13}C_6$/ $^{15}N_2$, CNLM-291, CK Gas Products) instead of light isotopic versions of L-arginine and L-lysine. The labeling was done in a course of about one to two weeks with considerations being taken of propagating cell cultures in order to dilute unlabeled cells under 1% (around seven cell division cycles).

On the day of the experiment, 1 x 10^8 cells/ sample on plates were treated for 15 minutes with 200 nM ISRIB (in 100% DMSO) or with equivalent amount of

DMSO as “untreated” control, then harvested, lysed in 3 x pellet volumes of lysis buffer [50 mM Tris pH 7.4, 150mM NaCl, 0.5% Triton, 5mM $MgCl_2$, 2mM DTT, 2 mM PMSF, 8 µg/ml aprotinin, 4 µg/mL pepstatin], and lysates were cleared as described in Section 4.5. 30 µL of anti-FLAG M2 affinity resin (A2220, Sigma Aldrich) resuspended 1:1 in lysis buffer was added to the equalized amounts of samples (4 mg each) mixed together 1:1 and rotated for 1 hour at 4°C. Resin was then quickly washed three times with 500 µL of lysis buffer (without triton and protease inhibitors) containing 150 mM NaCl to preserve eIF2*eIF2B interactions. All the liquid was discarded, 30 µL of elution buffer [50 mM Tris pH 7.4, 150mM NaCl, 5mM $MgCl_2$, 2mM DTT, 150 µg/ mL] was added to the resin with bound material, incubated for 1 hour at 1,200 rpm at 4°C, and 25 µL of eluted material was sent to mass-spectrometry (MS) analysis.

The MS data was analyzed using MaxQuant software. Summed peptide intensities reflect the abundance of the peptides and the accuracy of quantification. Protein ratios of “heavy” (H) to “light” (L) labeled peptides were calculated as the median of all labeled peptides ratios normalized to correct for unequal protein amounts. For more information on SILAC data analysis using MaxQuant software please refer to (Cox and Mann 2008).

4.8 Protein purification

4.8.1 eIF2

eIF2(α^{WT}), eIF2(αP) and eIF2(α^{S51A}) were either purified from CHO [Fv2E-PERK, human 3xFlag-eIF2α^{WT}] treated for one hour with 20 nM AP20187 (in 100% EtOH) to promote phosphorylation of eIF2α or with respective amount of EtOH as “untreated” control, or from CHO [Fv2E-PERK, human 3xFlag-eIF2α^{S51A}] using the following procedure. 1-2 x 10^8 of adherent cells were harvested, lysed in two pellet volumes of lysis buffer [50mM Tris-HCl pH7.4, 150mM NaCl, 0.5% Triton, 5 mM $MgCl_2$, 1mM DTT, 2 mM PMSF, 8 µg/ml aprotinin, 4 µg/mL pepstatin, 4 µM Leupeptin] supplemented with phosphatase inhibitors (17.5 mM β-glycerophosphate, 10 mM tetrasodium pyrophosphate, 100 mM NaF) for preserving phosphorylated eIF2, and

lysates were cleared as described in Section 4.5. Supernatants were precleared using protein A sepharose resin (10-1042, ZYMED) at 4˚C for 30 min. After removal of protein A sepharose resin, 30 µl of anti-FLAG M2 affinity gel (A2220, Sigma) was added to the supernatants, and incubated for 30-60 min at 4˚C. After the incubation, beads were washed once quickly with 1 mL of lysis buffer containing 500 mM NaCl, and twice with 1 mL of the same buffer for 10 min. Then, beads were washed quickly three times with 0.5 mL of GDP-mounting buffer [50 mM Tris pH7.4, 150 mM NaCl, 0.5 mM TCEP], and the bound material was eluted with 40 µl of GDP-mounting buffer supplemented with 125 µg/ ml 3X FLAG peptide (F4799, Sigma) after 30 min incubation at 4˚C. Approximately 0.5-1.5 µM of eIF2 was recovered after the procedure. This purified material was used for labeling with Bodipy-FL-GDP, and GDP-release assay (Section 4.9).

4.8.2 Human eIF2B

Human eIF2B was purified from 50 L of HeLa-2C2 cells (3xFlag-*EIF2B2* in/in) grown in suspension at a maximum density of 1 x 10^6 cells/ mL. Cell pellet (150 grams total) was harvested and washed twice with PBS at RT. Cells were then lysed at 4˚C in 2 x pellet volumes of chilled lysis buffer [50 mM Tris (pH 7.4), 150 mM NaCl, 0.5% Triton, 10% Glycerol, 5 mM $MgCl_2$, 1 mM DTT, 2 mM PMSF, 10 µg/ ml aprotinin, 4 µg/ µL pepstatin, 4 µM leupeptin]. For structural analysis lysis buffer was supplemented with 200 nM ISRIB. Lysates were cleared at 20,000 rpm (JA 25.50) at 4˚C, and supernatants were incubated with 5 mL of anti-FLAG M2 affinity gel (A2220, Sigma) for one hour at 4˚C. Resin with bound eIF2B was washed three times for 5 minutes with 10 mL of ice-cold lysis buffer containing 500 mM NaCl, then, washed three times for 5 minutes with 10 mL of washing buffer [50 mM Tris (pH 7.4), 150 mM NaCl, 0.1% CHAPS, 5m M $MgCl_2$, 1 mM DTT]. The bound protein was eluted twice sequentially in 10 mL of the washing buffer supplemented with 150 µg/ mL 3X FLAG peptide (F4799, Sigma), elution was concentrated to 2 mg/ mL using 100K MWCO PES concentrator (88503, Pierce), and 100 µL of concentrated protein complex was size-fractionated on a SEC-3 300 Å HPLC column (P.N. 5190-2513, Agilent) at a flow rate of 0.35 mL/ min in gel filtration

buffer [50 mM Tris (pH 7.4), 150 mM NaCl, 5 mM $MgCl_2$, 1 mM DTT]. The centre of the 280 nm absorbance peak eluting around 6 minutes was collected in 42 µL fraction, and applied onto cryo-grids for subsequent cryo-electron microscopy imaging. For the fluorescence polarization experiments the concentrated eIF2B eluate was used.

4.8.3 Hamster eIF2B

Hamster eIF2B from CHO-S7 [3xFlag-*Eif2b3* in/+; *Eif2b4*^{wt}], CHO-S9 [3xFlag-*Eif2b3* in/+; *Eif2b4*^{L180F} in/Δ], CHO [3xFlag-*Eif2b3* in/+; *Eif2b4*^{A392D} in/in] and CHO-B3 [3xFlag-*Eif2b3* in/+; *Eif2b2*^{H188K} in/ Δ] was purified similarly to human eIF2B (see Section 4.8.2) with following modifications.

Hamster eIF2B^{wt} and eIF2Bδ^{A392D} were purified from 3.5 L of respective CHO suspension cultures grown at maximum density of 1 x 10^6 cells/ mL. Cells were harvested, washed with PBS at RT, and lysed in 2 x pellet volumes of lysis buffer. Cleared lysate supernatant was incubated with 300 µL of anti-FLAG M2 affinity gel. The resin with bound material was washed three times for 5 minutes with 1 mL of lysis buffer containing 500 mM NaCl, then, washed three times for 5 minutes with 1 mL of washing buffer [50 mM Tris pH7.4, 150 mM NaCl, 2 mM $MgCl_2$, 0.01% Triton, 1 mM DTT]. Protein complex was eluted in 2 x resin volumes of washing buffer supplemented with 125 µg/ mL 3X FLAG peptide. 12 µg of eIF2B^{wt} and eIF2Bδ^{A392D} each were size fractionated on a SEC-3 300 Å HPLC column (P.N. 5190-2513, Agilent) at a flow rate of 0.35 mL/ min in gel filtration buffer (as in Section 4.8.2).

Hamster eIF2Bδ^{L180F} along with eIF2Bβ^{H188K} mutant cells (with total cell count of 5 x 10^8 cells each) were harvested, and lysed in 3 x pellet volumes of lysis buffer. Cleared lysate supernatant was incubated with 60 µL of anti-FLAG M2 affinity gel; resin with bound material was washed, and protein complex was eluted as described above.

4.9 GDP-release assay

The assay of GDP release from eIF2 was developed by combining features of a well-established [^{3}H]GDP release assay (Kimball et al. 1989) with a recently-described fluorescence intensity-based assay for nucleotide binding to other G-proteins (Sajid et al. 2011; Shang et al. 2012).

Substrates, Bodipy-FL-GDP labeled eIF2(α^{WT}), eIF2(αP), or eIF2(α^{S51A}) were prepared in the following manner. 40 µl of eIF2 eluate (approx. 1 µM) in GDP-mounting buffer (described in Section 4.8.1) was incubated for 20 min with 20 µL of 150 nM Bodipy-FL-GDP (G22360, Invitrogen) at 25°C. The reactant was mixed with 10 µL of 12 mM $MgCl_2$, and passed through a G-50 sephadex column (17-0855-01, GE healthcare) equilibrated with GEF-assay buffer [50 mM Tris pH7.4, 150 mM NaCl, 1 mM DTT, 2 mM $MgCl_2$, 0.01% Triton X-100]. It was then used as a substrate in the GEF assay at a working concentration of approx. 100 nM.

Human eIF2B was prepared as described in Section 4.8.2 and its eluate was used as a GEF at a working concentration of approx. 1.5 nM.

Cell lysates used as a source of GEF were prepared following an adapted published protocol (Kimball et al. 1989). CHO cells of indicated cell lines were harvested as described above, and mixed with homogenization buffer [50 mM Tris pH7.4, 375 µM magnesium acetate, 75 µM EDTA, 95 mM potassium acetate, 2.5 mg/ ml digitonin, 10% Glycerol, 1 mM DTT, 2 mM PMSF, 10 µg/ml aprotinin, 4 µg/µL pepstatin, 4 µM leupeptin] supplemented with phosphatase inhibitors (17.5 mM β-glycerophosphate, 10 mM tetrasodium pyrophosphate, 100 mM NaF) for preserving phosphorylated eIF2. The mixture was incubated on ice for 15 min and passed through 0.5 mL syringe with 29G needle five times. Lysate was then cleared at 21,130 x *g* for 15 min at 4°C, and GEF activity of the supernatant was measured.

For the assay, 2 µL of Bodipy-FL-GDP-eIF2, and 3 µL of GEF assay buffer containing 1.5 mM non-labeled GDP were pre-mixed with 0.5 µL of 10% DMSO or 0.5 µL of 4 µM ISRIB (200 nM final), and fluorescence reading was

started after addition of 4.5 µL of purified human eIF2B (1.5 nM final) or 4.5 µL cell lysate (approx. 0.5-1 µg/ µL to arrive at approx. 1.5 nM eIF2B content) in 384-well round bottom black polystyrene assay plates (3667, Corning). Fluorescence intensity (excitation wavelength: 485 ± 20 nm, emission wavelength: 535 ± 25 nm) was measured using a TECAN F500 plate reader every 20 seconds for indicated periods. GEF activity was calculated as a decrease of fluorescent intensity (ΔFI) per second at the initial linear phase of the reaction: $\Delta FI=FI_0/ FI_n$, where FI_0 is FI signal at time "0" and FI_n are subsequently measured FI points at time "n".

4.10 Fluorescence polarization assay

20 µL reactions were assembled in 384-well round bottom polystyrene plates (3677, Corning), equilibrated in the assay buffer [50 mM Tris pH7.4, 150 mM NaCl, 2 mM $MgCl_2$, 0.01% Triton, 1 mM DTT] for 10 minutes at room temperature, and either read directly or in 25 minutes after addition of unlabeled competitor on a CLARIOstar microplate reader (BMG Labtech) with filter settings of 482 nm (excitation) and 530 nm (emission). The fluorescein-labeled AAA2-101 compound was used in the range of 1-100 nM with corresponding amounts of purified eIF2B of 30-250 nM. Each measurement point was either an average of six readings every 30 seconds (for eIF2B concentration-response) or five readings every 60 seconds (for unlabeled competitor assay).

Binding of the fluorescent probe to eIF2B in the competition experiments was expressed as a fraction of relative polarization signal (%P) over the dynamic range of the assay. Relative polarization was calculated by subtracting background FP (P_{bg}) from experimental FP (P_{ex}) ($P= P_{ex}- P_{bg}$). The minimal FP (P_{min}) observed when no eIF2B was added, and the maximal FP (P_{max}) with eIF2B alone (in the presence of fluorescent probe and in the absence of non-fluorescent competitor compounds) defined the dynamic range of the assay. Values of relative polarization for any assay point ($\%P_n$) were calculated using the formula: $\%P_n=[(P_n-P_{min})/ (P_{max}-P_{min})]*100$.

4.11 Native PAGE

CHO-S7 [3xFlag-*Eif2b3* in/+; *Eif2b4*^{wt}] or parental CHO-C30 lysate supernatants were prepared as described before (Section 4.6.2) using lysis buffer [50 mM Tris pH7.4, 150 mM NaCl, 0.2% Triton, 5 mM $MgCl_2$, 10% glycerol, 1mM DTT, 2 mM PMSF, 10 µg/ ml aprotinin, 4 µg/ µL pepstatin, 4 µM leupeptin] except the times when 0.2% CHAPS or 0.2% digitonin was used instead of 0.2% triton, or when hypotonic buffer [10mM MOPS pH7.4, 1.5 mM $MgAc_2$, 0.1 mM EDTA, 1 mM DTT, 2 mM PMSF, 10 µg/ml aprotinin, 4 µg/ µL pepstatin, 4 µM leupeptin] was used. Lysate supernatants were treated with 2 µM ISRIB (in 100% DMSO) or with respective amount of DMSO, and 20-60 µg of samples were mixed with non-denaturing loading dye buffer [240 mM Tris pH 6.8, 30% glycerol, 0.03% bromophenol blue]. Then, the samples were run at constant voltage (120 V) for two hours on native PAGE system in running buffer [3 g/L Tris-base, 14.4 g/L glycine, not adjustable pH8.3-8.9] using gels made of 4.5% stacking [4.5% acrylamide, 120 mM Tris pH8.8, 0.1% APS, 0.1% TEMED] and 7.5% separation [7.5% acrylamide, 375 mM Tris pH8.8, 0.1% APS, 0.08% TEMED] partitions. After the run was completed, gels were washed for 5 min in transfer buffer [190 mM glycine, 25 mM Tris-base], and material was transferred at constant voltage (30 V) for 16 hours from the gel onto PVDF membrane activated in MetOH and washed with Bjerrum transfer buffer [5.8 g/ L Tris-base, 2.9 g/ L glycine, pH9.2 adjusted with Tris or glycine] supplemented with 0.04% SDS. Membrane with transferred material was then washed with Bjerrum transfer buffer, blocked with 5% milk for 1 hour at RT, and incubated for two hours at RT with primary monoclonal mouse anti-FLAG M2 antibodies (F1804, Sigma Aldrich) followed by incubation with secondary goat anti-mouse-IR800 for one hour at RT. Membranes were scanned on Odyssey imager (LI-COR Biosciences) and image analysis was done using ImageJ software.

Human eIF2B (600 nM in elution buffer) purified from HeLa [3xFlag-*EIF2B2*] cells (described in Section 4.8.2) was treated with 10 µM ISRIB (in 100% DMSO) or equivalent amount of DMSO, then, was mixed with non-denaturing loading dye buffer, run on native PAGE system (7.5% gel) at constant voltage

(120 V) for two hours as described above, and stained with InstantBlue Coomassie protein stain (ISB1L, Expedeon). Gel was scanned on Odyssey imager (LI-COR Biosciences) and image analysis was done using ImageJ software.

4.12 Acquisition of structural data

4.12.1 Electron microscopy

3 µL aliquots of the protein complex diluted to 2 µM in gel filtration buffer were applied on holey carbon grids (Quantifoil 300 mesh R2/2) rendered more hydrophilic with a 20 seconds 9:1 argon–oxygen plasma treatment (Fischione Model 1070). Grids were blotted for 7 seconds at 10°C in 100% humidity, and flash-frozen in liquid ethane using a Vitrobot mark II (Thermo Fisher). Data acquisition was performed on a Titan Krios microscope (Thermo Fisher) operated at 300 kV. The dataset was recorded on a back-thinned Falcon II detector (Thermo Fisher) at a calibrated magnification of x 80,000 (resulting in a pixel size of 1.75 Å on the object scale) with a defocus range of 2.5-3.5 µm. An in-house built system was used to intercept the videos from the detector at a speed of 25 frames for the 1.5-second exposures. Data were acquired automatically using the EPU software (Thermo Fisher).

4.12.2 Image processing

After visual inspection of the micrographs, 765 images were selected for further processing. The movie frames were aligned with MotionCorr (Li et al. 2013) for whole-image motion correction. Contrast transfer function parameters for the micrographs were estimated using Gctf (Zhang 2016). 237,486 particles were selected semi-automatically using the e2boxer routine from EMAN2 (Tang et al. 2007) (Figure 4.12.2a). All 2D and 3D classifications and refinements were performed using RELION (Scheres 2012a; Scheres 2012b).

First, reference-free 2D classification (Figure 4.12.2b) was performed followed by a 3D classification step using a low-pass filtered (60 Å) map calculated

from the tetrameric eIF2B $(\beta\delta)_2$ complex from *Chaetomium thermophilum* (PDB: 5DBO). An initial map was consistent with the presence of all five subunits in our sample and also with the existence of C2 symmetry. The particles were subclassified into eight 3D classes (Figure 4.12.2c). One class representing 17 % of the dataset (41,750 particles) was used for 3D refinement in C2 symmetry.

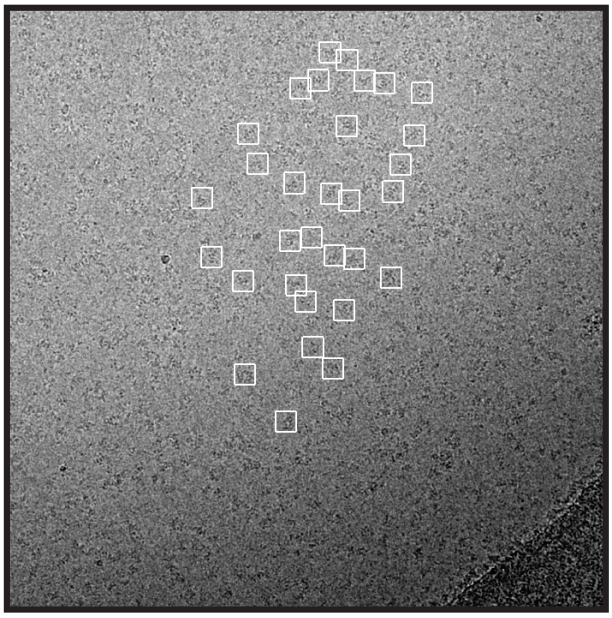

Figure 4.12.2a: Particles picking.

A representative cryo-EM micrograph with boxed human eIF2B-ISRIB protein particles as an example of manual particles picking using e2boxer EMAN2 software. Acquisition of micrographs on cryo-electron microscopy performed by F. Weis, Laboratory of Molecular Biology. Particles picking done by A. Zyryanova, University of Cambridge.

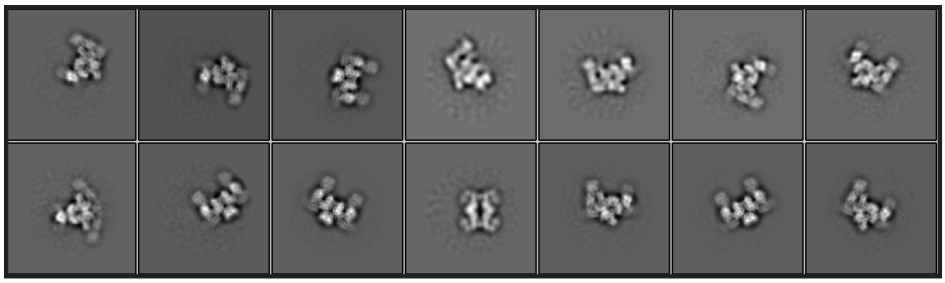

Figure 4.12.2b: 2D classification of particles.

Representative sample of the reference-free 2D class averages of eIF2B-ISRIB particles used for 3D classification and initial model generation. Analysis was performed using RELION and EMAN2 software by F. Weis, Laboratory of Molecular Biology.

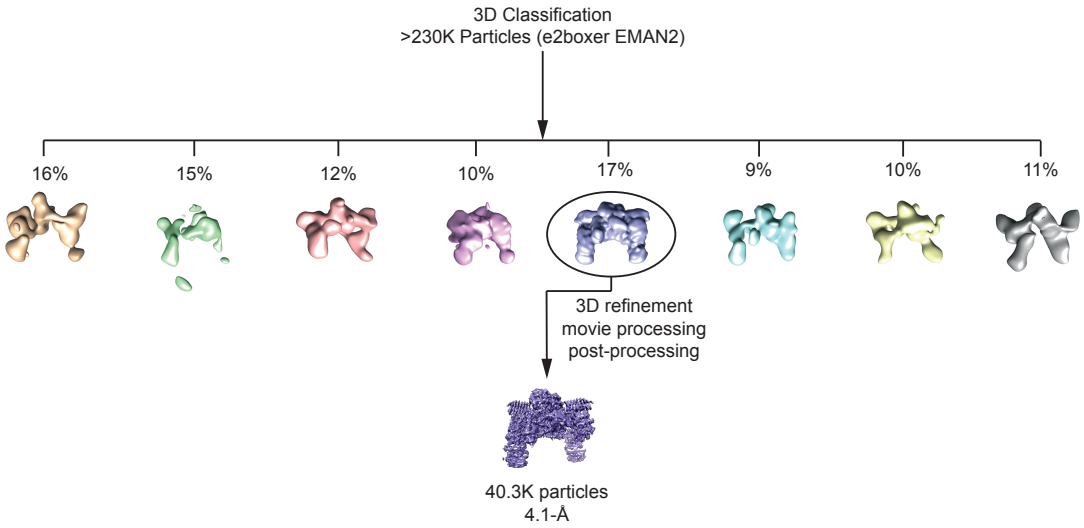

Figure 4.12.2c: 3D classification of particles.

After 3D classification was conducted on the whole particle dataset (237,213), 17% (40,326 particles) were used to generate and refine the final 3D map. Analysis was performed using RELION by F. Weis, Laboratory of Molecular Biology.

Statistical movie processing was performed as was described (Bai et al. 2013) including modeling of the fall-off of high-resolution information content by radiation damage in a dose-dependent manner as was described (Scheres 2014). The reported overall resolution of 4.1 Å was calculated using the gold-standard Fourier shell correlation (FSC) 0.143 criterion (Figure 4.12.2d) (Scheres and Chen 2012), and was corrected for the effects of a soft mask on the FSC curve using high-resolution noise substitution (Figure 4.12.2e) (Chen et al. 2013). The final density map was corrected for the modulation transfer function of the detector, and sharpened by applying a negative B factor that was estimated using automated procedures (Rosenthal and Henderson 2003).

As a control experiment, data were also processed without applying symmetry (C1). This generated a map at 4.2 Å resolution that still contained a density attributable to ISRIB in the core of the complex (data not shown).

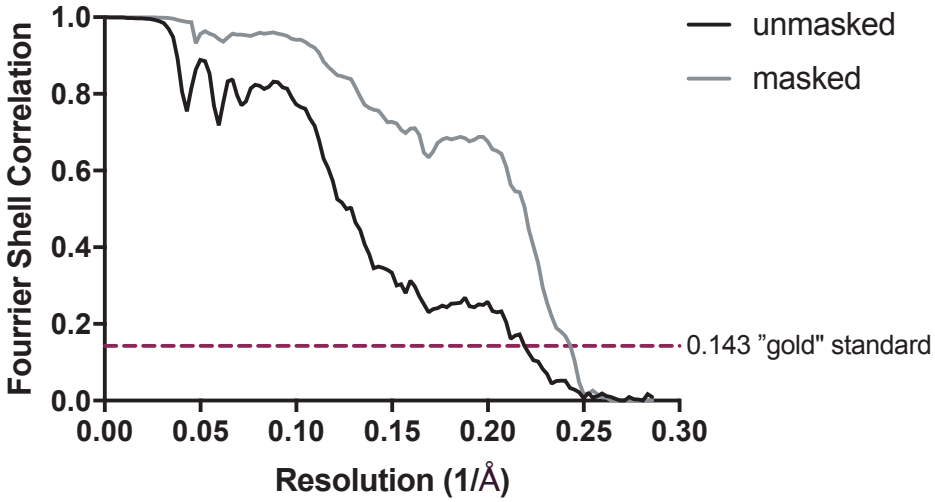

Figure 4.12.2d: Calculating resolution of the cryo-EM map.

Gold-standard Fourier shell correlation (FSC) curves. Unmasked map FSC curve is represented in black. Masked-corrected map FSC curve is represented in grey and crosses the 0.143 ‘gold standard’ purple line at a resolution of 4.1 Å indicating the resolution of the masked map. Co-generated by F. Weis, Laboratory of Molecular Biology, and A. Faille, University of Cambridge. Figure was assembled by A. Zyryanova, University of Cambridge.

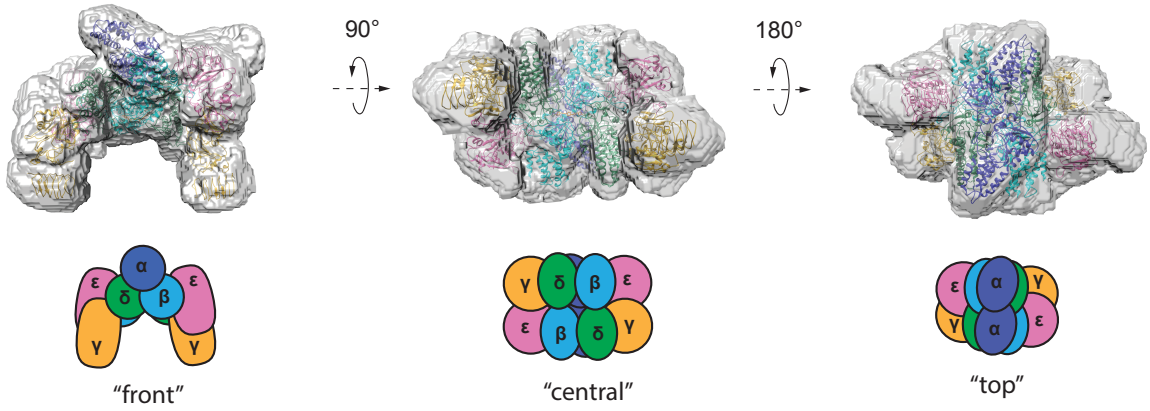

Figure 4.12.2e: "Soft" mask applied on the structural model.

Transparent representations of the "soft" mask used for post-processing of the final density map. Structures of eIF2B subunits are represented in cartoon, colored as below. Co-generated using RELION by F. Weis, Laboratory of Molecular Biology, and A. Faille, University of Cambridge. Figure was assembled by A. Zyryanova, University of Cambridge.

4.12.3 Model building and refinement

S. pombe eIF2B structure (PDB: 5B04) (Kashiwagi et al. 2016) was used as a starting model. A poly-alanine (glycines were immediately added to account for flexibility) model was generated, and subunits were individually fitted to the density map in Chimera (Pettersen et al. 2004). This model was then finely fitted using real space refinement, and loops found to be divergent between *S. pombe* and human were rebuilt in Coot (Emsley et al. 2010). All side chains, for which density was clearly resolved (up to 37% of non-Ala non-Gly residues in α and β subunits and as low as 8% in ε subunits), were positioned. The ISRIB molecule was then manually fitted in the density located at the regulatory core of eIF2B.

The model was refined using phenix.real_space_refine (Adams et al. 2010) to optimize both protein and ligand geometry, and limit clashes. Finally, REFMAC in CCP-EM (Burnley et al. 2017) was used to further refine the model, to automatically generate map vs. model FSC curves (Figure 4.12.3a), and to assess overfitting as was described (Brown et al. 2015). Briefly, the procedure involved initial random displacement of the atoms within the final model, and refinement against one of the two half maps to generate the FSC_{work} curve. A cross-validated FSC_{free} curve was calculated between the refined model and the other half map. The similarity between FSC_{work} and FSC_{free} curves should be indicative of the absence of overfitting. Maps were analyzed and visualized using Chimera (Pettersen et al. 2004). Figures were prepared using Chimera and Pymol (Molecular Graphics System, Version 2.0.6 Schrödinger, LLC, http://www.pymol.org).

Information on structural data processing is summarized in Table 4.12.3b.

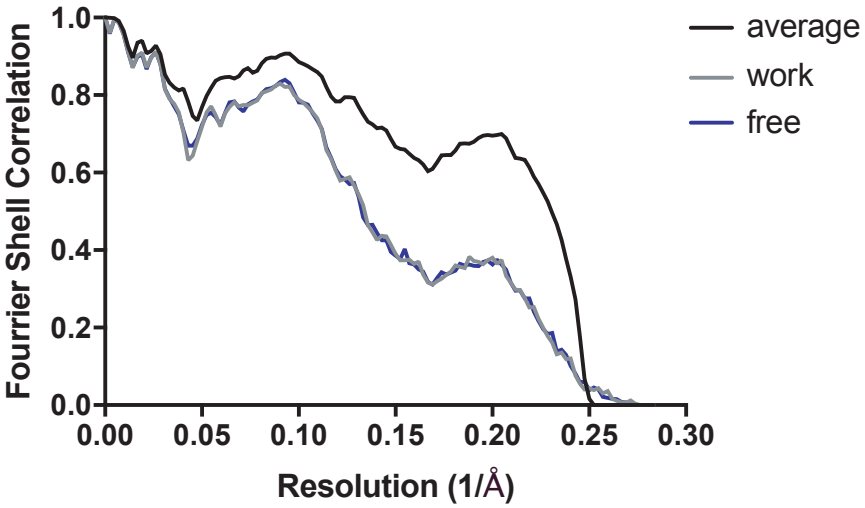

Figure 4.12.3a: Refinement and cross-validation of the eIF2B model.

The final map vs. model 'FSC average' curve is represented in black. For cross-validation, the model was 'shaken' (see Methods section) and refined against one of the two half-maps to generate the 'FSC work' curve (grey line). The 'FSC free' curve was calculated between this same refined model and the other half-map (blue line). Superimposition of the two FSC curves shows no sign of over-fitting. Co-generated using RELION by F. Weis, Laboratory of Molecular Biology, and A. Faille, University of Cambridge. Figure was assembled by A. Zyryanova, University of Cambridge.

Cryo-electron microscopy data collection	
Electron microscope	Titan Krios 300 kV
Detector	FEI Falcon II
Detector mode	Linear
Pixel size (Å)	1.75
Defocus range (μm)	-2.5 to -3.5
Dose rate (e^-.pixel^{-1}.s^{-1})	60
Electron dose (e^-.Å^{-2}.s^{-1})	20
Exposure time (s)	1.5
Total dose (e^-.Å^{-2})	30
Movies	765
Frames / movie	25
Reconstruction	
Software	Relion
Symmetry	C2
Particles used for 3D refinement	41750
Cell dimensions	
a, b, c (Å) A, β, γ (°)	240, 240, 240 90, 90, 90
Model refinement	
Resolution limit	4.1
Map sharpening factor (Å^2)	-140.4
$FSC_{average}$[3]	0.6931
RMS bonds deviation (Å)	0.0069
RMS angles deviation (Å)	1.3485
Model validation	
Molprobity score	2.33 (99th percentile)
Clashscore	6.84 (100th percentile)
Ramachandran favored	80.68%
Ramachandran allowed	18.57%
Ramachandran outliers	0.75%
Rotamer favored	91.44%
Rotamer outliers	0.20%

Table 4.12.3b: Data collection, map reconstruction, and model statistics.

[3] $FSC_{average} = \Sigma(N_{shell}\ FSC_{shell} / \Sigma(N_{shell})$, where FSC_{shell} is the FSC in a given shell, N_{shell} is the number of "structure factors" in the shell.
$FSC_{shell} = \Sigma(F_{model}\ FEM)/(\sqrt{(\Sigma(|F|2\ model))}\ \sqrt{(\Sigma(F2\ EM))}$.

4.13 ISRIB analogues chemistry

Compound design (Scheme 4.13)**.** To observe ISRIB's interaction with eIF2B directly, we designed a fluorescently labeled derivative (AAA2-101) (Figure 2.1.1e) based on known structure–activity relationships of ISRIB derivatives (Hearn et al. 2016). These show that major modifications of the central *trans*-cyclohexyl group and the glycolamide linkages are poorly tolerated, whereas changes to the terminal aryl groups in some cases maintain or enhance activity. Since conservative modifications of the glycolamide portions appeared possible (Hearn et al. 2016), we attempted to tether the glycolamide C^{α} of one of the cyclohexyl substituents to the neighboring phenyl in the form of a chromane group. We observed that the compound containing this group (AAA1-084, Figure 2.1.1e) retained activity and was only 8.5-fold less active than trans-ISRIB (Figure 2.1.1f). Molecular modeling with *S.pombe* eIF2B structure (PBD: 5B04) suggested that the benzylic C of the chromane system would face the solvent-accessible entry into the putative ISRIB-binding site of eIF2B. Replacement of the chromane with the dihydrobenzoxazine system afforded a compound (AAA1-075B, Figure 2.1.1e) only 3-fold less active than trans-ISRIB (Figure 2.1.1f). The aniline function in this compound was then used to elaborate the fluorescently labeled compound AAA2-101, which contains a flexible linker terminating in a 5/6-carboxyfluorescein moiety.

General. LC-MS analyses were performed using a Shimadzu UFLCXR system coupled to an Applied Biosystems API2000 mass spectrometer. The HPLC column used was Phenomenex Gemini-NX, 3 µm-110 Å, C_{18}, 50 x 2 mm with a flow rate of 0.5 mL/min and UV monitoring at 220 and 254 nm. Gradient elution: pre-equilibration for 1 min at 5% eluant B in eluant A; then 5 to 98% B over 2 min, 98% B for 2 min, 98 to 10% B over 0.5 min, then 10% B for one min. Eluant A: 0.1% HCOOH in H_2O; eluant B: 0.1% HCOOH in MeCN. ^{1}H-NMR spectra were recorded using a Bruker-AV 400 instrument operating at 400.13 MHz and ^{13}C-NMR spectra were recorded at 101.62 MHz. Chemical shifts (δ) are in parts per million (ppm) with reference to solvent

chemical shift. High-resolution time-of-flight electrospray (TOF-ES$^+$) mass spectra (HR-MS) were recorded using a Bruker micrOTOF spectrometer.

***N*,*N*'-((1*r*,4*r*)-Cyclohexane-1,4-diyl)*bis*(2-(4-chlorophenoxy)acetamide)** (**2a**; trans-ISRIB). This compound was prepared from *trans*-1,4-cyclohexanediamine (**1a**) and 4-chlorophenoxyacetyl chloride as described (2). ^{1}H-NMR (DMSO-d_6): δ 7.97 (d, J = 8.0 Hz, 2H), 7.33 (d, J = 8.8 Hz, 4H), 6.96 (d, J = 8.6 Hz, 4H), 4.44 (s, 4H), 3.58 (br s, 2H), 1.75 (br d, J = 7.5 Hz, 4H), 1.33 (quint, J = 10.2 Hz, 4H); ^{13}C-NMR (DMSO-d_6): δ 167, 157, 129, 125, 117, 67, 47, 31; LC-MS: *m/z* 451.3 [M + H]$^+$; HPLC: t_R 2.92 min (> 95%).

***N*,*N*'-((1*s*,4*s*)-Cyclohexane-1,4-diyl)*bis*(2-(4-chlorophenoxy)acetamide)** (**2b**; cis-ISRIB). This compound was prepared from *cis*-1,4-cyclohexanediamine (**1b**) and 4-chlorophenoxyacetyl chloride as described (2). ^{1}H-NMR (DMSO-d_6): δ 7.87 (d, J = 7.1 Hz, 2H), 7.34 (d, J = 9.5 Hz, 4H), 6.98 (d, J = 8.7 Hz, 4H), 4.49 (s, 4H), 3.73 (br s, 2H), 1.54-1.63 (m, 8H); ^{13}C-NMR (DMSO-d_6): δ 167, 157, 130, 125, 117, 67, 45, 28; LC-MS: *m/z* 451.4 [M + H]$^+$; HPLC: t_R 2.96 min (95%).

***N*,*N*'-((1*r*,4*r*)-Cyclohexane-1,4-diyl)*bis*(2-methoxyacetamide)** (**3**; AAA1-090). A stirred solution of **1a** (0.11 g, 1 mmol) and iPr_2NEt (0.37 mL, 2.2 mmol) in CH_2Cl_2 (5 mL) was cooled to 0 ^{o}C. Methoxyacetyl chloride (0.19 mL, 2.2 mmol) in CH_2Cl_2 (1 mL) was added dropwise. The resulting suspension was stirred at 0 ^{o}C for 30 min and at room temperature for 1 h. EtOAc was added and the solution was extracted successively with saturated aq solutions of NH_4Cl, $NaHCO_3$, and brine. The organic phase was dried with Na_2SO_4, filtered, and evaporated. The residue was triturated with Et_2O, collected and dried to afford the title compound as a white powder (0.219 g, 85%) ^{1}H-NMR (DMSO-d_6): δ 7.55 (d, J = 8.8 Hz, 2H), 3.75 (s, 4H), 3.55 (br s, 2H), 3.28 (s, 6H), 1.70 (d, J = 8.4 Hz, 4H), 1.33 (quint, J = 19.7 Hz, 4H); ^{13}C-NMR (DMSO-d_6): δ 168, 72, 59, 47, 31; HR-MS: *m/z* 259.1660 [M + H]$^+$, $C_{12}H_{23}N_2O_4$ requires 259.1652.

***N*-((1*r*,4*r*)-4-Aminocyclohexyl)-2-(4-chlorophenoxy)acetamide** (**4b**). A stirred solution of *tert*-butyl ((1*r*,4*r*)-4-aminocyclohexyl)carbamate (**1c**, 2.143

g, 10 mmol) and iPr_2NEt (1.9 mL, 11 mmol) in CH_2Cl_2 (50 mL) was cooled to 0 ^oC (ice bath). 4-Chlorophenoxyacetyl chloride (1.7 mL, 11 mmol) in CH_2Cl_2 (3 mL) was added dropwise. The resulting suspension was stirred at 0 ^oC for 30 min and at room temperature for 1 h. EtOAc was added and the solution was extracted successively with saturated aq solutions of NH_4Cl, $NaHCO_3$, and brine. The organic phase was dried with Na_2SO_4, filtered, and evaporated. The residue was triturated with Et_2O, collected, and dried to afford the Boc-protected intermediate **4a** as a white powder (3.63 g, 95%).

A suspension of **4a** (1.43 g, 3.5 mmol) in dioxane–MeOH (2:1; 6 mL) was treated with 4 M HCl in dioxane (7 mL, 28 mmol) with stirring for 2 h. The resulting solution was evaporated and the residue was triturated with Et_2O, collected, and dried to afford the HCl salt of the title compound **4b** as a white powder (1.071 g, 96%). ^{1}H-NMR (DMSO-d_6): δ 8.0 (d, J = 6.5 Hz, 1H), 7.33 (d, J = 8.7 Hz, 2H), 6.96 (d, J = 8.7 Hz, 2H), 5.98 (br s, 2H), 4.46 (s, 2H), 3.50-3.60 (m, 1H), 2.91 (br s, 1H), 1.97, 1.78 (dd, J = 10.9 Hz, J = 13.1 Hz, 4H), 1.36 (sext, 4H); ^{13}C-NMR (DMSO-d_6): δ 167, 157, 129 , 125 , 117, 67, 49, 47, 31, 29; HPLC: t_R 2.03 min (95%).

6-Chloro-*N*-((1*r*,4*r*)-4-(2-(4-chlorophenoxy)acetamido)cyclohexyl) chromane-2-carboxamide (**6**; AAA1-084). To a stirred solution of (*rac*)-6-chlorochromane-2-carboxylic acid (**5**; 0.1 g, 0.5 mmol; prepared as described (Dolle, R. E. C., Chu 2005)) and Et_3N (0.13 mL, 1 mmol) in CH_2Cl_2 (5 mL) was added *O*-(benzotriazol-1-yl)-*N*,*N*,*N*',*N*'-tetramethyluronium hexafluorophosphate (HBTU; 0.21 g, 0.6 mmol). The mixture was stirred for 10 min, when **4b** (0.16 g, 0.55 mmol) was added. Stirring was continued overnight, the reaction was diluted with H_2O, and was extracted with EtOAc. The organic layer was washed with aq NH_4Cl and brine, dried over Na_2SO_4, filtered, and evaporated. The residue was triturated with Et_2O, collected, and dried to afford the title compound as an off-white powder (0.155 g, 65%). ^{1}H-NMR (DMSO-d_6): δ 7.95 (d, J = 8.2 Hz, 1H), 7.83 (d, J = 7.5 Hz, 1H), 7.35 (d, J = 8.3, 2H), 7.14 (d, J = 7.2, 2H), 6.97 (d, J = 9.3, 2H), 6.89 (d, J = 9.0 Hz, 1H), 4.51, 4.49 (dd, J = 3.9 Hz, J = 3.0 Hz, 1H), 4.46 (s, 2H), 3.59 (br s, 2H), 2.84-2.76 (m, 1H), 2.72-2.65 (m, 1H), 2.17-2.10 (m, 1H), 1.90-1.82 (m, 1H),

1.78 (br s, 4H), 1.40-1.30 (m, 4H); ^{13}C-NMR (DMSO-d_6): δ 169, 168, 157, 152, 129, 126, 125, 124, 118, 117, 75, 67, 48, 31, 25, 23; HPLC: t_R 3.01 min (95%). HR-MS: *m/z* 477.1350 $[M + H]^+$, $C_{24}H_{27}Cl_2N_2O_4$ requires 477.1342.

6-Chloro-*N*-((1*r*,4*r*)-4-(2-(4-chlorophenoxy)acetamido)cyclohexyl)-3,4-dihydro-2*H*-benzo[*b*][1,4]oxazine-2-carboxamide (**8a**; AAA1-075B). A solution of (*rac*)-ethyl 6-chloro-3,4-dihydro-2*H*-1,4-benzoxazine-2-carboxylate (7a; 0.25 g, 1 mmol; prepared as described (Carr 1979)) in THF–H_2O (2:1) was treated with LiOH.H_2O (0.12 g, 3 mmol) and the resulting mixture was stirred for 3 h. The solution was neutralized with 1 M aq HCl solution and extracted with EtOAc. The organic phase was dried over Na_2SO_4, filtered and concentrated to afford 6-chloro-3,4-dihydro-2*H*-1,4-benzoxazine-2-carboxylic acid **7b** (0.19 g, 89%).

To a stirred solution of **7b** (0.15 g, 0.7 mmol) and Et_3N (0.18 mL, 1.4 mmol) in CH_2Cl_2 (5 mL) was added HBTU (0.3 g, 0.84 mmol). The mixture was stirred for 10 min, when **4b** (0.23 g, 0.77 mmol) was added. Stirring was continued overnight, the reaction was diluted with H_2O, and was extracted with EtOAc. The organic layer was washed with aq NH_4Cl and brine, dried over Na_2SO_4, filtered, and evaporated. The residue was dissolved in MeOH (1 mL) and the product was precipitated by addition of excess Et_2O. The precipitate was collected, washed with more Et_2O and dried to afford the title compound as an off-white powder (0.224 g, 67%). ^{1}H-NMR (DMSO-d_6): δ 8.08 (d, *J* = 8.4 Hz, 1H), 7.92 (d, *J* = 8.4 Hz, 1H), 7.34 (d, *J* = 8.7 Hz, 2H), 6.97 (d, *J* = 9.0 Hz, 2H), 6.78 (d, *J* = 8.4 Hz, 1H), 6.63 (d, *J* = 2.7 Hz, 1H), 6.50, 6.48 (dd, *J* = 3.3 Hz, *J* = 2.7 Hz, 1H), 6.31 (s, 1H), 4.47 (s, 2H), 4.44 (dd, *J* = 3.3 Hz, *J* =3.6 Hz, 1H), 3.57 (br s, 2H), 3.45, 3.42 (tt, *J* = 6.7 Hz, *J* = 6.2 Hz, 1H), 3.20-3.15 (m, 1H), 1.78-1.70 (m, 4H), 1.42-1.29 (m, 4H); ^{13}C-NMR (DMSO-d_6): δ 168, 166, 157, 141, 136, 129, 125, 118, 116, 114, 73, 68, 48, 42, 31; HPLC: t_R 2.90 min (95%). HR-MS: *m/z* 478.1286 $[M + H]^+$, $C_{23}H_{26}Cl_2N_3O_4$ requires 478.1295.

4- and 5-((2-(2-(2-(2-(6-Chloro-2-(((1*r*,4*r*)-4-(2-(4-chlorophenoxy) acetamido)cyclohexyl)carbamoyl)-2,3-dihydro-4*H*-benzo[*b*][1,4]oxazin-4-yl)acetamido)ethoxy)ethoxy)ethyl)carbamoyl)-2-(6-hydroxy-3-oxo-3*H*-xanthen-9-yl)benzoic acid (**8f**; AAA2-101). To a solution of **8a** (0.19 g, 0.4

mmol) in DMF (5 mL) was added K_2CO_3 (0.18 g, 1.2 mmol), NaI (0.09 g, 0.6 mmol), and methyl bromoacetate (0.1 mL, 0.48 mmol). The mixture was stirred at 125 ^oC for 16 h, cooled to room temperature, and diluted with H_2O (10 mL). The solution was extracted with EtOAc and the organic phase was washed with H_2O and brine, dried over Na_2SO_4, filtered, and evaporated. The residue was purified by silica gel column chromatography (CH_2Cl_2–THF gradient elution) to afford methyl ester **8b** (0.14 g, 65%).

A solution of **8b** (0.1 g, 0.18 mmol) in THF–H_2O (2:1) was treated with LiOH.H_2O (0.037 g, 0.9 mmol) and the resulting mixture was stirred for 3 h. The reaction was neutralized with 1 M aq HCl and extracted with EtOAc. The organic phase was dried over Na_2SO_4, filtered, and evaporated to afford the carboxylic acid derivative **8c** (0.09 g, 98%).

8c (0.09 g, 0.2 mmol) and Et_3N (0.06 mL, 0.5 mmol) were dissolved in CH_2Cl_2 (3 mL). HBTU (0.08 g, 0.22 mmol) was added and the mixture was stirred for 10 min, when *tert*-butyl (2-(2-(2-aminoethoxy)ethoxy)ethyl)carbamate (0.054 g, 0.22 mmol) in CH_2Cl_2 (1 mL) was added. The mixture was stirred overnight, diluted with H_2O, and extracted with EtOAc. The organic phase was washed with aq NH_4Cl and brine, dried over Na_2SO_4, filtered, and evaporated. The residue was purified by silica gel column chromatography (CH_2Cl_2–MeOH gradient elution) to afford the Boc-protected intermediate **8d** (0.12 g, 80%).

A solution of **8d** (0.12 g, 0.15 mmol) in dioxane (0.5 mL) was treated with 4 M HCl in dioxane (1 mL, 4 mmol). After stirring for 2 h the solution was evaporated. The residue was dissolved in MeOH (0.5 mL) and the product was precipitated by addition of excess Et_2O. The precipitate was collected and dried to afford the HCl salt of the amine derivative **8e** (0.10 g, 98%).

8c (14 mg, 0.02 mmol) and 5-(and 6-) carboxyfluorescein succinimidyl ester (9.4 mg, 0.02 mmol; NHS-fluorescein, 5/6-carboxyfluorescein succinimidyl ester mixed isomer (46410, ThermoFisher Scientific)), were dissolved in DMF (1 mL) with Et_3N (4 µL). The mixture was stirred overnight at 31℃ and was evaporated. The residue was fractionated by semi-preparative HPLC (Phenomenex Gemini 5 µm-110 Å, C_{18}, 150 x 10 mm column; 5 mL/min flow

rate) with linear gradient elution of H_2O–MeCN (containing 0.1% HCOOH) from 85:15 to 5:95 over 13 min to afford the title compound **8f** as an orange powder (0.015 g, 75%). ^{1}H-NMR (DMSO-d_6): δ 8.88, 8.74 (tt, J = 5.8 Hz, J = 11.7 Hz, 1H), 8.46 (s, 1H), 8.30 (br s, 1H), 8.22, 8.15 (dd, J = 8.6 Hz, J = 8.0 Hz, 1H), 8.05-8.11 (m, 1H), 7.96 (t, J = 8.1 Hz, 2H), 7.68 (s, 1H), 7.34 (t, J = 9.7 Hz, 2H), 6.95 (d, J = 8.6 Hz, 2H), 6.82 (d, J = 8.6 Hz, 1H), 6.67 (s, 2H), 6.58 (d, J = 8.9 Hz, 2H), 6.54 (s, 2H), 6.49 (d, J = 8.0 Hz, 1H), 4.61 (quint, J = 4.0 Hz, 1H), 4.44 (s, 2H), 4.44, 3.81-3.96 (m, 4H), 3.5-3.57 (m, 8H), 2.07 (s, 2H), 1.67-1.78 (m, 4H), 1.29-1.39 (m, 4H), 1.23 (s, 4H); HPLC: t_R 2.81 min (95%); HR-MS: *m/z* 1024.2920 $[M + H]^+$, $C_{52}H_{52}C_{l2}N_5O_{13}$ requires 1024.2933.

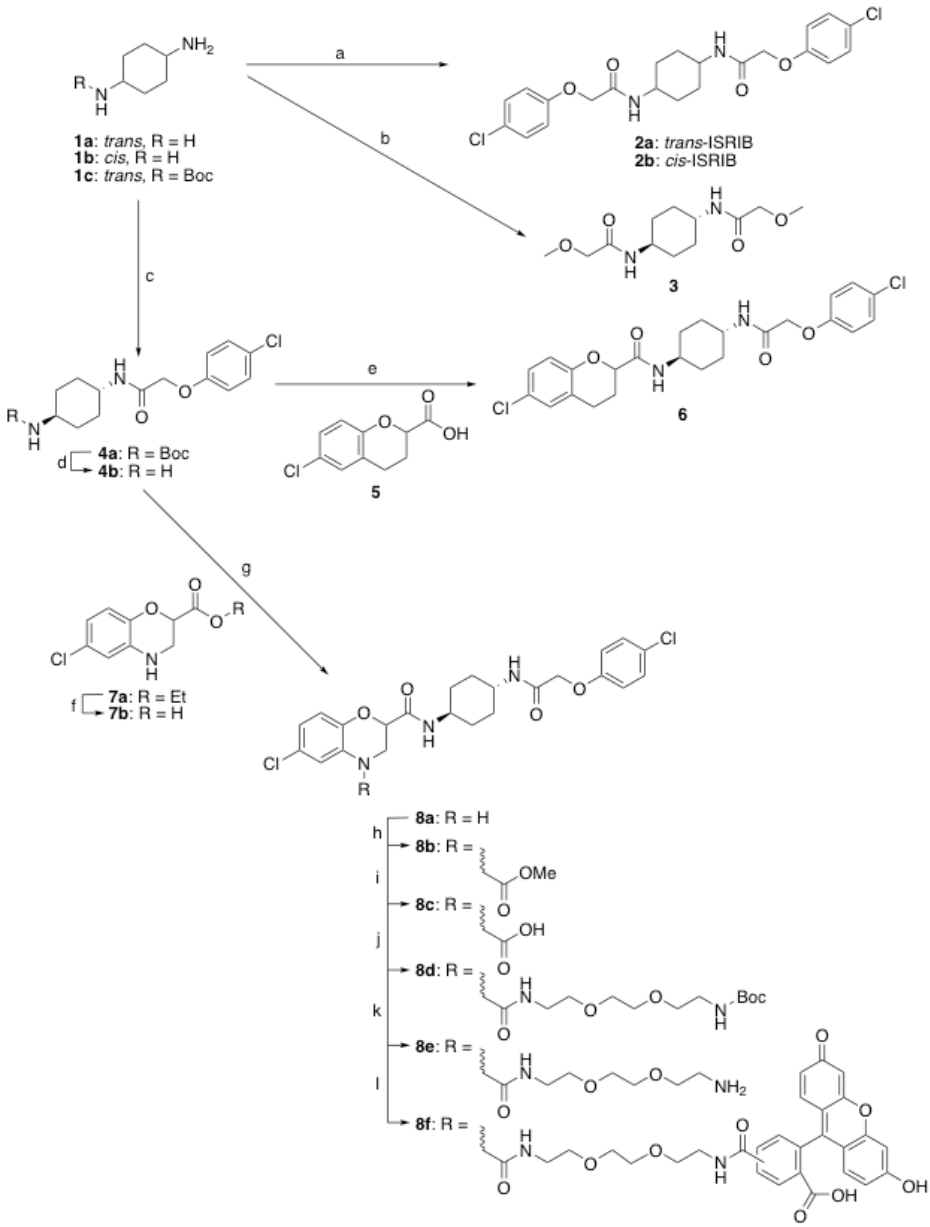

Figure 4.13. (a) **1a** or **1b**, 4-chlorophenoxyacetyl chloride, iPr_2NEt, CH_2Cl_2, 0 °C to rt (70-88%); (b) **1a**, methoxyacetyl chloride, iPr_2NEt, CH_2Cl_2, 0 °C to rt (85%); (c) **1c**, 4-chlorophenoxyacetyl chloride, iPr_2NEt, CH_2Cl_2, 0 °C to rt (95%); (d, f, and k) 4 M HCl in dioxane–MeOH (89-98%); (e) **4b** and **5**, HBTU, Et_3N, CH_2Cl_2 (65%); (g) **4b** and **7b**, HBTU, Et_3N, CH_2Cl_2 (67%); (h) methyl bromoacetate, K_2CO_3, NaI, DMF, 125 °C, 16 h (65%); (i) LiOH, THF–H_2O (98%); (j) *tert*-butyl (2-(2-(2-aminoethoxy)ethoxy)ethyl)carbamate, HBTU, Et_3N, CH_2Cl_2 (80%); (l) 5-(and 6-) carboxyfluorescein, iPr_2NEt, DMF, 31℃, 12 h (75%).

Bibliography

Adams, Paul D., Pavel V. Afonine, Gábor Bunkóczi, Vincent B. Chen, Ian W. Davis, Nathaniel Echols, Jeffrey J. Headd, et al. 2010. “PHENIX: A Comprehensive Python-Based System for Macromolecular Structure Solution.” *Acta Crystallographica Section D: Biological Crystallography* 66 (2): 213–21. doi:10.1107/S0907444909052925.

Alone, Pankaj V., and Thomas E. Dever. 2006. “Direct Binding of Translation Initiation Factor eIF2γ-G Domain to Its GTPase-Activating and GDP-GTP Exchange Factors eIF5 and eIF2Bε.” *Journal of Biological Chemistry* 281 (18): 12636–44. doi:10.1074/jbc.M511700200.

Amesz, Hans, Hans Goumans, Thea Haubrich-Morree, Harry O. Voorma, and Rob Benne. 1979. “Purification and Characterization of a Protein Factor That Reverses the Inhibition of Protein Synthesis by the Heme-Regulated Translational Inhibitor in Rabbit Reticulocyte Lysates.” *European Journal of Biochemistry* 98 (2): 513–20. doi:10.1111/j.1432-1033.1979.tb13212.x.

Anantharaman, Vivek, and L. Aravind. 2006. “Diversification of Catalytic Activities and Ligand Interactions in the Protein Fold Shared by the Sugar Isomerases, eIF2B, DeoR Transcription Factors, Acyl-CoA Transferases and Methenyltetrahydrofolate Synthetase.” *Journal of Molecular Biology* 356 (3): 823–42. doi:10.1016/j.jmb.2005.11.031.

Anthony, Tracy G., John R. Fabian, Scot R. Kimball, and Leonard S. Jefferson. 2000. “Identification of Domains within the ε-Subunit of the Translation Initiation Factor eIF2B That Are Necessary for Guanine Nucleotide Exchange Activity and eIF2B Holoprotein Formation.” *Biochimica et Biophysica Acta - Gene Structure and Expression* 1492 (1): 56–62. doi:10.1016/S0167-4781(00)00062-2.

Aroor, Annayya R, Nancy D Denslow, Lalit P Singh, Thomas W O’Brien, and Albert J Wahba. 1994. “Phosphorylation of Rabbit Reticulocyte Guanine Nucleotide Exchange Factor In Vivo. Identification of Putative Casein Kinase II Phosphorylation Sites.” *Biochemistry* 33 (11): 3350–57. doi:10.1021/bi00177a028.

Asano, K., T Krishnamoorthy, L Phan, G D Pavitt, and A G Hinnebusch. 1999. “Conserved Bipartite Motifs in Yeast eIF5 and eIF2Bepsilon, GTPase-Activating and GDP-GTP Exchange Factors in Translation Initiation, Mediate Binding to Their Common Substrate eIF2.” *The EMBO Journal* 18 (6): 1673–88. doi:10.1093/emboj/18.6.1673.

Ashe, M. P., J W Slaven, S K De Long, S Ibrahimo, and A B Sachs. 2001. “A Novel eIF2B-Dependent Mechanism of Translational Control in Yeast as a Response to Fusel Alcohols.” *The EMBO Journal* 20 (22): 6464–74. doi:10.1093/emboj/20.22.6464.

ATCC® Cell Culture Media. 2012. G DeliveReD.

Axten, Jeffrey M., Jesús R. Medina, Yanhong Feng, Arthur Shu, Stuart P. Romeril, Seth W. Grant, William Hoi Hong Li, et al. 2012. “Discovery of 7-Methyl-5-(1-{[3-(Trifluoromethyl)phenyl]acetyl}-2,3-Dihydro- 1H-Indol-5-Yl)-7H-pyrrolo[2,3-D]pyrimidin-4-Amine (GSK2606414), a Potent and Selective First-in-Class Inhibitor of Protein Kinase R (PKR)-like Endoplasmic Reticulum Kinase (PERK).” *Journal of Medicinal Chemistry* 55 (16): 7193–7207. doi:10.1021/jm300713s.

Axten, Jeffrey M., Stuart P. Romeril, Arthur Shu, Jeffrey Ralph, Jesús R. Medina, Yanhong Feng, William Hoi Hong Li, et al. 2013. “Discovery of GSK2656157: An Optimized PERK Inhibitor Selected for Preclinical Development.” *ACS Medicinal Chemistry Letters* 4 (10): 964–68. doi:10.1021/ml400228e.

Bai, Xiao-Chen, Israel S Fernandez, Greg McMullan, and Sjors Hw Scheres. 2013. “Ribosome Structures to near-Atomic Resolution from Thirty Thousand Cryo-EM Particles.” *eLife* 2 (January): e00461. doi:10.7554/eLife.00461.

Boesen, Thomas, Sarah S Mohammad, Graham D Pavitt, and Gregers R Andersen. 2004. “Structure of the Catalytic Fragment of Translation Initiation Factor 2B and Identification of a Critically Important Catalytic Residue.” *Journal of Biological Chemistry* 279 (11): 10584–92. doi:10.1074/jbc.M311055200.

Bogorad, Andrew M., Kai Ying Lin, and Assen Marintchev. 2017. “Novel

Mechanisms of eIF2B Action and Regulation by eIF2α Phosphorylation." *Nucleic Acids Research* 45 (20): 11962–79. doi:10.1093/nar/gkx845.

Bogorad, Andrew M, Kai Ying Lin, and Assen Marintchev. 2017. "Novel Mechanisms of eIF2B Action and Regulation by eIF2α Phosphorylation." *Nucleic Acids Research* 45 (20). Oxford University Press: 11962–79. doi:10.1093/nar/gkx845.

———. 2018. "eIF2B Mechanisms of Action and Regulation: A Thermodynamic View." *Biochemistry* 57 (9): 1426–35. doi:10.1021/acs.biochem.7b00957.

Bogorad, Andrew M, Bing Xia, Dana G Sandor, Artem B Mamonov, Tanya R Cafarella, Stefan Jehle, Sandor Vajda, Dima Kozakov, and Assen Marintchev. 2014. "Insights into the Architecture of the eIF2Bα/β/δ Regulatory Subcomplex." *Biochemistry* 53 (21): 3432–45. doi:10.1021/bi500346u.

Boyce, Michael, Kevin F Bryant, Céline Jousse, Kai Long, Heather P Harding, Donalyn Scheuner, Randal J Kaufman, et al. 2005. "A Selective Inhibitor of eIF2alpha Dephosphorylation Protects Cells from ER Stress." *Science* 307 (5711): 935–39. doi:10.1126/science.1101902.

Brown, Alan, Fei Long, Robert A. Nicholls, Jaan Toots, Paul Emsley, and Garib Murshudov. 2015. "Tools for Macromolecular Model Building and Refinement into Electron Cryo-Microscopy Reconstructions." *Acta Crystallographica Section D: Biological Crystallography* 71. International Union of Crystallography: 136–53. doi:10.1107/S1399004714021683.

Brush, Matthew H, Douglas C Weiser, and Shirish Shenolikar. 2003. "Growth Arrest and DNA Damage-Inducible Protein GADD34 Targets Protein Phosphatase 1 to the Endoplasmic Reticulum and Promotes Dephosphorylation of the Subunit of Eukaryotic Translation Initiation Factor 2." *Molecular and Cellular Biology* 23 (4): 1292–1303. doi:10.1128/MCB.23.4.1292-1303.2003.

Bumann, Mario, Siamak Djafarzadeh, Anselm Erich Oberholzer, Peter Bigler, Michael Altmann, Hans Trachsel, and Ulrich Baumann. 2004. "Crystal Structure of Yeast Ypr118w, a Methylthioribose-1-Phosphate Isomerase

Related to Regulatory eIF2B Subunits." *Journal of Biological Chemistry* 279 (35): 37087–94. doi:10.1074/jbc.M404458200.

Burnley, Tom, Colin M. Palmer, and Martyn Winn. 2017. "Recent Developments in the CCP-EM Software Suite." *Acta Crystallographica Section D: Structural Biology* 73 (6). International Union of Crystallography: 469–77. doi:10.1107/S2059798317007859.

Bushman, J L, M Foiani, A M Cigan, C J Paddon, and A G Hinnebusch. 1993. "Guanine Nucleotide Exchange Factor for Eukaryotic Translation Initiation Factor 2 in *Saccharomyces cerevisiae*: Interactions between the Essential Subunits GCD2, GCD6, and GCD7 and the Regulatory Subunit GCN3." *Molecular and Cellular Biology* 13 (8): 4618–31. doi:10.1128/MCB.13.8.4618.

Carr, J. B. 1979. Lipogenesis control by esters of benzoxazine carboxylic acids. US 4180572, issued 1979.

Chefalo, Peter Joseph, Jihyun Oh, Maryam Rafie-Kolpin, Beki Kan, and Jane-Jane Chen. 1998. "Heme-Regulated eIF-2alpha Kinase Purifies as a Hemoprotein." *European Journal of Biochemistry* 258 (2): 820–30. doi:10.1046/j.1432-1327.1998.2580820.x.

Chen, J.-J. 2006. "Regulation of Protein Synthesis by the Heme-Regulated eIF2 Kinase: Relevance to Anemias." *Blood* 109 (7): 2693–99. doi:10.1182/blood-2006-08-041830.

Chen, Jane-Jane, and Irving M London. 1995. "Regulation of Protein Synthesis by Heme-Regulated eIF-2α Kinase." *Trends in Biochemical Sciences* 20 (3): 105–8. doi:10.1016/S0968-0004(00)88975-6.

Chen, Shaoxia, Greg McMullan, Abdul R. Faruqi, Garib N. Murshudov, Judith M. Short, Sjors H W Scheres, and Richard Henderson. 2013. "High-Resolution Noise Substitution to Measure Overfitting and Validate Resolution in 3D Structure Determination by Single Particle Electron Cryomicroscopy." *Ultramicroscopy* 135 (December). Elsevier: 24–35. doi:10.1016/j.ultramic.2013.06.004.

Chen, Ting, Duygu Ozel, Yuan Qiao, Fred Harbinski, Limo Chen, Séverine Denoyelle, Xiaoying He, et al. 2011. "Chemical Genetics Identify eIF2α

Kinase Heme-Regulated Inhibitor as an Anticancer Target." *Nature Chemical Biology* 7 (9): 610–16. doi:10.1038/nchembio.613.

Choi, S Y, Bradley J Scherer, Joachim Schnier, Monique V Davies, Randal J Kaufman, and J W Hershey. 1992. "Stimulation of Protein Synthesis in COS Cells Transfected with Variants of the Alpha-Subunit of Initiation Factor eIF-2." *The Journal of Biological Chemistry* 267 (1): 286–93. http://www.ncbi.nlm.nih.gov/pubmed/1346129.

Chou, Austin, Karen Krukowski, Timothy Jopson, Ping Jun Zhu, Mauro Costa-Mattioli, Peter Walter, and Susanna Rosi. 2017. "Inhibition of the Integrated Stress Response Reverses Cognitive Deficits after Traumatic Brain Injury." *Proceedings of the National Academy of Sciences* 114 (31): E6420–26. doi:10.1073/pnas.1707661114.

Colthurst, D R, D G Campbell, and C G Proud. 1987. "Structure and Regulation of Eukaryotic Initiation Factor eIF-2. Sequence of the Site in the Alpha Subunit Phosphorylated by the Haem-Controlled Repressor and by the Double-Stranded RNA-Activated Inhibitor." *European Journal of Biochemistry* 166 (2): 357–63. doi:10.1111/j.1432-1033.1987.tb13523.x.

Conte, Maria R., Geoff Kelly, Jeff Babon, Domenico Sanfelice, James Youell, Stephen J. Smerdon, and Christopher G. Proud. 2006. "Structure of the Eukaryotic Initiation Factor (eIF) 5 Reveals a Fold Common to Several Translation Factors." *Biochemistry* 45 (14): 4550–58. doi:10.1021/bi052387u.

Costa-Mattioli, Mauro, Delphine Gobert, Elad Stern, Karine Gamache, Rodney Colina, Claudio Cuello, Wayne Sossin, et al. 2007. "eIF2alpha Phosphorylation Bidirectionally Regulates the Switch from Short- to Long-Term Synaptic Plasticity and Memory." *Cell* 129 (1): 195–206. doi:10.1016/j.cell.2007.01.050.

Cox, Jürgen, and Matthias Mann. 2008. "MaxQuant Enables High Peptide Identification Rates, Individualized P.p.b.-Range Mass Accuracies and Proteome-Wide Protein Quantification." *Nature Biotechnology* 26 (12): 1367–72. doi:10.1038/nbt.1511.

Craddock, Bridget L., and Christopher G. Proud. 1996. “The α-Subunit of the Mammalian Guanine Nucleotide-Exchange Factor eIF-2B Is Essential for Catalytic Activity in Vitro.” *Biochemical and Biophysical Research Communications* 220 (3): 843–47. doi:10.1006/bbrc.1996.0495.

Crespillo-Casado, Ana, Joseph E. Chambers, Peter M. Fischer, Stefan J. Marciniak, and David Ron. 2017. “PPP1R15A-Mediated Dephosphorylation of eIF2a Is Unaffected by sephin1 or Guanabenz.” *eLife* 6: 1–29. doi:10.7554/eLife.26109.

Crespillo-Casado, Ana, Zander Claes, Meng S. Choy, Wolfgang Peti, Mathieu Bollen, and David Ron. 2018. “A Sephin1-Insensitive Tripartite Holophosphatase Dephosphorylates Translation Initiation Factor 2α.” *Journal of Biological Chemistry* 293 (20): 7766–76. doi:10.1074/jbc.RA118.002325.

Das, Indrajit, Agnieszka Krzyzosiak, Kim Schneider, Lawrence Wrabetz, Maurizio D’Antonio, Nicholas Barry, Anna Sigurdardottir, and Anne Bertolotti. 2015. “Preventing Proteostasis Diseases by Selective Inhibition of a Phosphatase Regulatory Subunit.” *Science* 348 (6231): 239–42. doi:10.1126/science.aaa4484.

Das, Supratik, and Umadas Maitra. 2000. “Mutational Analysis of Mammalian Translation Initiation Factor 5 (eIF5): Role of Interaction between the Beta Subunit of eIF2 and eIF5 in eIF5 Function In Vitro and In Vivo.” *Molecular and Cellular Biology* 20 (11): 3942–50. doi:10.1128/MCB.20.11.3942-3950.2000.

de Haro, Cesar, and Severo Ochoa. 1978. “Mode of Action of the Hemin-Controlled Inhibitor of Protein Synthesis: Studies with Factors from Rabbit Reticulocytes.” *Proceedings of the National Academy of Sciences of the United States of America* 75 (6): 2713–16. http://www.ncbi.nlm.nih.gov/pubmed/275839.

———. 1979. “Further Studies on the Mode of Action of the Heme-Controlled Translational Inhibitor: Stimulating Protein Acts at Level of Binary Complex Formation.” *Proceedings of the National Academy of Sciences* 76 (5): 2163–64. doi:10.1073/pnas.76.5.2163.

Dev, Kamal, Hongfang Qiu, Jinsheng Dong, Fan Zhang, Dominik Barthlme, and Alan G Hinnebusch. 2010. “The /Gcd7 Subunit of Eukaryotic Translation Initiation Factor 2B (eIF2B), a Guanine Nucleotide Exchange Factor, Is Crucial for Binding eIF2 In Vivo.” *Molecular and Cellular Biology* 30 (21): 5218–33. doi:10.1128/MCB.00265-10.

Dever, Thomas E. 2002. “Gene-Specific Regulation by General Translation Factors.” *Cell* 108 (4): 545–56. doi:10.1016/S0092-8674(02)00642-6.

Dever, Thomas E, Jane-Jane Chen, Glen N Barber, Mark A Cigan, Lan Feng, Thomas F Donahue, Irving M London, Michael Katze, and Alan G Hinnebusch. 1993. “Mammalian Eukaryotic Initiation Factor 2 Alpha Kinases Functionally Substitute for GCN2 Protein Kinase in the GCN4 Translational Control Mechanism of Yeast.” *Proceedings of the National Academy of Sciences* 90 (10): 4616–20. doi:10.1073/pnas.90.10.4616.

Dever, Thomas E, Lan Feng, Ronald C Wek, A.Mark Cigan, Thomas F Donahue, and Alan G Hinnebusch. 1992. “Phosphorylation of Initiation Factor 2α by Protein Kinase GCN2 Mediates Gene-Specific Translational Control of GCN4 in Yeast.” *Cell* 68 (3): 585–96. doi:10.1016/0092-8674(92)90193-G.

Dever, Thomas E, Terri Goss Kinzy, and Graham D. Pavitt. 2016. “Mechanism and Regulation of Protein Synthesis in *Saccharomyces cerevisiae*.” *Genetics* 203 (1): 65–107. doi:10.1534/genetics.115.186221.

Dey, Madhusudan, Bruce Trieselmann, Emily G Locke, Jingfang Lu, Chune Cao, Arvin C Dar, Thanuja Krishnamoorthy, Jinsheng Dong, Frank Sicheri, and Thomas E Dever. 2005. “PKR and GCN2 Kinases and Guanine Nucleotide Exchange Factor Eukaryotic Translation Initiation Factor 2B (eIF2B) Recognize Overlapping Surfaces on eIF2.” *Molecular and Cellular Biology* 25 (8): 3063–75. doi:10.1128/MCB.25.8.3063-3075.2005.

Dey, Madhusudan, Algirdas Velyvis, John J. Li, Elaine Chiu, David Chiovitti, Lewis E. Kay, Frank Sicheri, and Thomas E. Dever. 2011. “Requirement for Kinase-Induced Conformational Change in Eukaryotic Initiation Factor 2alpha (eIF2alpha) Restricts Phosphorylation of Ser51.” *Proceedings of*

the National Academy of Sciences of the United States of America 108 (11): 4316–21. doi:10.1073/pnas.1014872108.

Dhaliwal, Simrit, and David W. Hoffman. 2003. “The Crystal Structure of the N-Terminal Region of the Alpha Subunit of Translation Initiation Factor 2 (eIF2α) from *Saccharomyces cerevisiae* Provides a View of the Loop Containing Serine 51, the Target of the eIF2α-Specific Kinases.” *Journal of Molecular Biology* 334 (2): 187–95. doi:10.1016/j.jmb.2003.09.045.

Dholakia, Jaydev N, Timothy C Mueser, Charles L Woodley, Lawrence J Parkhurst, and Albert J Wahba. 1986. “The Association of NADPH with the Guanine Nucleotide Exchange Factor from Rabbit Reticulocytes: A Role of Pyridine Dinucleotides in Eukaryotic Polypeptide Chain Initiation.” *Proceedings of the National Academy of Sciences* 83 (18): 6746–50. doi:10.1073/pnas.83.18.6746.

Dholakia, Jaydev N, and Albert J Wahba. 1988. “Phosphorylation of the Guanine Nucleotide Exchange Factor from Rabbit Reticulocytes Regulates Its Activity in Polypeptide Chain Initiation.” *Proceedings of the National Academy of Sciences* 85 (1): 51–54. doi:10.1073/pnas.85.1.51.

———. 1989. “Mechanism of the Nucleotide Exchange Reaction in Eukaryotic Polypeptide Chain Initiation. Characterization of the Guanine Nucleotide Exchange Factor as a GTP-Binding Protein.” *The Journal of Biological Chemistry* 264 (1): 546–50. http://www.ncbi.nlm.nih.gov/pubmed/2491852.

Dietrich, Jörg, Michelle Lacagnina, David Gass, Eric Richfield, Margot Mayer-Pröschel, Mark Noble, Carlos Torres, and Christoph Pröschel. 2005. “EIF2B5 Mutations Compromise GFAP+astrocyte Generation in Vanishing White Matter Leukodystrophy.” *Nature Medicine* 11 (3): 277–83. doi:10.1038/nm1195.

Dolle, R. E. C., Chu, G-H. 2005. Preparation of pyrrolidinylphenethyl benzoxepine-, tetrahydronaphthalene-, chroman-, and benzofurancarboxamides as κ-opioid agonists. US 2005/54630 A1, issued 2005.

Dooves, Stephanie, Marianna Bugiani, Nienke L Postma, Emiel Polder, Niels

Land, Stephen T. Horan, Anne-Lieke F. van Deijk, et al. 2016. “Astrocytes Are Central in the Pathomechanisms of Vanishing White Matter.” *Journal of Clinical Investigation* 126 (4): 1512–24. doi:10.1172/JCI83908.

Dubochet, Jacques, Joachim Frank, and Richard Henderson. 2018. “Cryo-EM in Drug Discovery: Achievements, Limitations and Prospects.” *Nature Reviews Drug Discovery*. Nature Publishing Group. doi:10.1038/nrd.2018.77.

Emsley, P., B. Lohkamp, W. G. Scott, and K. Cowtan. 2010. “Features and Development of Coot.” *Acta Crystallographica Section D: Biological Crystallography* 66 (4). International Union of Crystallography: 486–501. doi:10.1107/S0907444910007493.

Fabian, John R., Scot R. Kimball, Nina K. Heinzinger, and Leonard S. Jefferson. 1997. “Subunit Assembly and Guanine Nucleotide Exchange Activity of Eukaryotic Initiation Factor-2B Expressed in Sf9 Cells.” *Journal of Biological Chemistry* 272 (19): 12359–65. doi:10.1074/jbc.272.19.12359.

Fawcett, T W, J L Martindale, K Z Guyton, T Hai, and N J Holbrook. 1999. “Complexes Containing Activating Transcription Factor (ATF)/cAMP-Responsive-Element-Binding Protein (CREB) Interact with the CCAAT/enhancer-Binding Protein (C/EBP)-ATF Composite Site to Regulate Gadd153 Expression during the Stress Response.” *The Biochemical Journal* 339 (Pt 1 (1): 135–41. doi:10.1042/bj3390135.

Fogli, Anne, Raphael Schiffmann, Lynne Hugendubler, Patricia Combes, Enrico Bertini, Diana Rodriguez, Scot R Kimball, and Odile Boespflug-Tanguy. 2004. “Decreased Guanine Nucleotide Exchange Factor Activity in eIF2B-Mutated Patients.” *European Journal of Human Genetics* 12 (7): 561–66. doi:10.1038/sj.ejhg.5201189.

Gat-Viks, Irite, Tamar Geiger, Mali Barbi, Gali Raini, and Orna Elroy-Stein. 2015. “Proteomics-Level Analysis of Myelin Formation and Regeneration in a Mouse Model for Vanishing White Matter Disease.” *Journal of Neurochemistry* 134 (3): 513–26. doi:10.1111/jnc.13142.

Geva, Michal, Yuval Cabilly, Yaniv Assaf, Nina Mindroul, Liraz Marom, Gali Raini, Dalia Pinchasi, and Orna Elroy-Stein. 2010. “A Mouse Model for Eukaryotic Translation Initiation Factor 2B-Leucodystrophy Reveals Abnormal Development of Brain White Matter.” *Brain* 133 (8): 2448–61. doi:10.1093/brain/awq180.

Gogoi, Prerana, and Shankar Prasad Kanaujia. 2018. “A Presumed Homologue of the Regulatory Subunits of eIF2B Functions as Ribose-1,5-Bisphosphate Isomerase in Pyrococcus Horikoshii OT3.” *Scientific Reports* 8 (1). Springer US: 1891. doi:10.1038/s41598-018-20418-w.

Gomez, Edith, Sarah S. Mohammad, and Graham D. Pavitt. 2002. “Characterization of the Minimal Catalytic Domain within eIF2B: The Guanine-Nucleotide Exchange Factor for Translation Initiation.” *The EMBO Journal* 21 (19): 5292–5301. doi:10.1093/emboj/cdf515.

Gomez, Edith, and Graham D Pavitt. 2000. “Identification of Domains and Residues within the Varepsilon Subunit of Eukaryotic Translation Initiation Factor 2B (eIF2Bvarepsilon) Required for Guanine Nucleotide Exchange Reveals a Novel Activation Function Promoted by eIF2B Complex Formation.” *Molecular and Cellular Biology* 20 (11): 3965–76. doi:10.1128/MCB.20.11.3965-3976.2000.

Gordiyenko, Yuliya, Carla Schmidt, Martin D Jennings, Dijana Matak-Vinkovic, Graham D Pavitt, and Carol V Robinson. 2014. “eIF2B Is a Decameric Guanine Nucleotide Exchange Factor with a γ2ε2 Tetrameric Core.” *Nature Communications* 5 (1). Nature Publishing Group: 3902. doi:10.1038/ncomms4902.

Goss, Dixie J, Lawrence J Parkhurst, Harshvardhan B Mehta, Charles L Woodley, and A J Wahba. 1984. “Studies on the Role of Eukaryotic Nucleotide Exchange Factor in Polypeptide Chain Initiation.” *The Journal of Biological Chemistry* 259 (12): 7374–77. http://www.ncbi.nlm.nih.gov/pubmed/6330054.

Gromadski, Kirill B., Hans-Joachim Wieden, and Marina V. Rodnina. 2002. “Kinetic Mechanism of Elongation Factor Ts-Catalyzed Nucleotide Exchange in Elongation Factor Tu †.” *Biochemistry* 41 (1): 162–69.

doi:10.1021/bi015712w.

Gromadski, Kirill B, Tobias Schümmer, Anne Strømgaard, Charlotte R Knudsen, Terri Goss Kinzy, and Marina V Rodnina. 2007. “Kinetics of the Interactions between Yeast Elongation Factors 1A and 1Bα, Guanine Nucleotides, and Aminoacyl-tRNA.” *Journal of Biological Chemistry* 282 (49): 35629–37. doi:10.1074/jbc.M707245200.

Gross, Martin. 1975. “Reversal of the Inhibitory Action of the Hemin-Controlled Translational Repressor by a Post-Ribosomal Supernatant Factor from Rabbit Reticulocyte Lysate.” *Biochemical and Biophysical Research Communications* 67 (4): 1507–15. doi:10.1016/0006-291X(75)90197-7.

———. 1976. “Control of Protein Synthesis by Hemin. Isolation and Characterization of a Supernatant Factor from Rabbit Reticulocyte Lysate.” *BBA Section Nucleic Acids And Protein Synthesis* 447 (4): 445–59. doi:10.1016/0005-2787(76)90082-4.

Gross, Martin, and Mark S Rubino. 1989. “Regulation of Eukaryotic Initiation Factor-2B Activity by Polyamines and Amino Acid Starvation in Rabbit Reticulocyte Lysate.” *The Journal of Biological Chemistry* 264 (36): 21879–84. http://www.ncbi.nlm.nih.gov/pubmed/2600092.

Gross, Martin, Mark S. Rubino, and Suzanne M. Hessefort. 1991. “The Conversion of eIF-2·GDP to eIF-2·GTP by eIF-2B Requires Met-tRNAf Met.” *Biochemical and Biophysical Research Communications* 181 (3): 1500–1507. doi:10.1016/0006-291X(91)92109-W.

Gross, Martin, Mark S Rubino, and Timothy K Starn. 1988. “Regulation of Protein Synthesis in Rabbit Reticulocyte Lysate.” *Biochemistry* 263 (25): 12486–92.

Halliday, M, H Radford, Y Sekine, J Moreno, N Verity, J le Quesne, C A Ortori, et al. 2015. “Partial Restoration of Protein Synthesis Rates by the Small Molecule ISRIB Prevents Neurodegeneration without Pancreatic Toxicity.” *Cell Death and Disease* 6 (3). Nature Publishing Group: e1672. doi:10.1038/cddis.2015.49.

Han, A P, C Yu, L Lu, Y Fujiwara, C Browne, G Chin, M Fleming, P Leboulch,

S H Orkin, and J J Chen. 2001. “Heme-Regulated eIF2alpha Kinase (HRI) Is Required for Translational Regulation and Survival of Erythroid Precursors in Iron Deficiency.” *The EMBO Journal* 20 (23): 6909–18. doi:10.1093/emboj/20.23.6909.

Hannig, Ernest M, and Alan G Hinnebusch. 1988. “Molecular Analysis of GCN3, a Translational Activator of GCN4: Evidence for Posttranslational Control of GCN3 Regulatory Function.” *Molecular and Cellular Biology* 8 (11): 4808–20. doi:10.1128/MCB.8.11.4808.

Harding, Heather P., Alisa F. Zyryanova, and David Ron. 2012. “Uncoupling Proteostasis and Development in Vitro with a Small Molecule Inhibitor of the Pancreatic Endoplasmic Reticulum Kinase, PERK.” *Journal of Biological Chemistry* 287 (53): 44338–44. doi:10.1074/jbc.M112.428987.

Harding, Heather P, Isabel Novoa, Yuhong Zhang, Huiqing Zeng, Ron Wek, Matthieu Schapira, and David Ron. 2000a. “Regulated Translation Initiation Controls Stress-Induced Gene Expression in Mammalian Cells.” *Molecular Cell* 6 (5): 1099–1108. doi:10.1016/S1097-2765(00)00108-8.

Harding, Heather P, Huiqing Zeng, Yuhong Zhang, Rivka Jungries, Peter Chung, Heidi Plesken, David D Sabatini, and David Ron. 2001. “Diabetes Mellitus and Exocrine Pancreatic Dysfunction in Perk−/− Mice Reveals a Role for Translational Control in Secretory Cell Survival.” *Molecular Cell* 7 (6): 1153–63. doi:10.1016/S1097-2765(01)00264-7.

Harding, Heather P, Yuhong Zhang, Anne Bertolotti, Huiqing Zeng, and David Ron. 2000b. “Perk Is Essential for Translational Regulation and Cell Survival during the Unfolded Protein Response.” *Molecular Cell* 5 (5): 897–904. doi:10.1016/S1097-2765(00)80330-5.

Harding, Heather P, Yuhong Zhang, and David Ron. 1999. “Protein Translation and Folding Are Coupled by an Endoplasmic-Reticulum-Resident Kinase.” *Nature* 397 (6716): 271–74. doi:10.1038/16729.

Harding, Heather P, Yuhong Zhang, Huiquing Zeng, Isabel Novoa, Phoebe D Lu, Marcella Calfon, Navid Sadri, et al. 2003. “An Integrated Stress Response Regulates Amino Acid Metabolism and Resistance to Oxidative Stress.” *Molecular Cell* 11 (3): 619–33. doi:10.1016/S1097-

2765(03)00105-9.

Harris, Thurl E., An Chi, Jeffrey Shabanowitz, Donald F. Hunt, Robert E. Rhoads, and John C. Lawrence. 2006. “mTOR-Dependent Stimulation of the Association of eIF4G and eIF3 by Insulin.” *The EMBO Journal* 25 (8): 1659–68. doi:10.1038/sj.emboj.7601047.

Hearn, Brian R, Priyadarshini Jaishankar, Carmela Sidrauski, Jordan C Tsai, Punitha Vedantham, Shaun D Fontaine, Peter Walter, and Adam R Renslo. 2016. “Structure-Activity Studies of Bis- O -Arylglycolamides: Inhibitors of the Integrated Stress Response.” *ChemMedChem* 11 (8): 870–80. doi:10.1002/cmdc.201500483.

Hershey, John W B, Nahum Sonenberg, and Michael B Mathews. 2012. “Principles of Translational Control: An Overview.” *Cold Spring Harbor Perspectives in Biology* 4 (12): a011528–a011528. doi:10.1101/cshperspect.a011528.

Hinnebusch, Alan G. 1988. “Mechanisms of Gene Regulation in the General Control of Amino Acid Biosynthesis in *Saccharomyces cerevisiae*.” *Microbiological Reviews* 52 (2): 248–73. http://www.pubmedcentral.nih.gov/articlerender.fcgi?artid=373138&tool=pmcentrez&rendertype=abstract.

———. 2006. “eIF3: A Versatile Scaffold for Translation Initiation Complexes.” *Trends in Biochemical Sciences* 31 (10): 553–62. doi:10.1016/j.tibs.2006.08.005.

———. 2011. “Molecular Mechanism of Scanning and Start Codon Selection in Eukaryotes.” *Microbiology and Molecular Biology Reviews* 75 (3): 434–67. doi:10.1128/MMBR.00008-11.

Hinnebusch, Alan G, and Jon R Lorsch. 2012. “The Mechanism of Eukaryotic Translation Initiation: New Insights and Challenges.” *Cold Spring Harbor Perspectives in Biology* 4 (10): a011544–a011544. doi:10.1101/cshperspect.a011544.

Hinnebusch, Alan G, and Krishnamurthy Natarajan. 2002. “Gcn4p, a Master Regulator of Gene Expression, Is Controlled at Multiple Levels by Diverse Signals of Starvation and Stress.” *Eukaryotic Cell* 1 (1): 22–32.

doi:0.1128/EC.01.1.22-32.2002.

Hiyama, Takuya B, Takuhiro Ito, Hiroaki Imataka, and Shigeyuki Yokoyama. 2009. “Crystal Structure of the α Subunit of Human Translation Initiation Factor 2B.” *Journal of Molecular Biology* 392 (4). Elsevier Ltd: 937–51. doi:10.1016/j.jmb.2009.07.054.

Holz, Marina K., Bryan A. Ballif, Steven P. Gygi, and John Blenis. 2005. “mTOR and S6K1 Mediate Assembly of the Translation Preinitiation Complex through Dynamic Protein Interchange and Ordered Phosphorylation Events.” *Cell* 123 (4): 569–80. doi:10.1016/j.cell.2005.10.024.

Hopfield, J. J. 1974. “Kinetic Proofreading: A New Mechanism for Reducing Errors in Biosynthetic Processes Requiring High Specificity.” *Proceedings of the National Academy of Sciences* 71 (10): 4135–39. doi:10.1073/pnas.71.10.4135.

Hwang, Y W, and D L Miller. 1985. “A Study of the Kinetic Mechanism of Elongation Factor Ts.” *The Journal of Biological Chemistry* 260 (21): 11498–502. http://www.ncbi.nlm.nih.gov/pubmed/4044568.

Ito, Takuhiro, Assen Marintchev, and Gerhard Wagner. 2004. “Solution Structure of Human Initiation Factor eIF2α Reveals Homology to the Elongation Factor eEF1B.” *Structure* 12 (9): 1693–1704. doi:10.1016/j.str.2004.07.010.

Janssen, G M, and W Möller. 1988. “Elongation Factor 1 Beta Gamma from Artemia. Purification and Properties of Its Subunits.” *European Journal of Biochemistry* 171 (1–2): 119–29. http://onlinelibrary.wiley.com/store/10.1111/j.1432-1033.1988.tb13766.x/asset/j.1432-1033.1988.tb13766.x.pdf?v=1&t=ho1nj3tu&s=ca935bc5dd37c5d51562d177df52a7532ce5f287.

Jennings, Martin D., and Graham D. Pavitt. 2014. “A New Function and Complexity for Protein Translation Initiation Factor eIF2B.” *Cell Cycle* 13 (17): 2660–65. doi:10.4161/15384101.2014.948797.

Jennings, Martin D, Christopher J Kershaw, Tomas Adomavicius, and

Graham D Pavitt. 2017a. “Fail-Safe Control of Translation Initiation by Dissociation of eIF2α Phosphorylated Ternary Complexes.” *eLife* 6: e24542. doi:10.7554/eLife.24542.

———. 2017b. “Fail-Safe Control of Translation Initiation by Dissociation of eIF2α Phosphorylated Ternary Complexes.” *eLife* 6 (March): e24542. doi:10.7554/eLife.24542.

Jennings, Martin D, Christopher J Kershaw, Christopher White, Danielle Hoyle, Jonathan P. Richardson, Joseph L Costello, Ian J Donaldson, Yu Zhou, and Graham D Pavitt. 2016. “eIF2β Is Critical for eIF5-Mediated GDP-Dissociation Inhibitor Activity and Translational Control.” *Nucleic Acids Research* 44 (20): gkw657. doi:10.1093/nar/gkw657.

Jennings, Martin D, and Graham D Pavitt. 2010. “eIF5 Has GDI Activity Necessary for Translational Control by eIF2 Phosphorylation.” *Nature* 465 (7296). Nature Publishing Group: 378–81. doi:10.1038/nature09003.

Jennings, Martin D, Yu Zhou, Sarah S Mohammad-Qureshi, David Bennett, and Graham D Pavitt. 2013. “eIF2B Promotes eIF5 Dissociation from eIF2*GDP to Facilitate Guanine Nucleotide Exchange for Translation Initiation.” *Genes & Development* 27 (24): 2696–2707. doi:10.1101/gad.231514.113.

Jiang, H.-Y., S. A. Wek, Barbara C McGrath, Dan Lu, Tsonwin Hai, Heather P Harding, Xiaozhong Wang, David Ron, Douglas R Cavener, and Ronald C Wek. 2004. “Activating Transcription Factor 3 Is Integral to the Eukaryotic Initiation Factor 2 Kinase Stress Response.” *Molecular and Cellular Biology* 24 (3): 1365–77. doi:10.1128/MCB.24.3.1365-1377.2004.

Jin, Xiangshu, Miguel A Ballicora, Jack Preiss, and James H Geiger. 2005. “Crystal Structure of Potato Tuber ADP-Glucose Pyrophosphorylase.” *The EMBO Journal* 24 (4): 694–704. doi:10.1038/sj.emboj.7600551.

Kakuta, Yoshimitsu, Maino Tahara, Shigehiro Maetani, Min Yao, Isao Tanaka, and Makoto Kimura. 2004. “Crystal Structure of the Regulatory Subunit of Archaeal Initiation Factor 2B (aIF2B) from Hyperthermophilic Archaeon Pyrococcus Horikoshii OT3: A Proposed Structure of the Regulatory

Subcomplex of Eukaryotic IF2B." *Biochemical and Biophysical Research Communications* 319 (3): 725–32. doi:10.1016/j.bbrc.2004.05.045.

Kantor, Liraz, Heather P. Harding, David Ron, Raphael Schiffmann, Christine R. Kaneski, Scot R. Kimball, and Orna Elroy-Stein. 2005. "Heightened Stress Response in Primary Fibroblasts Expressing Mutant eIF2B Genes from CACH/VWM Leukodystrophy Patients." *Human Genetics* 118 (1): 99–106. doi:10.1007/s00439-005-0024-x.

Kashiwagi, Kazuhiro, Takuhiro Ito, and Shigeyuki Yokoyama. 2017. "Crystal Structure of eIF2B and Insights into eIF2-eIF2B Interactions." *The FEBS Journal* 284 (6): 868–74. doi:10.1111/febs.13896.

Kashiwagi, Kazuhiro, Mari Takahashi, Madoka Nishimoto, Takuya B Hiyama, Toshiaki Higo, Takashi Umehara, Kensaku Sakamoto, Takuhiro Ito, and Shigeyuki Yokoyama. 2016. "Crystal Structure of Eukaryotic Translation Initiation Factor 2B." *Nature* 531 (7592). Nature Publishing Group: 122–25. doi:10.1038/nature16991.

Kaufman, Randal J. 1999. "Double-Stranded RNA-Activated Protein Kinase Mediates Virus-Induced Apoptosis: A New Role for an Old Actor." *Proceedings of the National Academy of Sciences* 96 (21): 11693–95. doi:10.1073/pnas.96.21.11693.

Kaufman, Randal J, Monique V Davies, Vinay K Pathak, and John W Hershey. 1989. "The Phosphorylation State of Eucaryotic Initiation Factor 2 Alters Translational Efficiency of Specific mRNAs." *Molecular and Cellular Biology* 9 (3): 946–58. doi:10.1128/MCB.9.3.946.

Kaziro, Yoshito. 1978. "The Role of Guanosine 5'-triphosphate in Polypeptide Chain Elongation." *Biochimica et Biophysica Acta* 505 (1): 95–127. http://www.ncbi.nlm.nih.gov/pubmed/361078.

Khaperskyy, Denys A., Mohamed M. Emara, Benjamin P. Johnston, Paul Anderson, Todd F. Hatchette, and Craig McCormick. 2014. "Influenza A Virus Host Shutoff Disables Antiviral Stress-Induced Translation Arrest." Edited by Andrew Pekosz. *PLoS Pathogens* 10 (7): e1004217. doi:10.1371/journal.ppat.1004217.

Kimball, Scot R., Nina K. Heinzinger, Rick L. Horetsky, and Leonard S.

Jefferson. 1998. “Identification of Interprotein Interactions between the Subunits of Eukaryotic Initiation Factors eIF2 and eIF2B.” *Journal of Biological Chemistry* 273 (5): 3039–44. doi:10.1074/jbc.273.5.3039.

Kimball, Scot R, William V Everson, K E Flaim, and L S Jefferson. 1989. “Initiation of Protein Synthesis in a Cell-Free System Prepared from Rat Hepatocytes.” *American Journal of Physiology-Cell Physiology* 256 (1): C28–34. doi:10.1152/ajpcell.1989.256.1.C28.

Kimball, Scot R, William V Everson, Lethea M Myers, and Leonard S Jefferson. 1987. “Purification and Characterization of Eukaryotic Initiation Factor 2 and a Guanine Nucleotide Exchange Factor from Rat Liver.” *The Journal of Biological Chemistry* 262 (5): 2220–27.

Kimball, Scot R, and Leonard S Jefferson. 1995. “Allosteric Regulation of Eukaryotic Initiation Factor eIF-2B by Adenine Nucleotides.” *Biochemical and Biophysical Research Communications* 212 (3): 1074–81. doi:10.1006/bbrc.1995.2079.

Konieczny, Andrej, and Brian Safer. 1983. “Purification of the Eukaryotic Initiation Factor 2-Eukaryotic Initiation Factor 2B Complex and Characterization of Its Guanine Nucleotide Exchange Activity during Protein Synthesis Initiation.” *The Journal of Biological Chemistry* 258 (5): 3402–8.

Koonin, Eugene V. 1995. “Multidomain Organization of Eukaryotic Guanine Nucleotide Exchange Translation Initiation Factor eIF-2B Subunits Revealed by Analysis of Conserved Sequence Motifs.” *Protein Science* 4 (8): 1608–17. doi:10.1002/pro.5560040819.

Krishnamoorthy, Thanuja, Graham D Pavitt, F Zhang, Thomas E Dever, and Alan G Hinnebusch. 2001. “Tight Binding of the Phosphorylated Subunit of Initiation Factor 2 (eIF2) to the Regulatory Subunits of Guanine Nucleotide Exchange Factor eIF2B Is Required for Inhibition of Translation Initiation.” *Molecular and Cellular Biology* 21 (15): 5018–30. doi:10.1128/MCB.21.15.5018-5030.2001.

Kuhle, Bernhard, Nora K. Eulig, and Ralf Ficner. 2015. “Architecture of the eIF2B Regulatory Subcomplex and Its Implications for the Regulation of

Guanine Nucleotide Exchange on eIF2." *Nucleic Acids Research* 43 (20): gkv930. doi:10.1093/nar/gkv930.

Labauge, Pierre, Laetitia Horzinski, Xavier Ayrignac, Pierre Blanc, Sandra Vukusic, Diana Rodriguez, Francois Mauguiere, et al. 2009. "Natural History of Adult-Onset eIF2B-Related Disorders: A Multi-Centric Survey of 16 Cases." *Brain* 132 (8): 2161–69. doi:10.1093/brain/awp171.

Laurino, Jomar P, Glória M Thompson, Eliza Pacheco, and Beatriz A Castilho. 1999. "The β Subunit of Eukaryotic Translation Initiation Factor 2 Binds mRNA through the Lysine Repeats and a Region Comprising the C 2 -C 2 Motif." *Molecular and Cellular Biology* 19 (1): 173–81. doi:10.1128/MCB.19.1.173.

Leegwater, Peter A.J., Gerre Vermeulen, Andrea A.M. Könst, Sakkubai Naidu, Joyce Mulders, Allerdien Visser, Paula Kersbergen, et al. 2001. "Subunits of the Translation Initiation Factor eIF2B Are Mutant in Leukoencephalopathy with Vanishing White Matter." *Nature Genetics* 29 (4): 383–88. doi:10.1038/ng764.

Leibundgut, Marc, Christian Frick, Martin Thanbichler, August Böck, and Nenad Ban. 2005. "Selenocysteine tRNA-Specific Elongation Factor SelB Is a Structural Chimaera of Elongation and Initiation Factors." *The EMBO Journal* 24 (1): 11–22. doi:10.1038/sj.emboj.7600505.

Leroux, Alena, and Irving M London. 1982. "Regulation of Protein Synthesis by Phosphorylation of Eukaryotic Initiation Factor 2 Alpha in Intact Reticulocytes and Reticulocyte Lysates." *Proceedings of the National Academy of Sciences* 79 (7): 2147–51. doi:10.1073/pnas.79.7.2147.

Levin, Daniel, and Irving M London. 1978. "Regulation of Protein Synthesis: Activation by Double-Stranded RNA of a Protein Kinase That Phosphorylates Eukaryotic Initiation Factor 2." *Proceedings of the National Academy of Sciences* 75 (3): 1121–25. doi:10.1073/pnas.75.3.1121.

Li, Wei, Xuemin Wang, M. S. van der Knaap, and Christopher G Proud. 2004. "Mutations Linked to Leukoencephalopathy with Vanishing White Matter Impair the Function of the Eukaryotic Initiation Factor 2B Complex in

Diverse Ways." *Molecular and Cellular Biology* 24 (8): 3295–3306. doi:10.1128/MCB.24.8.3295-3306.2004.

Li, Xueming, Paul Mooney, Shawn Zheng, Christopher R. Booth, Michael B. Braunfeld, Sander Gubbens, David A. Agard, and Yifan Cheng. 2013. "Electron Counting and Beam-Induced Motion Correction Enable near-Atomic-Resolution Single-Particle Cryo-EM." *Nature Methods* 10 (6): 584–90. doi:10.1038/nmeth.2472.

Liu, Rui, Hannemieke D.W. van der Lei, Xuemin Wang, Noel C Wortham, Hua Tang, Carola G.M. van Berkel, Tsitsi Arikana Mufunde, et al. 2011. "Severity of Vanishing White Matter Disease Does Not Correlate with Deficits in eIF2B Activity or the Integrity of eIF2B Complexes." *Human Mutation* 32 (9): 1036–45. doi:10.1002/humu.21535.

Llácer, Jose L., Tanweer Hussain, Laura Marler, Colin Echeverría Aitken, Anil Thakur, Jon R. Lorsch, Alan G. Hinnebusch, and V. Ramakrishnan. 2015. "Conformational Differences between Open and Closed States of the Eukaryotic Translation Initiation Complex." *Molecular Cell* 59 (3): 399–412. doi:10.1016/j.molcel.2015.06.033.

Lu, Linrong, A.-P. Han, and J.-J. Chen. 2001. "Translation Initiation Control by Heme-Regulated Eukaryotic Initiation Factor 2alpha Kinase in Erythroid Cells under Cytoplasmic Stresses." *Molecular and Cellular Biology* 21 (23): 7971–80. doi:10.1128/MCB.21.23.7971-7980.2001.

Lu, Phoebe D, Céline Jousse, Stefan J Marciniak, Yuhong Zhang, Isabel Novoa, Donalyn Scheuner, Randal J Kaufman, David Ron, and Heather P Harding. 2004. "Cytoprotection by Pre-Emptive Conditional Phosphorylation of Translation Initiation Factor 2." *The EMBO Journal* 23 (1): 169–79. doi:10.1038/sj.emboj.7600030.

Ma, Tao, Mimi a Trinh, Alyse J Wexler, Clarisse Bourbon, Evelina Gatti, Philippe Pierre, Douglas R Cavener, and Eric Klann. 2013. "Suppression of eIF2α Kinases Alleviates Alzheimer's Disease–related Plasticity and Memory Deficits." *Nature Neuroscience* 16 (9): 1299–1305. doi:10.1038/nn.3486.

Manchester, Keith L. 1997. "Catalysis of Guanine Nucleotide Exchange on

eIF-2 by eIF-2B: Is It a Sequential or Substituted Enzyme Mechanism?" *Biochemical and Biophysical Research Communications* 239 (1): 223–27. doi:10.1006/bbrc.1997.7462.

Maracci, Cristina, and Marina V. Rodnina. 2016. "Review: Translational GTPases." *Biopolymers* 105 (8): 463–75. doi:10.1002/bip.22832.

Marciniak, Stefan J., Chi Y Yun, Seiichi Oyadomari, Isabel Novoa, Yuhong Zhang, Rivka Jungreis, Kazuhiro Nagata, Heather P Harding, and David Ron. 2004. "CHOP Induces Death by Promoting Protein Synthesis and Oxidation in the Stressed Endoplasmic Reticulum." *Genes & Development* 18 (24): 3066–77. doi:10.1101/gad.1250704.

Marintchev, Assen, and Gerhard Wagner. 2004. "Translation Initiation: Structures, Mechanisms and Evolution." *Quarterly Reviews of Biophysics* 37 (3–4): 197–284. doi:10.1017/S0033583505004026.

Marom, Liraz, Igor Ulitsky, Yuval Cabilly, Ron Shamir, and Orna Elroy-Stein. 2011. "A Point Mutation in Translation Initiation Factor eIF2B Leads to Function- and Time-Specific Changes in Brain Gene Expression." Edited by Bob Lightowlers. *PLoS ONE* 6 (10): e26992. doi:10.1371/journal.pone.0026992.

Martin, Leenus, Scot R Kimball, and Lawrence B Gardner. 2010. "Regulation of the Unfolded Protein Response by eIF2Bδ Isoforms." *Journal of Biological Chemistry* 285 (42): 31944–53. doi:10.1074/jbc.M110.153148.

Matsukawa, Takashi, Xuemin Wang, Rui Liu, Noel C. Wortham, Yuko Onuki, Akatsuki Kubota, Ayumi Hida, et al. 2011. "Adult-Onset Leukoencephalopathies with Vanishing White Matter with Novel Missense Mutations in EIF2B2, EIF2B3, and EIF2B5." *Neurogenetics* 12 (3): 259–61. doi:10.1007/s10048-011-0284-7.

Matts, Robert L, Daniel H Levin, and Irving M London. 1983. "Effect of Phosphorylation of the Alpha-Subunit of Eukaryotic Initiation Factor 2 on the Function of Reversing Factor in the Initiation of Protein Synthesis." *Proceedings of the National Academy of Sciences* 80 (9): 2559–63. doi:10.1073/pnas.80.9.2559.

McEwen, Dyke P., Kyle R. Gee, Hee C. Kang, and Richard R. Neubig. 2001.

"Fluorescent BODIPY-GTP Analogs: Real-Time Measurement of Nucleotide Binding to G Proteins." *Analytical Biochemistry* 291 (1): 109–17. doi:10.1006/abio.2001.5011.

Merk, Alan, Alberto Bartesaghi, Soojay Banerjee, Veronica Falconieri, Prashant Rao, Mindy I. Davis, Rajan Pragani, et al. 2016. "Breaking Cryo-EM Resolution Barriers to Facilitate Drug Discovery." *Cell* 165 (7). Elsevier Inc.: 1698–1707. doi:10.1016/j.cell.2016.05.040.

Merrick, William C. 1992. "Mechanism and Regulation of Eukaryotic Protein Synthesis." *Microbiological Reviews* 56 (2): 291–315. http://www.ncbi.nlm.nih.gov/pubmed/1620067.

Miller, David L, and Herbert W Weissbach. 1970. "Studies on the Purification and Properties of Factor Tu from E. Coli." *Archives of Biochemistry and Biophysics* 141 (1): 26–37. http://www.ncbi.nlm.nih.gov/pubmed/4921066.

Mohammad-Qureshi, Sarah S, Raphaël Haddad, Elizabeth J Hemingway, Jonathan P Richardson, and Graham D Pavitt. 2007. "Critical Contacts between the Eukaryotic Initiation Factor 2B (eIF2B) Catalytic Domain and Both eIF2 and -2 Mediate Guanine Nucleotide Exchange." *Molecular and Cellular Biology* 27 (14): 5225–34. doi:10.1128/MCB.00495-07.

Mohammad-Qureshi, Sarah S, Martin D Jennings, and Graham D Pavitt. 2008. "Clues to the Mechanism of Action of eIF2B, the Guanine-Nucleotide-Exchange Factor for Translation Initiation." *Biochemical Society Transactions* 36 (Pt 4): 658–64. doi:10.1042/BST0360658.

Moreno, Julie A, Mark Halliday, Colin Molloy, Helois Radford, Nicholas Verity, Jeffrey M Axten, Catharine A Ortori, et al. 2013. "Oral Treatment Targeting the Unfolded Protein Response Prevents Neurodegeneration and Clinical Disease in Prion-Infected Mice." *Science Translational Medicine* 5 (206): 206ra138-206ra138. doi:10.1126/scitranslmed.3006767.

Murtha-Riel, Patricia, Monique Davies, Bradley J Scherer, Sang-Yun Choi, John W B Hershey, and Randal J Kaufman. 1993. "Expression of a Phosphorylation-Resistant Eukaryotic Initiation Factor 2 Alpha-Subunit

Mitigates Heat Shock Inhibition of Protein Synthesis." *The Journal of Biological Chemistry* 268 (17): 12946–51. http://www.jbc.org/content/268/17/12946.short%5Cnhttp://www.ncbi.nlm.nih.gov/pubmed/8509427.

Nakamura, Akira, Masahiro Fujihashi, Riku Aono, Takaaki Sato, Yosuke Nishiba, Shosuke Yoshida, Ayumu Yano, Haruyuki Atomi, Tadayuki Imanaka, and Kunio Miki. 2012. "Dynamic, Ligand-Dependent Conformational Change Triggers Reaction of Ribose-1,5-Bisphosphate Isomerase from Thermococcus Kodakarensis KOD1." *Journal of Biological Chemistry* 287 (25): 20784–96. doi:10.1074/jbc.M112.349423.

Naveau, Marie, Christine Lazennec-Schurdevin, Michel Panvert, Yves Mechulam, and Emmanuelle Schmitt. 2010. "tRNA Binding Properties of Eukaryotic Translation Initiation Factor 2 from Encephalitozoon Cuniculi." *Biochemistry* 49 (40): 8680–88. doi:10.1021/bi1009166.

Nika, Joseph, Scott Rippel, and Ernest M. Hannig. 2001. "Biochemical Analysis of the eIF2βγ Complex Reveals a Structural Function for eIF2α in Catalyzed Nucleotide Exchange." *Journal of Biological Chemistry* 276 (2): 1051–56. doi:10.1074/jbc.M007398200.

Nika, Joseph, Weimin Yang, Graham D Pavitt, Alan G Hinnebusch, and Ernest M Hannig. 2000. "Purification and Kinetic Analysis of eIF2B from *Saccharomyces cerevisiae*." *Journal of Biological Chemistry* 275 (34): 26011–17. doi:10.1074/jbc.M003718200.

Nonato, M Cristina, Joanne Widom, and Jon Clardy. 2002. "Crystal Structure of the N-Terminal Segment of Human Eukaryotic Translation Initiation Factor 2." *Journal of Biological Chemistry* 277 (19): 17057–61. doi:10.1074/jbc.M111804200.

Novoa, Isabel, Huiqing Zeng, Heather P Harding, and David Ron. 2001. "Feedback Inhibition of the Unfolded Protein Response by GADD34 - Mediated Dephosphorylation of eIF2α." *The Journal of Cell Biology* 153 (5): 1011–22. doi:10.1083/jcb.153.5.1011.

Oldfield, Susan, Bridget L Jones, Deborah Tanton, and Christopher G Proud. 1994. "Use of Monoclonal Antibodies to Study the Structure and Function

of Eukaryotic Protein Synthesis Initiation Factor eIF-2B." *European Journal of Biochemistry* 221 (1): 399–410. doi:10.1111/j.1432-1033.1994.tb18752.x.

Oldfield, Susan, and Christopher G Proud. 1992. "Purification, Phosphorylation and Control of the Guanine-Nucleotide-Exchange Factor from Rabbit Reticulocyte Lysates." *European Journal of Biochemistry* 208 (1): 73–81. doi:10.1111/j.1432-1033.1992.tb17160.x.

Oyadomari, Seiichi, Heather P Harding, Yuhong Zhang, Miho Oyadomari, and David Ron. 2008. "Dephosphorylation of Translation Initiation Factor 2alpha Enhances Glucose Tolerance and Attenuates Hepatosteatosis in Mice." *Cell Metabolism* 7 (6): 520–32. doi:10.1016/j.cmet.2008.04.011.

Paddon, Christopher J, Ernest M Hannig, and Alan G Hinnebusch. 1989. "Amino Acid Sequence Similarity between GCN3 and GCD2, Positive and Negative Translational Regulators of GCN4: Evidence for Antagonism by Competition." *Genetics* 122 (3): 551–59. http://www.ncbi.nlm.nih.gov/pubmed/2668117.

Pakos-Zebrucka, Karolina, Izabela Koryga, Katarzyna Mnich, Mila Ljujic, Afshin Samali, and Adrienne M Gorman. 2016. "The Integrated Stress Response." *EMBO Reports* 17 (10): 1374–95. doi:10.15252/embr.201642195.

Palam, L. R., J. Gore, K. E. Craven, J. L. Wilson, and M. Korc. 2015. "Integrated Stress Response Is Critical for Gemcitabine Resistance in Pancreatic Ductal Adenocarcinoma." *Cell Death & Disease* 6 (10). Nature Publishing Group: e1913–e1913. doi:10.1038/cddis.2015.264.

Panniers, Richard, and Edgar C Henshaw. 1983. "A GDP/GTP Exchange Factor Essential for Eukaryotic Initiation Factor 2 Cycling in Ehrlich Ascites Tumor Cells and Its Regulation by Eukaryotic Initiation Factor 2 Phosphorylation." *The Journal of Biological Chemistry* 258 (13): 7928–34. http://www.ncbi.nlm.nih.gov/pubmed/6553052.

Panniers, Richard, Anne G Rowlands, and Edgar C Henshaw. 1988. "The Effect of Mg2+ and Guanine Nucleotide Exchange Factor on the Binding of Guanine Nucleotides to Eukaryotic Initiation Factor 2." *The Journal of*

Biological Chemistry 263 (12): 5519–25. http://www.ncbi.nlm.nih.gov/pubmed/3356694.

Pap, Marianna, and Geoffrey M Cooper. 2002. “Role of Translation Initiation Factor 2B in Control of Cell Survival by the Phosphatidylinositol 3-kinase/Akt/glycogen Synthase Kinase 3beta Signaling Pathway.” *Molecular and Cellular Biology* 22 (2): 578–86. doi:10.1128/MCB.22.2.578.

Pavitt, Graham D. 2005. “eIF2B, a Mediator of General and Gene-Specific Translational Control.” *Biochemical Society Transactions* 33 (Pt 6): 1487–92. doi:10.1042/BST20051487.

Pavitt, Graham D. 2018. “Regulation of Translation Initiation Factor eIF2B at the Hub of the Integrated Stress Response.” *Wiley Interdisciplinary Reviews: RNA*, no. March (July): e1491. doi:10.1002/wrna.1491.

Pavitt, Graham D., Weimin Yang, and Alan G Hinnebusch. 1997. “Homologous Segments in Three Subunits of the Guanine Nucleotide Exchange Factor eIF2B Mediate Translational Regulation by Phosphorylation of eIF2.” *Molecular and Cellular Biology* 17 (3): 1298–1313. doi:10.1128/MCB.17.3.1298.

Pavitt, Graham D, and Christopher G Proud. 2009. “Protein Synthesis and Its Control in Neuronal Cells with a Focus on Vanishing White Matter Disease.” *Biochemical Society Transactions* 37 (Pt 6): 1298–1310. doi:10.1042/BST0371298.

Pavitt, Graham D, Kolluru V A Ramaiah, Scot R Kimball, and Alan G Hinnebusch. 1998. “eIF2 Independently Binds Two Distinct eIF2B Subcomplexes That Catalyze and Regulate Guanine-Nucleotide Exchange.” *Genes & Development* 12 (4): 514–26. doi:10.1101/gad.12.4.514.

Pettersen, Eric F., Thomas D. Goddard, Conrad C. Huang, Gregory S. Couch, Daniel M. Greenblatt, Elaine C. Meng, and Thomas E. Ferrin. 2004. “UCSF Chimera - A Visualization System for Exploratory Research and Analysis.” *Journal of Computational Chemistry* 25 (13): 1605–12. doi:10.1002/jcc.20084.

Price, Nigel T, and Christopher G Proud. 1994. “The Guanine Nucleotide-Exchange Factor, eIF-2B.” *Biochimie* 76 (8): 748–60. doi:10.1016/0300-9084(94)90079-5.

Pronk, Jan C, Barbara van Kollenburg, Gert C Scheper, and Marjo S van der Knaap. 2006. “Vanishing White Matter Disease: A Review with Focus on Its Genetics.” *Mental Retardation and Developmental Disabilities Research Reviews* 12 (2): 123–28. doi:10.1002/mrdd.20104.

Proud, Christopher G. 2005. “eIF2 and the Control of Cell Physiology.” *Seminars in Cell & Developmental Biology* 16 (1): 3–12. doi:10.1016/j.semcdb.2004.11.004.

Qin, Qingsong, Kate Carroll, Craig Hastings, and Cathy L Miller. 2011. “Mammalian Orthoreovirus Escape from Host Translational Shutoff Correlates with Stress Granule Disruption and Is Independent of eIF2 Phosphorylation and PKR.” *Journal of Virology* 85 (17): 8798–8810. doi:10.1128/JVI.01831-10.

Rafie-Kolpin, Maryam, Peter J. Chefalo, Zareena Hussain, Joyce Hahn, Sheri Uma, Robert L. Matts, and Jane-Jane Chen. 2000. “Two Heme-Binding Domains of Heme-Regulated Eukaryotic Initiation Factor-2α Kinase.” *Journal of Biological Chemistry* 275 (7): 5171–78. doi:10.1074/jbc.275.7.5171.

Ralston, R O., A Das, A Dasgupta, R Roy, S Palmieri, and N K Gupta. 1978. “Protein Synthesis in Rabbit Reticulocytes: Characteristics of a Ribosomal Factor That Reverses Inhibition of Protein Synthesis in Heme-Deficient Lysates.” *Proceedings of the National Academy of Sciences* 75 (10): 4858–62. doi:10.1073/pnas.75.10.4858.

Ramaiah, K V, Monique V Davies, J J Chen, and Randal J Kaufman. 1994. “Expression of Mutant Eukaryotic Initiation Factor 2 Alpha Subunit (eIF-2 Alpha) Reduces Inhibition of Guanine Nucleotide Exchange Activity of eIF-2B Mediated by eIF-2 Alpha Phosphorylation.” *Molecular and Cellular Biology* 14 (7): 4546–53. doi:10.1128/MCB.14.7.4546.

Ran, F Ann, Patrick D Hsu, Jason Wright, Vineeta Agarwala, David a Scott, and Feng Zhang. 2013. “Genome Engineering Using the CRISPR-Cas9

System." *Nature Protocols* 8 (11): 2281–2308. doi:10.1038/nprot.2013.143.

Ranu, R S, and Irving M London. 1976. "Regulation of Protein Synthesis in Rabbit Reticulocyte Lysates: Purification and Initial Characterization of the Cyclic 3':5'-AMP Independent Protein Kinase of the Heme-Regulated Translational Inhibitor." *Proceedings of the National Academy of Sciences* 73 (12): 4349–53. doi:10.1073/pnas.73.12.4349.

Reid, Peter J., Sarah S. Mohammad-Qureshi, and Graham D. Pavitt. 2012. "Identification of Intersubunit Domain Interactions within Eukaryotic Initiation Factor (eIF) 2B, the Nucleotide Exchange Factor for Translation Initiation." *Journal of Biological Chemistry* 287 (11): 8275–85. doi:10.1074/jbc.M111.331645.

Richardson, Jonathan P, Sarah S Mohammad, and Graham D Pavitt. 2004. "Mutations Causing Childhood Ataxia with Central Nervous System Hypomyelination Reduce Eukaryotic Initiation Factor 2B Complex Formation and Activity." *Molecular and Cellular Biology* 24 (6): 2352–63. doi:10.1128/MCB.24.6.2352-2363.2004.

Roll-Mecak, Antonina, Pankaj Alone, Chune Cao, Thomas E. Dever, and Stephen K. Burley. 2004. "X-Ray Structure of Translation Initiation Factor eIF2γ: Implications for tRNA and eIF2α Binding." *Journal of Biological Chemistry* 279 (11): 10634–42. doi:10.1074/jbc.M310418200.

Ron, David. 2002. "Translational Control in the Endoplasmic Reticulum Stress Response." *Journal of Clinical Investigation* 110 (10): 1383–88. doi:10.1172/JCI16784.

Rosenthal, Peter B., and Richard Henderson. 2003. "Optimal Determination of Particle Orientation, Absolute Hand, and Contrast Loss in Single-Particle Electron Cryomicroscopy." *Journal of Molecular Biology* 333 (4): 721–45. doi:10.1016/j.jmb.2003.07.013.

Roux, Philippe P, and Ivan Topisirovic. 2012. "Regulation of mRNA Translation by Signaling Pathways." *Cold Spring Harbor Perspectives in Biology* 4 (11): 1–24. doi:10.1101/cshperspect.a012252.

Rowlands, Anne G, Richard Panniers, and E C Henshaw. 1988. "The

Catalytic Mechanism of Guanine Nucleotide Exchange Factor Action and Competitive Inhibition by Phosphorylated Eukaryotic Initiation Factor 2." *The Journal of Biological Chemistry* 263 (12): 5526–33. http://www.ncbi.nlm.nih.gov/pubmed/3356695.

Safer, Brian, M Grunberg-Manago, D Badman, F Bergman, C Freeman, G Galasso, Rosemary Jagus, and B Williams. 1982. "International Symposium on Translation/transcriptional Regulation of Gene Expression." *FEBS Letters* 147 (1): 1–10. doi:10.1016/0014-5793(82)81000-4.

Safer, Brian, and Rosemary Jagus. 1981. "The Regulation of eIF-2 Function during Protein Synthesis Initiation." *Biochimie* 63 (8–9): 709–17. doi:10.1016/S0300-9084(81)80219-2.

Sajid, Andaleeb, Gunjan Arora, Meetu Gupta, Anshika Singhal, Kausik Chakraborty, Vinay Kumar Nandicoori, and Yogendra Singh. 2011. "Interaction of Mycobacterium Tuberculosis Elongation Factor Tu with GTP Is Regulated by Phosphorylation." *Journal of Bacteriology* 193 (19): 5347–58. doi:10.1128/JB.05469-11.

Salimans, Marcel, Hans Goumans, Hans Amesz, Rob Benne, and Harry O Voorma. 1984. "Regulation of Protein Synthesis in Eukaryotes. Mode of Action of eRF, an eIF-2-Recycling Factor from Rabbit Reticulocytes Involved in GDP/GTP Exchange." *European Journal of Biochemistry* 145 (1): 91–98. doi:10.1111/j.1432-1033.1984.tb08526.x.

Sattlegger, Evelyn, and Alan G Hinnebusch. 2000. "Separate Domains in GCN1 for Binding Protein Kinase GCN2 and Ribosomes Are Required for GCN2 Activation in Amino Acid-Starved Cells." *The EMBO Journal* 19 (23): 6622–33. doi:10.1093/emboj/19.23.6622.

Scheper, Gert C., Christopher G. Proud, and Marjo S. van der Knaap. 2006. "Defective Translation Initiation Causes Vanishing of Cerebral White Matter." *Trends in Molecular Medicine* 12 (4): 159–66. doi:10.1016/j.molmed.2006.02.006.

Scheper, Gert C, Marjo S van der Knaap, and Christopher G Proud. 2007. "Translation Matters: Protein Synthesis Defects in Inherited Disease."

Nature Reviews. Genetics 8 (9): 711–23. doi:10.1038/nrg2142.

Scheres, Sjors H.W. 2012a. “A Bayesian View on Cryo-EM Structure Determination.” *Journal of Molecular Biology* 415 (2). Elsevier Ltd: 406–18. doi:10.1016/j.jmb.2011.11.010.

———. 2012b. “RELION: Implementation of a Bayesian Approach to Cryo-EM Structure Determination.” *Journal of Structural Biology* 180 (3). Elsevier Inc.: 519–30. doi:10.1016/j.jsb.2012.09.006.

Scheres, Sjors H W, and Shaoxia Chen. 2012. “Prevention of Overfitting in Cryo-EM Structure Determination.” *Nature Methods* 9 (9). Nature Publishing Group: 853–54. doi:10.1038/nmeth.2115.

Scheres, Sjors Hw. 2014. “Beam-Induced Motion Correction for Sub-Megadalton Cryo-EM Particles.” *eLife* 3 (August): e03665. doi:10.7554/eLife.03665.

Schiffmann, Raphael, and Orna Elroy-Stein. 2006. “Childhood Ataxia with CNS Hypomyelination/vanishing White Matter Disease-A Common Leukodystrophy Caused by Abnormal Control of Protein Synthesis.” *Molecular Genetics and Metabolism* 88 (1): 7–15. doi:10.1016/j.ymgme.2005.10.019.

Schimmel, Paul. 1993. “GTP Hydrolysis in Protein Synthesis: Two for Tu?” *Science* 259 (5099): 1264–65. doi:10.1126/science.8446896.

Schmitt, Emmanuelle, Marie Naveau, and Yves Mechulam. 2010. “Eukaryotic and Archaeal Translation Initiation Factor 2: A Heterotrimeric tRNA Carrier.” *FEBS Letters* 584 (2). Federation of European Biochemical Societies: 405–12. doi:10.1016/j.febslet.2009.11.002.

Schmitt, Emmanuelle, Michel Panvert, Christine Lazennec-Schurdevin, Pierre-Damien Coureux, Javier Perez, Andrew Thompson, and Yves Mechulam. 2012. “Structure of the Ternary Initiation Complex aIF2–GDPNP–methionylated Initiator tRNA.” *Nature Structural & Molecular Biology* 19 (4). Nature Publishing Group: 450–54. doi:10.1038/nsmb.2259.

Sekine, Yusuke, Alisa Zyryanova, Ana Crespillo-Casado, Peter M Fischer,

Heather P Harding, and David Ron. 2015a. “Stress Responses. Mutations in a Translation Initiation Factor Identify the Target of a Memory-Enhancing Compound.” *Science (New York, N.Y.)* 348 (6238): 1027–30. doi:10.1126/science.aaa6986.

Sekine, Yusuke, Alisa F Zyryanova, Ana Crespillo-Casado, Niko Amin-Wetzel, Heather P Harding, and David Ron. 2016. “Paradoxical Sensitivity to an Integrated Stress Response Blocking Mutation in Vanishing White Matter Cells.” *PLoS ONE* 11 (11): 1–18. doi:10.1371/journal.pone.0166278.

Sekine, Yusuke, Alisa F Zyryanova, Ana Crespillo-Casado, Peter M Fischer, Heather P Harding, and David Ron. 2015b. “Mutations in a Translation Initiation Factor Identify the Target of a Memory-Enhancing Compound.” *Science* 348 (6238): 1027–30. doi:10.1126/science.aaa6986.

Shang, Xun, Fillipo Marchioni, Nisha Sipes, Chris R. Evelyn, Moran Jerabek-Willemsen, Stefan Duhr, William Seibel, Matthew Wortman, and Yi Zheng. 2012. “Rational Design of Small Molecule Inhibitors Targeting Rhoa Subfamily Rho GTPases.” *Chemistry and Biology* 19 (6). Elsevier Ltd: 699–710. doi:10.1016/j.chembiol.2012.05.009.

Sharon, Eyal, and Niza Frenkel. 2017. “Human Herpesvirus 6A Exhibits Restrictive Propagation with Limited Activation of the Protein Kinase R-eIF2α Stress Pathway.” *Journal of Virology* 91 (9): e02120-16. doi:10.1128/JVI.02120-16.

Sidrauski, Carmela, Diego Acosta-Alvear, Arkady Khoutorsky, Punitha Vedantham, Brian R Hearn, Han Li, Karine Gamache, et al. 2013. “Pharmacological Brake-Release of mRNA Translation Enhances Cognitive Memory.” *eLife* 2 (May): e00498. doi:10.7554/eLife.00498.

Sidrauski, Carmela, Jordan C Tsai, Martin Kampmann, Brian R Hearn, Punitha Vedantham, Priyadarshini Jaishankar, Masaaki Sokabe, et al. 2015. “Pharmacological Dimerization and Activation of the Exchange Factor eIF2B Antagonizes the Integrated Stress Response.” *eLife* 4 (April): 1–27. doi:10.7554/eLife.07314.

Siekierka, John, Veeraswamy Manne, and Severo Ochoa. 1984. “Mechanism of Translational Control by Partial Phosphorylation of the Alpha Subunit

of Eukaryotic Initiation Factor 2." *Proceedings of the National Academy of Sciences* 81 (2): 352–56. doi:10.1073/pnas.81.2.352.

Siekierka, John, Ljubica Mauser, and Severo Ochoa. 1982. "Mechanism of Polypeptide Chain Initiation in Eukaryotes and Its Control by Phosphorylation of the Alpha Subunit of Initiation Factor 2." *Proceedings of the National Academy of Sciences of the United States of America* 79 (8): 2537–40. doi:10.1073/pnas.79.8.2537.

Siekierka, John, Ken-Ichiro Mitsui, and Severo Ochoa. 1981. "Mode of Action of the Heme-Controlled Translational Inhibitor: Relationship of Eukaryotic Initiation Factor 2-Stimulating Protein to Translation Restoring Factor." *Proceedings of the National Academy of Sciences* 78 (1): 220–23. doi:10.1073/pnas.78.1.220.

Singh, Chingakham Ranjit, Bumjun Lee, Tsuyoshi Udagawa, Sarah S Mohammad-Qureshi, Yasufumi Yamamoto, Graham D Pavitt, and Katsura Asano. 2006. "An eIF5/eIF2 Complex Antagonizes Guanine Nucleotide Exchange by eIF2B during Translation Initiation." *The EMBO Journal* 25 (19): 4537–46. doi:10.1038/sj.emboj.7601339.

Singh, Lalit P., Nancy D. Denslow, and Albert J. Wahba. 1996. "Modulation of Rabbit Reticulocyte Guanine Nucleotide Exchange Factor Activity by Casein Kinases 1 and 2 and Glycogen Synthase Kinase 3." *Biochemistry* 35 (10): 3206–12. doi:10.1021/bi9522099.

Singh, Lalit P, Annayya R. Aroor, and Albert J Wahba. 1994. "Phosphorylation of the Guanine Nucleotide Exchange Factor and Eukaryotic Initiation Factor 2 by Casein Kinase II Regulates Guanine Nucleotide Binding and GDP/GTP Exchange." *Biochemistry* 33 (31): 9152–57. doi:10.1021/bi00197a018.

Singh, Lalit P, Annayya R Aroor, and Albert J Wahba. 1995. "Inhibition of Rabbit Reticulocyte Guanine Nucleotide Exchange Factor Activity by Heparin and Its Reversal by Polyamines." *Biochemical and Biophysical Research Communications* 212 (3): 1007–14. doi:10.1006/bbrc.1995.2070.

Sokabe, Masaaki, Christopher S. Fraser, and John W B Hershey. 2012. "The

Human Translation Initiation Multi-Factor Complex Promotes Methionyl-tRNA I Binding to the 40S Ribosomal Subunit." *Nucleic Acids Research* 40 (2): 905–13. doi:10.1093/nar/gkr772.

Sokabe, Masaaki, Min Yao, Naoki Sakai, Shingo Toya, and Isao Tanaka. 2006. "Structure of Archaeal Translational Initiation Factor 2 Betagamma-GDP Reveals Significant Conformational Change of the Beta-Subunit and Switch 1 Region." *Proceedings of the National Academy of Sciences of the United States of America* 103 (35): 13016–21. doi:10.1073/pnas.0604165103.

Sonenberg, Nahum, and Alan G Hinnebusch. 2009. "Regulation of Translation Initiation in Eukaryotes: Mechanisms and Biological Targets." *Cell* 136 (4). Elsevier Inc.: 731–45. doi:10.1016/j.cell.2009.01.042.

Stolboushkina, Elena, Stanislav Nikonov, Alexei Nikulin, Udo Bläsi, Dietmar J Manstein, Roman Fedorov, Maria Garber, and Oleg Nikonov. 2008. "Crystal Structure of the Intact Archaeal Translation Initiation Factor 2 Demonstrates Very High Conformational Flexibility in the α- and β-Subunits." *Journal of Molecular Biology* 382 (3): 680–91. doi:10.1016/j.jmb.2008.07.039.

Stolboushkina, Elena, Stanislav Nikonov, Natalia Zelinskaya, Valentina Arkhipova, Alexei Nikulin, Maria Garber, and Oleg Nikonov. 2013. "Crystal Structure of the Archaeal Translation Initiation Factor 2 in Complex with a GTP Analogue and Met-tRNAfMet." *Journal of Molecular Biology* 425 (6). Elsevier Ltd: 989–98. doi:10.1016/j.jmb.2012.12.023.

Sudhakar, Akulapalli, Thanuja Krishnamoorthy, Anjali Jain, Udayan Chatterjee, Seyed E. Hasnain, Randal J. Kaufman, and Kolluru V.A. Ramaiah. 1999. "Serine 48 in Initiation Factor 2α (eIF2α) Is Required for High- Affinity Interaction between eIF2α(P) and eIF2B." *Biochemistry* 38 (46): 15398–405. doi:10.1021/bi991211n.

Sudhakar, Akulapalli, Aruna Ramachandran, Sudip Ghosh, Seyed E Hasnain, Randal J Kaufman, and K V Ramaiah. 2000. "Phosphorylation of Serine 51 in Initiation Factor 2 Alpha (eIF2 Alpha) Promotes Complex Formation between eIF2 alpha(P) and eIF2B and Causes Inhibition in the Guanine

Nucleotide Exchange Activity of eIF2B." *Biochemistry* 39 (42): 12929–38. doi:10.1021/bi0008682.

Tang, Guang, Liwei Peng, Philip R. Baldwin, Deepinder S. Mann, Wen Jiang, Ian Rees, and Steven J. Ludtke. 2007. "EMAN2: An Extensible Image Processing Suite for Electron Microscopy." *Journal of Structural Biology* 157 (1): 38–46. doi:10.1016/j.jsb.2006.05.009.

The Molecular Probes Handbook. a Quide to Fluorescent Probes and Labeling Technologies. 2010.

Tsai, Jordan C, Lakshmi E Miller-Vedam, Aditya A Anand, Priyadarshini Jaishankar, Henry C Nguyen, Adam R Renslo, Adam Frost, and Peter Walter. 2018. "Structure of the Nucleotide Exchange Factor eIF2B Reveals Mechanism of Memory-Enhancing Molecule." *Science* 359 (6383): eaaq0939. doi:10.1126/science.aaq0939.

Tsaytler, Pavel, Heather P Harding, David Ron, and Anne Bertolotti. 2011. "Selective Inhibition of a Regulatory Subunit of Protein Phosphatase 1 Restores Proteostasis." *Science* 332 (6025): 91–94. doi:10.1126/science.1201396.

van der Knaap, Marjo S, Peter A J Leegwater, Andrea A M Könst, Allerdien Visser, Sakkubai Naidu, Cees B M Oudejans, Ruud B H Schutgens, and Jan C Pronk. 2002. "Mutations in Each of the Five Subunits of Translation Initiation Factor eIF2B Can Cause Leukoencephalopathy with Vanishing White Matter." *Annals of Neurology* 51 (2): 264–70. doi:10.1002/ana.10112.

van der Voorn, J Patrick, Barbara van Kollenburg, Gesina Bertrand, Keith Van Haren, Gert C Scheper, James M Powers, and Marjo S van der Knaap. 2005. "The Unfolded Protein Response in Vanishing White Matter Disease." *Journal of Neuropathology and Experimental Neurology* 64 (9): 770–75. http://www.ncbi.nlm.nih.gov/pubmed/16141786.

van Kollenburg, Barbara, Adri A M Thomas, Gerre Vermeulen, Gesina A M Bertrand, Carola G M van Berkel, Jan C. Pronk, Christopher G. Proud, Marjo S. van der Knaap, and Gert C. Scheper. 2006. "Regulation of Protein Synthesis in Lymphoblasts from Vanishing White Matter

Patients." *Neurobiology of Disease* 21 (3): 496–504. doi:10.1016/j.nbd.2005.08.009.

Vattem, Krishna M, and Ronald C Wek. 2004. "Reinitiation Involving Upstream ORFs Regulates ATF4 mRNA Translation in Mammalian Cells." *Proceedings of the National Academy of Sciences of the United States of America* 101 (31): 11269–74. doi:10.1073/pnas.0400541101.

Vazquez de Aldana, Carlos R, Thomas E Dever, and Alan G Hinnebusch. 1993. "Mutations in the Alpha Subunit of Eukaryotic Translation Initiation Factor 2 (eIF-2 Alpha) That Overcome the Inhibitory Effect of eIF-2 Alpha Phosphorylation on Translation Initiation." *Proceedings of the National Academy of Sciences of the United States of America* 90 (15): 7215–19. http://www.ncbi.nlm.nih.gov/pubmed/8102207.

Vazquez de Aldana, Carlos R, and Alan G Hinnebusch. 1994. "Mutations in the GCD7 Subunit of Yeast Guanine Nucleotide Exchange Factor eIF-2B Overcome the Inhibitory Effects of Phosphorylated eIF-2 on Translation Initiation." *Molecular and Cellular Biology* 14 (5): 3208–22. doi:10.1128/MCB.14.5.3208.

Walsh, Derek, Michael B Mathews, and Ian Mohr. 2013. "Tinkering with Translation: Protein Synthesis in Virus-Infected Cells." *Cold Spring Harbor Perspectives in Biology* 5 (1): a012351. doi:10.1101/cshperspect.a012351.

Walton, Gordon M., and Gordon N. Gill. 1975. "Nucleotide Regulation of a Eukaryotic Protein Synthesis Initiation Complex." *Biochimica et Biophysica Acta (BBA) - Nucleic Acids and Protein Synthesis* 390 (2): 231–45. doi:10.1016/0005-2787(75)90344-5.

Wang, Lijun, Brian Popko, and Raymond P. Roos. 2014. "An Enhanced Integrated Stress Response Ameliorates Mutant SOD1-Induced ALS." *Human Molecular Genetics* 23 (10): 2629–38. doi:10.1093/hmg/ddt658.

Wang, Xuemin, Fiona E M Paulin, Linda E Campbell, Edith Gomez, Kirsty O'Brien, Nicholas Morrice, and Christopher G Proud. 2001. "Eukaryotic Initiation Factor 2B: Identification of Multiple Phosphorylation Sites in the Epsilon-Subunit and Their Functions in Vivo." *The EMBO Journal* 20 (16):

4349–59. doi:10.1093/emboj/20.16.4349.

Wang, Xuemin, and Christopher G Proud. 2008. “A Novel Mechanism for the Control of Translation Initiation by Amino Acids, Mediated by Phosphorylation of Eukaryotic Initiation Factor 2B.” *Molecular and Cellular Biology* 28 (5): 1429–42. doi:10.1128/MCB.01512-07.

Wang, Xuemin, Noel C Wortham, Rui Liu, and Christopher G Proud. 2012. “Identification of Residues That Underpin Interactions within the Eukaryotic Initiation Factor (eIF2) 2B Complex.” *Journal of Biological Chemistry* 287 (11): 8263–74. doi:10.1074/jbc.M111.331553.

Webb, Benjamin L J, and Christopher G Proud. 1997. “Eukaryotic Initiation Factor 2B (eIF2B).” *The International Journal of Biochemistry & Cell Biology* 29 (10): 1127–31. doi:10.1016/S1357-2725(97)00039-3.

Wei, Jia, Minze Jia, Cheng Zhang, Mingzhu Wang, Feng Gao, Hang Xu, and Weimin Gong. 2010. “Crystal Structure of the C-Terminal Domain of the Ɛ Subunit of Human Translation Initiation Factor eIF2B.” *Protein & Cell* 1 (6): 595–603. doi:10.1007/s13238-010-0070-6.

Wek, Ronald C, Belinda M Jackson, and Alan G Hinnebusch. 1989. “Juxtaposition of Domains Homologous to Protein Kinases and Histidyl-tRNA Synthetases in GCN2 Protein Suggests a Mechanism for Coupling GCN4 Expression to Amino Acid Availability.” *Proceedings of the National Academy of Sciences* 86 (12): 4579–83. doi:10.1073/pnas.86.12.4579.

Welsh, Gavin I., Christa M. Miller, A. Jane Loughlin, Nigel T. Price, and Christopher G. Proud. 1998. “Regulation of Eukaryotic Initiation Factor eIF2B: Glycogen Synthase Kinase-3 Phosphorylates a Conserved Serine Which Undergoes Dephosphorylation in Response to Insulin.” *FEBS Letters* 421 (2): 125–30. doi:10.1016/S0014-5793(97)01548-2.

Welsh, Gavin I, and Christopher G Proud. 1992. “Regulation of Protein Synthesis in Swiss 3T3 Fibroblasts. Rapid Activation of the Guanine-Nucleotide-Exchange Factor by Insulin and Growth Factors.” *Biochemical Journal* 284 (1): 19–23. doi:10.1042/bj2840019.

———. 1993. “Glycogen Synthase Kinase-3 Is Rapidly Inactivated in

Response to Insulin and Phosphorylates Eukaryotic Initiation Factor eIF-2B." *Biochemical Journal* 294 (3): 625–29. doi:10.1042/bj2940625.

Williams, Daniel D., Graham D. Pavitt, and Christopher G. Proud. 2001. "Characterization of the Initiation Factor eIF2B and Its Regulation in Drosophila Melanogaster." *Journal of Biological Chemistry* 276 (6): 3733–42. doi:10.1074/jbc.M008041200.

Wong, Yao Liang, Lauren LeBon, Rohinton Edalji, Hock Ben Lim, Chaohong Sun, and Carmela Sidrauski. 2018. "The Small Molecule ISRIB Rescues the Stability and Activity of Vanishing White Matter Disease eIF2B Mutant Complexes." *eLife* 7 (February): 1–23. doi:10.7554/eLife.32733.

Woods, Y L, P Cohen, W Becker, R Jakes, M Goedert, X Wang, and C G Proud. 2001. "The Kinase DYRK Phosphorylates Protein-Synthesis Initiation Factor eIF2Bepsilon at Ser539 and the Microtubule-Associated Protein Tau at Thr212: Potential Role for DYRK as a Glycogen Synthase Kinase 3-Priming Kinase." *The Biochemical Journal* 355 (Pt 3): 609–15. doi:10.1042/bj3550609.

Wortham, Noel C., and Christopher G. Proud. 2015. "Biochemical Effects of Mutations in the Gene Encoding the Alpha Subunit of Eukaryotic Initiation Factor (eIF) 2B Associated with Vanishing White Matter Disease." *BMC Medical Genetics* 16 (1). BMC Medical Genetics: 1–8. doi:10.1186/s12881-015-0204-z.

Wortham, Noel C, Magdalena Martinez, Yuliya Gordiyenko, Carol V Robinson, and Christopher G Proud. 2014. "Analysis of the Subunit Organization of the eIF2B Complex Reveals New Insights into Its Structure and Regulation." *The FASEB Journal* 28 (5): 2225–37. doi:10.1096/fj.13-243329.

Wortham, Noel C, Joanna D Stewart, Sean Harris, Mark J Coldwell, and Christopher G Proud. 2016. "Stoichiometry of the eIF2B Complex Is Maintained by Mutual Stabilization of Subunits." *Biochemical Journal* 473 (5): 571–80. doi:10.1042/BJ20150828.

Yang, Weimin, and Alan G Hinnebusch. 1996. "Identification of a Regulatory Subcomplex in the Guanine Nucleotide Exchange Factor eIF2B That

Mediates Inhibition by Phosphorylated eIF2." *Molecular and Cellular Biology* 16 (11): 6603–16. doi:10.1128/MCB.16.11.6603.

Yatime, Laure, Yves Mechulam, Sylvain Blanquet, and Emmanuelle Schmitt. 2007. "Structure of an Archaeal Heterotrimeric Initiation Factor 2 Reveals a Nucleotide State between the GTP and the GDP States." *Proceedings of the National Academy of Sciences of the United States of America* 104 (47): 18445–50. doi:10.1073/pnas.0706784104.

Yatime, Laure, Emmanuelle Schmitt, Sylvain Blanquet, and Yves Mechulam. 2005. "Structure - Function Relationships of the Intact aIF2α Subunit from the Archaeon Pyrococcus Abyssi." *Biochemistry* 44 (24): 8749–56. doi:10.1021/bi050373i.

Ye, Jiangbin, Monika Kumanova, Lori S. Hart, Kelly Sloane, Haiyan Zhang, Diego N. De Panis, Ekaterina Bobrovnikova-Marjon, J. Alan Diehl, David Ron, and Constantinos Koumenis. 2010. "The GCN2-ATF4 Pathway Is Critical for Tumour Cell Survival and Proliferation in Response to Nutrient Deprivation." *The EMBO Journal* 29 (12). Nature Publishing Group: 2082–96. doi:10.1038/emboj.2010.81.

Zhang, Kai. 2016. "Gctf: Real-Time CTF Determination and Correction." *Journal of Structural Biology* 193 (1). Elsevier Inc.: 1–12. doi:10.1016/j.jsb.2015.11.003.

Zhou, Donghui, L. Reddy Palam, Li Jiang, Jana Narasimhan, Kirk A. Staschke, and Ronald C. Wek. 2008. "Phosphorylation of eIF2 Directs ATF5 Translational Control in Response to Diverse Stress Conditions." *Journal of Biological Chemistry* 283 (11): 7064–73. doi:10.1074/jbc.M708530200.

Zhu, Shuhao, and Ronald C. Wek. 1998. "Ribosome-Binding Domain of Eukaryotic Initiation Factor-2 Kinase GCN2 Facilitates Translation Control." *Journal of Biological Chemistry* 273 (3): 1808–14. doi:10.1074/jbc.273.3.1808.

Zyryanova, Alisa F, Félix Weis, Alexandre Faille, Akeel Abo, Ana Crespillo-casado, Heather P Harding, Felicity Allen, et al. 2017. "Binding of the Integrated Stress Response Inhibitor , ISRIB , Reveals a Regulatory Site

in the Nucleotide Exchange Factor , eIF2B Corresponding Authors :" *BioRxiv*, 1–61. doi:10.1101/224824.

Zyryanova, Alisa F, Félix Weis, Alexandre Faille, Akeel Abo Alard, Ana Crespillo-Casado, Yusuke Sekine, Heather P Harding, et al. 2018. "Binding of ISRIB Reveals a Regulatory Site in the Nucleotide Exchange Factor eIF2B." *Science* 359 (6383): 1533–36. doi:10.1126/science.aar5129.